An Integrated Fuzzy Rule-Based Image Segmentation Framework

by

Gour Chandra Karmakar

B.Sc. (Computer Science and Engineering), Master of Computing

A dissertation submitted in fulfilment of the requirements for the

degree of

Doctor of Philosophy

Gippsland School of Computing and Information Technology

Monash University, Melbourne, Australia.

November 2002

Abstract

Fuzzy rule-based image segmentation techniques are able to incorporate human expert and/or domain specific knowledge, however, they tend in general, to be image and application dependent with predefined membership function structures and in certain cases, the corresponding parameters being manually determined. This thesis proposes a new flexible integrated fuzzy rule-based image segmentation (object-based) framework, which automates many aspects of previous systems as well as enabling new rules, special domain information, and high-level semantics of an object to be easily incorporated.

The framework comprises four novel dedicated fuzzy rule-based segmentation algorithms that seek to exploit particular image attributes for perceptual grouping. These are: a *generic fuzzy rule based image segmentation (GFRIS)* algorithm, which is both application and image independent and also importantly exploits inter-pixel spatial relationships. The second algorithm comprises a series of refinement rules which are collectively called *fuzzy rules for image segmentation (FRIS)* and are primarily based on region *splitting and merging* techniques, combining uniquely the topological feature of connectedness and object surroundedness. The third algorithm, *fuzzy rule for image segmentation incorporating texture features (FRIST)*, integrates the fractal dimension and contrast features of a texture by considering image domain specific information within the GFRIS algorithm. Finally, since GFRIS, FRIS, and FRIST are developed for gray level images, a new *fuzzy rule based colour image segmentation (FRCIS)* algorithm is introduced, which is an extension of GFRIS and includes a special algorithm for calculating the average of hue components of the HSV (hue, saturation, and value) colour model.

A comprehensive qualitative and quantitative evaluation is presented together with a time complexity analysis for all four major algorithms. A statistical significance test, namely the *sign test* is used to assess the performance improvement achieved by each algorithm. This new flexible framework provides significant segmentation improvements over traditional fuzzy c-means (FCM) and possibilistic c-means (PCM) algorithms for many different image types and with the single exception of FRIS, without any increase in the overall order of computational complexity.

i

Declaration

I certify that this dissertation does not incorporate without acknowledgment any material previously submitted for a degree or diploma in any university; and that to the best of my knowledge and belief it does not contain any material previously published or written by any author except where due reference is made in the text.

Gour Chandra Karmakar

Date: 21·11·02.

ii

Acknowledgments

I would like to express my sincerest gratitude and greatest appreciation to my main supervisor Prof. Laurence S. Dooley and associate supervisor Dr. Manzur Murshed for their patience, guidance, innovative ideas, encouragement, motivation, observations, and suggestions, which helped me so much in successfully completing this research. I have enjoyed working with them - brainstorming, writing, and presenting. This dissertation would not have been possible without their support.

I am also grateful to Professor Syed Mahbubur Rahman (who to my great pleasure was my Masters supervisor) for his sincere help and support.

The other members of the multimedia research group and all 7N colleagues. I appreciate their help with the dissertation and have enjoyed interacting with them on other research issues. I would particularly like to thank Dr. Kai Ming Ting, Dr. Joarder Kamruzzaman, and Dr. John Arkinstall for their help and suggestions.

I wish to greatly express my gratitude to the Gippsland School of Computing and Information Technology for all help they have extended to me. The support from the Monash University in the form of scholarships and professional development program is also greatly acknowledged.

I wish to thank Bangladesh Open University for granting me study leave, my cousin Gopal Chandra Karmakar for his help, and all the Bengali Community in Gippsland for their well wishes and encouragement.

Last but not the least, my special thanks to my wonderful wife, Soma for her love, patience, sacrifice, and care, my affectionate little daughter, Anwseha, my parents and parents-in-laws.

Acronyms and Abbreviations

asd	Average sum of differences.
CAT	Computed axial topography.
DBC	Differential box counting.
FCM	Fuzzy c-means.
FD	Fractal dimension.
FDF	Fractal dimension based feature.
FRCIS	Fuzzy rule-based colour image segmentation.
FRIS	Fuzzy rules for image segmentation: a refinement algorithm.
FRIST	Fuzzy rule for image segmentation incorporating texture features.
GFRIS	Generic fuzzy rule-based image segmentation.
HSV	Hue, saturation, and value.
MRI	Magnetic resonance image.
nasd	Normalised average sum of differences.
OCA	Object-count-agreement.
PCM	Possibilistic c-means.
RGB	Red, green, and blue.
sofd	Absolute sum of differences.

Nomenclature

Symbols	Denotation
b	Number of bits.
C_j	The total number of both surrounded and connected objects of other regions with the *main object* of region R_j.
$contrast(O_{ij})$	Contrast of object O_{ij}.
$C(R_j)$	Centre of region R_j.
$diff(h_1, h_2)$	Difference between two hue angles h_1 and h_2.
$d(P_{x,y}, P_{s,t})$	The *city block* distance between pixels $P_{x,y}$ and $P_{s,t}$.
$FD(W_{h,h}(s,t))$	The *fractal dimension based feature (FDF)* of a candidate pixel $P_{s,t}$.
$f_{iR_j}(.)$	Polynomial for the pixel distribution for the ith colour component of region R_j.
$f_{R_j}(.)$	Polynomial for the pixel distribution of region R_j for gray level image.
h_i	The ith hue angle.
$hist(P_i)$	Gray level histogram $hist(P_i)$ for pixel intensity P_i.
K	An arbitrary constant.
$large(O_{m_k k}, R_k)$	Function that determines whether the *main object* $O_{m_k k}$ is sufficiently large with respect to its own region R_k.
O_{ij}	The ith object of region R_j.
$O_{m_j j}$	The *main object* of region R_j.
$outer(R_k)$	Function that determines whether R_k is an outer region.
$P_{s,t}$	A pixel with a gray level or colour value $P_{s,t}$ at location (s,t).
R	A set of all regions.

Symbols	Denotation
r	Neighbourhood radius.
R_j	The jth region.
$\mathrm{similar}\left(O_{m_k k}, O_{ik}\right)$	Membership function that measures the similarity between two objects, $O_{m_k k}$ and O_{ik} .
S_j	The total number of objects that are surrounded by the *main object* of region R_j.
T	The threshold for the variations of gray level pixel intensity.
T_a	Approximate threshold.
$\mathit{uniformity}\left(O_{ij}\right)$	The entropy which measures the uniformity of the gray level distribution of object O_{ij} .
V	A set of centre pairs of all regions.
$W_{h,h}(s,t)$	A window $W_{h,h}(s,t)$ of size $h \times h$ with its centre at (s,t) .
w_i	The weighting factor for the ith membership function.
$x(P_i)$	The x coordinate of pixel P_i .
$y(P_i)$	The y coordinate of pixel P_i .
χ	Threshold for similarity measure.
τ	Scale down ratio.
ϕ	The number of colour components.
λ_1	A threshold that defines the minimum size of a *main object*.
λ_2	A threshold that defines the maximum size of the *main object*.
μ	Membership function.
$\mu_{AR_j}(.)$	The overall membership value for region R_j .
$\mu_{CR_j}(.)$	Membership function to measure the closeness of a region for region R_j .
$\mu_{C_i R_j}(.)$	Membership function to measure the closeness of region for the ith colour component of region R_j .
$\mu_{C_t R_j}(.)$	Membership function for the contrast of region R_j .

Symbols	Denotation
$\mu_{DR_j}(.)$	Membership function for the pixel distribution of region R_j.
$\mu_{D_iR_j}(.)$	Membership function for the pixel distribution for the ith colour component of region R_j.
$\mu_{FR_j}(.)$	Membership function $\mu_{FR_j}(P_{s,t})$ of fractal dimension based feature for region R_j.
$\mu_l(.)$	Membership function to determine the size of *main object*.
$\mu_\ell(O_{m_kk}, R_k)$	The size of the *main object* within its own region R_k.
$\mu_{NR_j}(.)$	Membership function for spatial relations for region R_j.
$\mu_{N_iR_j}(.)$	Membership function for spatial relations for the ith colour component of region R_j.
$\mu_s(.)$	Membership function for estimating the degree of surroundedness.
σ_{R_j}	Standard deviation of region R_j.
ξ	A threshold that determines the minimum degree of surroundedness.
$\zeta(P_{s,t}, r)$	Neighbourhood system with radius r, of a candidate pixel $P_{s,t}$.
$\Re$	The number of segmented regions.

Contents

Introduction

1.1 Image Segmentation Background

The use of digital images is increasing rapidly due to the development of the Internet and related multimedia technologies, such that the focus of much recent research has been directed towards the field of digital image processing. Digital image processing covers a wide range of application areas from medical science to document processing. In general terms, it refers to the manipulation and analysis of pictorial information and is mainly classified into five categories: (i) enhancement, (ii) restoration, (iii) analysis, (iv) compression, and (v) synthesis. Image analysis in particular, includes image segmentation, feature extraction, and object classification [11].

Image segmentation is the process of separating mutually exclusive homogeneous regions (objects) of interest from other regions (objects) in an image. It is one of the most important and challenging tasks of digital image processing and analysis systems, due to the potentially inordinate number of objects and the myriad of variations among them. Most natural objects are not homogeneous, which contradicts the above definition for object-based image segmentation. This is because in general there is no universal standard definition of image segmentation. It is essentially an ad hoc process, which depends on the emphasis given to particular desired properties and a trade-off between them [2, 12].

Image segmentation has been extensively used in a wide range of diverse applications. These include, but are not limited to, automatic car assembly in robotic vision, airport identification from aerial photographs, object based image identification and retrieval, object recognition, second generation image coding, criminal investigation, computer graphic, and medical science (cancerous cell detection, segmentation of brain images, skin treatment, and intrathoracic airway trees) [13-15].

Many of the above applications, however, require different types of digital images. The most commonly used are light intensity (LI) images, range images (RI), computed tomography (CT) images, thermal images, and magnetic resonance images (MRI). However, much of the research

published in the image segmentation area is highly dependent on the type of image, its dimension, and its application domain. No single unified technique is suitable for every type of image [14].

The literature reveals a wide variety of image segmentation techniques that are broadly classified into two approaches: region-based and boundary or contour-based [16, 17]. The former uses the homogeneity of pixels or features, while the latter finds the contour of a region of interest. Two types of contours are: active contours [18-21] and deformable contours [17, 22, 23].

Haralic [24] went a step further and divided image segmentation techniques into four classes: -

1. Measurement space guided spatial clustering (e.g. thresholding and multidimensional measurement space clustering) [25-28].

2. Region growing (e.g. single linkage, hybrid linkage, and centroid linkage region growing approaches) [29-32].

3. Spatial clustering [33-35].

4. Split and merge [36-39].

The first technique assigns each pixel a *cluster index* of an appropriate cluster of the measurement space. Pixels having the same *cluster index* are treated as the connected component and in the same class. Generally, clustering and histogram mode seeking techniques are used in this approach, though they do not work well when the gray level intensity of an object of interest for segmentation varies extensively and the background is not uniform.

In the second of the above categories, the image is divided into an arbitrary number of regions. The gray level intensity variation of all the pixels of a region lies within the limit of a specified threshold. The region is grown by taking a pixel as a starting point and then adding all pixels into the region whose gray level intensity variation lies within the threshold [40]. This technique is expensive both in terms of computation and memory [41]. A short review of the three linkage approaches identified above is now provided. The single linkage region growing approach applies graph theory to segment the image with each vertex of the graph representing a pixel of the image. Pixels containing similar characteristics are connected by the links of the graph. This approach suffers from the problem of chaining, whereby if a chain is broken, it loses all the pixels of the other part. The hybrid linkage region growing approach allocates a property vector to each pixel, which is a function of its $k \times k$ neighbourhood values. In the centroid linkage region growing approach, the image is firstly scanned and then a region is formed by comparing the pixel value with the mean of that region. Pixels are added into the region if they are close enough and then the

mean of the region is updated. Similar regions (if any) are merged. The effectiveness of this approach depends on the combining criteria.

The third segmentation approach, spatial clustering, forms the clusters by considering both the measurement space as well as spatial space between the parent pixels and their neighbours, while the fourth approach initially assumes the image as one segment and then divides it into a number of sub-divisions (4^n where $n = 1, 2, ...$) based on a *quadtree* [40, 42]. Adjacent regions are merged if they are sufficiently homogenous, while the quadrants are further subdivided if they are not.

Pal and Pal [14] stated that image segmentation approaches could be generally classified into two approaches: classical and fuzzy mathematical. Classical approaches include histogram thresholding, edge detection, and semantic and syntactic. Fuzzy mathematical approaches are categorized as edge detection, thresholding, and relaxation. They also mentioned some other approaches [43-46] that are not classified into either of the above-mentioned classes. They classified all image segmentation into six main classes: -

1. Gray level thresholding [47-49].
2. Iterative pixel classification (e.g. relaxation, Markov random field (MRF) based techniques, and neural network based approaches) [50-59].
3. Surface based segmentation [60-62].
4. Segmentation of colour images [63, 64].
5. Edge detection [65-68].
6. Methods based on fuzzy set theory (e.g. fuzzy thresholding and fuzzy edge detection).

Although the final category describes fuzzy segmentation approaches, [14] did not include the segmentation approaches based on fuzzy rule, fuzzy integral, genetic algorithms, and soft computing. Genetic algorithm based image segmentation is described in [69-71]. Zadeh [72] first introduced the term soft computing in the early 1990s and it includes all of the approaches that are a synergistic combination of artificial neural networks, fuzzy logic, genetic algorithms, and probabilistic computing.

Image segmentation is one of the most complicated tasks in image processing and computer vision due to many factors, some of which are summarized as follows [14, 17, 24]:

- Any image processing system possesses some inherent constraints, so the resulting image is not perfect and will contain artifacts.

- Image data can be susceptible and ambiguous. For example, SPECT (Single Photon Emission Computed Tomography) imaging often deforms the high frequency information of the image data and produces fuzzy and non-reliable edges.

- The shape of the same object can differ from image to image. The structures of the objects are not well defined in most natural images and it is very difficult to find the accurate contour of an object.

- The gray level pixel values and their distributions of the same object are not the same for all images. Even in the same image, pixels belonging to same class may differ in their pixel intensities and distributions.

- The objects to be segmented are highly domain and application dependent.

- The properties of an object can differ in their representation, depending upon the type of the image and their domain It also needs a trade off between the desired properties. For example, gray level distribution follows the Poisson distribution for some visual images but this is not valid in the case of both MRI and RI images, so segmentation techniques need semantic and prior information on the type of image, in addition to other properties.

It may be easily deduced from these observations that most images contain some form of ambiguity. For example, it is not possible to define precisely the contour of an object in an image, region, and the relation between the regions, edge, surface, and corner. Pal and Pal [14] confirmed that LI images contain ambiguities because of their multi-valued gray level pixel intensity. This ambiguity may be defined in two ways: grayness and spatial. The former represents the whiteness or blackness of a pixel, while the latter covers the shape and geometry of a region contained in an image. In classical methods, each is taken as a crisp or hard decision. Hard decisions are however not suitable for image processing because of the aforementioned ill-defined data. It is of paramount importance that image processing systems should have a recognition strategy, which can handle all types of uncertainty arising at any level of the processing. Prewitt [73] recognized this when he introduced image segmentation by exploiting fuzzy regions.

In a fuzzy system, each image consists of a number of zy regions, $R_1,...,R_n$ where n is the number of regions [74]. Each region contains a set of pixels, with each pixel assigned a grade (a degree of membership value), which measures the possibility of a pixel belonging to a region. The membership function maps each of the feature values $f(x,y)$ of a pixel $I(x,y)$ of image I having

coordinate (x,y) into the closed range from 0 to 1. The membership function μ for image I can be defined as: -

$$\mu(f(x,y)):\Omega \to [0,1] \qquad\qquad (1.1)$$

where Ω represents a universal set of all feature values for all pixels in image I.

It is evident that the fuzzy approach can handle uncertainty better and use the membership value (varying grade) to define the imprecise or ill-defined property of an image. It was previously mentioned that the membership value denotes the possibility of a pixel belonging to a region (or more than one region), which distinguishes the fuzzy from the classical (hard decision-based) approach. The fuzzy approach can also interpret very well linguistic variables such as VERY BRIGHT, BRIGHT, and BLACK. Medasani, Krishnapuram, and Keller [74] measured geometric (area, perimeter, height, and length) and non-geometric (average pixel intensity, entropy, and homogeneity) properties for both real and artificial images using both fuzzy and crisp approaches. Experimental results proved that the fuzzy approach gave more accurate values for both geometric and non-geometric properties than the crisp approach. They also examined their performance by adding different levels of noise for both approaches. Again the fuzzy approach produced improved estimates compared with the crisp approach for both properties, even in the noisy image. They also proved that there was no need for noise removal during the measuring of fuzzy properties, which is especially useful in overcoming some of the difficulties raised in eliminating noise in textured images.

One of the most intractable tasks in image segmentation is to define the properties for perceptual grouping, which requires human expert knowledge to be incorporated in order to achieve superior segmentation results. Fuzzy rule-based image segmentation techniques are able to incorporate such expert knowledge and this was one of the key factors behind the motivation to investigate fuzzy image segmentation techniques. Before exploring which particular fuzzy based system was applied in this research, a brief overview of fuzzy image segmentation techniques is presented.

1.2 Fuzzy Image Segmentation Techniques

Fuzzy image segmentation has increased in popularity because of the rapid extension and development of fuzzy set theory based on mathematical modelling, synergistic combination of fuzzy, genetic algorithms, and neural networks, and its successful and practical application in image

processing, pattern recognition, and computer vision systems. Fuzzy image segmentation techniques may be broadly classified into the following six categories [75]: -

1. Fuzzy clustering-based image segmentation.
2. Fuzzy geometry-based image segmentation.
3. Fuzzy thresholding-based image segmentation.
4. Fuzzy integral-based image segmentation.
5. Soft computing-based image segmentation.
6. Fuzzy rule-based image segmentation.

A brief review of each of these techniques is now presented.

1.2.1 Fuzzy Clustering

Clustering is known as class discovery [76] or unsupervised grouping of data based on a similarity measure [13, 77]. There are mainly two types of clustering: hard and fuzzy clustering. In the former, a datum is classified into only one group, i.e. the groups are mutually exclusive, while in fuzzy clustering a membership value is assigned to a datum, which supports the group to which it belongs. A datum may belong to more than one class. The basis of fuzzy clustering is on the iterative minimization of an objective function, with the most widely used and popular algorithms being fuzzy c-means algorithm (FCM) [78-80] and possibilistic c-means algorithm (PCM) [81-83]. The main problems associated with fuzzy clustering algorithms are [2]: -

- The initialisation of the membership functions.
- The objective function is unable to achieve a local minimum in the case of FCM or a global in the case of PCM.
- It cannot directly incorporate human expert knowledge.
- Number of clusters must be known a priori.

Despite these apparent drawbacks, fuzzy clustering algorithms such as FCM are frequently used to achieve initial segmentation of an image and it is in this context that FCM will be applied in this thesis.

1.2.2 Fuzzy Geometry

Geometrical properties such as perimeter, area, length, width, extrinsic diameter, intrinsic diameter, index of area coverage (IOAC), and compactness are used to describe any object [84-88]. Such properties can be derived using fuzzy membership values without segmenting the object from

the image and hence they are dependent on the fuzzy membership function (μ). Segmentation is achieved through the utilization of a minimum value of compactness or *IOAC* [88-90].

The optimum value of *IOAC* is calculated by considering the predefined membership function called standard *S* type and in terms of area, length, and breath of an object. It is very difficult to accurately calculate the area, length, and breath of an object with a wide range of gray level pixel intensity variations. The resultant segmentation will not be good if there exists a significant number of overlapping pixels. This technique is also computationally expensive, as it needs to calculate the value of the membership function for each pixel, every time the cross-over point that is the point at which the value of the membership function is 0.5, is adjusted.

1.2.3 Fuzzy Thresholding

Thresholding-based image segmentation is one of the oldest and well-known techniques with its main function being background and foreground separation [77]. It is very difficult to produce appropriate threshold since the real image is itself ambiguous and there is almost always overlap between background and foreground pixels. Fuzzy thresholding based image segmentation has the potential to handle imprecise data, and to date there are generally two ways to calculate the optimal threshold in the fuzzy system: -

1. Techniques based on minimum values of index of fuzziness and entropy [91].
2. Fuzzy image thresholding based on minimization of fuzziness using histogram [77, 92].

In the first technique, the optimal threshold is determined by adjusting the cross-over point so that optimal (minimum) values of index of fuzziness and entropy are achieved. Thresholding is not however a good solution for image segmentation if there is a significant overlap between the background and the object pixels, which is a typical characteristic of many real world images.

1.2.4 Fuzzy Integral

Keller [93] proposed image segmentation based on the fuzzy integral. Fuzzy integral is a fuzzy aggregator operator on multi-attribute fuzzy information and provides a natural coupling of objective evidence and expectation. Besides this, it was used in combining the results from different classifiers i.e. in *classifier fusion* [94]. The segmentation of colour image using fuzzy integral and mountain clustering has also been reported in [95]. The techniques used in colour image segmentation of this method contain the following two steps: -

1. Determination of the number of clusters and the initial values of the cluster centres using mountain clustering and fuzzy integral.

2. FCM classification of colour image pixels by measuring the similarity between a colour image pixel and cluster centres using fuzzy integral.

The potential of this technique depends on the number of grid points and the value of the threshold T used in the mountain clustering algorithm. Very few techniques on image segmentation based on fuzzy integral have been published to date, due to the high mathematical complexity involved.

1.2.5 Soft Computing

Soft computing is an integrated method, which is a synergistic combination of fuzzy logic (FL), neurocomputing (NC), genetic computing (GC), and probabilistic computing (PC) [96]. Each of these techniques has a distinguished capability to solve problems that enables soft computing to manipulate imprecision, uncertainty, and partial truth in a better way compared to traditional approaches and to yield promising results.

Image segmentation based on fuzzy-genetic computing has been presented in [97, 98]. In [97] the objective function of FCM algorithm is optimised using a genetic algorithm. Ishibuchi and Murata [98] classified the high dimensional patterns by genetically selecting the minimum number of fuzzy rules that maximize the classification performance. A method of MRI segmentation based on neuro-fuzzy computing has been described in [99], where the MRI scan of the brain was segmented using a fuzzy algorithm for unsupervised linear vector quantisation neural network. Due to the synergistic combination of techniques, most soft computing based techniques are computationally expensive.

1.2.6 Fuzzy Rule

Fuzzy (IF-THEN) rule-based modelling is a very promising field of research because of its increasingly usage in a wide range of applications including the fields of industrial robotic, control engineering, medical imaging, and complex non-linear system recognition. The advantages of this approach are [72, 100]: -

1. Potential capability to represent the knowledge explicitly using IF-THEN rule and capture the knowledge from imprecise information in linguistic as well as numerical terms.

2. The ability of partial reasoning in human understandable terms. It determines the similarity based on the degree of condition satisfied in the antecedent clause of the rule. This is in contrast with the classical approach.

3. Humans can more easily understand the problems by using the linguistic representation of numeric variables.

4. Approximating capability of complex non-linear systems.

Fuzzy rule-based segmentation techniques are generally used in MRI and are dependent on image type and application domain. The performance of the technique is sensitive to the selection of the structure of the membership functions as well as their associated parameters [101].

In evaluating the above fuzzy image segmentation techniques, they all have advantages and disadvantages. From the viewpoint of object-based image segmentation however, whose applications encompass such diverse and challenging areas as MPEG-4 video object (VO) segmentation for content-based video coding [102] through to object-based description of multimedia content for MPEG-7 [103], the requirement for considering the human expert and/or domain specific knowledge is paramount. Indeed without such knowledge, accurate and effective segmentation would be impossible and thus fuzzy rule-based image segmentation is the only technique so far, which affords the potential for achieving this goal.

1.3 Motivation and Contributions

While fuzzy rule-based image segmentation techniques are able to incorporate human expert knowledge, they are very much application domain and image dependent. The structures of all of the membership functions are manually defined and their parameters are either manually or automatically derived. The performance of fuzzy rule-based techniques depends on selecting the structure and their associated parameters of the membership function. Fuzzy rule-based techniques have been popular engineering tools, but their application has been limited because of their exponential complexity property [104]. This dissertation is motivated by the following three key factors: -

1. Development of a general fuzzy rule-based image segmentation (object-based) framework considering the most important general attributes for perceptual grouping so that they can be applied in a wide range of image types and applications.

2. Incorporation of human expert and/or domain specific knowledge into the framework for a particular application.

3. Heuristic definition of a small number of rules in order to reduce the complexity of the
    algorithms.

It was to directly address these three key objectives that the integrated fuzzy rule-based
segmentation framework shown in the block diagram Fig. 1.1. was formulated and developed. The
original and segmented images are included as a representative example. The framework
specifically incorporates four innovative fuzzy rule-based image segmentation algorithms, which
are identified as **Blocks 1, 2, 3,** and **4** in Fig. 1.1. An important feature of this framework is its
flexibility as while the research has focused on perceptual grouping and other related key features,
new rules relevant to special domain and/or applications can be integrated easily into the
framework.
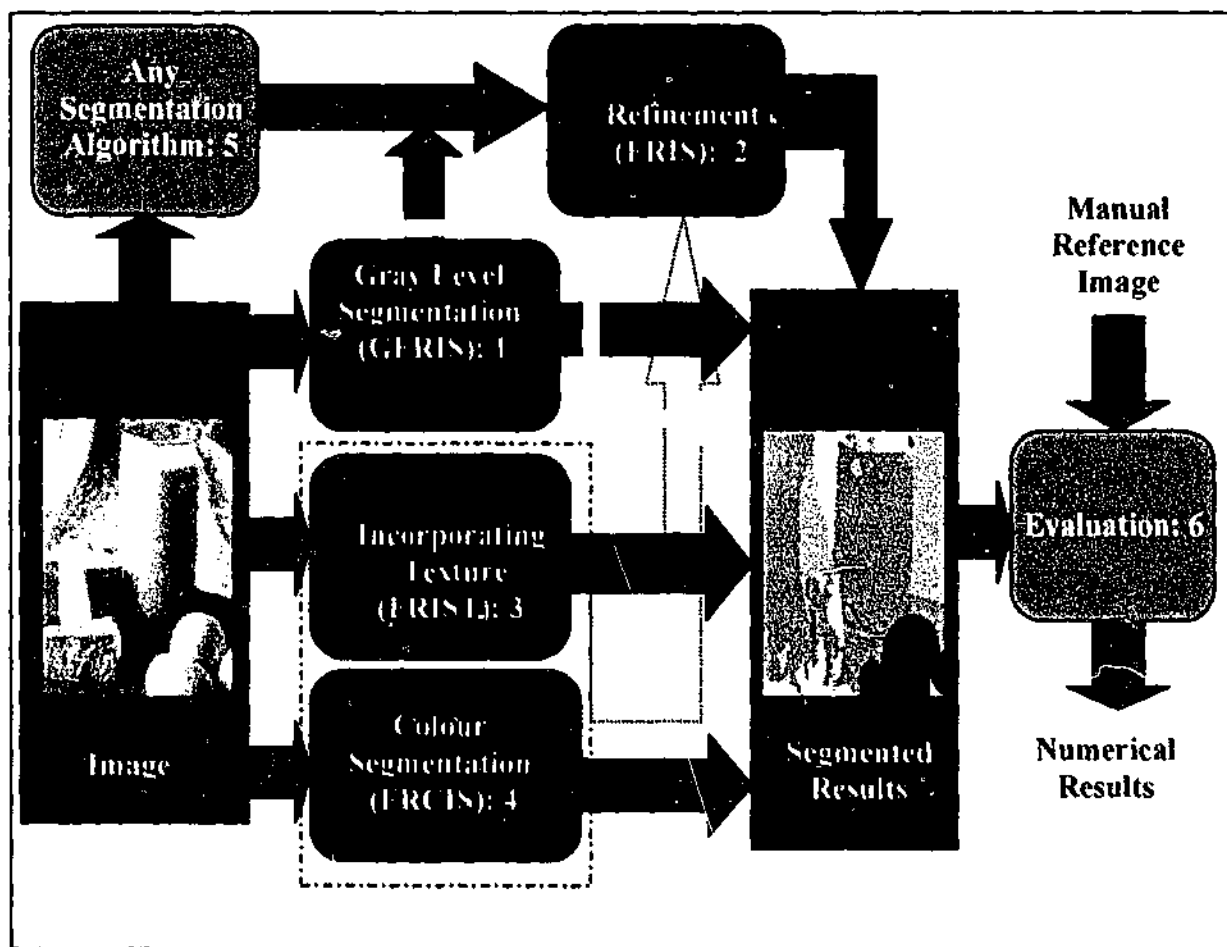
Fig. 1.1: Block diagram of the integrated fuzzy rule-based image segmentation framework.

The theory and performance of these constituent blocks will be fully analysed in subsequent chapters. The key contributions to the research can be identified as follows: -

- Development of a *generic fuzzy rule-based image segmentation (GFRIS)* algorithm, which considers region pixel distributions, similarity based on gray level pixel intensity, and the proximity and good continuation principles (**Block 1** in Fig. 1.1). This algorithm is both application and image-type independent and exploits inter-pixel spatial relationships [3, 4, 6].

- Development of an algorithm for the automatic data mining of the key weighting factor and threshold for the GFRIS algorithm (**Block 1** in Fig. 1.1).

- While GFRIS has provided significant improvements in the overall segmentation performance compared with FCM and PCM, it has proved to be ineffective for image regions that are characterised by either being non-homogeneous or possessing sharp variations in pixel intensity. To address this, a new *segmentation refinement* algorithm called *fuzzy rules for image segmentation (FRIS)* is presented for integration into the generic fuzzy rule-based framework. This utilises a combination of an object's connectedness, surroundedness, uniformity, and contrast properties (**Block 2** in Fig. 1.1) [5, 7, 9].

- The performance of the FRIS algorithm depends entirely on the results of the initial segmentation algorithms. This is because FRIS is a refinement algorithm, so in order to improve the performance of the GFRIS algorithm for non-homogeneous and textural regions, a new algorithm, namely *fuzzy rule for image segmentation incorporating texture features (FRIST)* is proposed. This integrates two new membership functions based upon the texture features of fractal dimension and contrast considering image domain specific information into the GFRIS algorithm. (**Block 3** in Fig. 1.1) [8].

- While the main focus of the research has been on gray level images, the framework is also able to process colour information. A *fuzzy rule-based colour image segmentation (FRCIS)* algorithm is developed by extending the GFRIS algorithm (**Block 4** in Fig. 1.1) and implemented using one of the popular perceptual colour models, namely HSV (hue, saturation, and value) and the basic colour model, namely RGB (red, green, and blue). An algorithm for calculating the average of hue angles of the HSV colour model is also presented.

- Detailed *computational complexity analysis* of all algorithms in the framework has been undertaken and is included in each representative chapter.

- The segmentation performance of all the key constituent blocks is analysed and numerically evaluated using the two powerful objective and quantitative segmentation evaluation techniques, namely *discrepancy based on the number of miss-segmented pixels* and *discrepancy based on the number of objects in the image.* A statistical significance test, namely *the sign test* is applied to test the statistical significance improvements of all proposed algorithms. A comparison is made with GFRIS, FCM and PCM algorithms using many different image types (**Block 6** in Fig. 1.1).

Finally, **Block 5** in Fig. 1.1 represents the initial segmentation algorithms that are needed for the FRIS algorithm. In principal, this includes any segmentation algorithm such as FCM, PCM, and GFRIS, which does not consider the perceptual properties of connectedness and surroundedness. Given the large reservoir of literature covering basic segmentation techniques (see the comprehensive literature review in Chapter 2), this block will not be considered further in the thesis.

1.4 Structure of the Thesis

The thesis is organised as follows: -

Chapter 2 includes a contemporary review of fuzzy clustering, fuzzy based and colour image segmentation techniques and explores some of the existing texture estimation techniques and colour models. The advantages and disadvantages of each technique are described in this chapter. Sections from this chapter have previously been published by Karmakar *et al.* in [1] and as a book chapter in [2].

Chapter 3 proposes the new *generic fuzzy rule-based image segmentation (GFRIS)* algorithm, which considers region pixel distribution, closeness to a region and spatial relations. The algorithm for automatically data-mining both the key fuzzy rule weighting factor and the threshold is also discussed in this chapter. This work has already been published by Karmakar *et al.* in [3, 4, 6].

Chapter 4 introduces the *fuzzy rule-based refinement* (FRIS) algorithm, which unifies the properties of connectedness, surroundedness, uniformity, and contrast and has previously been published by Karmakar *et al.* in [5, 7, 9].

Chapter 5 presents a new algorithm, *fuzzy rules for image segmentation incorporating texture features* (FRIST) by integrating two new membership functions into the set of GFRIS membership

functions, based upon fractal dimension and contrast, and image domain specific information, which has been published by Karmakar *et al.* in [8].

Chapter 6 details the *fuzzy rule-based colour image segmentation (FRCIS)* algorithm by extending the GFRIS algorithm from gray level to colour images. This algorithm is applied to both the HSV and RGB colour models. This chapter also defines a novel algorithm for calculating the average of hue components of the HSV colour model.

Chapter 7 provides a comprehensive qualitative and quantitative analysis of the performance of all the proposed algorithms in the framework. These are compared with the FCM and PCM algorithms and analysed using many different types of image. This chapter also examines the implementation details of all algorithms, the methods of numerical evaluation, and a statistical significant test for the overall segmentation performances.

Finally, Chapter 8 details the conclusions derived from this research as well as defining future potential directions for this work.

A Review of Relevant Fuzzy Clustering, Rule-Based, and Colour Image Segmentation Techniques

Sections 1.2.1 and 1.2.6 have respectively identified the potential of both fuzzy clustering and fuzzy rule-based image segmentation algorithms to be used for image segmentation. This chapter provides a comprehensive overview of the various methods used in fuzzy clustering and rule-based image segmentation techniques [2] as well as brief descriptions of a number of texture representation techniques, popular colour models, and fuzzy colour image segmentation techniques. Fuzzy clustering algorithms are used in pixel-based classifications for image segmentation, while fuzzy rule-based modelling is a very challenging field of research. It is widely used in the field of industrial applications including robotics, control engineering, medical imaging, and complex non-linear system recognition. Fuzzy rule-based segmentation techniques are able to incorporate domain expert knowledge and manipulate numerical as well as linguistic data. They are also capable of drawing partial inference using fuzzy IF-THEN rules [72, 100]. For these reasons they have been extensively applied in medical imaging. Fuzzy rule-based image segmentation techniques tend in general, to be application dependent with the structure of the membership functions being predefined and in certain cases, the corresponding parameters being manually determined. The overall performance of these segmentation techniques is very sensitive to parameter value selections. Chapter 3 will address these issues by introducing a generic fuzzy rule-based image segmentation (GFRIS) algorithm, which is both application independent and exploits inter-pixel spatial relationships.

This chapter is organized as follows: In Section 2.1, fuzzy clustering algorithms are described, with fuzzy rule-based image segmentation techniques being presented in Section 2.2. A brief description of texture feature approximation techniques are given in Section 2.3. Section 2.4 looks at colour models in the context of image segmentation, while Section 2.5 provides a brief outline of various popular fuzzy colour image segmentation techniques.

14

2.1 Fuzzy Clustering Based Image Segmentation

Clustering means unsupervised grouping of data based on a similarity measure [77]. An example of four clusters having different colours is given in Fig. 2.1.
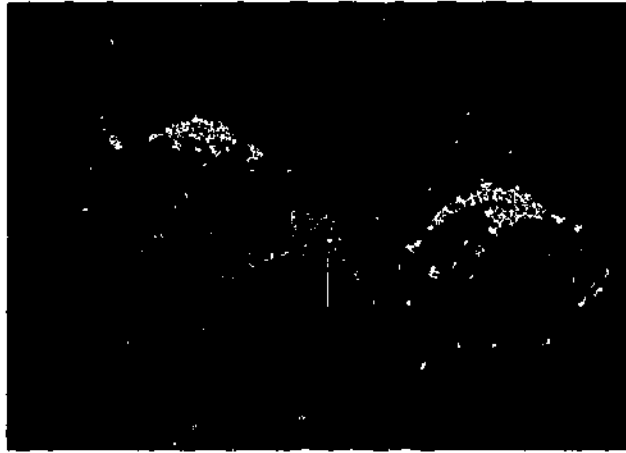
Fig. 2.1: An example of clusters.

There are mainly two types of clustering: hard clustering and fuzzy clustering. In the former, a datum is clearly classified into only one group i.e. the groups are mutually exclusive, while in fuzzy clustering a membership value is assigned to a datum, which supports the group to which it belongs. A datum may also belong to more than one class. The two most popular and extensively used fuzzy clustering algorithms are [2]: -

    1.   Fuzzy c-means algorithm (FCM).

    2.   Possibilistic c-means algorithm (PCM).

These will now be discussed in greater detail.

2.1.1 Fuzzy C-Means Algorithm (FCM)

FCM is the oldest and most popular fuzzy based clustering technique. It was developed by Bezdek [79] and is still being applied in image segmentation. It performs classification based on the iterative minimization of the following objective function and constraints [77-81, 105, 106]: -

$$f_m(\mu, V, X) = \sum_{i=1}^{c} \sum_{j=1}^{n} (\mu_{ij})^m d(x_j, v_i)^2 \qquad (2.1)$$

$$0 \le \mu_{ij} \le 1; \qquad i \in \{1, \ldots, c\} \text{ and } j \in \{1, \ldots, n\} \qquad (2.2)$$

$$\sum_{i=1}^{c} \mu_{ij} = 1; \qquad j \in \{1,...,n\} \tag{2.3}$$

$$0 < \sum_{j=1}^{n} \mu_{ij} < n; \quad i \in \{1,...,c\} \tag{2.4}$$

where c and n are respectively the number of clusters and data, μ is a fuzzy partition matrix containing membership values $[\mu_{ij}]$, V is a prototype vector containing the values of cluster centres $[v_i]$, m is the fuzzifier $1 < m \leq \infty$, X is a data vector $[x_j]$, and $d(x_j, v_i)$ is the distance between x_j and v_i. The following two equations are derived by minimizing the function $f_m(\mu, V, X)$ in (2.1) with respect to μ and V.

$$\mu_{ij} = \frac{1}{\sum_{k=1}^{c} \left(\frac{d(x_j, v_i)}{d(x_j, v_k)} \right)^{2/(m-1)}} \tag{2.5}$$

$$v_i = \frac{\sum_{j=1}^{n} (\mu_{ij})^m x_j}{\sum_{j=1}^{n} (\mu_{ij})^m} \tag{2.6}$$

The set of cluster centres is initialised either randomly or by using an approximation method and the membership values and cluster centres are updated through an iterative process until the maximum change in μ_{ij} becomes less than or equal to a specified threshold.

The number of clusters, the fuzzifier (m), and the threshold need to set empirically in FCM. Equations (2.5) and (2.6) are insufficient to achieve the local minimum of $f_m(\mu, V, X)$ [107]. The selection of the value of m is especially important, as if it is equal to 1 then FCM produces a crisp instead of a fuzzy partition. If any of the distance values $d(x_j, v_i) = 0$, then (2.5) will be undefined. FCM strongly supports probability as it has set the constraint in (2.3), which prevents the trivial solution $\mu = 0$.

2.1.2 Possibilistic C-Means Algorithm (PCM)

FCM arbitrarily divides the data set based on a selected number of clusters. The membership values generated by FCM represent the degrees of sharing. In order to eliminate the constraints in (2.3), Krishnapuram and Keller introduced PCM whose membership values represent the degrees of *typicality*, instead of degrees of sharing and all clusters are independent to each other [82, 83]. They modified the FCM objective function and defined the PCM objective function as,

$$f_m(\mu,V,X) = \sum_{i=1}^{c}\sum_{j=1}^{n}\left(\mu_{ij}\right)^m d^2\left(x_j,v_i\right) + \sum_{i=1}^{c}\eta_i\sum_{j=1}^{n}\left(1-\mu_{ij}\right)^m \tag{2.7}$$

with the corresponding constraints given by: -

$$0 \le \mu_{ij} \le 1; \qquad i \in \{1,...,c\} \text{ and } j \in \{1,...,n\} \tag{2.8}$$

$$0 < \sum_{j=1}^{n}\mu_{ij} < n; \qquad i \in \{1,...,c\} \tag{2.9}$$

$$\max \mu_{ij} > 0; \qquad j \in \{1,...,n\} \tag{2.10}$$

where η_i is the scale parameter, which determines the zone of influence of a point and the suggested value for η_i is the variance of cluster i and other parameters are as defined in Section 2.1.1. The membership values μ_{ij} and prototype centres v_i are obtained by minimizing the objective function $f_m(\mu,V,X)$ in (2.7) and then iteratively updating using the following two equations.

$$\mu_{ij} = \frac{1}{1+\left(\dfrac{d^2\left(x_j,v_i\right)}{\eta_i}\right)^{1/(m-1)}} \tag{2.11}$$

$$v_i = \frac{\sum_{j=1}^{n}(\mu_{ij})^m x_j}{\sum_{j=1}^{n}(\mu_{ij})^m} \qquad\qquad (2.12)$$

When fuzzifier $m = 1$, PCM produces a crisp partition. PCM gives promising results in the presence of noise but it is highly dependent on initialisation and estimation of the scale parameters. The output of FCM can be used for initialisation and scale estimation however FCM is very sensitive to noise. Barni also noted that PCM achieves local minimum but is unable to minimize $f_m(\mu,V,X)$ globally [108]. The overall time complexity of the PCM algorithm is $O(ncp)$ where p is the dimension of the feature.

2.2 Fuzzy Rule-Based Image Segmentation

As discussed in Section 1.2.6, this approach offers considerable potential for exploitation in image segmentation. Initially fuzzy IF-THEN rules were extensively used in control engineering problems but now their application in image segmentation is increasing. Their advantages may be summarised as follows [109, 110]: -

- Human can easily understand the problems due to the linguistic representation of numeric variables.
- Computationally less expensive than fuzzy clustering methods.
- Has the potential ability to integrate domain expert knowledge.

The general format of fuzzy IF-THEN rule can be defined as follows: -

IF <antecedent -condition> THEN <consequence>

There are two parts to this fuzzy rule: the antecedent-condition and the consequence. The rule evaluates the former and determines its amount of truthfulness. The consequence is measured based on the quantity satisfied in the antecedent condition. The general model of the fuzzy rule-based system is given in Fig. 2.2 [75, 111].

Fuzzy rule-based image segmentation mainly consists of three parts: image fuzzification, fuzzy rules, and defuzzification (if necessary). The first step is to fuzzify the pixels of the image and determine the degrees for the regions to which they belong using the appropriate membership functions. The model can, if required, take into account human expert knowledge. Once the pixels are fuzzified, the rules are applied to determine the outcome (consequence) of each rule. In this

step, if essential, human expert knowledge is used to define the fuzzy rules and/or for some models feedback is taken from human experts in order to reduce the conflicts arising among the rules. The results of the fuzzy rules can be applied to the output membership functions if needed. Finally, if there is more than one non-mutually exclusive rule, the results are combined and defuzzified in order to calculate a single output value.
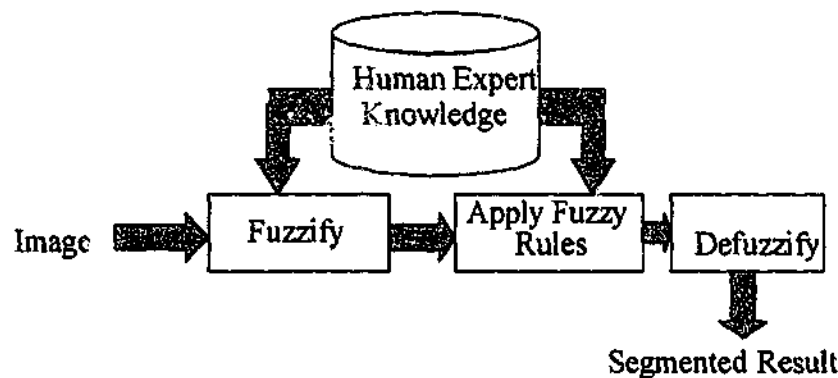
Fig. 2.2: General model of fuzzy rule-based image segmentation system.

Due to its limited application and dependency on image types, fuzzy rule-based image segmentation has generally only been applied to three image types: light intensity (LI), magnetic resonance (MR), and computed tomography (CT) images [1]. The various fuzzy rule-based image segmentation techniques relevant to these 3 image types are described in the following sections. Each technique is discussed in detail to highlight the problems and drawbacks of contemporary fuzzy rule-based techniques, and to place in context the originality of the research findings presented in this thesis.

2.2.1 Fuzzy Rule-Based LI Image Segmentation

Chi and Yan utilized the fuzzy IF-THEN rules in the segmentation (separation of background and foreground pixels) of 8-bit (256 gray levels) geographic map images. These composed text, streets, roads, and boundaries, which were considered foreground pixels [77, 112]. The main processing steps of this approach are described as follows: -

Features Used in Segmentation

Three features, difference between pixel intensity (DI), local standard deviation (SD) and local contrast of darker pixel (CD) were used in the segmentation and defined as: -

$$DI(x, y) = PI(x, y) - LA(x, y) \qquad (2.13)$$

$$SD(x,y) = \sqrt{\frac{\sum_{i=x-3}^{x+3}\sum_{j=y-3}^{y+3}(PI(i,j) - LA(i,j))^2}{49}} \qquad (2.14)$$

$$CD(x,y) = \frac{\max(0, BR(x,y) - PI(x,y))\,\text{sgn}(CI(x,y))}{LA(x,y)} \qquad (2.15)$$

where $PI(x,y)$ is pixel intensity in the location (x,y), $LA(x,y)$ is local average pixel intensity in a 7x7 window, $\text{sgn}(CI(x,y))$ is the sign operator, which is -1 when $CI(x,y) \le 0$ for a brighter pixel $PI(x,y)$; otherwise it is 1, $CI(x,y)$ is the difference of pixel intensity at location (x,y), and the average of its neighbours and can be defined as: -

$$CI(x,y) = \frac{1}{8}\left[\sum_{\substack{i=-3\\|i|\ge 2}}^{3} PI(x+i,y) + \sum_{\substack{j=-3\\|j|\ge 2}}^{3} PI(x,y+j)\right] - PI(x,y) \qquad (2.16)$$

$BR(x,y)$ is the average of relative brighter pixels and is defined as:-

$$BR(x,y) = \frac{1}{N}\sum_{\substack{x-4\le i\le x+4\\ y-4\le j\le y+4\\ CI(i,j)\le 0}} PI(i,j) \qquad (2.17)$$

where N indicates the number of brighter pixels $(CI(x,y) \le 0)$ contained in a 9x9 window.

Membership Functions

The input domain is divided into five fuzzy regions named as L2, L1, M, H1 and H2 while the output domain is split into two fuzzy regions, background and foreground. Triangular membership functions are utilized for the input regions. The input and output membership functions are shown in Fig. 2.3 (a) and 2.3(b) respectively.

Development of Fuzzy Rules

Fuzzy rules are developed by learning from examples [113], with the input and output domains divided into the fuzzy regions shown in Fig. 2.3. The membership values of all regions for each input are calculated and each input is assigned to the region having the maximum

membership values. So a pair of rules is generated for each training sample. An example of such a rule could be

IF DI is L1 AND SD is H1 AND CD is H2 THEN it is a foreground pixel

IF DI is H1 AND SD is M AND CD is L1 THEN it is a background pixel
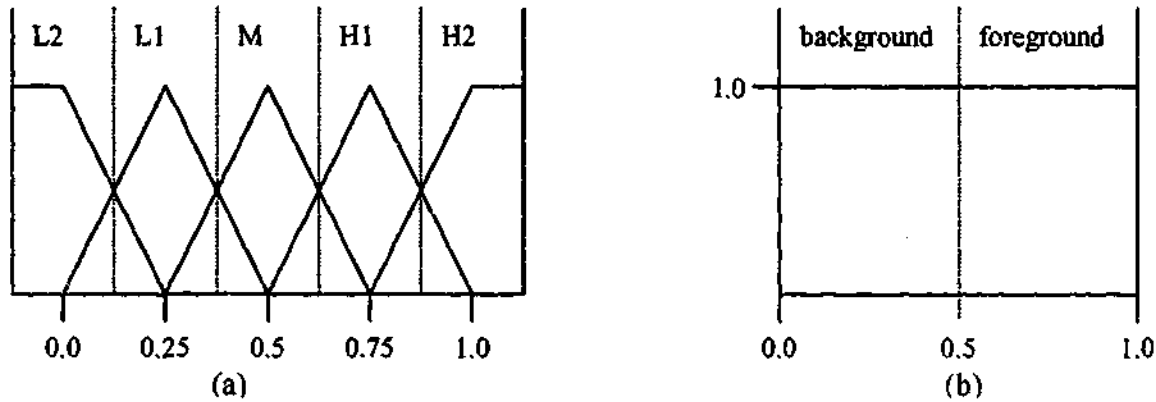
Fig. 2.3: Input and output membership functions, (a) Input membership functions, (b) Output membership functions.

DI=L2	L2	L1	M	H1	H2
L2					
L1					
M					
H1		F	F	F	
H2			F	F	F
			F	F	F

CD (right) — SD (bottom)

DI=L1	L2	L1	M	H1	H2
L2				F	F
L1					
M			F	F	F
H1		F	F	F	F
H2			F	F	F

CD (right) — SD (bottom)

DI=M	L2	L1	M	H1	H2
L2	F	F	F	F	B
L1	B	B	B	F	B
M	F	F	F	F	F
H1	F	F	F	F	F
H2		F	F	F	F

CD (right) — SD (bottom)

DI=H1	L2	L1	M	H1	H2
L2		F	F	B	B
L1	B	B	B	B	B
M		F	B	B	B
H1			B	B	B
H2			B		B

CD (right) — SD (bottom)

DI=H2	L2	L1	M	H1	H2
L2					B
L1		B	B	B	B
M					
H1					
H2					

CD (right) — SD (bottom)

Fig. 2.4: Fuzzy rule bank for geographic map image segmentation.

The learning set produced by this method may contain a larger number of rules including repeated and conflicting rules. To avoid these, the rules are selected that are supported by a large number of examples. Each rule is kept in a fuzzy rule bank, which is shown in Fig. 2.4.

Defuzzification

The centroid defuzzication method used to calculate the output for each input pixel is defined as: -

$$C_P = \frac{\sum_{i=1}^{n} M_p^i C_i}{\sum_{i=1}^{n} M_p^i} \tag{2.18}$$

where C_i is the class produced by the ith rule, n is the number of rules and M_p^i is the matching degree of the antecedent of ith rule for the pth pattern. If $C_p \leq 0.5$, the input pixel is categorised as a background pixel otherwise it is categorised as a foreground pixel, which works well for two class problems, but a large number of fuzzy rules are needed for multiple classes [114].

Concluding Comments

This approach is faster than neural network techniques but it has been found that some parts of the text characters of the maps are missed for standard triangular function [77], because the shape and parameters of the membership functions were intuitively selected. For this they used an automatic method based upon FCM to determine the parameters of the membership functions. The drawback however was the fundamental problem of manual determining the shape of the membership function. Heuristic rules were also not used in this technique.

2.2.2 Fuzzy Rule-Based MRI Segmentation

Magnetic resonance images (MRI) are one of the most important and complicated images used in medical imaging. They are extensively used in various types of disease diagnostic tasks. Medical experts generally draw the conclusion in regard to the disease by manually scanning such images [109], which is both a tedious and time-consuming task. Analysis, especially segmentation of MR images using automated computer techniques saves time and helps the

doctor to detect irregularity in diagnosis. Fuzzy rule-based MRI image segmentation techniques may be broadly classified into two classes:

1. Hybrid fuzzy rule-based MRI segmentation.
2. Conventional fuzzy rule-based MRI segmentation.

Both methods are discussed fully in the following sections.

2.2.2.1 Hybrid Fuzzy Rule-Based MRI Segmentation

A hybrid fuzzy rule-based segmentation system combines fuzzy rules with a fuzzy c-means clustering algorithm. Clustering is computational expensive, does not incorporate human expert knowledge, and thus does not produce appropriate class [115]. For these reasons, a set of fuzzy rules is applied to classify the pixels/voxels, where a voxel represents a pixel in three-dimensional space. It is very difficult to define fuzzy rules that cover all pixels/voxels, so the FCM algorithm is used to classify the remaining pixels/voxels and those classified by the fuzzy rules are used to initialise the centre of the clusters. Hybrid fuzzy rule-based segmentation systems are faster than clustering.

Two examples of a hybrid fuzzy rule-based system are: - (i) adapting fuzzy rules for the brain issue segmentation [115] and (ii) a rule-based segmentation system with automatic generation of membership functions for pathological brain MR tissues [109]. A description of these two systems is now given.

Adapting Fuzzy Rules for the Brain Tissue Segmentation

The technique [115] utilising adapting fuzzy rules for segmenting the brain tissue into six classes: white matter (WM), gray matter (GM), cerebro-spinal fluid (CSF), pathology, skull tissues, and background is described in the following.

Database and Features

105 axial brain slices, 5 mm thick from 15 people (39 normal slices from 8 people and 66 abnormal slices from 7 patients) are used for experimental purposes. Relative pixel intensities of T1, T2, and Proton Density (PD) weighted images are used as features.

Membership Functions

The triangular and trapezoidal membership functions used in the experiment are shown in Fig. 2.5. The parameters of the membership functions (a1, a2, b1, b2, b3, b4, b5, and b6) are calculated by determining the turning points of intensity histograms based on a training set

consisting of 6 normal and 4 abnormal slices and incorporating suggestions from expert radiologists. The turning points are regarded as peaks, valleys or the starting point of the histogram, and indicate the estimated boundary of the tissue types.   The turning points of the histograms are shown in Fig. 2.6.

(a)

(b)   (c)
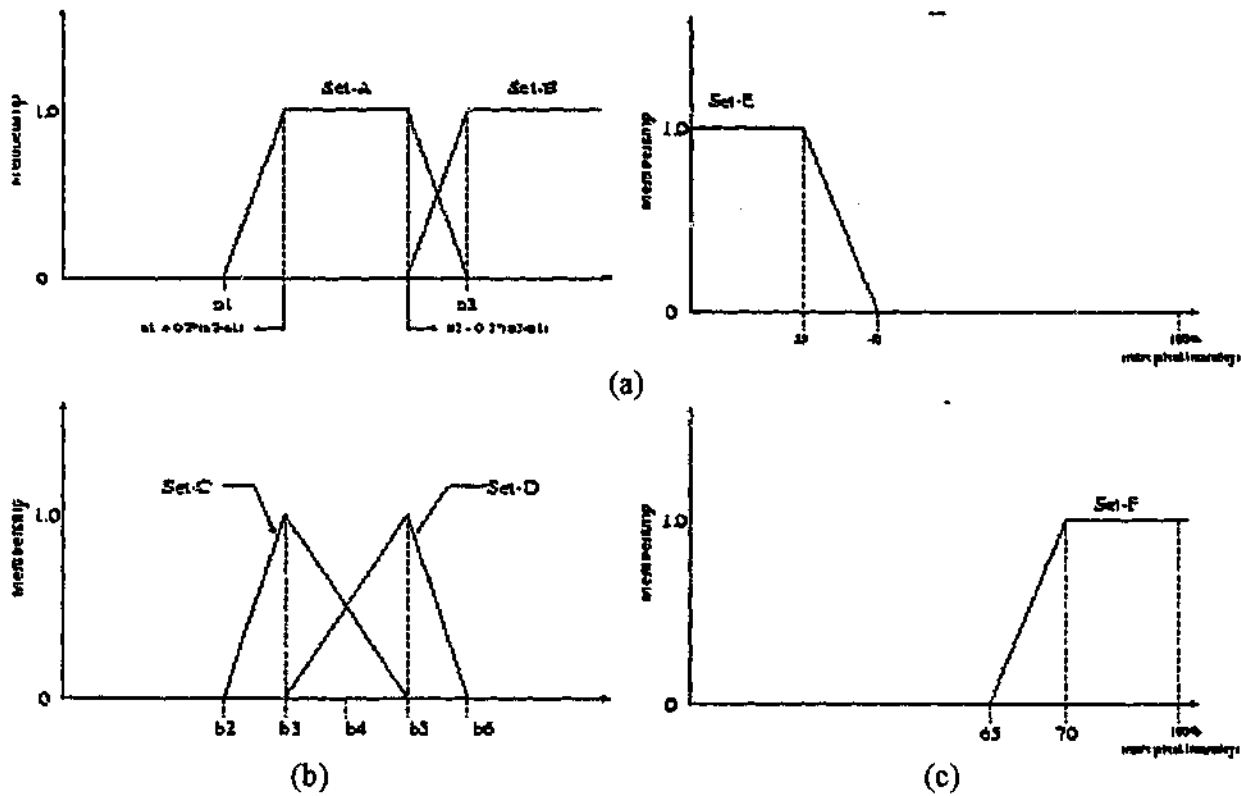
Fig. 2.5: Definition of membership functions [115], (a) Membership functions for T1 weighted image, (b) Membership function for T1 weighted image, (c) Membership function for T2 weighted image.

Patients having brain tumours usually receive radiation and chemotherapy treatment. For this the PD histogram of the patient with a brain tumour becomes like the PD histogram for abnormal slice shown in Fig. 2.6 due to the change of properties of gray and white matter. The turning points of this histogram are obscure and difficult to select. An edge detection technique [116] is used in order to sharpen the boundary between gray and white matter and utilizes a suitable threshold to detect the peaks. The initial value of threshold is chosen as 5 and increased by 5 until two peaks have been found. If peaks are not found, two peaks are assumed at 1/3 and 2/3 of the region between b1 and b2.

Fuzzy Rule Generation

The turning points of three histograms (T1, T2, and PD histograms) are used to separate the tissue into white matter, gray matter, cerebro-spinal fluid (CSF), pathology, background (air), and other skull tissues. The heuristics used here to generate the rules are that all voxels between b2 and b4 are usually white matter, below b1 are air in PD histogram, and between a1 and a2 are a mixture of white and gray matter in the T1 weighted histogram. A set of rules used to classify the brain tissue is described as follows: -

IF voxel in T1 in set-E AND voxel in T2 in set-F THEN voxel is CSF

IF voxel in PD is set-C AND voxel in T1 in set-A THEN voxel is white matter

IF voxel in PD is set-D AND voxel in T1 in set-A AND NOT (voxel in T2 is set-F AND voxel in T1 is Set-E) THEN voxel is gray matter

IF voxel in T1 is set-B AND voxel in T2 is set-F THEN voxel is pathology

IF voxel in T1 is set-B AND NOT (voxel in T2 is set-F) THEN voxel is other

IF PD voxel intensity < b1 AND T2 voxel intensity < c1 THEN voxel is background

Rules adapt themselves to each slice during processing as they are generated from the turning points of the histograms.

Abnormal PD image Slice   PD Intensity

Fig. 2.6: Histograms with turning points [116].

Classification Techniques

Voxels are classified into six classes by applying the above rules. The unclassified and isolated voxels (voxels whose membership values are 1 but have no neighbourhoods) for each class are assigned the membership values with the average membership values of their neighbourhoods and zero respectively. Finally the voxel membership values are normalized (0 to 1) using the following equation.

$$\mu_i = \frac{\mu_i(v)}{\sum_j \mu_j(v)} \tag{2.19}$$

where i and j represent each of the six classes. The incorrectly classified voxels (voxels whose membership values is ≤ 0.80) are classified using the semi-supervised clustering algorithm [117]. The correctly classified voxels are used as training set and weighted by 100.

Concluding Comments

This system is faster than FCM, but while the parameters of the membership functions are adjusted automatically during the processing of each slice, it does not produce superior results compared with FCM. Rules are generated based on turning points of the histogram but the turning points are not sufficient to distinguish the voxels if there is a significant number of overlapping voxels. The spatial information is not well considered as it is taken into account for only unclassified voxels. The threshold and approximate peaks (when there is no peak in the PD histogram) are chosen empirically and extra cranial tissues are not removed before classification.

The second of the hybrid fuzzy rule-based systems is discussed in the next section.

A Rule-Based Fuzzy Segmentation System with Automatic Generation of Memberships for Pathological Brain MR Images

This hybrid fuzzy rule-based brain MR image segmentation system automatically generates the memberships for pathological brain MRI images   [109] in order to separate white matter (WM), gray matter (GM), cerebro-spinal fluid (CSF), and cytomegalovirus (CMV) lesion from the brain. It works as follows: -

Database

A set of T1, T2 and PD weighted images containing 12 normal images and 3 abnormal images with lesions are used for experimental purposes. GE Signa 1.5T MRI and a Technicare 0.6T instruments are used to access these images.

Preprocessing Stage

This comprises image registration and the selection of a region of interest (ROI). The former ensures the same coordinates for the same pixels in two different images using the method of shifting of coordinates. For example, if the two images T2 and PD weighted are not matched, the coordinates of the PD image are shifted to match with T2 weighted image. The shifted coordinates of the PD image are recorded and the shifted PD image is regarded as a registered image.

The intracranial region of the brain is selected as the ROI, which has to be separated from the skull and scalp. It is anatomically separated from the scalp and skull by a layer of CSF, except for the fact that there are a few connections, where the layer of CSF is thin. To separate the intracranial region, the image is first threshold and then a region growing technique is applied to grow the empty space surrounding the intracranial region. The problem of the connections between brain and scalp is solved by applying the two morphological operators, erosion and dilation [118].

Determination of Parameters of the Membership Functions

The membership functions are perceptually identified. Three different types of tissue, namely WM, GM and CSF were identified for T2 weighted images. The T2 weighted images as well as its edges that are determined by Cohen's edge detection method described in [84] are classified into five classes WM, GM, CSF, WM-GM, and GM-CSF using the standard FCM algorithm. The mean intensity (μ_i) and variance (σ_i) of ith class are used to calculate the parameters of the membership function for i^{th} class. The membership functions for the T2 weighted images are shown in Fig. 2.7.

The PD weighted image and its edge values are used by FCM to classify them into four classes. The class containing the highest pixel intensity is discarded in order to eliminate the high edge values at the boundary of the brain. The techniques used to generate the membership function for PD weighted images are the same as for T2 weighted images. The membership function for PD weighted images is shown in Fig. 2.8.
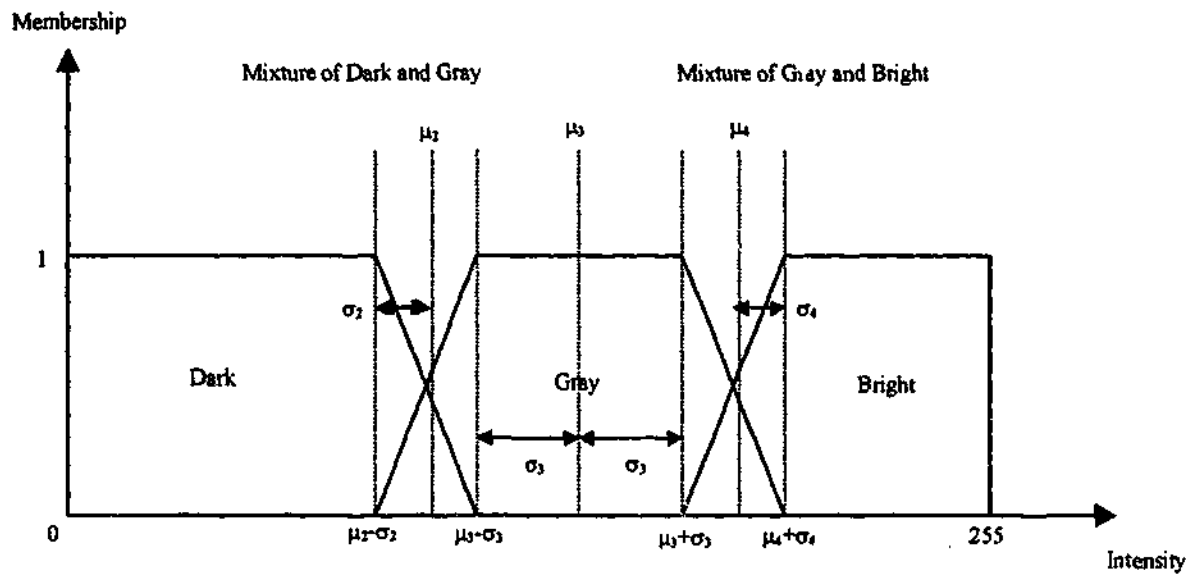
Fig. 2.7: Membership function for T2 weighted images.
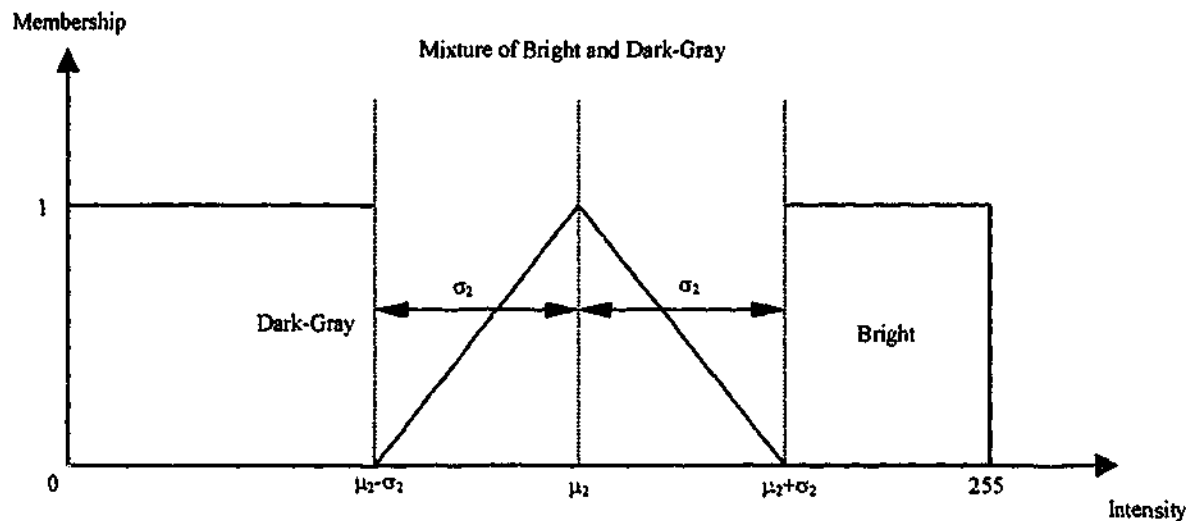
Fig. 2.8: Membership function for PD weighted images.

PD weighted abnormal images contain periventricular hyperintensity, which have higher pixel intensities in brighter class than other pixels in the same class. So the membership function for PD weighted abnormal image is presented in Fig. 2.9.

A membership function to represent the closeness of a pixel from the centre of the brain as the ventricle is considered a major connected CSF area adjacent to the centre of the brain. This membership function is used to discover the periventricular hyperintensity, which represents the lesions of the PD weighted images. The membership function to measure the closeness to the ventricle is given in Fig. 2.10.
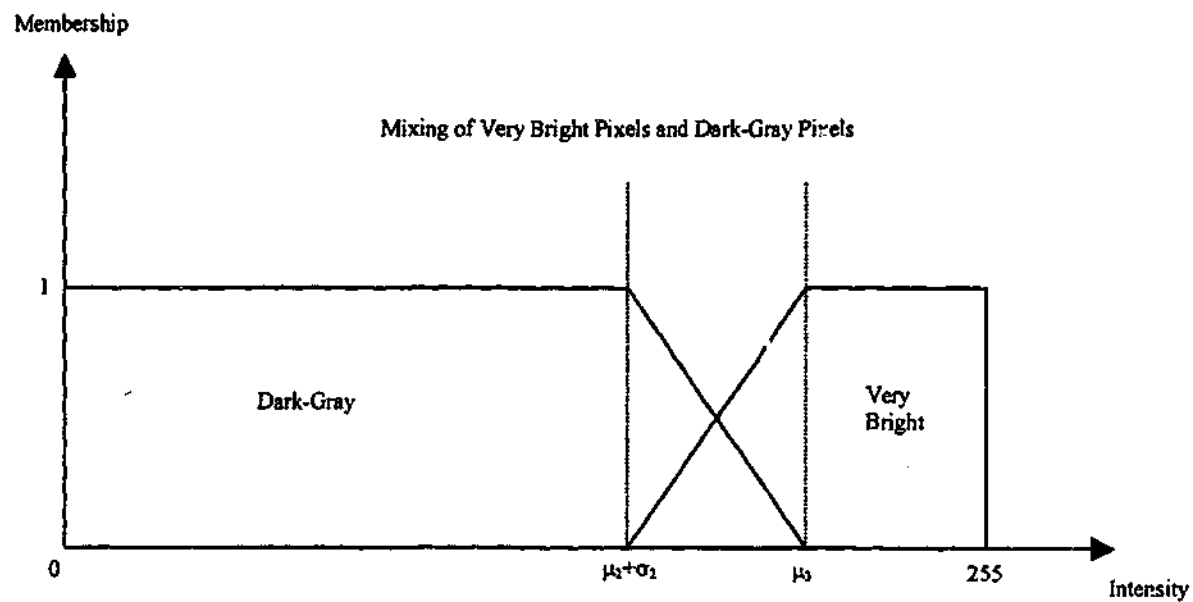
Fig. 2.9: Membership function for PD weighted abnormal images.
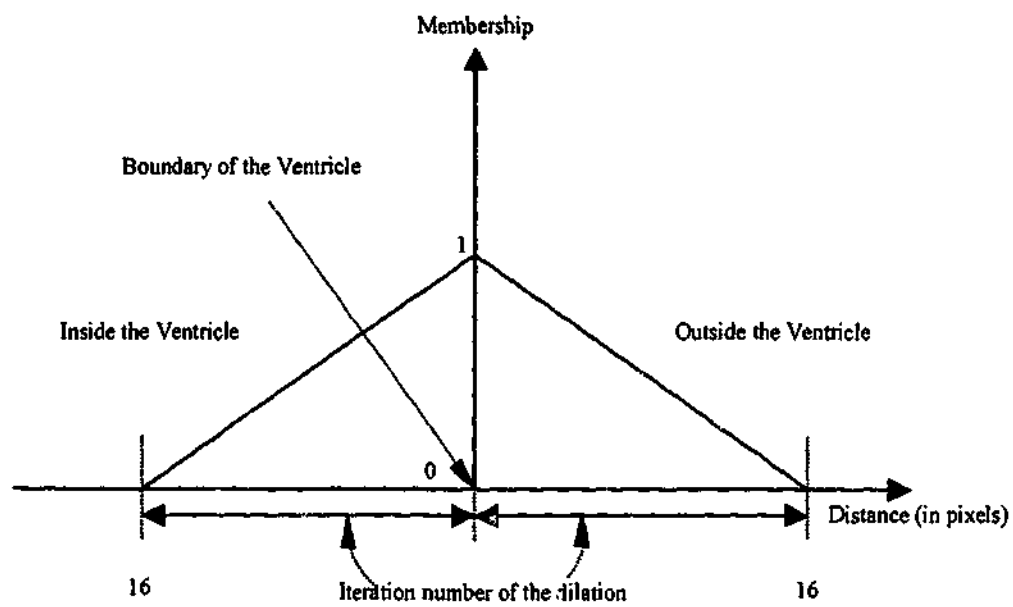
Fig. 2.10: Membership function to represent the closeness to ventricle.

Development of Fuzzy Rule-Based Segmentation

Two groups of fuzzy rules have been developed. The first group is used to segment the T2 weighted images and to recognize CMV lesions.

First Group:

IF pixel in T2 is Dark THEN pixel is White Matter

IF pixel in T2 is Grey THEN pixel is Grey Matter

IF pixel in T2 is Bright THEN pixel is CSF

The second group is formulated by splitting the last rule of the first group into three new rules that discriminate between CSF and CMV lesions.

Second Group:

IF pixel in T2 is Dark THEN pixel is White Matter

IF pixel in T2 is Grey THEN pixel is Grey Matter

IF pixel in T2 is Bright AND pixel in PD is Dark-Grey THEN pixel is CSF

IF pixel in T2 is Bright AND pixel in PD is Very Bright AND pixel is not close to the ventricle THEN pixel is CSF

IF pixel in T2 is Bright AND pixel in PD is Very Bright AND pixel is close to the ventricle THEN pixel is CMV lesion

The AND operator is evaluated by applying the fuzzy logic minimum operator [119]. All pixels are classified using the above rules, with those whose membership values<0.5 and the pixel having two maximum membership values being declared as unclassified pixels.

Modified FCM Segmentation

The initial value of each cluster centre is derived from the average value of each respective classified class. All unclassified pixels are classified using FCM with the derived initial cluster centres. If the number of classified pixels in CMV lesion is very small (from 10 to 20), they are reclassified as CSF.

Concluding Comments

This system is 10 to 20 times faster than FCM, and produces better results for abnormal images containing lesions but it does not exhibit such promising result compared to FCM for normal images. The parameters of the membership functions have been derived automatically but the structure of the membership functions have been defined according to the knowledge of medical experts. Although anatomical position of the lesion has been taken into account, inter-

pixel correlations have not been considered. Some additional criteria may be included in addition to gradient and pixel intensity in order to define the membership functions' parameters.

2.2.2.2 Conventional Fuzzy Rule-Based MRI Segmentation

Conventional fuzzy rule-based segmentation techniques use only fuzzy rules to segment the MR image and do not apply FCM in addition to the fuzzy rules. Sasaki *et al.* introduced such a fuzzy rule-based method to segment the menisci region from MR images [120].

Database

Five normal MR data sets consisting of three normal and two injured knees are used in the experiments. T1 weighted 3D SPGR with TR=100 msec, TE=15 msec, and flip angle=30 degree images are acquired with Genesis Sigma 1.5 Tesla MRI scanner. Each image contains 60 separate 1.5 mm thick slices.

Knowledge Used to Segment the Menisci Region

The anatomical position of the menisci region is shown in Fig. 2.11. The following knowledge is used to generate the fuzzy rules.
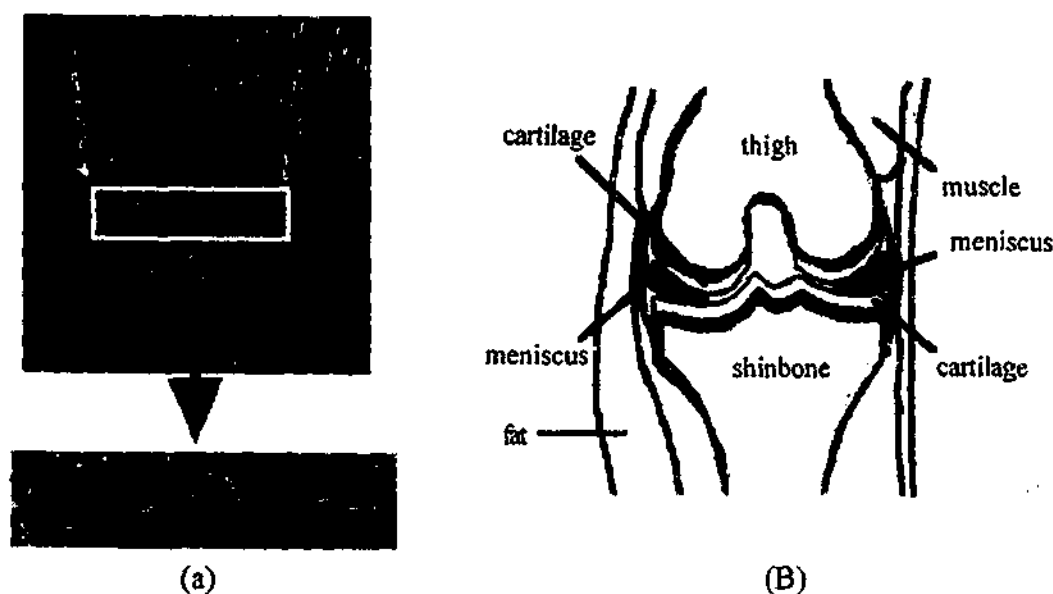
Fig. 2.11: Anatomical location of menisci region [120], (a) MRI and enlarged Image, (b) Anatomical location of knee.

1. Voxel intensities of cartilage regions are high.
2. The menisci region lies in between the thigh and shinbone.
3. The cartilage regions are adjacent to the centre of gravity of the knees.

4.   The menisci are automatically located near the cartilage.

5.   The voxel intensities of the menisci regions are coherent.

Fuzzy Rules Generation and Segmentation

Two different sets of fuzzy rules are developed as the segmentation is performed in two stages. Firstly the candidate region of the menisci is segmented whereas the menisci are extracted from the candidate region in the second stage. The candidate region is defined as the region between the cartilages as menisci are located between the cartilages. A set of voxels represented by straight contiguous two-dimensional $data(x,z)$ is called $unit(x,z)$. Two types of units, A and B are defined to segment the candidate region. Unit A contains the candidate region while unit B does not contain any candidate region voxels. Fig. 2.12 shows the model of candidate region and representation of the smallest unit.
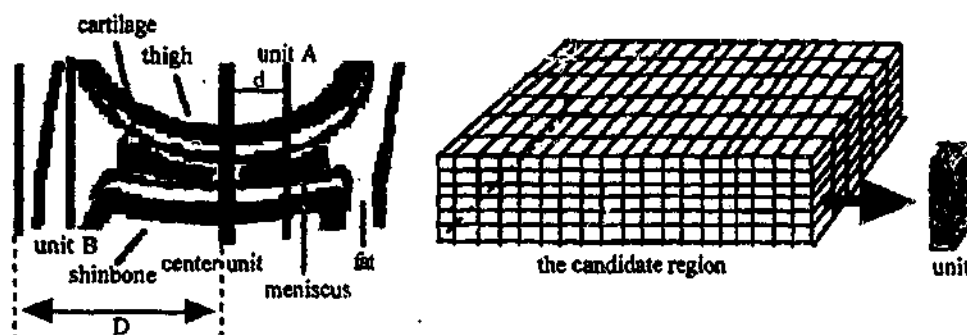
Fig. 2.12: A model of candidate region and representation of the smallest unit [120].

D and d denote the constant distance of the most distance unit and distance of the interested unit from the centre. Unit A and B are shown in Fig. 2.13.
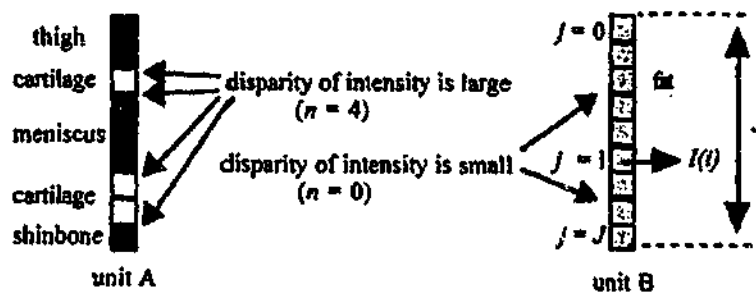
Fig. 2.13: Unit A and unit B [120].

The number of disparity between two adjacent voxel intensities on a unit is defined as: -

$$n = \sum_{j=0}^{J-1} C(j) \tag{2.20}$$

where $C(j)$ is calculated as: -

$$C(j) = \begin{cases} 1, & for \ |v(j)-v(j+1)| > T; \\ 0, & otherwise. \end{cases} \tag{2.21}$$

and J is the range of candidate region, $v(j)$ is the voxel intensity at coordinate j and T is the threshold.

The membership functions of distance and disparity to measure the values of linguistic variables, *small* and *large* are shown in Fig. 2.14.

Fig. 2.14: Membership functions for distance and disparity of intensity [120].

From the previously defined knowledge 1, 2, and 3, the following two rules are defined using the membership functions shown in Fig. 2.14 in order to segment the candidate region.

IF d is small AND n is large THEN degree of belonging to unit A is large

IF d is large AND n is small THEN degree of belonging to unit B is large

The degrees of belonging to units A and B are calculated using the following equations.

$$gradeA = w_1 \times udsmall(d) + w_2 \times unl \arg e(n) \tag{2.22}$$

$$gradeB = w_1 \times udl \arg e(d) + w_2 \times unsmall(n) \tag{2.23}$$

where w_1 and w_2 are weights. The unit is classified into unit A if $gradeA > gradeB$, otherwise the unit is classified into unit B.
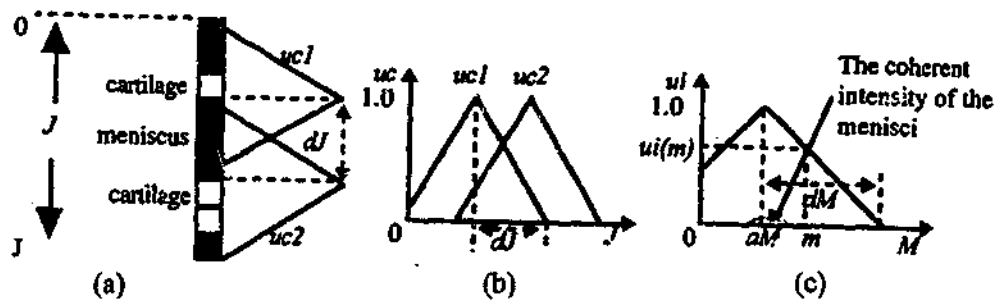
Fig. 2.15: Membership functions for segmenting menisci from cartilage region [120]), (a) Distance from cartilage, (b) Membership functions for distance from cartilage, (c) Membership functions for voxel intensity.

From the above defined knowledge 4 and 5, two membership functions uc and ui shown in Fig. 2.15 are derived for segmenting the menisci from the candidate region. Fig. 2.15(a) shows that the menisci exist near the cartilage. Both uc and ui calculate respectively the degree of belonginess to the menisci from the distance of a voxel from the cartilage region and the voxel intensity. The parameters dj and dM used in the membership functions shown in Fig. 2.15(b) and Fig. 2.15(c) respectively are the widths of the one side of the triangles whereas aM is the coherent intensity.

The calculation of uc for two cartilages is defined: -

$$uc(j) = \begin{cases} uc1(j) + uc2(j), & \text{for } uc1(j) + uc2(j) < 1; \\ 1, & \text{otherwise.} \end{cases} \qquad (2.24)$$

while for one cartilage it is: -

$$uc(j) = uc1(j) \qquad (2.25)$$

The following two rules are developed from the membership functions shown in Fig. 2.15 and the knowledge 4 and 5.

IF a voxel is anatomically adjacent to the cartilage THEN the degree of menisci voxel for uc is high

IF the intensity of the voxel is the same as coherent intensity of the menisci voxel THEN the degree for ui is high

The total degree, $gradeM = w_3 uc(j) + w_4 ui(m)$ $\qquad (2.26)$

where w_3 and w_4 are the weights. If *gradeM* > arbitrary threshold T then the voxel is classified as a menisci voxel.

Concluding Comments

This method can successfully separate the menisci. 3D construction and display of menisci has been performed for both normal and injured knees in order to identify cartilage tears. The rules have been heuristically defined from the anatomical position and coherent intensity of the menisci voxels. The structure of the membership function is predefined with the corresponding parameters being directly determined from the MR device parameters.

2.2.3 Fuzzy Rule-Based CAT Image Segmentation

CT imaging is also known as Computed Axial Tomography (CAT) scanning [121] and is one of the most important medical imaging techniques and used in various types of disease and wound diagnosis. A fuzzy rule-based segmentation of intrathoracic airway trees on CAT image has been described in [101].

Database

Five canine data sets are scanned using EBCT scanner from five anaesthetised dogs. Each data set contains 40 slices of 3mm thick. 40 slices, 8 per data set are randomly selected and their airways are perceptually determined by an expert in order to determine both the training and test sets.

Stages in Airway Tree Segmentation

This consists of the following five steps: -
   1.   Separation of lungs from the volumetric data set.
   2.   Definition of primary airway tree.
   3.   Preprocessing of all individual image slices.
   4.   Fuzzy rule-based identification of airways in all image slices.
   5.   Construction of airway tree using 3-D connectivity.

The techniques used for steps 1, 2, and 3 are described in [101, 122-124]. The primary airway tree contains the major branches of the tree and is defined as the 3-D connected components of the image voxels below a threshold, which is formed by 3-D seeded region growing approach

[125, 126]. The main task of this preprocessing step is to identify the background and all possible locations of airways and vessels for each slice. The pixels having from 55 to 110 gray level intensities are considered background pixels. Voxels darker and brighter than background are treated as candidate airways and vessels respectively.

Fuzzy Rule-Based Identification of Airways in All Image Slices

The following anatomical information is used to determine the airways.

1. Airways are generally dark
2. Airways are encompassed by airways wall
3. Airways are near to airway vessels

The anatomical position of airways and their vessels are shown in Fig. 2.16.
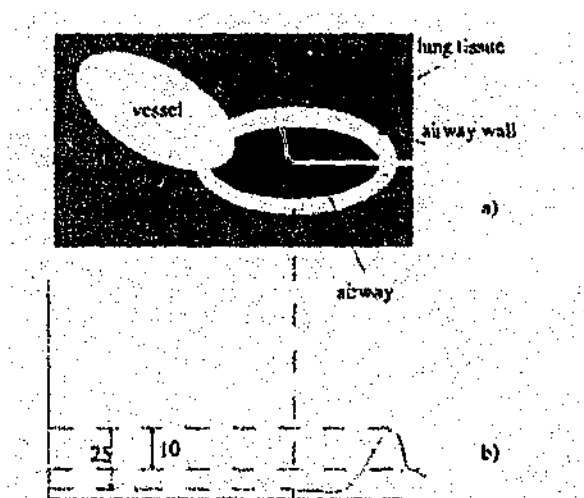
Fig. 2.16:   Anatomical position of airways [101], (a) Airways detection principles, (b) Assessment of wall evidence.

The following three features are defined according to a region adjacency graph property [127].

1. Brightness: Uses minimum and maximum grey level regions to represent the airways and vessels candidate regions respectively.
2. Adjacency: Represents the grey level of the brightest adjacent region.
3. Degree of Wall Existence: Determines the existence of the wall and is calculated by the ratio of the total number of concentric rays possessed dark-bright-dark profile and the total number of concentric rays directed from the centre of the candidate region.

The membership functions for Brightness, Adjacency and Degree_of_Wall _Existence including their linguistic variables are shown in Fig. 2.17.

The parameters of the membership function are determined from a manually tracking training set containing eight randomly selected slices of a single volumetric data set. The conflict arising amongst membership functions is solved manually in order to obtain optimum classification results [128, 129]. The rule banks developed for the segmentation are represented in tabular form and shown in Fig. 2.18.
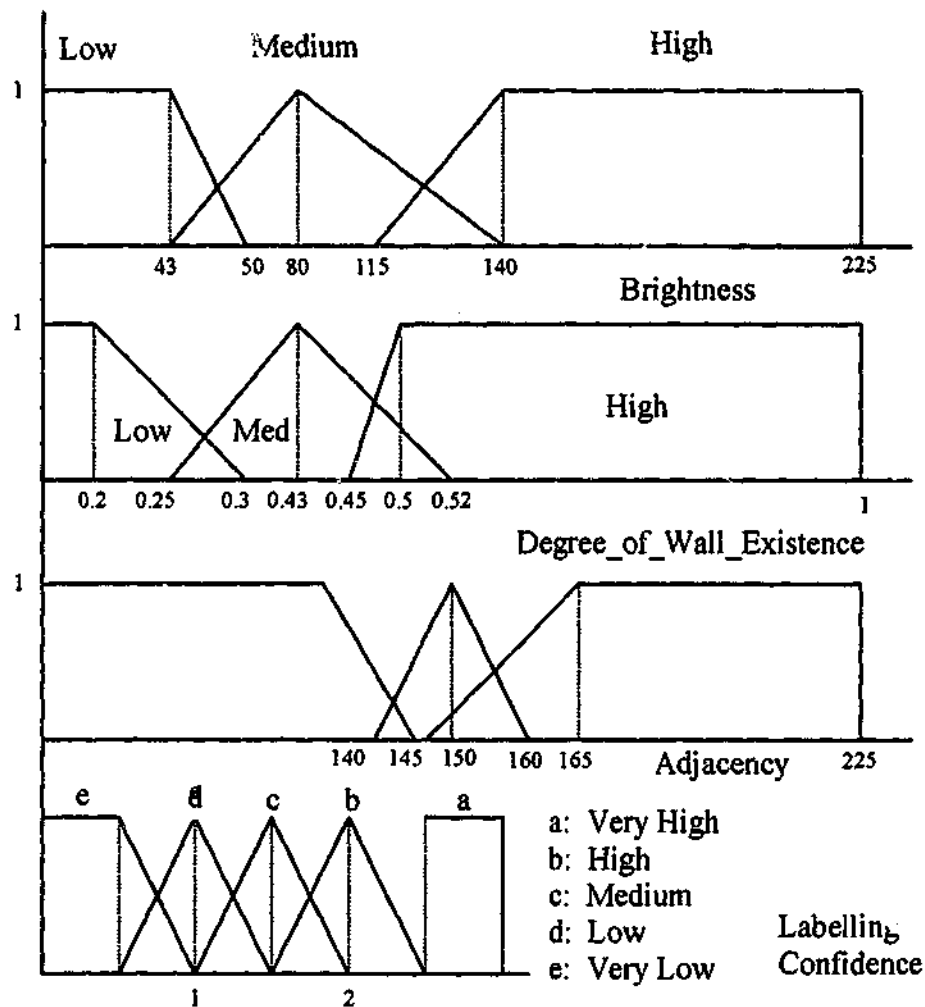
Fig. 2.17: Membership Functions for Brightness, Adjacency, and Degree _of_ Wall_Existence.

Adjacency=High

	Degree_of_Wall_Existence Low	Med	High
Brightness Low	Med	High	Very High
Med	Low	Med	High
High	Very Low	Low	Med

Adjacency=Med

	Degree_of_Wall_Existence Low	Med	High
Brightness Low	Low	Med	High
Med	Very Low	Low	Med
High	Very Low	Very Low	Low

Adjacency=Low

	Degree_of_Wall_Existence Low	Med	High
Brightness Low	Very Low	Low	Med
Med	Very Low	Very Low	Low
High	Very Low	Very Low	Very Low
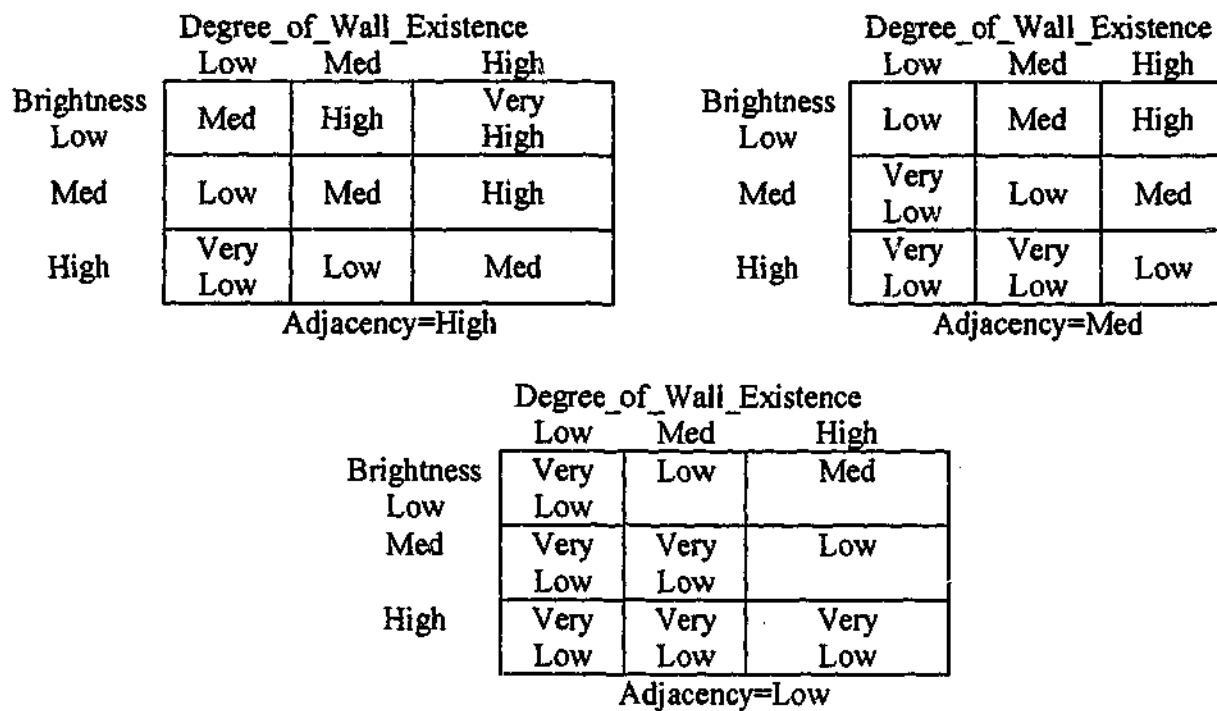
Fig. 2.18: Fuzzy rule banks to determine the confidence level of airway.

The value of each cell indicates the confidence level of airway, as for example in the following rule.

IF Brightness is Low AND Adjacency is Low AND Degree_of_Wall_Existence is High THEN
region is airway with Medium confidence

Finally, centroid defuzzification is applied in order to obtain numerical confidence level for each region, which indicates the possibility that the region belongs to airway.

Construction of Airway Tree Using 3-D Connectivity

Airway tree named C-tree is constructed by stacking all the regions whose airway confidence level is greater than 73% utilizing shape based interpolation along the z-axis [130]. From C-tree, A-tree and B-tree are created. A-tree is defined as a 3-D connected region and subset of C-tree, which contains the airway-tree root. B-tree is the combination of A-tree and disconnected airway tree branches of C-tree that contains above the empirically selected threshold for volume.

Concluding Comments

This method has constructed three trees named A-tree, B-tree, and C-tree. The medical specialist may use any of the trees according to their needs though the parameters of the membership function are not automatically derived. It showed good performance *in vivo* analysis of 3-D human CAT image data sets.

While each of the reviewed fuzzy rule-based systems has particular merits, they also each have some inherent limitations. They may be summarised as follows: -

1. The systems are both image and application dependent.
2. The structures of the membership functions are manually defined.
3. Spatial relations of pixels are not exploited by all systems.
4. In certain cases, the parameters of the membership functions are perceptually derived.
5. None of the systems considered texture.

As will be proven in subsequent chapters, the fuzzy rule-based framework solution proposed in this thesis specifically addresses all of the above limitations.

2.3 Texture Features

Texture representation is one of the fundamental problems of digital image processing since there is no widely accepted definition of texture and generally it represents the structural arrangement of the surfaces and their relationships. Most natural objects contain texture and are usually identified by shape, colour, and texture [10], so it is crucial to give consideration to texture feature for object based image segmentation. There are a large number of techniques available in the literature to estimate the texture. Some of the most common techniques are [10, 131]: -

- Gray level histogram.
- Gray-tone co-occurrence matrix.
- Fourier transform energy.
- Dominant local orientation and frequency.
- Gradient analysis.
- Relative extrema density.
- Markov random field model.
- Gibbs random field model.
- Gabor filters.
- Fractal dimension.

A brief description of the gray level histogram technique will be given in Section 4.3 where it is employed for measuring the uniformity. The main limitation of this approach is that the gray level histogram only considers first order statistics and so does not consider the relative position of the pixels [10]. Sharma *et al.* [132] performed an evaluation between five different texture

extraction techniques for image analysis and proved the gray-tone co-occurrence matrix the best. This technique measures the second order joint probability between a pair of pixels separated by a particular distance in a specific direction [10]. The features obtained from the gray-tone co-occurrence matrix however are not truly rotation invariant and thus not suitable in the context of the framework because in calculating the membership functions for texture for each pixel, a small window is used, typically of size 4×4. Higher sized windows are not suitable to calculate the membership function for each pixel.

A broad tutorial review of many of these different techniques including their advantages and disadvantages is given in [10][133]. Of the above, in the context of the thesis and particularly the role of texture in the fuzzy based framework, the fractal dimension (FD) is especially advantageous for the following reasons:

1.   It is relatively scale insensitive and corresponds to human perception of texture that is, there exists uniformity between the human perception and the surface roughness [131].

2.   It is suitable for describing the erratic and complex behaviour of the surface of natural objects [134].

3.   The FD based feature is also appropriate to consider image domain specific information based on a window in segmentation.

This final attribute is very important in being able to take image domain specific information into account and was one of the key reasons for selecting FD in the fuzzy rule-based framework (Fig. 1.1) for texture segmentation purposes. This will be discussed in greater detail in Chapter 5.

2.4 Colour Models

Colour is a physiopsychological phenomenon and exists in every aspect of human life. Colour analysis has been essential in computer vision based on the simple notion *the more information helps to more accurately represent the visual scene* [135]. The following two primary aspects inspire the application of colour in image processing [84]: -

1.   Colour is a very important attribute, which makes easier the object recognition and extraction from the image.

2.   Colour has a huge number of shades and intensities, whereas gray level has only about 24 shades of gray.

All colours are generated by the combination of three primary colours: red, green, and blue. The amounts of red, green, and blue used to generate a particular colour are known as tristimulus

values. So a colour is represented by a point within a subspace of 3-D coordinate system. The specifications of 3-D arrangements of the colour sensations are called colour models or colour spaces or colour coordinate systems. The colour models used in image processing are generally developed from following sources [136]: -

- Human visual systems: for example, RGB, opponent, and HSV colour models.
- Technical Domain: for example, XYZ (colorimetry) and YUV (television) colour models.
- Developed specifically for image processing: for example, Otha and Kodak Photo YCC models.

A brief description of some of the colour models is presented in the following sections.

2.4.1 RGB Colour Model
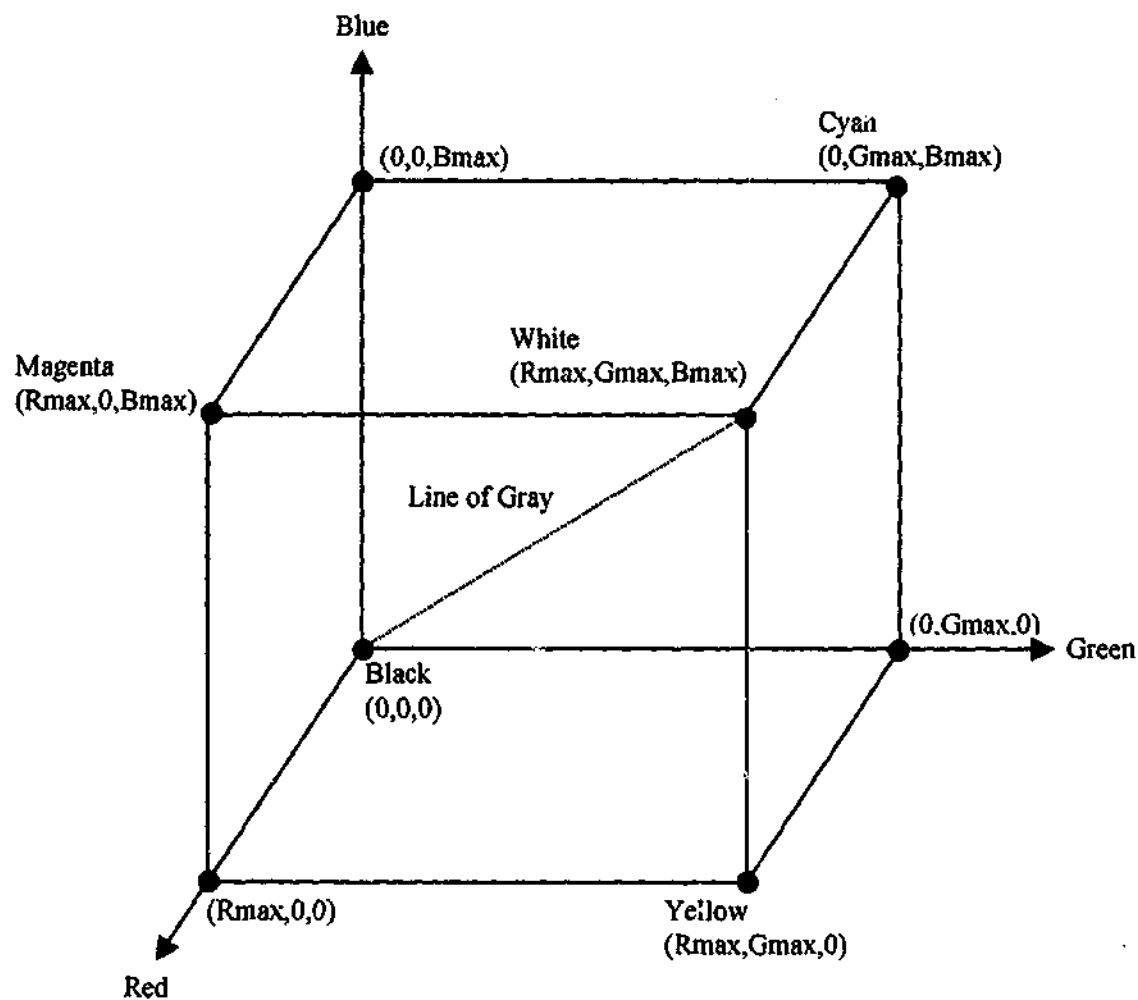
Fig. 2.19: RGB Colour Model (RGB Cube).

RGB model is the basic colour model and in general it is used to derive other colour models. Each colour is represented by the three components: red (R), green (G), and blue (B) using 3-D Cartesian coordinate system. The RGB colour gamut uses a unit cube called RGB cube shown in Fig. 2.19 assuming all three components are normalized within [0, 1], in which the positions of red, yellow, green, white, magenta, cyan, blue, and black are shown. The gray level is shown by the dotted lines connecting the black (0,0,0) and white (1,1,1) points [84, 136].

While the RGB colour model is used in many colour applications, such as cameras, scanners, and displays and aerial and multispectral image processing [84], it has some significant disadvantages when considered from a segmentation perspective.

- The R, G, and B components are highly correlated.
- A non-intuitive colour model, which means that it is very difficult to perceive the colour based on the values of the R, G, and B components.
- A non-uniform colour model, which means that usually the perceptual difference between two colours does not conform to the corresponding Cartesian distance.

As mentioned earlier, since RGB is the fundamental colour model and extensively used in colour image processing, its application to image segmentation will be examined in detail in Chapter 7.

2.4.2 HSV Colour Model

HSV is one of the perceptual colour models, in which human can easily perceive the basic attributes: hue (H), saturation (S), and value (V) [136]. Hue represents the dominant wavelength of the colour stimulus, while saturation denotes the relative purity of the colour. V corresponds to the gray level intensity of a colour that is, the luminance. HSV colour system uses a cylindrical coordinate system and the colour subspace is a hexcone, as shown in Fig. 2.20 [137].

The angle around the vertical line starting with 0 represents the hue and the saturation is measured by the distance of the colour point from the vertical line (V axis) within the normalised range of [0,1]. The advantages of the HSV colour model may be summarised as follows [136]: -

- Intuitive colour model.
- Separation of chrominance from luminance.
- Only hue component (H) can be used in object recognition and segmentation.

The main disadvantages of this model are: -

- Perceptually non-uniform.

- The inevitable singularities arising during the transformation from the RGB to HSV model.

- Difficulties in some arithmetic operations on hue angles e.g. averaging.
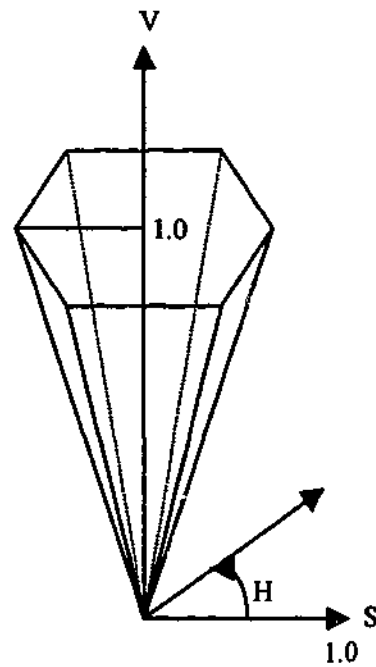
Fig. 2.20: HSV Colour model (Hexcone).

Since hue is expressed using the cylindrical coordinate system, the calculation of the average of hue angles based on Cartesian coordinates does not make sense. For this reasons, an alternative strategy be specifically proposed in Section 6.4, where an algorithm is developed for calculating the average of hue angles for the processing.

HIS (hue, intensity, and saturation) and HLS (hue, lightness, and saturation) are the same as the HSV colour model. In the light of the above mentioned advantages, especially its potential capability for object recognition and segmentation, the HSV colour model will be utilised in the proposed fuzzy rule-based colour image segmentation (FRCIS) algorithm (**Block 4** in Fig. 1.1) and analysed in greater detail in Chapter 7.

2.4.3 Television Colour Models

The television models were mainly created in order to reduce the bandwidth of the composite video signal (CVS), so that it can be transmitted through existing TV channels used by monochrome television systems [136]. These are opponent colour models, where the luminance (Y) and chrominance components (U and V or 1 and Q) are separated. The two chrominance

components are derived from the colour difference signals: R-Y and B-Y. YUV and YIQ colour models are used in the analogue PAL (625 lines) and NTSC (525 lines) TV signal coding systems respectively, while YC_bC_r is independent of the actual TV signal coding system and is suitable for the digital coding of TV pictures [136].

2.5 Fuzzy Colour Image Segmentation Techniques

As alluded in Section 2.4, the human eye can discern a huge number of shades and intensities of colour but only around two-dozen shades of gray. Using this additional information, objects, which are not possible to be segmented using gray level information, may potentially be able to be segmented using colour information [138].

Lim and Lee [139] proposed a colour image segmentation using multilevel thresholding and the FCM algorithm. There are two stages: coarse and fine, associated with this algorithm. In the coarse stage, the segmentation is performed using multilevel thresholding, while in the fine stage, the segmented results produced by the coarse stage are refined using the FCM algorithm. Its application is limited due to applying the histogram mode seeking technique [138], which usually uses the peaks in the histogram to determine the number of regions (clusters). It is difficult to calculate the number of regions (clusters), if there is no distinct peak in the histogram.

Another colour image segmentation technique using fuzzy integral and the RGB colour model has previously been discussed in Section 1.2.4.

Moghaddamzadesh and Bourbakis [140] introduced a fuzzy region growing approach for colour image segmentation, by defining a function $contrast(v, w)$ to measure the contrast between two pixels with v and w colour vectors in the following way: -

$$contrast_{v,w} = \sqrt{(R_v - R_w)^2 + (G_v - G_w)^2 + (B_v - B_w)^2}$$

(2.27)

The fuzzy membership function for the contrast is defined as:

$$\mu_c = \begin{cases} 0, & \text{if } contrast \le a_1; \\ 1, & \text{if } contrast > a_2; \\ (contrast - a_1)/(a_2 - a_1), & \text{otherwise.} \end{cases}$$

(2.28)

where a_1 and a_2 are two predefined thresholds. The contrast is deployed to measure the homogeneity during region-growing approach. Two types of contrast are determined, namely absolute contrast (contrast between a pixel and a region) and relative contrast (contrast between a

pixel and its neighbours in the growing direction). The membership function for farness, μ_f, which is used in classifying a pixel to the appropriate cluster is defined as: -

$$\mu_f = \mu_d \times \mu_c \tag{2.29}$$

where μ_d is the membership function for measuring the distance. The contrast defined by this technique is not reliable because of the high correlation between the colour components of the RGB colour model and not being illumination invariance [138].

Chien and Cheng [141] proposed a colour image segmentation approach based on fuzzy similarity measure by defining a set of fuzzy colours based on hue and tone using the HLS colour model. The tone is developed based on lightness and saturation. The predefined triangular membership functions are used for both hue and tone. Each pixel is represented by a set of fuzzy colours that are defined in the colour palette selected by human. They also defined a fuzzy similarity measure to calculate the similarity between two fuzzy colours. The adjacent pixels are merged based on their similarity value.

Cheng *et al.* [142] introduced a fuzzy colour image segmentation technique based on homogram mode seeking approach using the RGB and HSI colour model. In this technique, a homogram is defined in terms of gray level occupancies and fuzzy homogeneity among the neighbouring pixels. The two main processing steps of this technique are as follows:

1. The image is classified into major homogeneous regions by the homogram analysis based on entropy.
2. The final segmented results are produced by merging the smaller and closest regions with their closet regions in order to avoid over segmentation.

The segmented regions produced by these techniques are not perceptually meaningful objects and as mentioned before, the mode seeking approach is not suitable for object based image segmentation. This technique fails to separate the regions if there is no peak in the homogram at all. The approach also omits how to actually calculate the similarity for the HSI colour model, especially for the hue values.

2.6 Summary

This chapter has outlined some of the popular fuzzy clustering and rule-based image segmentation techniques. The simplest, oldest, and most widely used clustering algorithm is fuzzy c-means clustering algorithm (FCM), which arbitrarily divides the data sets and the

equations provided for the cluster centre and the membership function are not sufficient to achieve the local minimum of the object function. It also strongly follows the probability, which avoids the trivial solution for the membership function. Although the possibilistic c-means algorithm (PCM) considers the underlying meaning of data and hence has solved the problems for the degrees of sharing and strongly supporting the probability of the FCM membership function, its objective function cannot achieve a global minimum. The main two drawbacks of these clustering algorithms are the number of clusters and their initial values.

In contrast, fuzzy rule-based image segmentation techniques are able to integrate expert knowledge and are less computationally expensive compared with fuzzy clustering. They are also able to interpret linguistic as well as numeric variables. The performance of fuzzy rule-based segmentation in many applications however, is sensitive to both the structure of the membership functions and associated parameters used in each membership function. The example in Section 2.2.1 of a rule-based LI segmentation technique for geographic map images, intuitively defined the structure of the membership functions with the related parameters being automatically determined.

It is evident from the various examples and commenting that fuzzy rule-based image segmentation techniques offer much greater potential, though both the structure of membership functions and derivation of their relevant parameters are still very much application domain and image dependent.

The chapter has also reviewed ways of representing both texture and colour in images. The motivation for choosing fractal dimension (FD) to incorporate texture together with the image domain specific information for segmentation and the descriptions of different colour models including their respective advantages and disadvantages have been provided. Colour image segmentation techniques based on histogram/homogram mode seeking or thresholding have also been reviewed for few suitability for object based image segmentation.

The next chapter will introduce a new generic fuzzy rule-based image segmentation (GFRIS) algorithm, which will address a number of the aforementioned issues, most crucially by incorporating spatial pixel information and automatically data-mining both the key fuzzy rule weighting factor and its threshold.

A Generic Fuzzy Rule-Based Image Segmentation Algorithm

The literature review in Chapter 2 highlighted that fuzzy rule-based image segmentation techniques tend in general, to be application dependent with the structure of the membership functions being predefined and in certain cases, the corresponding parameters being manually determined. The net result is that the overall segmentation performance of a technique is very sensitive to parameter value selections. This chapter addresses these issues by introducing a *generic fuzzy rule-based image segmentation (GFRIS)* algorithm (**Block 1** in Fig. 1.1), which is both application independent and exploits inter-pixel spatial relationships. The GFRIS algorithm automatically approximates both the key weighting factor and threshold value in the definitions of the fuzzy rule and neighbourhood system respectively. A detailed time complexity analysis of this algorithm is also presented in this chapter. A complete quantitative evaluation will be presented between the segmentation results obtained using GFRIS and the two popular fuzzy c-means (FCM) and possibilistic c-means (PCM) algorithms in Chapter 7.

This Chapter is organised as follows: In Section 3.1, the three membership functions used in the GFRIS algorithm are defined. The fuzzy rule definition and underlying theory, together with the data-mining algorithm for obtaining both the key weighting factor and threshold are presented in Sections 3.2 and 3.3 respectively. Section 3.4 details the full GFRIS algorithm, together with a full time complexity analysis, while Section 3.5 addresses the performance of the GFRIS algorithm.

3.1 Defining the Membership Functions

The definition of the membership function lies at the heart of any fuzzy logic system and the capability of fuzzy rule-based techniques significantly depend upon it. The Gestalt principle states that visual elements may be perceptually grouped together based on the principles of: proximity, similarity, common fate, good continuation, surroundedness, closure, relative size, and symmetry [143]. Of these perceptual characteristics, three membership function types are defined based on the

47

Gestalt principles of similarity, proximity, and good continuation, to respectively represent the: (i) region pixel distributions, (ii) closeness to a region's centre, and (iii) pixel spatial relations. The first and second membership functions characterise similarity based on a region's pixel distribution and gray level pixel intensity respectively, while the third reflects the characteristics of both proximity and good continuation. Each membership function has a corresponding membership value for every region, which indicates the degree of belonging to that region. These three membership functions will now be individually discussed.

3.1.1 Membership Function for Region Pixel Distributions

In gray level images, every region has a distinctive pixel distribution, which characterises to some extent that region's properties. The approach adopted here is to automatically define the membership function including its structure from the pixel distribution of that particular region. This is achieved in three steps: -

1. Segment the original image into a desired number of regions by applying a clustering algorithm such as fuzzy c-means (FCM).
2. Generate the gray level pixel intensity histogram for every region and normalise the frequency for each gray level into the range [0 1].
3. Use a polynomial representation to approximate each region. The polynomial value of a region, for every gray level pixel corresponds to the membership value of that pixel in that region, with the actual gray level intensity values being the parameters of the membership function.

As an example, the reference image shown in Fig. 3.1(a) is classified into two separate regions, namely R_1 (cloud) and R_2 (urban scene) using the standard FCM algorithm. The respective pixel distribution of each region is used to produce the corresponding membership function and a gray level intensity histogram (*gray level histogram*) is generated for both regions, with the frequencies of occurrence being normalized. A polynomial then approximates the histogram of each region. As an example, a 3rd order polynomial is given by: -

$$f(x) = a_0 + a_1 x + a_2 x^2 + a_3 x^3 \qquad (3.1)$$

where x is an independent variable, which in this example is the 8-bit gray level pixel intensity.

The coefficients a_0, a_1, a_2, and a_3 are computed by applying a least squares (LS) fit to the histogram for each region. The values of $f(x)$ are constrained between 0 and 1, and represent the membership value of each gray level pixel. The 3rd order polynomials for the segmented regions R_1 and R_2 in the example image are shown in Fig. 3.1(b) and 3.1(c) respectively.

(a)   (b)   (c)
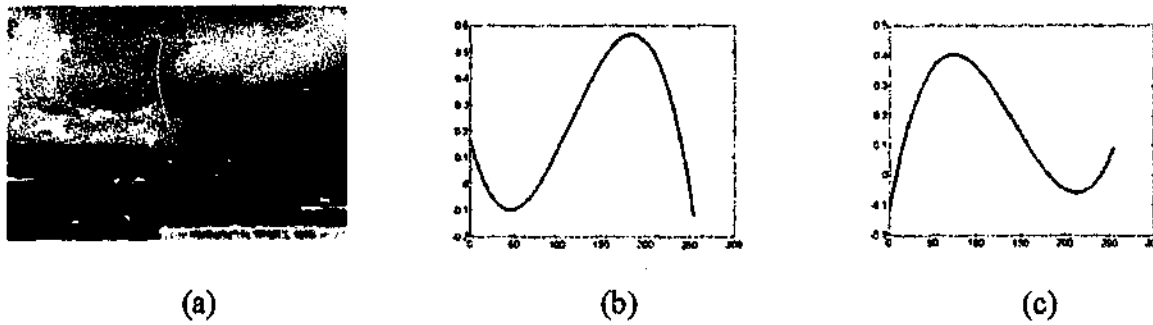
Fig. 3.1: Reference image and its membership function for each region: (a) Original image, (b) Membership function for R_1, (c) Membership function for R_2.

The degree of belonging to a region of a candidate pixel, that is the pixel to be classified, is determined from the respective membership function. Hence, for a pixel having a gray level value of 150, the membership values for regions R_1 and R_2 can be easily determined from the respective polynomials as 0.425 and 0.125 respectively. Considering the general case of a pixel with a gray level value of $P_{s,t}$ at location (s,t), then the two membership functions $\mu_{DR1}(P_{s,t})$ and $\mu_{DR_2}(P_{s,t})$ for the pixel distribution of regions R_1 and R_2 respectively, are expressed as: -

$$\mu_{DR_1}(P_{s,t}) = f_{R_1}(P_{s,t})$$

(3.2)

and

$$\mu_{DR_2}(P_{s,t}) = f_{R_2}(P_{s,t})$$

(3.3)

where $f_{R_1}(P_{s,t})$ and $f_{R_2}(P_{s,t})$ are the respective polynomials of regions R_1 and R_2.

3.1.2 Membership Function to Measure the Closeness of a Region

This membership function represents the similarity between a candidate pixel and the centre of a region based on gray level pixel intensity. A pixel must always be closer to the belonging region than any other region and the degree of *belongingness* of a candidate pixel to a region is determined from the k-means clustering algorithm [144]. When a candidate pixel joins its nearest region, the centre of that particular region is recomputed. The centroid of a region R_j is defined as: -

$$C(R_j) = \frac{1}{N_j} \sum_{i=1}^{N_j} P_j(i)$$
(3.4)

where N_j is the number of pixels and $P_j(i)$ represents the ith pixel gray level intensity in the jth region.

A membership function should reflect the axiom that *the closer a pixel is to a region, the larger the membership value that pixel should have*. Hence, the membership function $\mu_{CR_j}(P_{s,t})$, which determines the degree of belongingness of a candidate pixel $P_{s,t}$ at location (s,t), to a region R_j is defined as: -

$$\mu_{CR_j}(P_{s,t}) = 1 - \frac{|C(R_j) - P_{s,t}|}{(2^b - 1)}$$
(3.5)

where a b-bit gray level image is assumed.

Lemma 3.1: The maximum value of the membership function $\mu_{CR_j}(P_{s,t})$ will always be at the centre of the region and the structure of the function will be symmetrical about a vertical line that passes through the centre of the region.

Proof: For positive values of $(2^b - 1)$, $\frac{|C(R_j) - P_{s,t}|}{(2^b - 1)} \geq 0$. The function $\mu_{CR_j}(P_{s,t})$ will therefore be a maximum whenever $|C(R_j) - P_{s,t}| = 0$, i.e. when $C(R_j) = P_{s,t}$, so the maximum always occurs at $C(R_j)$, which is the centre of region R_j.

To prove the membership function is symmetrical about $C(R_j)$, consider the values of $\mu_{CR_j}(P_{s,t})$ for $P_{s,t} = C(R_j) + \delta$ and $P_{s,t} = C(R_j) - \delta$, where δ is an arbitrary constant.

$$\mu_{CR_j}(C(R_j) + \delta) = 1 - \frac{|C(R_j) - C(R_j) - \delta|}{(2^b - 1)} = 1 - \frac{|\delta|}{(2^b - 1)}$$

$$\mu_{CR_j}(C(R_j) - \delta) = 1 - \frac{|C(R_j) - C(R_j) + \delta|}{(2^b - 1)} = 1 - \frac{|\delta|}{(2^b - 1)}$$

Since $\mu_{CR_j}(C(R_j) + \delta) = \mu_{CR_j}(C(R_j) - \delta)$, $\mu_{CR_j}(P_{s,t})$ is also symmetrical about a vertical line passing through the centre of region R_j. ∎

3.1.3 Membership Function for Spatial Relations

The principles of proximity and good continuation are used to define this particular membership function. Wherever pixels are close together and exhibit relatively smooth variations, there is an obvious expectation that strong spatial relationships will exist between neighbouring pixels within that region. In the preceding two sections, the respective membership functions have been constructed using only feature values, i.e. gray level pixel intensities. Spatial relations between pixels within an identified region have not been considered, yet are vital since they characterise the geometric features of a region as any spatial object contains two descriptors: feature and geometric [145, 146].

In many natural images, there are a large number of overlapping pixels between regions, so that effective segmentation cannot be expected unless these overlapping pixels are taken into account. By considering the neighbourhood relationship between the candidate pixel and the pixels of a region that surround it, a large number of overlapping pixels can be reduced. Based on the neighbourhood relations, the candidate pixel can then be assigned to the appropriate region.

Many approaches exist to define neighbourhood relations [147], such as minimum spanning tree, fixed size neighbourhoods, and Voronoi tessellation. This paper concentrates upon only fixed size neighbourhoods around the candidate pixel, since the number of pixels and their distances from a candidate pixel has to be calculated.

The neighbourhood pixel configurations for $r=1$, $r=2$, and $r=4$ are shown in Fig. 3.2(a), 3.2(b), and 3.2(c) respectively [148] where $r \geq 1$ denotes the neighbourhood radius, while O and # represent the candidate and neighbourhood pixels respectively. The number of neighbours will be $(r+1)^2$ for $r=1$ and $(r+1)^2 - 1$ otherwise.

```
                                              #   #   #   #   #
          #                 #   #   #         #   #   #   #   #
      #   O   #             #   O   #         #   #   O   #   #
          #                 #   #   #         #   #   #   #   #
                                              #   #   #   #   #
      (a)  r=1             (b)  r=2               (c)  r=4
```
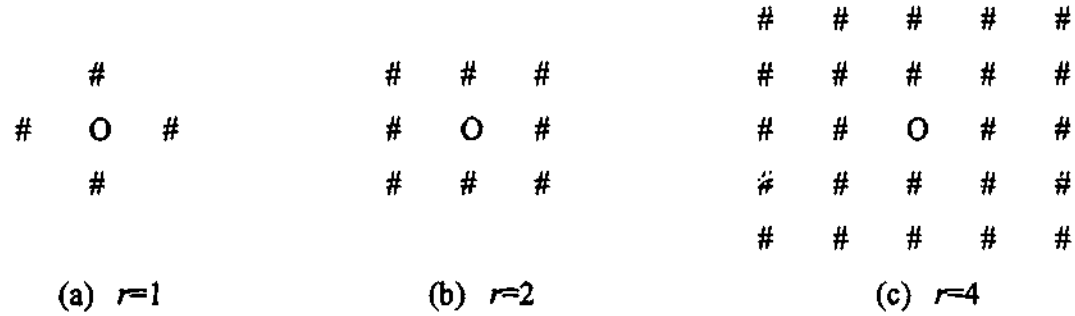
Fig. 3.2: Neighbourhood configurations.

As previously mentioned, the principles of proximity and good continuation imply that pixels, which are close together and have smooth variations should be part of the same region, that is, segmented regions are homogeneous and mutually exclusive. It is thus assumed that the variation of neighbouring pixels in a region is limited to some threshold T, and the neighbourhood system of a region based on this premise is defined as: -

Definition 3.1—A Neighbourhood System: A neighbourhood system $\zeta(P_{s,t}, r)$ with radius r, of a candidate pixel $P_{s,t}$ is the set of all pixels $P_{x,y}$ such that $\zeta(P_{s,t}, r) = \{P_{x,y} | (d(P_{x,y}, P_{s,t}) \leq r) \wedge (|P_{x,y} - P_{s,t}| \leq T)\}$ where the distance, $d(P_{x,y}, P_{s,t}) = |x - s| + |y - t|$, $P_{x,y}$ is the gray level value of the pixel at Cartesian coordinates (x, y), and T is the threshold.

To construct a membership function, the number of neighbourhood pixels and their distances from the candidate pixel must be considered, while to achieve proximity and good continuation, the membership function μ should possess the following properties: -

    1. $\mu \propto N$ where N is the number of neighbours.

2. $\mu \propto \dfrac{1}{d(P_{x,y}, P_{s,t})}$

where $d(P_{x,y}, P_{s,t})$ is the distance between pixels $P_{x,y}$ and $P_{s,t}$. The second property may intuitively be interpreted as the *smaller the distance between a candidate pixel $P_{s,t}$ and its neighbour $P_{x,y}$, the larger the value of the membership function μ.*

The summation of all inverse distances of a region R_j is: -

$$G_{R_j} = \sum_{i=1}^{N_j} \frac{1}{d_i(P_{x,y}, P_{s,t})} \qquad (3.6)$$

where $N_j = \left| \varsigma(P_{s,t}, r) \right|$ is the number of neighbourhood pixels of the candidate pixel $P_{s,t}$ in the region R_j and $d_i(P_{x,y}, P_{s,t})$ is the *city block distance* between the ith pixel $P_{x,y}$ of region R_j and the candidate pixel $P_{s,t}$.

By considering the number of neighbours N_j and the sum of their inverse distances G_{R_j} from the candidate pixel $P_{s,t}$, the membership function $\mu_{NR_j}(P_{s,t}, r)$ of the region R_j becomes,

$$\mu_{NR_j}(P_{s,t}, r) = \frac{N_j \times G_{R_j}}{\sum_{j=1}^{\Re}\left(N_j \times G_{R_j}\right)} \qquad (3.7)$$

where $\Re$ is the number of segmented image regions. Eq. (3.7) shows that the greater the number of neighbours in a region, the larger the membership function value will be for that region. Hence, if all neighbours fall into a single region, the corresponding membership function value will be one for that region, since the sum of the membership function values for all regions always equals unity.

It is worth mentioning that (3.7) is not a probability function, since it is does not use any random data or samples to develop the membership function. Rather it uses actual data to approximate spatial relationships. The sum of all the membership function values for all regions is deliberately kept equal to unity in order to reward regions that have and are close to neighbours, and to do the converse for regions that is further away and have a smaller number of neighbours. Experiments were performed with this restriction relaxed, but they did not produce very promising results.

3.2 Defining the Fuzzy Rule

Having defined the three membership functions, the next step is to combine them using a fuzzy rule. The definition of the fuzzy rule is the single most important and challenging aspect of fuzzy rule-based image segmentation, as its effectiveness is vital to the overall performance. In this section, the fuzzy rule is heuristically defined using the three membership functions defined in Section 3.1, in combination with the widely used fuzzy IF-THEN rule structure.

The overall membership value $\mu_{AR_j}(P_{s,t},r)$ of a pixel $P_{s,t}$ for region R_j represents the overall degree of belonging to that region, and is defined by the weighted average of the three individual membership function values $\mu_{DR_j}(P_{s,t})$, $\mu_{CR_j}(P_{s,t})$ and $\mu_{NR_j}(P_{s,t},r)$, which were given in (3.2), (3.5) and (3.7) respectively.

$$\mu_{AR_j}(P_{s,t},r)=\frac{w_1\mu_{DR_j}(P_{s,t})+w_2\mu_{CR_j}(P_{s,t})+w_3\mu_{NR_j}(P_{s,t},r)}{w_1+w_2+w_3} \tag{3.8}$$

where w_1, w_2, and w_3 are the weightings of the membership values for pixel distribution, closeness to the cluster centres, and neighbourhood relations respectively. The overall membership value $\mu_{AR_j}(P_{s,t},r)$ is used in the antecedent condition of the fuzzy IF-THEN rule.

Definition 3.2—Fuzzy Rule: IF $\mu_{AR_j}(P_{s,t},r)=\max_{1\leq i\leq \Re}\{\mu_{AR_i}(P_{s,t},r)\}$ THEN pixel $P_{s,t}$ belongs to region R_j.

This rule is made deliberately generic so that it can be applied to any image type thus adhering to one of the key objectives that the GFRIS algorithm should be both image and application independent. Clearly the weightings in (3.8) applied to each membership function have to be calculated and play a vital role in the performance of the GFRIS algorithm. In the next section, a strategy will be discussed to calculate each weighting value.

3.3 Determination of Weighting Factors and the Threshold

The threshold value T introduced in Section 3.1.3, plays a major role in defining the spatial relationship between pixels in any region, because it regulates the level of variation between the candidate pixel and its neighbours. The greater the variation between a candidate pixel and its

neighbours, the larger the standard deviation will be, which pro rata results in poor continuation. Two issues need to be considered in determining the threshold value: -

1. The degree to which pixels of one region overlap with those of another region.
2. The pixel standard deviations in each region.

The approximate threshold T_a is computed using step 1, by considering the centres of the initially segmented regions, while the status of this approximate threshold as to whether it is actually an overestimation of the final threshold value, is determined using step 2. Estimation of both the status and final threshold value is detailed in Algorithm 3.1. If the centre of a particular region is two standard deviations away from the boundary of another region and the pixels in that region are normally distributed, there is at best a 5% probability that the pixels of that region will overlap with the other. The procedure to determine the approximate threshold T_a for two regions may be formalized as follows: -

Theorem 3.1: *If two regions with centres c_1 and c_2 have pixels that are normally distributed, then for at least 5% levels of significance, the approximate threshold will be bounded by* $T_a \le |c_1 - c_2|/4$.

Proof: Assuming that the pixels are normally distributed, then in a region having a centre c_1 and standard deviation σ_1, the 5% level of significance means the probability of pixels falling outside $c_1 \pm 2\sigma_1$ will be 0.05 [149]. The same is also true for the other region, which has a centre c_2 and standard deviation σ_2. Thus, for at least 5% levels of significance,

$$2(\sigma_1 + \sigma_2) \le |c_1 - c_2|$$

Since the threshold is considered the same for both regions, it may be written as $T_a = \dfrac{\sigma_1 + \sigma_2}{2}$ such that,

$$4T_a \le |c_1 - c_2| \Rightarrow T_a \le \frac{|c_1 - c_2|}{4} \qquad \blacksquare$$

This theory may be extended to an arbitrary number of regions for determining the weight and the threshold values. If the approximate threshold is overestimated, the minimum value between the

standard deviations and the approximate threshold is used as the final threshold. This is conditional on the value not being either zero or very small (less than some arbitrary percentage of T_a), so ensuring that some spatial relationship exists. The weight w_1 in (3.8) governs the importance assigned to region pixel distributions, and extensive empirical observations revealed that the resultant segmentation was not very sensitive to variations in this particular parameter.

The important weighting factors are w_2 and w_3, as their values represent a trade-off between the gray level pixel intensity and spatial relationship. Prominence was initially given to the former, because it contributed more to the human visual perception and for this reason, following empirical evaluation; w_2 was set equal to 1.8, with the other two weighting factors being set to one. If the standard deviation in a number of regions is high with respect to the approximate threshold, then the spatial relationship will be ineffective and greater emphasis needs to be given to w_2 by increasing its value. In all other instances, importance should be given to the pixel spatial relationships so that the value of w_2 should be reduced. The following details the various stages of the algorithm to automatically determine this key weighting factor and its threshold.

Algorithm 3.1 Determining the weighting factors and threshold T

1. Set the initial values for the three weighting factors as $w_1 = 1$; $w_2 = 1.8$; $w_3 = 1$.

2. Define a set of all regions (R) and a set of centre pairs of all regions (V).

$$R = \{R_j \mid (1 \le j \le \Re)\}$$

$$V = \{(C(R_i), C(R_j)) \mid (\forall i, j \; R_i, R_j \in R) \wedge (i \ne j)\}$$

3. Compute the absolute sum of differences (*sofd*) between the elements of all pairs.

$$sofd = \sum_{i=1}^{\binom{\Re}{2}} |V_i(1) - V_i(2)|$$

where $\binom{\Re}{2}$ is the number of combination pairs of all regions.

4. Determine the approximate threshold T_a using Theorem 3.1.

$$T_a = \frac{sofd}{\binom{\Re}{2} \times 4}$$

5. Calculate the average sum of differences (asd) between the various standard deviations and approximate threshold.

$$asd = \frac{\sum_{j=1}^{\Re}\left(\sigma_{R_j} - T_a\right)}{\Re}$$

where σ_{R_j} is the standard deviation of region R_j.

6. If the approximate threshold is overestimated, i.e. $asd < 0$ then the minimum of the standard deviation and T_a, is taken as the final threshold value T, provided this value is neither too small (less than $K\%$ of T_a, where K is positive arbitrary constant) nor zero. Otherwise T_a becomes the final threshold, T.

7. Normalise the average sum of differences between the standard deviation and approximate threshold.

$$nasd = \frac{asd}{\max\left(\max_{1 \leq i \leq \Re}\left\{\sigma_{R_j}\right\}, T_a\right)}$$

8. Adjust the weight w_2 accordingly.

$$w_2 = w_2 + nasd$$

This algorithm has been experimentally tested upon various different image types and as results will prove in Chapter 7, the automatic data mining of the key weighting factor and threshold value is a significant reason for the superior performance of the GFRIS algorithm compared with other segmentation techniques such as FCM and PCM. The complete GFRIS algorithm is now discussed.

3.4 The GFRIS Algorithm

3.4.1 The Algorithm

As discussed before, the GFRIS algorithm is specifically designed so that it can be applied to any type of image and application. The detailed stages involved in the GFRIS algorithm may be formalised as follows: -

Algorithm 3.2 GFRIS

---

1. Classify the pixels of an image into a desired number of regions using any appropriate clustering algorithm.

2. Derive the key weight w_2 and threshold value by applying the data-mining Algorithm 3.1 and the membership function for each region pixel distribution (Section 3.1.1).

3. Initialise the centre of all regions required to define the membership function in Section 3.1.2, with the respective centres produced in step 1.

4. Sequentially select an unclassified pixel from the image and calculate each membership function value in each region for that pixel.

5. Classify the pixel into a region applying the fuzzy rule (Definition 3.2).

6. Return to step 4 until every pixel is classified.

It is also noteworthy from a computational perspective, that since all three membership functions are independent of each other, the GFRIS algorithm possesses a high degree of inherent concurrency, which could be exploited by a parallel implementation, with a dedicated processor being used for each function.

3.4.2 Time-Complexity Analysis of the GFRIS Algorithm

3.4.2.1   Fundamental Assumption for the complexity analysis of GFRIS

Without loss of any generality, the following assumption is made for the sake of simplicity in the complexity analysis. Any perceptually meaningful object is considered the *region of interest* for

object-based image segmentation and hence the number of regions to be segmented is limited to a certain extent.

Assumption 3.1: The number of regions $\Re$ is so small compared with the total number of pixels n such that $\Re$ can be considered a constant, i.e. $O(1)$ with respect to n.

Unless otherwise annotated, the above assumption holds for the remainder of the thesis.

3.4.2.2   *Time-Complexity Analysis*

In the results in Chapter 7, FCM is applied to segment the original image into a desired number of regions to calculate region pixel distributions (Section 3.1.1). The following two Lemmas 3.2 and 3.3 describe the computational processing time required to derive the membership function for region pixel distributions, including the initial FCM segmentation: -

Lemma 3.2: Given n pixels in an image, the FCM algorithm can be completed in $O(n)$ time for calculating the region pixel distribution.

Proof: Let $\Re$ and ρ be the number of regions and the dimensions of a feature vector respectively. The overall time complexity of the FCM algorithm is $O(\Re^2 \rho n)$ [150]. Since the gray level pixel intensity is the only feature used to calculate the region pixel distributions, $\rho = 1$. Moreover, by applying Assumption 3.1, $\Re = O(1)$, so the overall complexity of the FCM algorithm in determining region pixel distributions will be $O(n)$.   ∎

Lemma 3.3: For an image containing n pixels, the membership function for region pixel distributions in Section 3.1.1, based on the initial segmentation using FCM, can be computed in $O(n)$ time.

Proof: Given n pixels in an image, the initial segmentation using FCM can be performed in $O(n)$ time using Lemma 3.2. The calculation of histograms and their normalisation also requires $O(n)$ time, while the polynomial approximation requires $O(256) = O(1)$ time [151]. The total time required for the region pixel distribution membership function is $O(n) + O(n) + O(1) = O(n)$.   ∎

The next pair of lemma deal with the computational complexity of the other two membership functions used in GFRIS.

Lemma 3.4: The membership function measuring the closeness of a region (Section 3.1.2) requires $O(n)$ time.

Proof: Let $\Re$ be the number of segmented regions then, the time to progressively calculate the centres using the previous centres and the membership function for each pixel in each region is $O(n)$ and $O(n\Re)$ respectively. As $\Re = O(1)$, the total time is $O(n) + O(n\Re) = O(n)$.   ∎

Lemma 3.5: Membership function for spatial relations (Section 3.1.3) can be computed in $O(n)$ time.

Proof: Let the number of neighbours considered in segmentation be η. The time required to count the neighbours and to calculate the membership function for each pixel of all regions can be determined in $O(n\eta)$ and $O(n\Re)$ respectively. Total time is $O(n\eta) + O(n\Re) = O(n)$ since η is a $f(r)$ where $r = O(1)$ with respect to n.   ∎

Lemma 3.6: The implementation time of the fuzzy rule (Section 3.2) is $O(n)$.   ∎

Lemma 3.7: Determining the weighting factors and the threshold values in Algorithm 3.2, can be completed in $O(n)$ time.

Proof: To calculate the standard deviations for all regions requires $O(n)$ time. Steps 2 and 6 of the Algorithm 3.2 can be computed at $O(\Re^2)$ time while the other remaining steps can be performed in $O(\Re)$. As $\Re = O(1)$, this algorithm needs time in $O(n) + O(\Re^2) + O(\Re) = O(n)$.   ∎

Lemma 3.8: The time-complexity of the GFRIS algorithm (Algorithm 3.2) is $O(n)$ time.

Proof: By applying Lemma 3.2, step 1 of requires time in $O(n)$. From Lemmas 3.3 and 3.7, steps 2 and 3 can be performed in $O(n)$ time. Steps 4 to 6 can also be completed in $O(n)$ time using the Lemmas 3.2 to 3.7.   ∎

In conclusion, Lemmas 3.2 and 3.8 and Section 2.1.2 prove that GFRIS has exactly the same computational complexity as FCM and PCM, $O(n)$ and as Chapter 7 will show, it provides significantly enhanced segmentation performance.

3.5 Discussion of the Performance of the GFRIS Algorithm

Section 7.5 will provide a complete analysis of the performance of the GFRIS algorithm, however in order to qualitatively illustrate the improvement obtained and also some limitations of using GFRIS, an example is included in this chapter.

The cloud image shown in Fig. 3.3(a) contains two regions (objects), namely cloud (R_1) and urban scene (R_2). The cloud (R_1) region is homogeneous, while the urban scene (R_2) has sharp variations in pixel intensity, i.e. it is non-homogeneous. The segmented results of the cloud image in Fig. 3.3(a) into two regions produced by GFRIS for $r=1$, FCM, and PCM algorithms are presented in Fig. 3.3 using a separate colour for each region so that both correctly and incorrectly classified pixels are visible.

(a) Cloud Image   (b) GFRIS, $r=1$ (c) FCM   (d) PCM
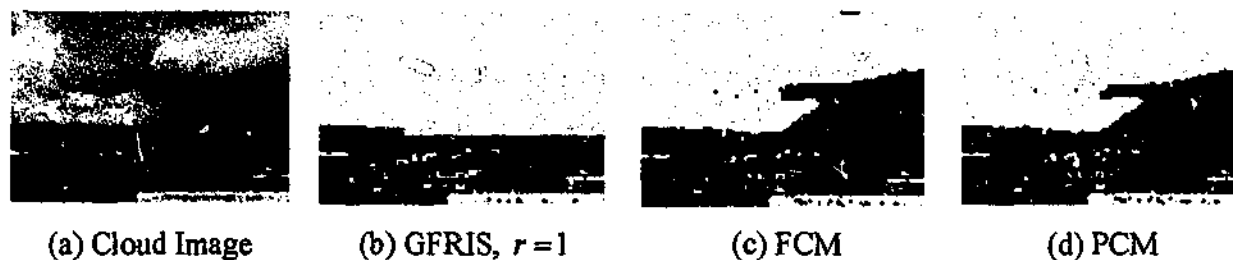
Fig. 3.3: The segmented results of the cloud image in Fig. 3.3(a) into two regions using the GFRIS, $r=1$, FCM, and PCM algorithms.

From the Fig. 3.3(b), it is clear that almost all of the pixels of the cloud (R_1) region have been correctly classified by GFRIS using $r=1$ because it is essentially a homogeneous region. A qualitative comparison of Fig. 3.3(b) to 3.3(d) reveals that GFRIS exhibited a substantial improvement over both FCM and PCM. The example in Fig. 3.3(b) also highlights however that GFRIS did not produce superior results for the urban scene (R_2) region, because it is a non-homogeneous region. A number of pixels in (R_2) have been misclassified into (R_1), which means a poorer performance for the non-homogeneous region. The reason for this is that one of the fundamental principles of GFRIS is proximity and good continuation and non-homogeneous regions violate this premise. Solutions to this problem will be presented in the subsequent chapters.

3.6 Summary

This Chapter has presented a new generic fuzzy rule-based image segmentation (GFRIS) algorithm, which crucially has incorporated spatial relationships between pixels. Chapter 7 will provide the analysis of performance of the GFRIS algorithm in comparison with both FCM and PCM.

A single fuzzy rule has been defined in order to classify the pixels, and three weighting factors w_1, w_2, and w_3 applied to stress the importance attached to feature based and spatial information in the image. Another important advantage of the GFRIS algorithm was that the structure of the membership functions and associated parameters were automatically derived and a new data-mining algorithm presented to determine both the key weighting factor and threshold value. The vital role of the threshold to the performance of GFRIS in controlling the maximum permitted pixel intensity variation between neighbouring and candidate pixels was highlighted.

A full computational complexity analysis has been presented and shown that it has exactly the same order $O(n)$ complexity as other segmentation algorithms FCM and PCM.

As GFRIS is fuzzy rule-based, the algorithm has the capability of incorporating any type of image attribute in any special application, by simply defining new membership functions, so making this solution both image and application independent.

As alluded in Section 3.5, the one major drawback of GFRIS is that it does not produce improved results for such regions. In order to improve the effectiveness of the GFRIS algorithm for non-homogeneous regions, the next chapter will introduce a generic segmentation refinement algorithm based on connectivity, surroundedness, uniformity, and contrast properties.

Fuzzy Rules for Image Segmentation: A Refinement Algorithm

The generic fuzzy rule-based image segmentation (GFRIS) algorithm, which has been articulated in the preceding chapter, attempted to solve a number of the identified limitations of modern fuzzy-based segmentation techniques. While GFRIS outperformed both FCM and PCM in segmenting many images, it did not prove to be so effective for image regions characterised by either being non-homogeneous or possessing sharp variations in pixel intensity. This is because it is developed mainly based on homogeneity and does not consider the two important properties of perceptual grouping, namely surroundedness and connectedness (see Section 3.5). To address these disadvantages, this chapter introduces *a new fuzzy rule-based refinement algorithm* called FRIS, which unifies the aforementioned properties of connectedness, surroundedness, uniformity and contrast (**Block 2** in Fig. 1.1). A full time-complexity analysis of the proposed FRIS algorithm is also presented in this chapter. An analysis and numerical evaluation of the results produced by this new refinement algorithm will be undertaken in Chapter 7.

This chapter is organised as follows: Section 4.1 illustrates the connectedness and surroundedness properties. Section 4.2 provides a brief description on the region splitting techniques and image preprocessing used. The underlying theory of the various membership and other functions used is described in Section 4.3, while the fuzzy rules applied in the FRIS algorithm are given in Section 4.4. The FRIS algorithm is formalised in Section 4.5, together with a detailed time-complexity analysis. Section 4.6 presents a representative performance of the FRIS algorithm to illustrate its potential.

4.1 Connectedness and Surroundedness

A topological relation of the parts or features of the data represents their mutual spatial as well as structural relationships [152]. Connectedness, a topological feature, indicates whether a

topological space is contiguous or not. A topological space, which cannot be divided into two disjoint, nonempty and closed sets, is called the *connected space*. For example, suppose φ_1 and φ_2 are two nonempty and closed sets of the set φ. φ will be disconnected when $\varphi_1 \cap \varphi_2 = 0$ and $\varphi = \varphi_1 \cup \varphi_2$ [153]. The neighbourhood system has already been defined in Definition 3.1, however in this chapter, a slightly different representation of neighbourhood system is defined for connectivity. For the sake of consistency, the definitions of δ – neighbourhood and δ – connectivity [154] are formally provided: -

Definition 4.1—δ-neighbourhood: The δ -neighbourhood $\zeta_\delta(P)$ of a candidate pixel P, is the set of all pixels P_i, such that $\zeta_\delta(P) = \left\{ P_i \middle| d(P_i, P) \le \frac{\delta}{4} \right\}$ where $\delta \in \{4,8\}$, $d(P_i, P) = |x(P_i) - x(P)| + |y(P_i) - y(P)|$ is the *city block distance*, with $x(P_i)$ and $y(P_i)$ being the x and y coordinates respectively of pixel P_i.

Definition 4.2—δ-connectivity: Let P_i and P_j be two neighbouring pixels, and R_i and R_j be two regions. Then $\delta - connected(P_i, P_j)$ and $\delta - connected(R_i, R_j)$ are defined as follows: -

$$\delta - connected(P_i, P_j) = \begin{cases} \text{true,} & \text{if } P_i \in \zeta_\delta(P_i); \\ \text{false,} & \text{otherwise.} \end{cases}$$

$$\delta - connected(R_i, R_j) = (\exists P_i \in R_i) \wedge (\exists P_j \in R_j) \wedge \\ \delta - connected(P_i, P_j)$$

As alluded in the previous chapter, surroundedness is one of the eight Gestalt perceptual principles, which implies that the surrounded areas could be interpreted as a single object [155, 156]. The surfaces of most natural objects are connected, oriented, and closed [157], so effective segmentation cannot be expected unless properties such as connectedness and surroundedness (closeness) have been incorporated. Exploitation of these two properties is rare in the image segmentation literature, and this is the first fuzzy rule-based segmentation technique to propose [2,

14, 12, 158] using them. In addition, other key features such as uniformity and the contrast properties of a group of pixels comprising an object are also incorporated with the overall goal of reducing the segmentation error due to non-homogeneity.

4.2 Region Splitting and Image Preprocessing

4.2.1 Initial Segmentation

The initial image segmentation phase may be undertaken using any standard segmentation algorithm [2, 14] (**Block 1** in Fig. 1.1). In this paper, the initial segmentation was performed using one of following three algorithms: - GFRIS [6], FCM [79], and PCM [82]. The results were subsequently refined using fuzzy rules based on the principles of connectedness, surroundedness, uniformity, and contrast criteria.

4.2.2 Region Splitting Techniques

This section discusses the splitting techniques applied to the initially segmented $\Re$ regions, represented by $R_j, j = 1,..., \Re$. Each region is split into a number of mutually exclusive objects using the 4-connected neighbourhood property. The reason for applying 4-connectedness in the splitting process, instead of the more usual 8-connectedness is to avoid weak connections within an object and also to maximize the number of possible objects in any region.

Let the set of all objects in region R_j be denoted as $\{O_{1j}, O_{2j}, ..., O_{n_j j}\}$ where n_j represents the number of 4-connected objects in that region. It is interesting to note that $O_{1j} \cup O_{2j} \cup ... \cup O_{n_j j} = R_j$ and $O_{1j} \cap O_{2j} \cap ... \cap O_{n_j j} = \phi$. Now let object $O_{m_j j}$, be the *main object* of region R_j, where $|O_{m_j j}| = \max\{|O_{1j}|, |O_{2j}|, ..., |O_{n_j j}|\}$ and $|Q|$ denotes the number of pixels in object (region) Q.

4.2.3 Image Preprocessing

The result from the initial segmentation of each region is split into a number of objects exploiting the connectedness property for refinement. Connectedness however assumes all background pixels have a gray level intensity of zero, so a DC level ΔI shift is introduced to ensure all pixel values are non-zero and positive. This requirement is also essential for the numerical evaluation of the segmented results, which will be discussed in Section 7.3. Concomitant with this objective is that any DC bias must not affect the visual perception of the image, and so it was empirically chosen that $\Delta I = 5$ during the preprocessing phase, as this provides an imperceptible change to 8-bit gray level images [84].

4.3 Defining the Membership and the Other Functions

Before detailing the new refining fuzzy rules, a collection of membership and other functions are firstly defined.

Surroundedness is by its very nature fuzzy, since any object may either be or not be entirely surrounded by another object. This leads to the definition of a membership function for estimating the degree of surroundedness of an object (region) A by another object (region) B as: -

$$\mu_S(A,B) = \frac{|A \cap B|}{|A|} \tag{4.1}$$

The largest object within a region R_k is designated as the *main object*, and its size is defined by the membership function $\mu_\ell(O_{m_k k}, R_k)$ as follows: -

$$\mu_\ell\left(O_{m_k k}, R_k\right) = \frac{\left|O_{m_k k}\right|}{|R_k|} \tag{4.2}$$

The segmented results of the Indira Gandi image shown in Fig. 4.1(a) for two regions, namely the person Indira Gandi (R_1) and background (R_2) produced by GFRIS, $r=1$ are shown in Fig. 4.1. The segmented result for the R_1 region and its main object are shown in Fig. 4.1(b) and

4.1(d) respectively. The size of the main object with respect to the segmented R_1 region (Fig. 4.1(b)) is 0.947 that is in this example, the main object is 94.7% of region R_1.

Two other functions, namely $\text{outer}(R_k)$ and $\text{large}(O_{m_k k}, R_k)$ can now be defined using (4.1) and (4.2) respectively. The former determines whether R_k is an outer region, which is the region not surrounded by any other region and encompassing all regions. This function is true provided the degree of surroundedness of every region, except R_k, is greater than or equal to the specified threshold ξ : -

$$\text{outer}(R_k) = \prod_{\substack{i=1 \\ i \neq k}}^{\Re} \left(\mu_S(R_i, R_k) \geq \xi \right) \tag{4.3}$$

The segmented result in Fig. 4.1(c) for the background R_2 region is an example of an outer region because it is not surrounded by any other region and also encloses the segmented R_1 region in Fig. 4.1(b).

| (a) | (b) | (c) | (d) |
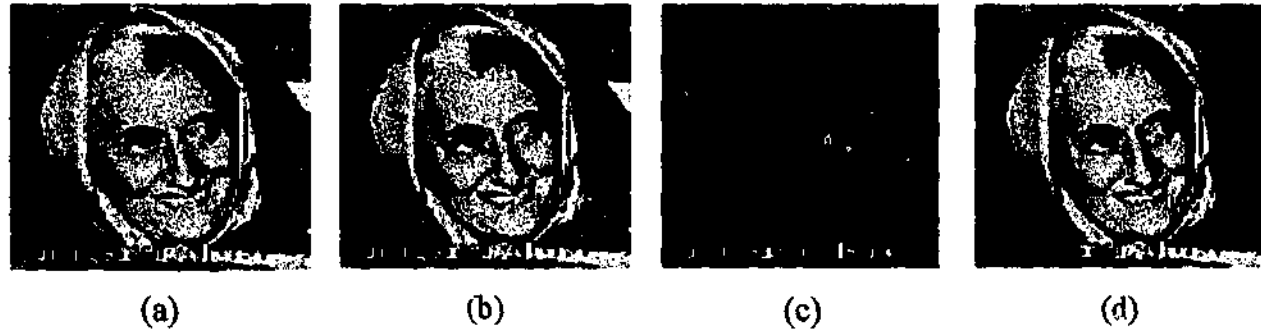
Fig. 4.1: Segmentation results of the Indira Gandi Image for two regions produced by GFRIS, $r = 1$, (a) Original Indira Gandi image, (b) Segmented Indira Gandi (R_1) region, (c) Segmented background (R_2) region, (d) The main object of the segmented Indira Gandi (R_1) region.

The $\text{large}(O_{m_k k}, R_k)$ function determines whether the *main object* $O_{m_k k}$ is sufficiently large with respect to its own region R_k, by using a threshold λ_1 that defines the minimum size of a *main object*. This function is formalized as follows: -

$$\text{large}\big(O_{m_k k}, R_k\big) = \begin{cases} \text{true,} & \text{if } \mu_\ell\big(O_{m_k k}, R_k\big) > \lambda_1; \\ \text{false,} & \text{otherwise.} \end{cases} \tag{4.4}$$

As mentioned above, the size of the main object in Fig. 4.1(d) for the segmented R_1 region (Fig. 4.1(b)) is 0.947. This is sufficiently large with respect to R_1 as it is greater than the predefined threshold λ_1 in (4.4), which is empirically set for all the experiments at 0.70.

Two other functions $uniformity\big(O_{ij}\big)$ and $contrast\big(O_{ij}\big)$ are also defined at this stage. Using a gray level histogram $hist(P_i)$, the occurrence probability for pixel intensity P_i in object O_{ij} is obtained, where n discrete gray-level values are assumed. The entropy is then used as a measure of the uniformity of the gray level distribution of object O_{ij} [10]: -

$$uniformity\big(O_{ij}\big) = -\sum_{i=0}^{n} hist(P_i)\log[hist(P_i)] \tag{4.5}$$

The standard deviation σ of the gray level probability distribution reflects the dynamic range of pixel values and is the preferred measure of contrast [144]. The kurtosis α, which represents the polarization of the distribution of the black and white on the gray level histogram (the ratio of black and white areas in the image), is given as [159]: -

$$\alpha = \frac{\Omega_4}{\sigma^4} \tag{4.6}$$

where Ω_4 is the fourth moment about the mean and the contrast of an object O_{ij}, $contrast\big(O_{ij}\big)$ is defined as: -

$$contrast\big(O_{ij}\big) = \frac{\sigma}{(\alpha)^\varsigma} \tag{4.7}$$

where ς is a positive number in the range $\left[\frac{1}{8}, 8\right]$, which is empirically selected as 0.25.

By now using (4.5) and (4.7), the membership function $\text{similar}(O_{m_k k}, O_{ik})$ can be defined as a measure of the similarity between a main object $O_{m_k k}$ and its siblings (all other objects O_{ik} belonging to the same region): -

$$\text{similar}(O_{m_k k}, O_{ik}) = \begin{pmatrix} |\text{uniformity}(O_{m_k k}) - \text{uniformity}(O_{ik})| \\ \leq \chi |\text{uniformity}(O_{m_k k})| \end{pmatrix}$$
$$\wedge \left(|\text{contrast}(O_{m_k k}) - \text{contrast}(O_{ik})| \leq \chi |\text{contrast}(O_{m_k k})| \right) \tag{4.8}$$

where χ is the maximum permitted percentage variation in the similarity measure.

To define the final function, let

$$\text{maxs}(O_{ij}) = \left\{ k \middle| \mu_S(O_{ij}, O_{m_k k}) = \max_{\substack{1 \leq l \leq \Re \\ l \neq j}} (\mu_S(O_{ij}, O_{m_l l})) \right\}$$

be the set of indices of all regions for which the degree of surroundedness of an object O_{ij} of another region, by the *main objects* of those regions, is a maximum. The function $\text{connect}_\delta(O_{ij})$ represents the set of indices of those regions returned by $\text{maxs}(O_{ij})$ for which object O_{ij} is $\delta - connected$ (Definition 4.2) with the *main object* of another region $O_{m_k k}$.

$$\text{connect}_\delta(O_{ij})$$
$$= \left\{ k \middle| k \in \text{maxs}(O_{ij}) \wedge \delta - \text{connected}(O_{ij}, O_{m_k k}) \right\} \tag{4.9}$$

All these functions are now used in defining the FRIS rules in the following section.

4.4 Defining Fuzzy Rules

As was discussed in Chapter 3, the fuzzy rule definitions are the most important and challenging aspect of fuzzy rule-based image segmentation. In the refinement phase, three different classes of fuzzy rules are heuristically defined covering three totally different scenarios.

There will always exist the possibility after the initial image segmentation, of obtaining a small *main object*, that is an object less than or equal to $\lambda_1 \times 100\%$ of its region (see (4.4)), after splitting. This is very much dependent upon the pixel distribution of the regions and the type of objects in an image. If the *main object* of a region is not sufficiently large it will be unable to enclose all the other objects or components in that region. To address such a problem, any small *main objects* (except the *main object* of the outer region) need to be grown, as otherwise the new refinement algorithm will wrongly classify these objects, leading to poor segmentation results.

The *main object* of the outer region is prevented from being grown as otherwise objects inside this region may be incorrectly merged with its *main object*. As mentioned in Section 4.3, the outer region encapsulates all other regions and in general, the outer region is a background region. The first fuzzy rule definition, called the *growing up rule*, has the express purpose of growing small *main objects* according to the similarity between the *main object* and its *siblings*, provided the *main object* is not the *main object* of the outer region. The growing up rule is defined as: -

Definition 4.3—Growing Up Rule: *IF NOT* $\text{large}\!\left(O_{m_k k}, R_k\right)$ *AND NOT* $\text{outer}\!\left(R_k\right)$ *AND* $\text{similar}\!\left(O_{m_k k}, O_{ik}\right)$ *THEN merge* O_{ik} *with* $O_{m_k k}$.

(a)   (b)   (c)
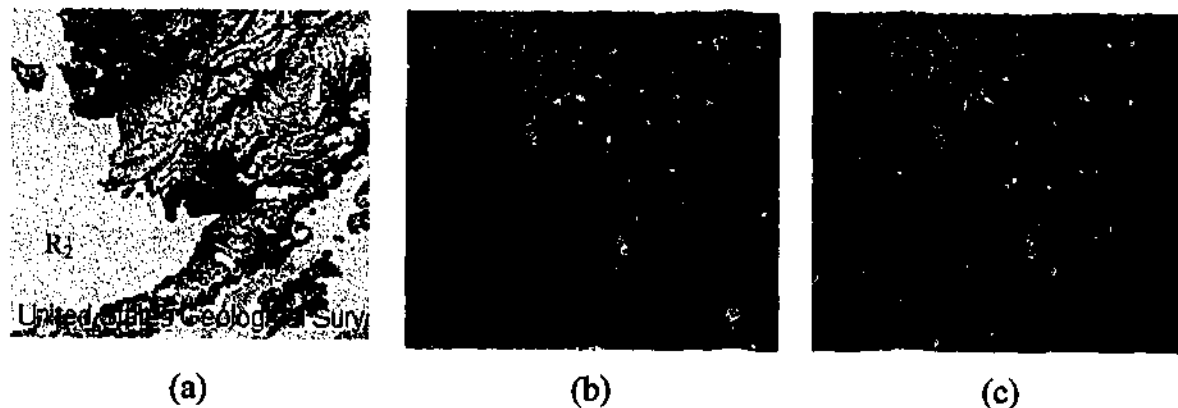
Fig. 4.2: Example of a main object, (a) Original aerial image (b) Segmented land region $\left(R_1\right)$ of the aerial image produced by GFRIS, $r = 1$, (c) The main object of the land region after splitting based on 4-connectedness.

Some objects of a region may be enclosed by the *main object* of another region, but not covered by their own *main object*. In such circumstances, the objects will be misplaced even though their own *main object* is large. For example, the aerial image in Fig. 4.2(a) has two regions, namely land

(R_1) and water (R_2). The segmented land (R_1) region produced by GFRIS, $r = 1$ and its main object are shown in Fig. 4.2(b) and 4.2(c) respectively. It is obvious that the main object in Fig. 4.2(c) of the land (R_1) region does not cover all the objects in R_1 and that all the parts, except the main object of R_1 are enclosed by the other region, namely the water (R_2) region.

To address this matter, three conditions are tested to see if (a) such objects are similar to their *main object*, (b) whether the size of their *main object* lies between the range $(\lambda_1, \lambda_2]$, and (c) their region is not an outer region. If all three conditions are met then these objects are prevented from merging with any other *main object* by applying the following fuzzy definition, called the *preventive rule*.

Definition 4.4—Preventive Rule: *IF* similar$(O_{m_k k}, O_{ik})$*AND* $\lambda_1 < \mu_\ell(O_{m_k k}, R_k) \le \lambda_2$ *AND NOT* outer(R_k)*THEN prevent* O_{ik} *from merging.*

The final set of definitions concern a group of mutually exclusive merging rules, which are applied to coalesce suitable objects with the *main objects* of other regions, based upon the principles of connectedness and surroundedness. 8-connectedness is selected for merging in order to consider all possible connected objects, including those with weak connections. If there is one maximum degree of surroundedness of an object by the *main object* of another region, the degree of surroundedness is greater than or equal to the threshold ξ, and the object is 8-connected with that main object, the object is merged using the first merging *rule*: -

Definition 4.5—Merging Rule 1: IF $|maxs| = 1$ AND $\mu_S(O_{ij}, O_{m_k k}) \ge \xi$ AND $8-$connected$(O_{ij}, O_{m_k k})$ THEN merge O_{ij} with $O_{m_k k}$.

Two other merging rules (2 and 3) are also defined for selecting the most suitable surrounding main object. If there is more than one maximum degree of surroundedness of an object, the smallest 4-connected main object is selected, provided there are 4-connected main objects (merging rule 2), otherwise the smallest 8-connected main object is chosen for merging (merging rule 3).

Definition 4.6—Merging Rule 2:   IF $|maxs| > 1$ AND $\mu_S\left(O_{ij}, O_{m_k k}\right) \geq \xi$ AND

$4 - \text{connected}\left(O_{ij}, O_{m_k k}\right)$ THEN   merge O_{ij} with $O_{m_k k}$ such   that

$\mu_I\left(O_{m_k k}, R_k\right) = \min\limits_{reconnect_4\left(O_{ij}\right)}\left\{\mu_\ell\left(O_{m,r}, R_r\right)\right\}$.

Definition 4.7—Merging Rule 3:   IF $|\text{maxs}| > 1$ AND $\mu_S\left(O_{ij}, O_{m_k k}\right) \geq \xi$ AND

$8 - \text{connected}\left(O_{ij}, O_{m_k k}\right)$ THEN   merge O_{ij} with $O_{m_k k}$ such   that

$\mu_I\left(O_{m_k k}, R_k\right) = \min\limits_{reconnect_8\left(O_{ij}\right)}\left\{\mu_\ell\left(O_{m,r}, R_r\right)\right\}$.

Note, that in all the above definitions, it is assumed $k \neq j$ to ensure that object O_{ij} always merges with the main object $O_{m_k k}$, of another region. The perceptual selection of all the various parameters used by the fuzzy rules namely, λ_1, λ_2, ξ, and χ have been also proven to be suitable for all image types. The complete FRIS algorithm will now be described using the defined membership and other functions (Section 4.3) and the above fuzzy rules.

4.5 The FRIS Algorithm

4.5.1 The Algorithm

The FRIS segmentation refinement algorithm can be formalised in the following steps: -

Algorithm 4.1 FRIS

Precondition: Initially segmented image regions using any standard segmentation algorithm such as FCM [79] or PCM [82] or GFRIS [6] (**Block 5** in Fig. 1.1).

Postcondition: Refined segmented regions.

1. Each segmented regions is split into a number of objects based upon 4-connected neighbourhoods. The *main object*, that is the object in each region containing the maximum number of pixels, is then determined.

2. If the size of the *main object* of a region is small, and it is NOT an outer region, then it is grown using *the growing rule* (Definition 4.3).

3. Objects in a region, except the outer region, which are similar to their *main object*, are prevented from merging with the *main object* of another region by applying the *preventive rule* (Definition 4.4).

4. A candidate object is tested for merging with the main objects of another region based on one of the three merging rules (Definitions 4.5, 4.6, and 4.7).

5. If the object is merged, the algorithm repeats for all other objects, which were previously surrounded but not connected to the merged *main object*.

6. Return to step 4 until all candidate objects have been merged.

4.5.2 Time-Complexity Analysis of the FRIS Algorithm

As with GFRIS, a computational complexity of the FRIS algorithm is presented by applying a series of lemmas. In order to calculate the degree of surroundedness, firstly the boundary, i.e the convex hull of the main object, needs to be computed and secondly a decision needs to be made as to whether a particular pixel lies inside the convex hull. The first pair of lemmas consider the former.

Lemma 4.1 [151]: The convex hull of n pixels can be computed in $O(n \log n)$ time.   ∎

Lemma 4.2: Consider a region of n pixels whose height and width are of $O(\sqrt{n})$. The convex hull of this region can be computed in $O(n)$ time.

Proof: The region can have at most $4 \times O(\sqrt{n}) = O(\sqrt{n})$ boundary pixels and these boundary pixels can be found for both the average and worst cases in $O(n)$ time. The convex hull of the region can now be computed using only the boundary pixels in $O(\sqrt{n} \log \sqrt{n})$, so that the total time required to construct the convex hull is $O(n) + O(\sqrt{n} \log \sqrt{n}) = O(n)$.   ∎

The next is to calculate the computational complexity for deciding whether a pixel lies inside the convex hull of the main object i.e. the convex polygon. This is defined using the following lemma: -

Lemma 4.3 [151]: The decision as to whether a pixel lies inside the convex polygon having N vertices can be determined in $O(\log N)$ time. ■

Lemma 4.4: The decision as to whether a pixel lies inside the convex hull of a region of n pixels, whose height and width are of $O(\sqrt{n})$, can be determined in $O(\log\sqrt{n})$ time.

Proof: In the proof for Lemma 4.2, it was shown that such a region has a maximum of $O(\sqrt{n})$ boundary pixels and hence the convex hull of that region will be a polygon of at most $O(\sqrt{n})$ vertices. Applying Lemma 4.3, the decision can therefore be made in $O(\log\sqrt{n})$ time. ■

Let A and B be two objects (regions) whose height and width are bounded by $O(\sqrt{|A|})$ and $O(\sqrt{|B|})$ respectively. By using Lemma 4.4, it can be easily shown that the number of pixels $\in A$ that lie inside the convex hull of B can be determined in $O(|A|\log\sqrt{|B|})$ time. In the worst case, both $|A|$ and $|B|$ will be $O(n)$, where n is the number of pixels in the image. Thus, for an image with n pixels, the membership function for the degree of surroundedness defined in (4.1), and the two functions (4.3) and (4.9) can computed in $O(n\log\sqrt{n})$ time, while membership functions (4.2) and (4.8), as well as function (4.4) can be computed in $O(n)$ time.

Lemma 4.5 [160]: The connected components of a set of n pixels can be found in $O(n)$ time.

■

Lemma 4.6: Given n pixels in an image, the FRIS algorithm can be completed in $O(n\log n)$ time.

Proof: Based on Lemma 4.5, step 1 of the FRIS algorithm (Section 4.5) can be performed in $O(n)$ time. All the membership and other functions (Section 4.3) required for steps 2 and 3 can be computed in $O(n)$ time, so by inference steps 2 and 3 can also be completed in $O(n)$ time. To evaluate the time-complexity for steps 4, 5, and 6, let S_j be the total number of surrounded objects, and C_j be the total number of both surrounded and connected objects of other regions with the *main object* of the jth region, where $C_j \le S_j$. As step 5 of the FRIS algorithm points out, after the

merging of an object, all other objects that were previously surrounded, but not connected to the *main object*, are recursively tested for connectedness and hence for merging. Step 6 confirms the iterative nature of the algorithm for all candidate objects. Given $\Re$ segmented regions, in the worst case, the total number of recursions required to check for connectedness is: -

$$n_c = \sum_{j=1}^{\Re} \sum_{i=0}^{C_j-1} (S_j - i) = \sum_{j=1}^{\Re} \left[S_j C_j - C_j (C_j - 1)/2 \right] \qquad (4.10)$$

Main objects will dominate the major proportion of image pixels and even if this is relatively small, it will be increased using the growing-up rule (Definition 4.3 in Section 4.4). The number of objects will therefore be negligible compared with the number of pixels. All split objects may not be surrounded by the main objects of other regions and some objects, similar to their main object, will be prevented from merging in the algorithm (Definition 4.4), so the total number of surrounded objects is generally less than the total number of split objects, so $C_j \leq S_j$, which yields $n_c \ll n$. Since the maximum order of the time-complexity of the membership functions and functions in steps 4 and 5 is $O(n \log \sqrt{n})$, the time-complexity for the entire FRIS algorithm will be the same $O(n \log \sqrt{n})$, i.e., $O(n \log n)$.   ∎

4.6 Discussion of the Performance of the FRIS Algorithm

As with GFRIS, a qualitative example is included in this chapter to illustrate the main advantages and problems associated with using this refinement algorithm. Overall, the FRIS algorithm has shown significantly improved results when the initial algorithm is able to separate the regions. The results produced by GFRIS, $r = 1$ and PCM for the Brodatz texture segmentation for two regions, namely d8 (R_1) and d94 (R_2) without and with the FRIS algorithm are shown in Fig. 4.3. If the segmented result produced by GFRIS, $r = 1$ shown in Fig. 4.3(b) is compared with the result produced by GFRIS, $r = 1$ incorporating the new refinement rules (Fig. 4.3(c)), it is visually apparent that FRIS gives an improved segmentation. This will be discussed fully in Chapter 7.

Since FRIS is a refinement algorithm, however, its performance depends very much on the effectiveness of the initial segmentation. If the result of the initial segmentation is poor for a region

(object), the FRIS algorithm will produce little or no improvement for that particular region (object).

To confirm this, the segmented result in Fig. 4.3(c) shows that PCM could not separate d8 (R_1) from d94 (R_2) at all and for this reason, FRIS provided very little improvement upon the results produced by PCM for this image, especially the d8 (R_1) region (Fig. 4.3(d)).

(a)   (b)   (c)   (d)   (e)
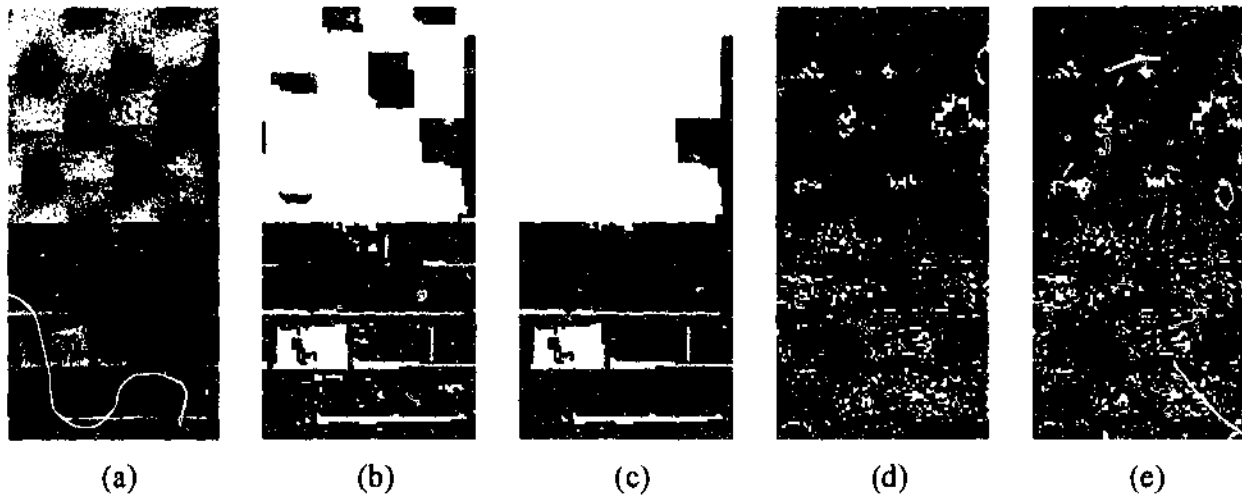
Fig. 4.3: An example of Brodatz texture segmentation into two regions, (b) Original Brodatz texture (d8 and d94), (b) Segmented results produced by GFRIS, $r=1$, (c) Segmented results produced by GFRIS, $r=1$ with using FRIS, (d) Segmented results produced by PCM, (e) Segmented results produced by PCM with using FRIS.

Thus far in the framework (Fig. 1.1), texture has not been directly considered. The GFRIS algorithm described in Chapter 3 was unable to resolve accurately non-homogeneous regions, while the refinement rules in FRIS are very dependent on the initial segmentation. There is clearly scope for integrating texture into the basic GFRIS algorithm. This is the motivation behind the algorithm that will be presented in the next chapter.

4.7 Summary

This chapter has shown that the characteristics of both connectedness and surroundedness are not only very important in providing high-level visual features, but also can play a vital role in reducing and eliminating segmentation errors. A new image segmentation refinement algorithm

called, *fuzzy rule-based refinement algorithm* (FRIS) has been presented that exploits the principles of connectedness, surroundedness, uniformity, and contrast properties amongst an object's pixels. Objects were defined as a 4-connected component of a region's pixels, when splitting the regions into objects to avoid weak connections between objects. During the merging however, 8-connectedness was used to explore all possible connections. A set of fuzzy rules covering the growing of a small main object, preventing similar siblings from merging with other main objects, and selecting the best surrounding main object were defined in this new algorithm. The growing and prevention rules handled a disconnected object if there existed some similarity based on uniformity and contrast between the different components of that object. The algorithm was tested using a wide variety of images types containing different numbers of regions.

The time complexity of the new algorithm was analysed and shown to be $n \log n$. The initial segmentation can be performed using any suitable standard segmentation algorithm.

The FRIS algorithm produced significant improvement, however, it depends very much on the initial segmentation (see Section 4.5). As mentioned in Section 3.5, GFRIS could not produce good results for non-homogeneous region and does not directly consider texture. In this context, it needs to develop the original GFRIS algorithm by incorporating texture, which will be fully explained in the next chapter.

Fuzzy Rule for Image Segmentation Incorporating Texture Features

Section 4.6 has shown that the segmentation performance of the FRIS algorithm depends very much on the initial segmentation. The generic fuzzy rule-based image segmentation (GFRIS) algorithm does not produce good results for images containing non-homogeneous regions (see Section 3.5). This means it does not directly consider texture, however, texture is one of the most important attributes of any image. It represents the structural arrangement of the surfaces as well as the relations among them and is widely used in image segmentation [131]. Most natural images contain textures, some examples of which include the Brodatz (d12) and background textures given in Fig. 5.1.

(a)   (b)
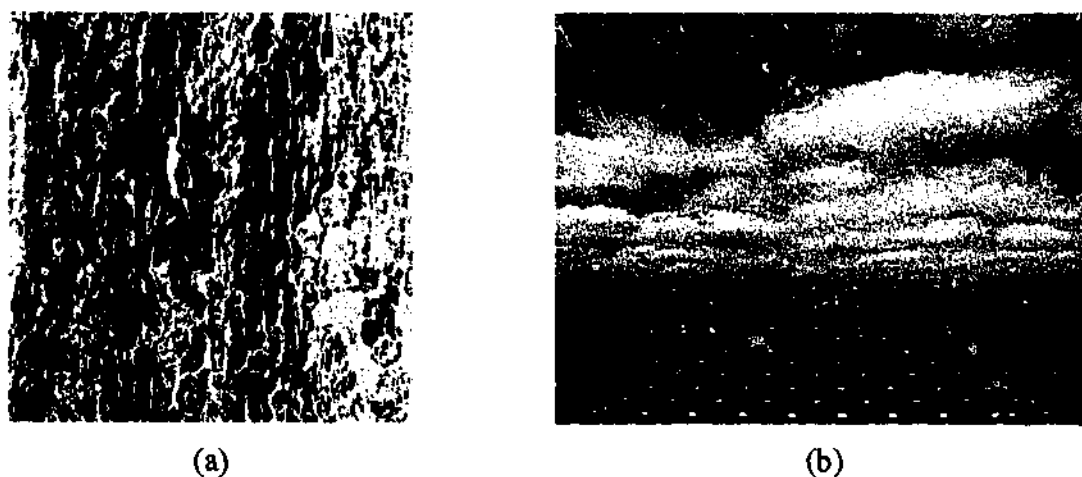
Fig. 5.1: Examples of textural images, (a) Brodatz texture (d12), (b) Background texture.

It needs to be emphasised that this chapter deals with a very challenging task, incorporating texture together with spatial relations. This is however, a fundamental contradiction since texture directly opposes spatial relations. The latter as has been highlighted in Chapter 3, is usually

measured based on the principles of proximity and good continuation, while texture clearly is not. For this reason, the variation amongst neighbourhood pixels must be controlled and kept within a limit using a threshold for spatial relations. If the variation exceeds this limit for a pixel, it will not be considered a neighbourhood of the candidate pixel. Using this rationale, highly textural surfaces, which exhibit sharp variations that oppose the principle of spatial relations defined in Section 3.1.3, can therefore still be considered and membership functions that represent texture can be integrated in the fuzzy rule-based framework.

In this chapter a new algorithm called *fuzzy rule for image segmentation incorporating texture features (FRIST)* is proposed, which includes two additional membership functions to those already defined in the framework (**Block 1** in Fig. 1.1). FRIST (**Block 3** in Fig. 1.1) incorporates the fractal dimension (FD) and contrast features of a texture by considering image domain specific information. Quantitative evaluation of the performance of FRIST will be discussed and contrasted with GFRIS in Chapter 7.

This chapter is organised as follows: Section 5.1 briefly describes the fractal dimension and the differential box-counting method. In Section 5.2, the membership functions used in the FRIST algorithm are described. The definition of the fuzzy rule, and also the determination of the weighting factors are presented in Sections 5.3 and 5.4 respectively. The FRIST algorithm as well as its time-complexity analysis is given in Section 5.5. The performance of the FRIST algorithm is discussed in Section 5.6.

5.1 Fractal Dimension Representation

A set whose Hausdorff-Besicovitch dimension is strictly greater than its topological dimension is called a fractal set [161]. The central notion of fractal is the concept of self-similarity, which is used in estimating the fractal dimension. A self-similar set (A) is the union of N_r mutually exclusive copies of itself that are similar to A and scaled down by a ratio r where $r < 1$. The FD of A can then be defined as,

$$1 = N_r r^{FD} \Rightarrow FD = \frac{\log N_r}{\log(1/r)} \tag{5.1}$$

Most natural objects are full of textures, which are very complex and erratic in nature and cannot be readily approximated using classical geometry. Fractal dimension (FD) has been chosen to describe these high degrees of irregularity and complex behaviour of the surface of the natural

objects [134] because as described in Section 2.3, it offers scale insensitive and uniform surface behaviour. In describing such erratic behaviour of objects, it is very important to consider the domain specific information of that object for image segmentation, which will be discussed shortly. A brief overview of texture representation and the rationale of choosing fractal dimension to estimate the texture have already been presented in Section 2.3. FD can be derived in a variety of ways but the motivation in this research is to use an efficient differential box-counting (DBC) method as it is faster and more efficient than other methods [131] and is suitable for incorporating image domain specific information.

5.1.1 Differential Box Counting (DBC) Method

The estimation of FD using the DBC method [134] is described as follows: -
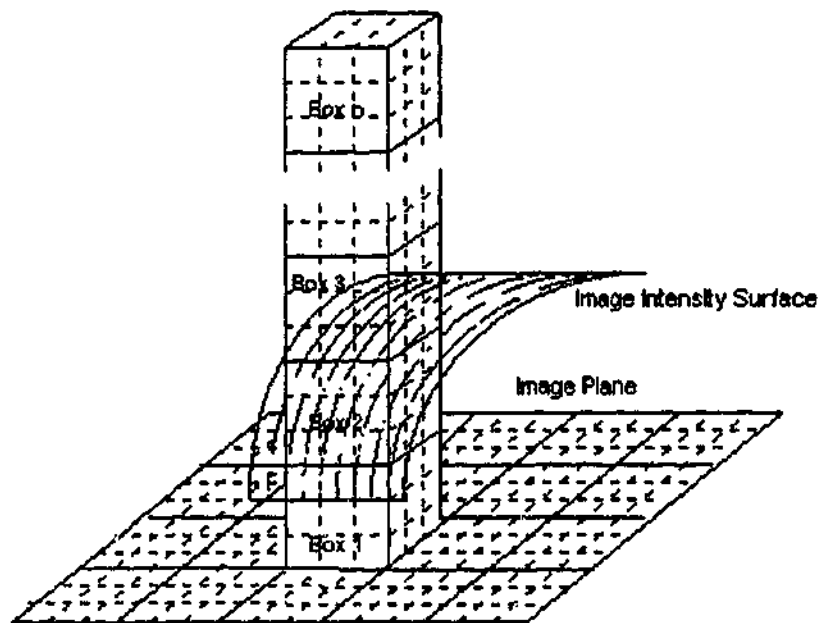
Fig. 5.2: Estimation of n_r using the DBC method [162].

For an image of size $M \times M$ to be scaled down to a size of $x \times x$ where $2 \leq x \leq \lfloor M/2 \rfloor$, the ratio of scale down is $\tau = x/M$. The image is then extended into 3-D space by introducing a 3rd co-ordinate for the 8-bit gray level intensity of 256 levels. If the image is partitioned into grids of size $x \times x$, then each grid will comprise a column of boxes of size $x \times x \times x'$ shown in Fig. 5.2, which implies $\lfloor 256/x' \rfloor = \lfloor M/x \rfloor$. If the maximum and minimum gray level values in the $(u, v)^{th}$ grid are

in the lth and k^{th} boxes, the thickness of the blanket (surface variations) covering the image surface on the grid (u,v) is: -

$$n_\tau(u,v) = l - k + 1 \tag{5.2}$$

Since the blanket effectively describes the surface variations of the image, the smaller the size of the grid, the greater their number and the finer the variations of the surface though of course this commensurately increases computational complexity. For the example, in Fig. 5.2, the blanket thickness is $n_\tau(u,v) = 3 - 1 + 1 = 3$. The contribution from all the grids defining the blanket is: -

$$N_\tau = \sum_{u,v} n_\tau(u,v) \tag{5.3}$$
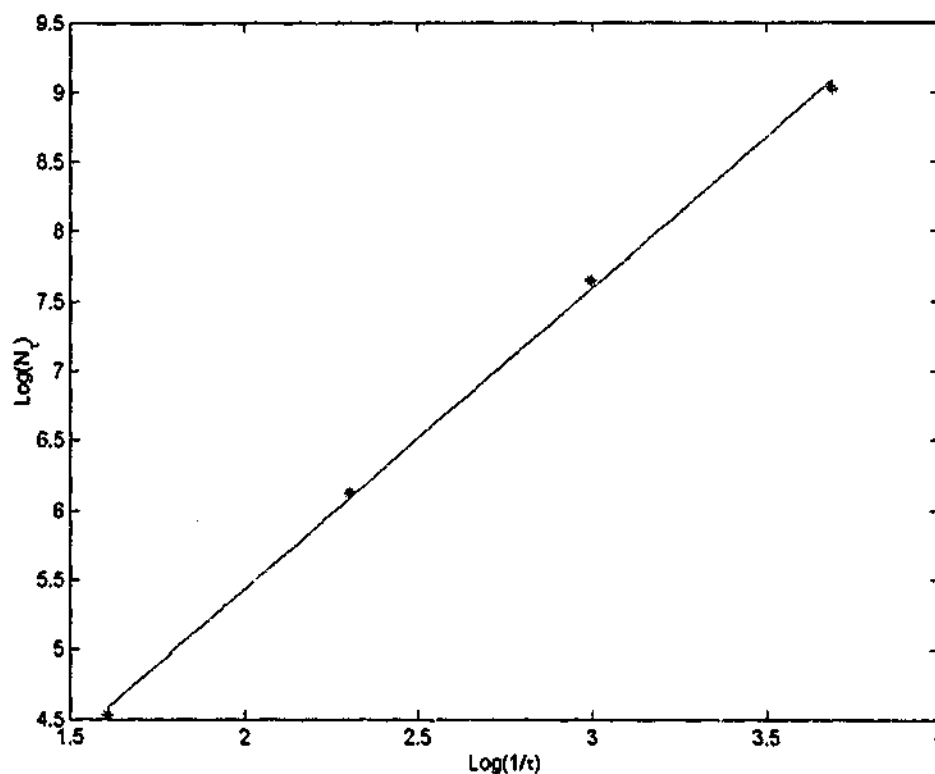
Fig. 5.3: Least square linear fit of $\log(N_\tau)$ versus $\log(1/\tau)$ of the cloud image in Fig. 3.1(a).

The value of N_τ is calculated using different values of τ. The FD can then be estimated as the slope of the least square (LS) linear fit of $\log(N_\tau)$ against $\log(1/\tau)$ using (5.1), an example of which, for the cloud image in Fig. 3.1(a), is shown in Fig. 5.3.

5.2 Membership Functions

The GFRIS algorithm, described in Chapter 3, uses three types of membership functions to represent the region pixel distributions (Section 3.1.1), the closeness to their centres (Section 3.1.2), and the spatial relations among the pixels in a particular region (Section 3.1.3). Each membership function possesses a membership value for every region, which indicates the degree of belonging to that particular region. FIRST incorporates two additional membership functions based on the fractal dimension and contrast features of a texture by considering image domain specific information. A detailed description of these new membership functions is provided in the following section.

5.2.1 Membership Functions for Fractal Dimension

Fractal dimension (FD) is used to estimate the texture in an image. To define the membership function for fractal dimension, *the fractal dimension based feature* (FDF) of a candidate pixel $P_{s,t}$ is used. Since the DBC method has been chosen to calculate the FDF for a candidate pixel, it is necessary to consider all the neighbourhoods around the candidate pixel in a window. The FDF of a candidate pixel $P_{s,t}$ is calculated on a window $W_{h,h}(s,t)$ of size $h \times h$ with its centre at (s,t) (see Fig. 5.4) rather than the entire image and defined as: -

$$FDF(P_{s,t}) = FD(W_{h,h}(s,t)) \tag{5.4}$$

where $FD(W_{h,h}(s,t))$ denotes the FDF on $W_{h,h}(s,t)$ derived using the DBC method in the following manner. The bound of the grid size is chosen as $2 \leq \xi \leq \lfloor h/2 \rfloor$, the scale down ratio $\tau = \lfloor \xi/h \rfloor$ and in order to consider the finer variations of the gray level values or the surface, x' is taken as $\lfloor 256 \times \xi / height \rfloor$ where $height$ is the height of the image.

The value of $FD(W_{h,h}(s,t))$ will not be the exact fractal dimension of the window $W_{h,h}(s,t)$ because the height of the image is used in calculating x' rather than the height of the window, h.
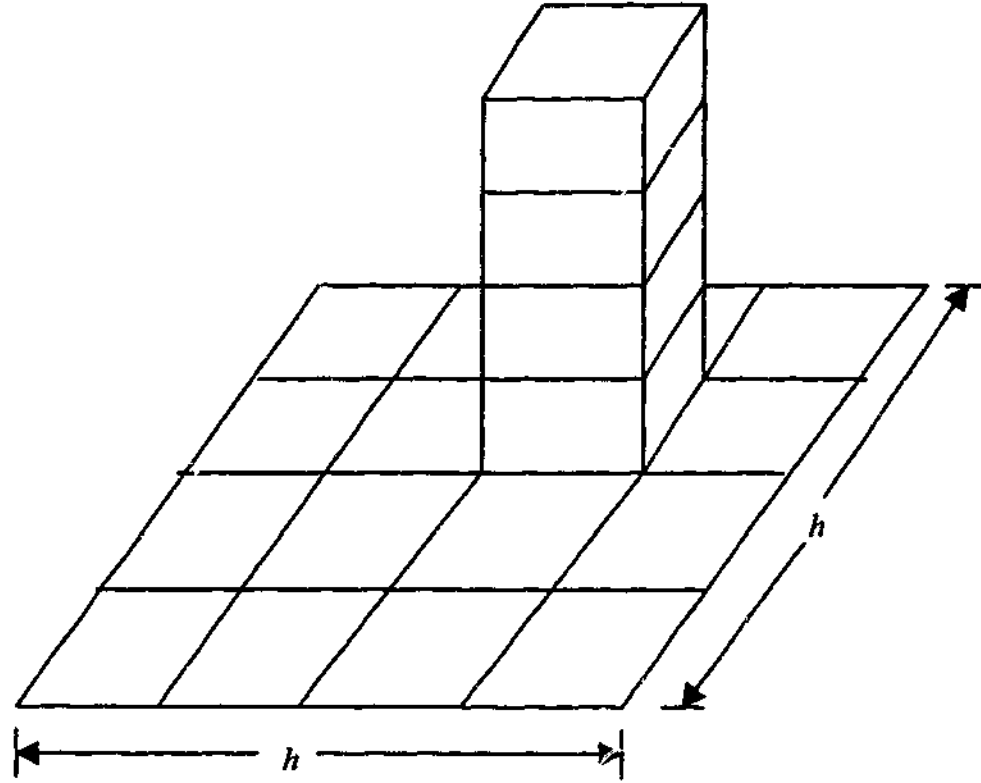
Fig. 5.4: A column of boxes on the (s,t) grid in the window $W_{h,h}(s,t)$ for calculating the fractal dimension based feature (FDF).

Fig. 5.4 shows an example of a window $W_{h,h}(s,t)$ together with all its grids and the column of boxes on grid (s,t) required to calculate the FDF of the candidate pixel $P_{s,t}$. Instead of considering the log-log plot in Fig. 5.3 to reduce computational complexity, the average value of $\log(N_\tau)/\log(1/\tau)$ is used to obtain the fractal dimension. The membership function $\mu_{FR_j}(P_{s,t})$ of fractal dimension based feature for the region R_j and the pixel $P_{s,t}$ is formulated as: -

$$\mu_{FR_j}(P_{s,t}) = 1 - \frac{\left| FDF_{R_j}(P_{s,t}) - FDF_I(P_{s,t}) \right|}{\max\{FDF_{R_j}(P_{s,t}), FDF_I(P_{s,t})\}} \tag{5.5}$$

where $FDR_{R_j}(P_{s,t})$ and $FDF_I(P_{s,t})$ are the fractal dimension based features for the segmented region R_j and the original image respectively, so this membership function does consider image domain specific information for segmentation. $FDF_I(P_{s,t})$ is determined from the ratio of the

number of contributory and total grids during the corresponding $FDF_{R_j}(P_{s,t})$ calculation for each value of τ.

As an example, the window $W_{h,h}(s,t)$ shown in Fig. 5.5 is scaled down by a ratio $\tau = 1/2$, so the four resulting grids are represented by different colours. Some grids in the window of a segmented region will not be filled with previously classified pixels, especially those grids containing pixels that have already been classified into another region and that will be referenced later. Assume that the grids containing the blue circles are already classified into a segmented region R_j. These grids are called contributory grids for the regions R_j as only these grids will be used in calculating the FDF for this region.

In the Fig. 5.5 example there are four grids in total and two of them are contributory, so the ratio of the contributory grids in this example will therefore be $2/4 = 0.5$. For the sake of accuracy, it is essential that in the membership function defined in (5.5) between the region R_j and the original image, the proportion of the FDF of the original image, for a specific value of the ratio of the scale down, is always considered.
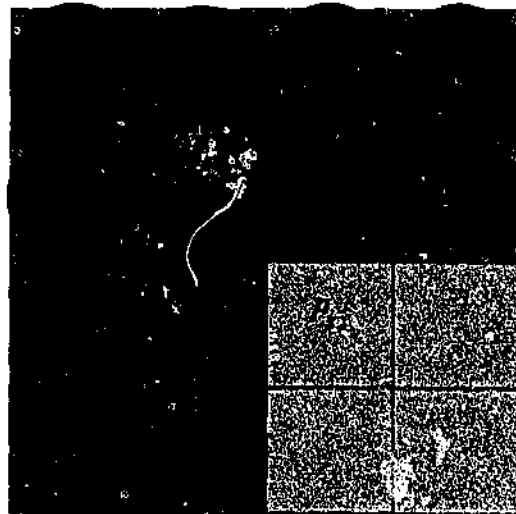
Fig. 5.5: Window $W_{h,h}(s,t)$ located in a segmented region R_j

for a specific value of the scale down ratio $\tau = 0.5$.

5.2.2 Membership Functions for Contrast

Contrast provides the measure of the texture of an image and is measured by considering the dynamic range of gray levels and the polarization of the distribution of black and white on the gray level histogram. The contrast of a window $W_{h,h}(s,t)$ in an image is calculated using the technique described in [159]. The membership function for the contrast of the region R_j and the pixel $P_{s,t}$ can be defined as: -

$$\mu_{C_t R_j}(P_{s,t}) = 1 - \frac{\left| contrast_{R_j}(P_{s,t}) - contrast_I(P_{s,t}) \right|}{\max\left(contrast_{R_j}(P_{s,t}), \ contrast_I(P_{s,t}) \right)} \tag{5.6}$$

where $contrast_{R_j}(P_{s,t})$ and $contrast_I(P_{s,t})$ represent the contrast of the portions of the segmented region R_j and the original image covered by the window $W_{h,h}(s,t)$ respectively. Again note that image domain specific information is incorporated into this membership function.

5.3 Defining the Fuzzy Rule

The original fuzzy rule defined in Section 3.2 has utilised three membership functions. In this section the fuzzy rule is heuristically defined incorporating two additional membership functions, which relate to texture, namely FD and contrast.

The overall membership value $\mu_{AR_j}(P_{s,t}, r)$ of a pixel $P_{s,t}$ for region R_j represents the overall degree of belonging to that region, and is defined by the weighted average of the five individual membership function values $\mu_{DR_j}(P_{s,t})$, $\mu_{CR_j}(P_{s,t})$, $\mu_{NR_j}(P_{s,t}, r)$, $\mu_{FR_j}(P_{s,t})$, and $\mu_{C_t R_j}(P_{s,t})$.

$$\mu_{AR_j}(P_{s,t}, r) = \frac{w_1 \mu_{DR_j}(P_{s,t}) + w_2 \mu_{CR_j}(P_{s,t}) + w_3 \mu_{NR_j}(P_{s,t}, r)}{\sum_{i=1}^{5} w_i}$$
$$+ \frac{w_4 \mu_{FR_j}(P_{s,t}) + w_5 \mu_{C_t R_j}(P_{s,t})}{\sum_{i=1}^{5} w_i} \tag{5.7}$$

where w_1, w_2, w_3, w_4, and w_5 are the weightings of the membership values for pixel distribution, closeness to the cluster centres, neighbourhood relations, fractal dimension, and contrast respectively.

Definition 1—Rule: *IF* $\mu_{AR_j}(P_{s,t},r) = \max_{1 \leq i \leq \Re} \{\mu_{AR_i}(P_{s,t},r)\}$ *THEN pixel* $P_{s,t}$ *belongs to region*

R_j.

This straightforward extension of the original fuzzy rule in Section 3.2 illustrates how new membership functions (attributes) can be integrated and highlights one of the key advantages of the approach adopted in this research, which is the flexibility of the framework or the fuzzy rule-based system. As with the original rule, this new rule is also generic and thereby application and image type independent. Further attributes or new features, such as for example, object motion in video segmentation can easily be included into the framework. Since all of the membership functions are independent of each other, one other interesting feature to highlight is that they each can be implemented concurrently using a parallel algorithm.

5.4 Determining the Parameters

The weighting factors w_1, w_2, and w_3, and threshold T for neighbourhood system are automatically determined using the algorithm by Karmakar *et al.* [6]. The other two weighting factors w_4 and w_5 are approximated based on the FD of the entire image and the standard deviations (*rstd*) of pixel intensities of the initially segmented regions, as follows: -

$$w_4 = w_5 = a(FD-2)/\text{var}(rstd) \tag{5.8}$$

where var *(rstd)* is the variance of the standard deviations of all segmented regions.

Since $2 \leq FD \leq 3$ and 2 is the topological dimension of the 2D image, this value is deducted from the FD thereby keeping the original contribution of the fractal within [0,1]. This ensures that the contributions of all the weights are constrained within their limits. From the observations, it was found that the regions having high texture suppressed regions containing less texture because they produced higher FD values. The standard deviation approximates the texture and the variance of the standard deviations of all regions measures the spread across the regions, that is the variability of

the texture in those regions. In order to prevent high textured regions from suppressing the less textured regions, the weights w_4 and w_5 are normalised using the variance of the standard deviations var($rstd$) of the initially segmented regions i.e. the higher the value of the var($rstd$) then the lower the values of the weights w_4 and w_5 and hence smaller their contributions to the segmentation. This will be experimentally tested upon various image types in Chapter 7.

The following section describes the steps of the complete FRIST algorithm utilising the membership functions (Sections 3.1 and 5.2) and the fuzzy rule defined in Section 5.3.

5.5 The FRIST Algorithm

5.5.1 The Algorithm

The detailed stages involved in the FRIST algorithm can now be formalised are as follows: -

Algorithm 5.1 FRIST

---

1. Classify the pixels of an image into a desired number of regions using any appropriate clustering algorithm (**Block 5** in Fig. 1.1).
2. Derive the weights and threshold value by applying the data-mining algorithm, Algorithm 3.1 and (5.8).
3. Derive the membership function for each region pixel distribution (Section 3.1).
4. Initialise the centre of all regions required to define the membership function in Section 3.1.2, with the respective centres produced in step 1.
5. Sequentially select an unclassified pixel from the image and calculate each membership function value in each region for that pixel.
6. Classify the pixel into a region applying the fuzzy rule defined in Section 5.3.
7. Return to step 5 until every pixel is classified.

It is important to reiterate that the FRIST algorithm considers image domain specific information when segmenting. The reason for this is that the membership functions for both the fractal dimension based feature (5.5) and the contrast (5.6) of a candidate pixel are developed for each region by comparing the physical structural characteristics of the surface of the respective segmented region with that of the original image within a window i.e. the segmentation is based on

information directly related to the original image. If a group of pixels is close together and has sharp variations, the membership function (3.7) for spatial relations will be ineffective, but the membership functions (5.5) and (5.6) for texture will be effectual and vice versa. This is because the variations among the pixel intensities are not limited by the threshold T for the membership functions (5.5) and (5.6). In this way, the algorithm addresses the obvious contraction that has been identified at the beginning of this chapter, between spatial relations of pixels and texture.

5.5.2 Time-Complexity Analysis of the FRIST Algorithm

Lemma 5.1: The fractal dimension (FD) using the differential box counting (DBC) method can be computed in $O(n)$ time for an image of n pixels.

Proof: To calculate the $n_\tau(i,j)$ for a grid of size $x \times y$, needs $O(xy)$ time in the worst case. The whole image consists of $\dfrac{n}{xy}$ grids and hence N_τ can be computed in $\dfrac{n}{xy} \times O(xy) = O(n)$ time. To calculate the FD using DBC method for υ different values of τ can be estimated in $\upsilon \times O(n) = O(n)$ since υ can be considered constant with respect to n. ■

Lemma 5.2: The time complexity of the FRIST algorithm (Algorithm 5.1) is $O(n)$ for an image containing n pixels.

Proof: The initial segmentation can be performed in $O(n)$ time using the FCM algorithm (Lemma 3.2), while the membership functions defined in Section 3.1 are determined in $O(n)$ time (Lemmas 3.3 to 3.5). From Lemma 5.1, the membership functions of FDF and contrast for each pixel on the window of size $h \times h$ require $O(h^2)$ time. The FRIST algorithm (Algorithm 5.1) for the whole image can be performed in $O(n) + n \times O(h^2) = O(n)$ since h can be considered constant with respect to n. ■

Here, the order of computational time of the FRIST algorithm remains the same as the GFRIS algorithm (Section 3.4.1) i.e. $O(n)$, although it incurs some additional computational cost for calculating the FD and the two related membership functions for texture, namely FDF and contrast.

5.6 Discussion of the Performance of the FRIST Algorithm

For completeness and to present a qualitative evaluation of the potential capability of the FRIST algorithm, the segmented results of the Brodatz texture image in Fig. 5.6(a) containing two regions, namely d8 (R_1) and d94 (R_2) produced by the GFRIS and FRIST algorithms using the neighbourhood radius $r = 1$ are shown in Fig. 5.6. If the result (Fig. 5.6(b)) produced by GFRIS, $r = 1$ is contrasted with the result (Fig. 5.6(c)) produced by FRIST, $r = 1$, it is perceptually apparent that the FRIST algorithm exhibits considerable improved segmentation results compared with the GFRIS algorithm. FRIST correctly classified in Fig. 5.6(c) a significant number of pixels that GFRIS misclassified in Fig. 5.6(b) for both d8 (R_1) and d94 (R_2) regions. A detailed performance analysis of the FRIST algorithm will be given in Chapter 7.

(a)   (b) GFRIS, $r = 1$ (c) FRIST, $r = 1$
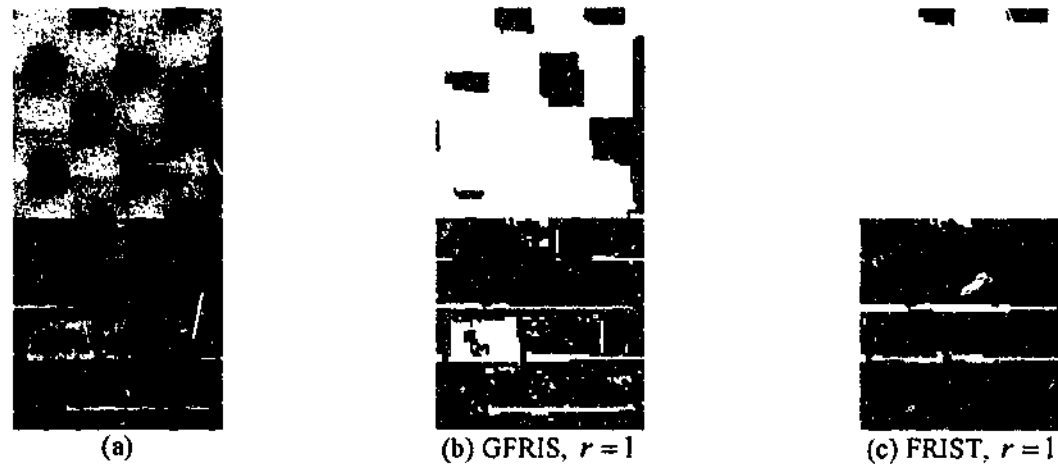
Fig. 5.6: The segmented results of the Brodatz texture (d8 and d94) image shown in Fig. 5.6(a) into two regions produced by GFRIS and FRIST using $r = 1$.

5.7 Summary

This chapter has outlined the development of a new general fuzzy rule-based image segmentation algorithm, namely *fuzzy rule for image segmentation incorporating texture features* (FRIST) by integrating fractal dimension and contrast and also considers domain specific information about an object. The weighing factors for the membership functions for FD and contrast have been automatically derived by considering the FD of the entire image and the variability of the texture in all regions produced by the initial segmentation.

The analysis of the computational complexity of the FRIST algorithm has been performed and proven that it requires $O(n)$ time for an image containing n pixels.

So far all of the algorithms in the framework have been developed for gray level image segmentation. In many real world images, there exist some information of an object such as edges, that cannot be separated using gray level information alone but that can be separated using colour information. Colour provides more information concerning an object and hence plays an important role in enabling the separation of an object (region) from an image, which is the main motivation to develop a fuzzy rule-based colour image segmentation algorithm. This will be the focus of the next chapter.

A Fuzzy Rule-Based Colour Image Segmentation Algorithm

Colour is a very common attribute of all natural and artificial objects, which contains far more information about an object than gray level intensity [163] and plays an important role in separating an object from its domain. There is some information about an object, such as edge, that is only visible in the colour domain. So the greater the visual information concerning an object potentially helps to improve the accuracy of the segmentation of that object. For these reasons, it is frequently easier to segment a colour image than a gray level image [135]. An example of a colour image separated into its gray level (luminance) and colour (chrominance) components is shown in Fig. 6.1. This confirms that perceptually colour provides additional information (Fig. 6.1(b)) to the gray level information (Fig. 6.1(a)) of the original object crocodile shown in Fig. 6.1(c).

A brief review of fuzzy colour image segmentation techniques has been provided in Section 2.5. To date, most fuzzy rule-based segmentation techniques are based on gray level pixel intensity (see Section 2.2). This chapter introduces a new colour image segmentation algorithm, namely a *fuzzy rule-based colour image segmentation (FRCIS)* algorithm by extending the GFRIS algorithm described in Chapter 3, from gray level to colour and developing a new algorithm for averaging hue angles (**Block 4** in Fig. 1.1). The proposed FRCIS algorithm will be both perceptually and numerically evaluated and compared with FCM and PCM using the HSV and RGB colour models (see Section 2.4) in the next chapter.

This chapter is organised as follows: In Section 6.1, the membership functions used in the FRCIS algorithm are defined. The definition of the fuzzy rule, and also the determination of the weighting factors are presented in Sections 6.2 and 6.3 respectively. The algorithm required for averaging the hue angles together with the operator for measuring the difference between two hue angles is described in Section 6.4. The complete FRCIS algorithm with its time-complexity analysis is given in Section 6.5. Finally, a qualitative performance analysis of this algorithm using the HSV colour model is provided in Section 6.6.

(a)   (b)

(c)
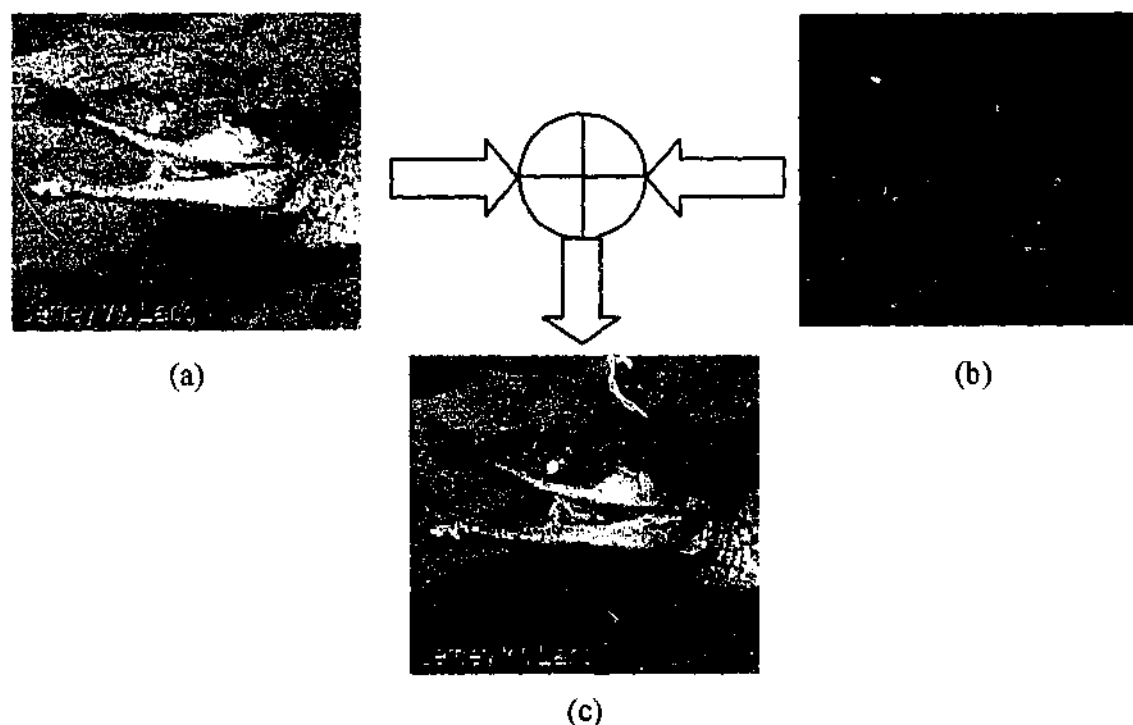
Fig. 6.1: An example of colour image, (a) Gray level (luminance) information, (b) Colour (chrominance) information, (c) Original image.

6.1 Defining Membership Functions

The FRCIS algorithm uses three membership functions namely, the membership function for region pixel distributions, the closeness to their centres, and the spatial relations among the pixels in a particular region. These have already been fully described in Section 3.1 and are the bedrock of the GFRIS algorithm. However, all these membership functions have been defined for only gray level pixel intensity. In this section, these membership function definitions are extended for each colour component of each region. As mentioned in Section 2.4, each colour is represented by a point within the colour space of a 3D-coodinate system, so each colour will have three components. All of the membership functions for each colour component are defined in the following sections.

6.1.1 Membership Function for Region Pixel Distributions

As alluded above, a detailed description of this membership function has been provided in Section 3.1.1. The membership function for the pixel distribution of region R_j, $\mu_{D_i R_j}(P_{s,t})$ of a pixel with a gray level value of $P_{s,t}$ at location (s,t) for the ith colour component can be defined as: -

$$\mu_{D_i R_j}(P_{s,t}) = f_{i R_j}(P_{s,t}) \tag{6.1}$$

where $f_{i R_j}(P_{s,t})$ is the polynomial for the ith colour component of region R_j and $i \in \{1, ..., \phi\}$ where ϕ is the number of components for a particular colour model, i.e. $\phi = 3$ for HSV, though in certain cases it may not be equal to 3.

6.1.2 Membership Function to Measure the Closeness of a Region

The definition of this particular membership function differs slightly from the definition presented in Section 3.1.2. This is because it uses a normalised difference with respect to the maximum value of the candidate pixel $P_{s,t}$ and the respective centre $C_i(R_j)$ of a region R_j, instead of fixed value $(2^b - 1)$ where b-bit gray levels or colour components are presumed. The membership function for the closeness to a region R_j, $\mu_{C_i R_j}(P_{s,t})$ of a candidate pixel $P_{s,t}$ for the ith colour component is defined as: -

$$\mu_{C_i R_j}(P_{s,t}) = 1 - |C_i(R_j) - P_{s,t}| / \max\{C_i(R_j), P_{s,t}\} \tag{6.2}$$

where $C_i(R_j)$ is the centre of the ith colour component of region R_j. This membership function considers more accurately the human visual perception than (3.5) in the GFRIS algorithm. For example, if the difference i.e. $|C_i(R_j) - P_{s,t}|$ is the same for a luminance component for two regions, namely R_1 and R_2, the membership function (3.5) will generate exactly the same value for both regions. However, the new membership function (6.2) will produce a different value thereby reducing the inclination towards the less bright region.

To illustrate this, let the values of the centres of regions R_1 and R_2 for a luminance component be 60 and 200 respectively. If a candidate pixel value is 130, the difference $|60 - 130| = |200 - 130| = 70$ is the same for the two regions. It is essential to determine which region would be more appropriate for this pixel. Perceptually 130 is closer to region R_2 than R_1 because R_2 possesses a lower percentage difference. The ratio of the difference for region R_1 is $|60 - 13|/\max(60,130) = 7/13$, while it is $|200 - 130|/\max(200,13) = 7/20$ for R_2 where

$7/20 < 7/13$. The corresponding values of the membership function (6.2) for this example for regions R_1 and R_2 are $(1 - 7/13) = 6/13 = 0.46$ and $(1 - 7/20) = 13/20 = 0.65$ respectively. Since the value of the membership function for R_2 is greater than that of R_1, (6.2) conforms more to human visual perception, which was the main reasoning for defining this membership function. While the above example only considered the luminance component, it can also be extended to include the chrominance components.

6.1.3 Membership Functions for Spatial Relation

The membership function for spatial relation between the pixels of the ith colour component of a region R_j, $\mu_{N_i R_j}(P_{s,t}, r)$ for the neighbourhood radius r is defined as: -

$$\mu_{N_i R_j}(P_{s,t}) = \left(N_{ij} \times G_{iR_j}\right) / \sum_{i=1}^{\phi} \sum_{j=1}^{\Re} \left(N_{ij} \times G_{iR_j}\right) \tag{6.3}$$

where N_{ij} and G_{iR_j} are respectively the number of neighbours and the sum of the inverse distances of the ith colour component of a region R_j from the candidate pixel $P_{s,t}$. $\Re$ is the number of segmented regions.

6.2 Defining the Fuzzy Rule

In contrast to the fuzzy rule defined in Section 3.2 for only one component (gray level pixel intensity), in this section a fuzzy rule is heuristically defined for all three colour components.

The overall membership value $\mu_{AR_j}(P_{s,t}, r)$ of a pixel $P_{s,t}$ for a region R_j represents the overall degree of belonging to that region for all colour components. This is defined by the weighted average of all membership functions for all colour components $\mu_{D_i R_j}(P_{s,t})$, $\mu_{C_i R_j}(P_{s,t})$, and $\mu_{N_i R_j}(P_{s,t}, r)$.

$$\mu_{AR_j}(P_{s,t}, r) = \frac{\sum_{i=1}^{\phi} w_{1i} \mu_{D_i R_j}(P_{s,t}) + \sum_{i=1}^{\phi} w_{2i} \mu_{C_i R_j}(P_{s,t}) + \sum_{i=1}^{\phi} w_{3i} \mu_{N_i R_j}(P_{s,t}, r)}{\sum_{k=1}^{3} \sum_{i=1}^{\phi} w_{ki}} \tag{6.4}$$

where w_{1i}, w_{2i}, and w_{3i} are the weightings of the membership values of ith colour component for pixel distribution, closeness to the cluster centres, and neighbourhood relations respectively.

Definition 6.1—Rule: IF $\mu_{AR_j}(P_{s,t},r) = \max\limits_{1 \le i \le \Re}\{\mu_{AR_i}(P_{s,t},r)\}$ THEN pixel $P_{s,t}$ belongs to region R_j.

As in Section 3.2, this rule is general enough to ensure that this algorithm is both application and image independent. The effectiveness of this rule will be assessed using one of the perceptual colour models (HSV) and the basic colour model (RGB) in Chapter 7.

6.3 Determining the Weighting Factors and the Threshold

The data mining Algorithm 3.1, which was articulated in Section 3.3, is extended to incorporate colour components and determine the weighting factors w_{1i}, w_{2i}, and w_{3i}, and threshold T_j. The spatial relationship weighting factors w_{31} and w_{32} for the hue and saturation colour components of the HSV colour model were empirically chosen as 0.2. The reason for the low value of both parameters is that hue denotes the dominant colour and already represents spatial relations by suppressing the minor variations of a colour, while saturation represents the relative colour purity, that is the whiteness of hue [136].

6.4 Arithmetic Operators for Hue in the HSV Colour Model

The hue in the HSV colour model represents the dominant wavelength of the colour stimulus. The HSV colour model is represented by a cone shown in Fig. 2.20, where the hue is the angle of each colour within the cone starting from 0 point on the x-axis [164]. Hue angles are used in calculating the membership functions defined in Sections 6.1.2 and 6.1.3 and automatically deriving the key weighting factors and thresholds described in Section 6.3 for the hue component of the HSV colour model. Since hue is expressed in angles, the arithmetic operations for Cartesian coordinates are not suitable for hue and as mentioned in Section 2.4.2 this leads to some difficulties when applying certain arithmetic operations on hue angles e.g. averaging. The definition of the difference between two hue angles h_1 and h_2 where both h_1 and h_2 are bounded in the range the $[0, 2\pi]$ and the formula for calculating the average of n hue angles are given as follows: -

Definition 6.2—Difference Between Two Angles: The difference between two hue angles h_1 and h_2, $diff(h_1, h_2)$ is defined as: -

$$diff(h_1, h_2) = \min(|h_1 - h_2|, 2\pi - |h_1 - h_2|) \tag{6.5}$$

As mentioned in Section 3.1.2, when a candidate pixel joins its nearest region, the centre of that particular region is recomputed. The rationale behind recomputing the centre of a region, which considers the previous values of the centre and its candidate pixels, is best understood using an analogy from basic force analysis.

Let the initial hue value of the centre of a particular region be h_1 shown in Fig. 6.2. If the saturation is assumed as 1, this can be considered a unit force F_1 with direction h_1. If a candidate pixel h_2 joins this region, this can be regarded as a unit force F_2 with direction h_2. The resultant force of F_1 and F_2, namely R_1 and resultant hue angle ψ_1 of h_1 and h_2 shown in Fig. 6.2 are computed using the force analysis technique, which will be formalised in Algorithm 6.1. Note, that the magnitude of R_1 may not be unity. If another candidate pixel h_3 with unit force F_3 joins this region, the resultant force of R_1 and F_3, namely R_2 and resultant hue angle ψ_2 of ψ_1 and h_3 can also be calculated in exactly the same way. Therefore, ψ_2 is the average angle of h_1, h_2, and h_3. A similar process is applied to recalculate the centre of this region for all candidate pixels that join this region.

This process can be formalised as follows: -

1. The initial value of the centre of a region and the first candidate pixel are considered two angles of unit force, since the respective saturation values are always one.

2. The resultant angle of the two forces (the initial value of the centre and the candidate pixel) is regarded as the current value of the centre.

3. When another candidate pixel joins this region, the resultant force (angle and magnitude) for the current centre and the force for the candidate pixel are used to recalculate the centre of this region. This process is repeated for all candidate pixels that join this particular region.
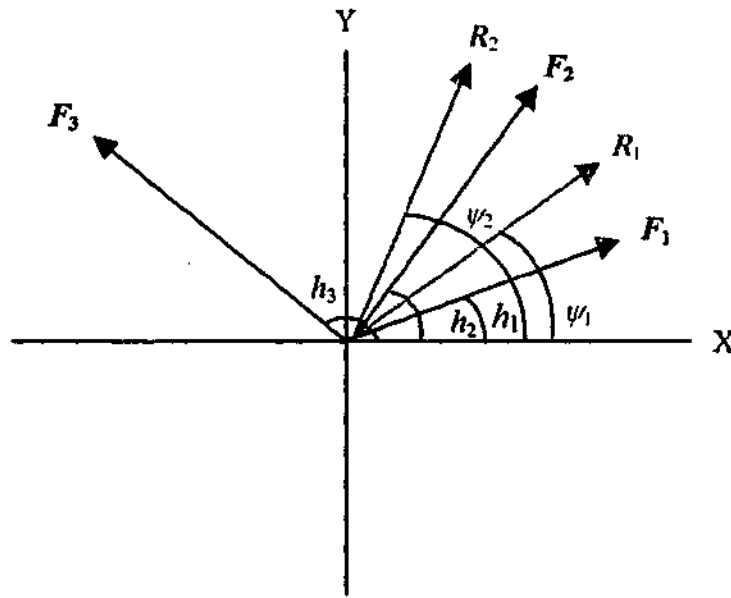
Fig. 6.2: Resultant (average) hue angle ψ_2 of h_1, h_2, and h_3.
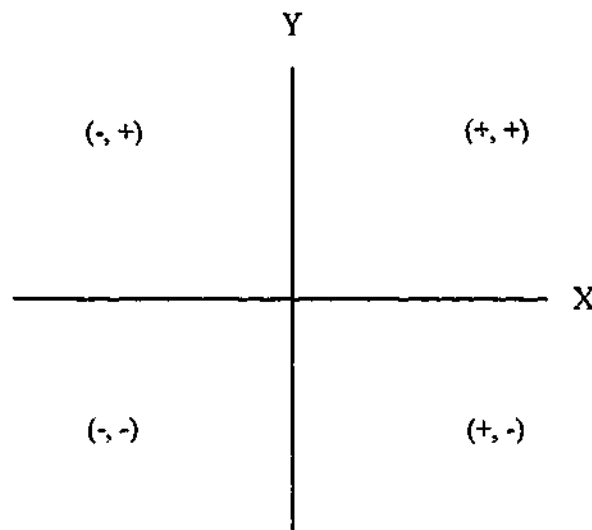
Fig. 6.3: The sign of X and Y components of the resultant force.

The actual magnitude of the resultant angle depends on the sign of both the X and Y components of the resultant force because of the π radians periodicity of the tangent function shown in Fig. 6.3. This means that the resultant angle will be in first, second, third, and fourth quadrant depending on the respective signs of the X and Y components.

The algorithm for calculating the average angle of two hue angles based on force analysis is formalised as follows: -

Algorithm 6.1 Calculation of the average of two hue angles

Precondition: Two hue angles h_1 and h_2 with magnitudes F_1 and F_2 of the forces F_1 and F_2 respectively.

Postcondition: Resultant direction ψ (average angle) and magnitude R of the force R.

1. Calculate the X and Y components of the resultant force R.

$$R_x = F_1 \cos(h_1) + F_2 \cos(h_2)$$

$$R_y = F_1 \sin(h_1) + F_2 \sin(h_2)$$

2. Compute the magnitude of the resultant force R. If it is zero, mark the resultant angle ψ as undefined by setting its value as -1 and go to step 4.

$$R = \sqrt{R_x^2 + R_y^2}$$

IF $(R = 0)$ THEN

   $\psi = -1$

   GOTO step 4

3. Determine the resultant direction (average angle).

$$\psi = \tan^{-1}\left(\frac{|R_y|}{|R_x|}\right)$$

IF $(R_x \geq 0)$ THEN

   IF $(R_y < 0)$ THEN

      $\psi = 2\pi - \psi$

ELSE

   IF $(R_y > 0)$ THEN

      $\psi = \pi - \psi$

   ELSE

      $\psi = \pi + \psi$

4. STOP

All those pixel values, for which the average angle becomes undefined are blocked from the process for modification of each region centre in Section 6.1.2.

6.5 The FRCIS Algorithm

Many of the steps of the FRCIS algorithm are the same as the GFRIS algorithm in Algorithm 3.2, described in Section 3.4. There are however some subtle differences in certain the stages of processing, so for completeness, the entire FRCIS algorithm is formalised in Algorithm 6.2.

Algorithm 6.2 FRCIS

---

1. This step is same as Algorithm 3.2, however the initial segmentation uses (6.5) to calculate the distance between two hue angles for the HSV colour model.

2. Derive the weighting factors and threshold values by applying the data-mining Algorithm 3.1 and the membership function for each region pixel distribution for each colour component (Section 6.1.1). This step again uses (6.5) for the hue component in the HSV colour model.

3. Initialise the centre of all regions for each colour component required to define the membership function in Section 6.1.2, with the respective centres produced in step 1.

4. Sequentially select an unclassified pixel from the image and calculate the membership function value for each colour component in each region for that pixel. This step uses (6.5) and Algorithm 6.1 for the hue component of the HSV colour model.

5. Classify the pixel into a region applying the fuzzy rule (Definition 6.2).

6. Return to step 4 until every pixel is classified.

It is important to reiterate that as with GFRIS, this algorithm is image and application independent. The time complexity of this algorithm is described using the following lemma.

Lemma 6.1: The computational complexity of the FRCIS algorithm is $O(n)$ for an image containing n pixels.

Proof: For a specific colour component, the time complexity for the FRCIS algorithm (Algorithm 6.2) is same as the GFRIS algorithm (Algorithm 3.2) assuming the same initial

segmentation. This is because the computational time of the membership functions defined in Section 6.1 is the same as those defined in Section 3.1 for a particular colour component. Although steps 2 and 4 of Algorithm 6.2 uses (6.5) and step 4 also uses Algorithm 6.1 for the hue component of the HSV colour model, these do not change the order of the computational time. The computational time complexity of the FRCIS algorithm is greater than the GFRIS algorithm because three colour components are considered, so the order of time complexity of the FRCIS algorithm is three times of that of the GFRIS algorithm, i.e. $3 \times O(n) = O(n)$ (see Section 3.4.2) where n is the total number of pixels of an image. ∎

6.6 Discussion of the Performance of the FRCIS algorithm

As in other chapters, a representative sample of the performance of this algorithm in segmenting the cloud image in Fig. 6.4(a) for two regions, namely the cloud (R_1) and urban scene (R_2) produced by the FRCIS using $r = 1$, FCM, and PCM algorithms using the HSV colour model is shown in Fig. 6.4.

(a)	(b) FRCIS, $r = 1$	(c) FCM	(d) PCM
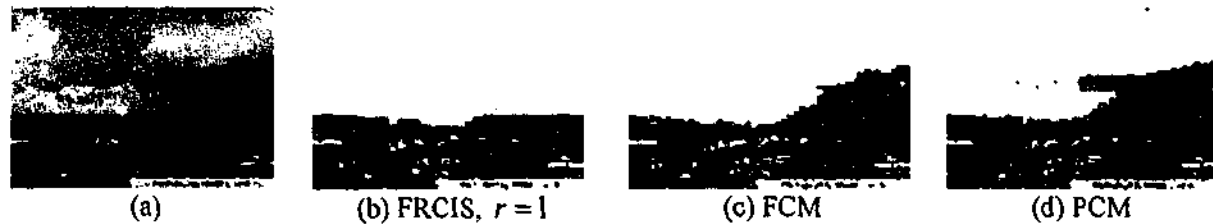
Fig. 6.4: The segmented results of the cloud image in (a) into two regions for the HSV colour model produced by the FRCIS using $r = 1$, FCM, and PCM algorithms.

The segmented results shown in Fig. 6.4(b) visually confirm that FRCIS using $r = 1$, separated almost the entire cloud (R_1) region from the urban scene (R_2). It also exhibits considerable improvement over both the FCM and PCM algorithms (Fig. 6.4(c) and 6.4(d)) with FCM again produced better results especially for the cloud (R_1) region than PCM. An extensive performance analysis of this algorithm will be presented in the next chapter using both the HSV and RGB colour models.

6.7 Summary

Colour is an additional attribute of an object, which leads to more appealing and easy interpretation of the object. There are some edges of an object that are only visible in the colour

domain. In this chapter, a new fuzzy rule-based colour image segmentation algorithm called FRCIS has been proposed by extending the original gray level fuzzy rule-based image segmentation algorithm GFRIS described in Chapter 3. The difference operator and an algorithm for calculating the average of hue components of the HSV colour model have been defined.

The computational complexity of the FRCIS algorithm is also the same as the GFRIS algorithm i.e. $O(n)$ for an image containing n pixels.

Numerical evaluation of this algorithm using one of the perceptual colour models, namely HSV and the basic colour model RGB will be performed in the next chapter.

Experimental Results and Discussions

In this chapter, the performance of all the various constituent blocks in the fuzzy rule-based image segmentation framework shown in Fig. 1.1 is analysed and discussed. The GFRIS (**Block 1**), FRIS (**Block 2**), FRIST (**Block 3**), and FRCIS (**Block 4**) algorithms are applied to a wide range of real images containing different features and number of objects/regions (**Block 6**). The results produced by the proposed algorithms are compared with those obtained using FCM and PCM, and a numerical evaluation is undertaken using the two powerful objective and quantitative segmentation evaluation methods, namely *discrepancy based on the number of mis-segmented pixels* and *discrepancy based on the number of objects in the image*. A statistical significance test, called the *sign test*, is also applied to determine the worthiness of any improvement in each segmentation algorithm's performance. All algorithms including FCM and PCM were implemented using MATLAB version 6.0.

This chapter is organised as follows: In Section 7.1, the segmentation evaluation methods used in the experiments are described. The statistical significance test (*sign test*), the image database and manually segmented reference images, and the parameter settings are presented in Sections 7.2, 7.3, and 7.4 respectively. The performance analysis of the GFRIS, FRIS, FRIST, and FRCIS algorithms are given in Sections 7.5, 7.6, 7.7, and 7.8 respectively. Finally, some general issues relating to the framework are discussed in Section 7.9.

7.1 Segmentation Evaluation Methods

Segmentation evaluation methods can be generally categorised into the following two classes [165]: -

1. Analytical methods
2. Empirical methods

Analytical methods directly assess the segmentation algorithms by examining their principles, requirements, utilities, and complexity, while empirical methods indirectly evaluate the results of the segmentation algorithms based on some test images and by measuring the quality of the segmented results. Empirical methods are generally divided into two classes: goodness and discrepancy. Goodness methods appraise the performance of a segmentation algorithm by determining the quality of the results based on primarily some predefined *goodness* parameters such as entropy and gray-level uniformity. Discrepancy based methods judge the segmentation performance by calculating the disparity between the segmentation results and the corresponding ideal or expected results (reference images). It has been experimentally shown that generally, discrepancy methods are more powerful than other methods [165]. In this chapter, the numerical evaluation of each segmentation algorithm in the framework (Fig. 1.1) is performed based on two powerful discrepancy methods, namely: -

1. Discrepancy based on the number of mis-segmented pixels.
2. Discrepancy based on the number of objects in the image.

These are discussed in the following sections.

7.1.1 Discrepancy Based on the Number of Mis-segmented Pixels

This measures the percentage error of misclassified pixels due to the segmentation. The confusion matrix C is a $\Re$ by $\Re$ square matrix, where $\Re$ is the number of segmented regions and C_{ij} denotes the number of jth region pixels that are wrongly classified in region i by the segmentation algorithm. Two error measures Type I, $errorI_i$ and Type II, $errorII_i$, are defined as performance measures [165, 166] as follows: -

$$errorI_i = \frac{\left(\sum_{j=1}^{\Re} C_{ji} - C_{ii}\right)}{\sum_{j=1}^{\Re} C_{ji}} \times 100 \qquad (7.1)$$

$$errorII_i = \frac{\left(\sum_{j=1}^{\Re} C_{ij} - C_{ii}\right)}{\left(\sum_{i=1}^{\Re}\sum_{j=1}^{\Re} C_{ij} - \sum_{j=1}^{\Re} C_{ji}\right)} \times 100 \qquad (7.2)$$

Type I, *errorI$_i$* gives the percentage error of ith region pixels that are not classified in the ith region, whereas Type II, *errorII$_i$*, is the percentage error of all other region pixels wrongly classified in the ith region. For the case of $\Re = 2$ (two regions), the error rates (7.1) and (7.2) for one region will therefore be the reverse of those of the other region.

7.1.2 Discrepancy Based on the Number of Objects in the Image

The total number of objects in any region of a segmented image should be equal to that in the respective region of the reference image where ideal segmentation is assumed. Any discrepancy in the number of objects between the segmented and reference images leads to poorer results. Let S_i and R_i be the respective number of objects in the ith region of the segmented and reference images. The probability that both S_i and R_i are taken from the same distribution that is used to measure the object-count-agreement (OCA) is defined as [165, 167]: -

$$P_{OCA} = \int_{\zeta}^{\infty} \frac{1}{2^{\eta/2}\Gamma(\eta/2)} x^{(\eta-2)/2} e^{-x/2} dx \qquad (7.3)$$

where $\eta = \Re - 1$ and $\Gamma(.)$ are the degrees of freedom and the gamma function respectively. The value of ζ is determined from the following: -

$$\zeta = \sum_{i=1}^{\Re} \frac{S_i - R_i}{\theta \times R_i} \qquad (7.4)$$

where θ is the correlation parameter. This evaluation is important because for example, the principle behind the refinement algorithm described in Chapter 4 is fundamentally based upon splitting and merging of region objects. Every segmented and reference region is split into objects using 8-connected neighbourhood for the purpose of this evaluation. The reason for using 8-connected instead of 4-connected neighbourhood is to find as many as possible perceptually meaningful objects by considering all weak connections between the pixels.

7.2 Statistical Significance Test

To determine whether or not the results of one algorithm provided a significant improvement, i.e. positive differences over the other, a statistical significance test was applied. The *sign test* has

been extensively used to measure the differences between related samples, considering as it does, only the direction and not the magnitude of any differences [168]. The *sign test* is appropriate for determining the differences between two segmentation results for the same image or a region produced by two different algorithms, since it only checks whether a pixel has been correctly classified or not. If A_1 and A_2 are two algorithms, the null hypothesis A_1 *is not better than* A_2 can be assessed based on the classification of each pixel of an image, by applying the truth table in Table 7.1.

Table 7.1: Truth table for A_1 is better than A_2.

A_1	A_2	A_1 is better than A_2
Correct	Incorrect	+
Correct	Correct	×
Incorrect	Correct	-
Incorrect	Incorrect	×

Correct and Incorrect respectively denote the classification of a pixel, either by algorithm A_1 or A_2 ; × means don't care.

If the number of plus signs is considerably greater than the minus signs, the *sign test* detects a significant difference using the equation for the z value defined in [168] and hence the null hypothesis is rejected. This z value yields the significance level of the differences from the table of the standard normal curve. Note, that the *sign test* is only performed on the Type I error since it only considers correctly classified pixels for a particular region and not those pixels from other regions that are misclassified into that region, which is what the Type II error in (7.2) measures.

7.3 Image Database and Manually Segmented Reference Images

The image database used throughout the evaluation comprised 18 different natural images consisting of two (9), three (8) and five (1) regions. The images were collected from the IMSI[‡], Brodatz album[*], and the Internet. In order to fully evaluate the performance and potential of the GFRIS, FRIS, FRIST, and FRCIS algorithms, these different natural 18 images were selected because they possessed a range of disparate features such as homogeneous and non-homogeneous regions, low pixel contrast regions, perceptually distinct regions, different types of natural objects, Brodatz textures, and colours.

[‡] IMSI's Master Photo Collection, 1895 Francisco Blvd. East San Rafael, CA 94901-5506, USA.
[*] Brodatz Textures, http://www.ux.his.no/~tranden/brodatz.html.
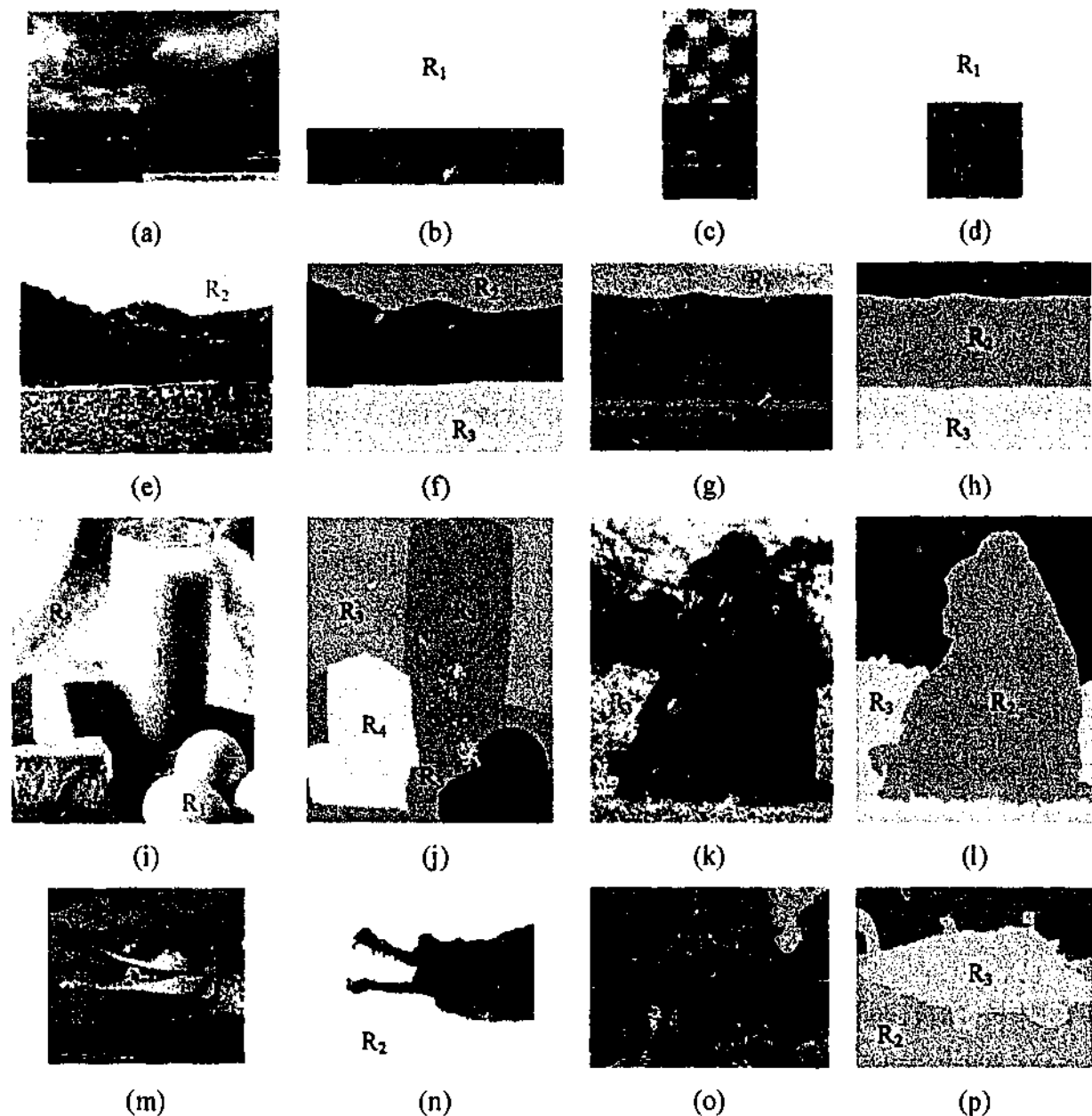
Fig. 7.1: A sample of original and their manually segmented reference images, (a) and (b) The cloud and its reference image (2 regions), (c) and (d) The Brodatz texture (d8 and d94) and its reference image (2 regions), (e) and (f) The forest and its reference image (3 regions), (g) and (h) The hill and its reference image (3 regions), (i) and (j) The food and its reference image (5 regions), (k) and (l) The gorilla and its reference image (3 regions), (m) and (n) The crocodile and its reference image (2 regions), (o) and (p) The fish and its reference image (3 regions).

As mentioned in Section 4.2.3, for the sake of the numerical evaluation and the connectedness property, all zero pixel values were pre-processed by adding 5 to each of them before applying any

of the segmentation algorithms. This has not effect upon the visual perception of the images [84]. A representative sample of these and their manually segmented reference images are shown in Fig. 7.1. The remainder of the images are included in Appendix B.

7.4 Setting the Framework Parameters

For the implementation of all algorithms in the framework (Fig. 1.1) as well as the PCM and FCM algorithms, the derivation of key algorithm parameter values were as follows: -

For FCM, initialisation of the cluster centre was performed randomly. The maximum number of iterations, the minimum level of improvement, and the value of the fuzzifier (m) were empirically selected as 100, 0.00001 and 2, respectively. Note, that the threshold (the maximum level of improvement) was chosen as 0.00001, which is a very small value and sufficient to ensure good convergence. FCM converged at this threshold in all our experiments with the number of iterations, always being less than the maximum number of iterations i.e. 100.

For PCM, initialisation of the cluster centres used the output of FCM. The value of the scale parameter η_i was taken as the variance of the cluster i produced by FCM. The maximum number of iterations, minimum level of improvement and value of fuzzifier (m) were empirically chosen as 200, 0.00001 and 1.5, respectively. The maximum number of iterations was chosen to be greater than for FCM (100) as PCM took more iterations than FCM to converge. The approach adopted to set the values of the threshold and the maximum number of iterations for PCM was exactly the same as FCM.

For GFRIS, FRIST, and FRCIS, the membership function for region pixel distribution $\mu_{DR_f}(P_{s,t})$ was developed using the clusters produced by the initial segmentation results using the fuzzy c-means (FCM) algorithm [80]. The centre values were used to initialise the centres of the clusters required to define the membership function for the closeness of a region. The respective weighting and threshold values were automatically data-mined by the algorithm delineated in [6], using the arbitrary constant $K = 0.25$. The neighbourhood radius (r) was taken as 1, 2, and 4, with the size of the window $W_{h,h}(s,t)$ used in the FRIST algorithm (see Section 5.2.1) being 4×4 pixels.

In FRIS, the values of the three thresholds ξ, λ_1, and λ_2 were empirically selected as 0.8, 0.7, and 0.9 respectively. The dependency of the overall segmentation performance to slight variations in the values of these three parameters has proven to be negligible. The values of χ were also intuitively chosen as 1 and 0.8 for the *growing up* and *preventive* rules respectively.

In the numerical segmentation evaluation, namely *discrepancy based on the number of objects in the image* described in Section 7.1.2, the value of the correlation parameter θ was empirically selected as 200.

7.5 Performance Analysis of the GFRIS Algorithm

While some sample preliminary results of the GFRIS algorithm were included in Section 3.5, this section provides a complete analysis and evaluation of this algorithm. The segmentations were performed using eight different gray level images containing two regions. A representative sample of the segmented results of the two images in Fig. 7.1(a) and 7.1(c) for the two regions, cloud (R_1) and urban scene (R_2) of the cloud image and d8 (R_1) and d94 (R_2) of the Brodatz texture produced by GFRIS, FCM, and PCM respectively are shown in Fig. 7.2 and 7.3. The segmentation results for the remaining six images shown in Fig. B.1, are included in Fig. C.1 (Appendix C).

(a) GFRIS, $r=1$ (b) GFRIS, $r=2$ (c) GFRIS, $r=4$ (d) FCM   (e) PCM
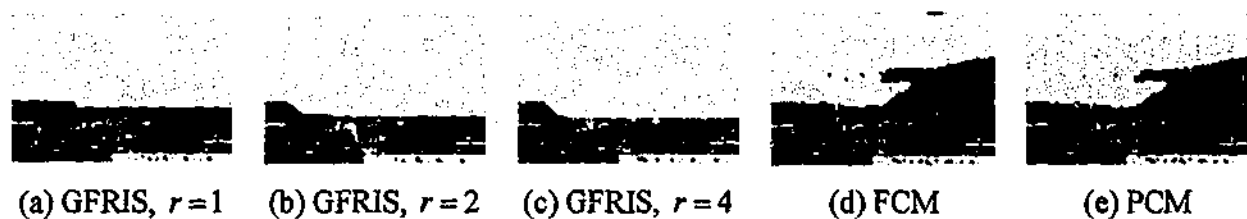
Fig. 7.2: The segmented results of the cloud image in Fig. 7.1(a) into two regions using the GFRIS, FCM, and PCM algorithms.

The results confirm that GFRIS separated almost the entire cloud (R_1) and Brodatz texture d8 (R_1) regions from the urban scene (R_2) and Brodatz texture d94 (R_2) regions respectively. It produced significantly better results than both FCM and PCM for these two as well as the other six images shown in Fig. B.1. FCM and PCM gave approximately equal performance for the cloud image (Fig. 7.1(a)), since as alluded earlier, both algorithms do not consider the spatial relationships between the pixels in each region, while PCM could not separate the Brodatz texture regions at all (Fig. 7.3(e)). GFRIS also exhibited better results for larger values of neighbourhood radius r (Fig. 7.2(b) and 7.2(c), and Fig. 7.3(b) and 7.3(c)), since the region pixels in both the cloud (R_1) and Brodatz texture d8 (R_1) possess strong spatial correlation. Evaluation of the segmentation results for the cloud and Brodatz texture images, compared with the manually segmented reference images in Fig. 7.1(a) and 7.1(c), are shown in Table 7.2 with the results for other images shown in

Table D.1 (Appendix D). Note, that only the error rates for the segmented cloud (R_1) and Brodatz texture d8 (R_1) regions are displayed in Table 7.2, since as explained in Section 7.1.1 for two regions, the error rate of one region will be the reverse of the other region. The shaded entries correspond to the best GFRIS results. While GFRIS provided particularly good performance in segmenting the cloud (R_1) and Brodatz texture d8 (R_1) regions, it is worth noting that the error rates of GFRIS for the Type II error of the cloud (R_1) and Brodatz texture d8 (R_1) regions respectively were higher than those for both PCM and FCM. This was because not all the pixels in these regions possessed good continuation due to the abrupt changes in the Brodatz texture d94 (R_2) region as well as in the urban scene (R_2). The urban scene for instance does not constitute a single object and so opposes the necessary condition for good inter-pixel relationships. This issue has been addressed by the refinement (FRIS) algorithm described in Chapter 4 and will be analysed further in Section 7.6.

(a) GFRIS, $r = 1$ (b) GFRIS, $r = 2$ (c) GFRIS, $r = 4$ (d) FCM   (e) PCM
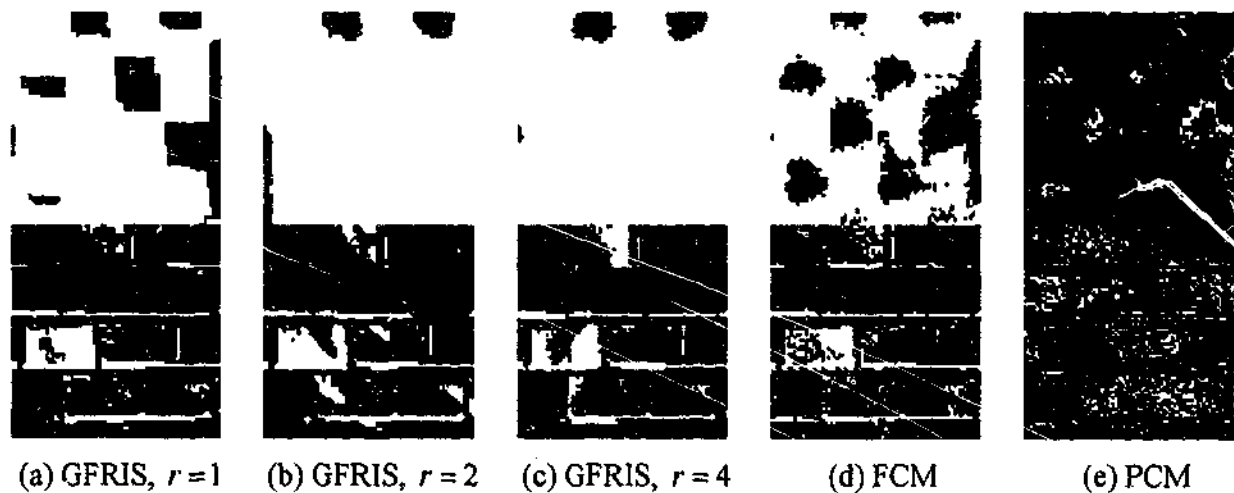
Fig. 7.3: The segmented results of the Brodatz texture image (d8 and d94) in Fig. 7.1(c) into two regions using the GFRIS, FCM, and PCM algorithms.

The average GFRIS error rates (the average of Type I and Type II errors) with respect to the corresponding manually segmented reference regions are plotted in Fig. 7.4 for the Brodatz texture, the cloud, and an average of all eight sample images. This shows that GFRIS performed significantly better than both FCM and PCM for each value of the neighbourhood radius r. The overall error improvements for GFRIS were 35.1% and 51.5% over FCM and PCM respectively for the eight images. Note, that the overall average error for GFRIS was calculated considering all

values of the neighbourhood radius r. Unless otherwise stated, this will hold for the remainder of this chapter.

Table 7.2: Error percentages for the cloud (R_1) and Brodatz texture d8 (R_1) regions of the cloud (Fig. 7.1(a)) and Brodatz texture (Fig. 7.1(c)) image segmentations respectively using the GFRIS, FCM, and PCM algorithms.

Algorithm	Cloud (R_1) Region		Brodatz Texture d8 (R_1) Region	
	Type I	Type II	Type I	Type II
GFRIS r=1		17.0513		13.991
GFRIS r=2		21.2500		14.542
GFRIS r=4		23.6218		13.600
FCM	28.0000	15.7372	29.920	13.156
PCM	26.8939	16.3141	96.089	10.044
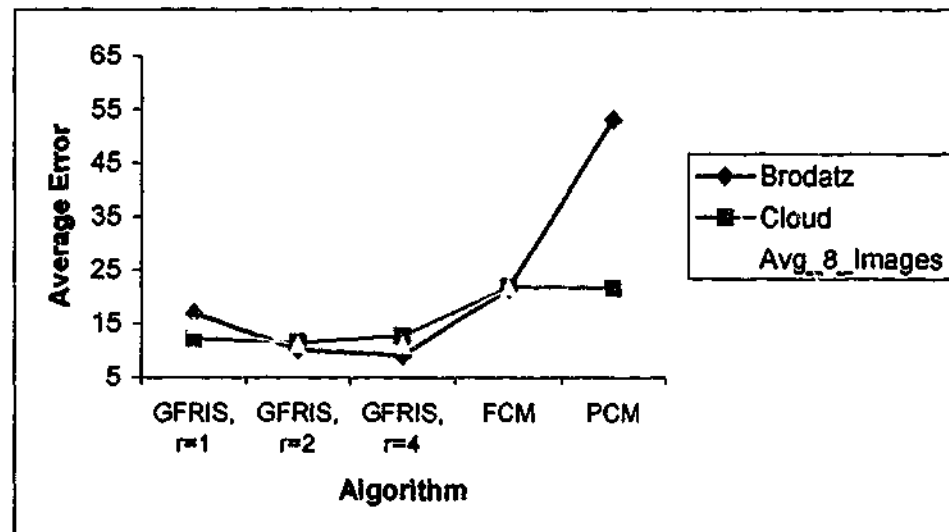
Fig. 7.4: Average error rates of GFRIS, FCM, and PCM for the Fig. 7.1(a) and 7.1 (c), and average of the eight image segmentations.

Another evaluation was conducted utilising the method of *discrepancy based on the number of objects* for all eight images. The probabilities of object-count-agreement (OCA) for each algorithm for the cloud and Brodatz texture images are given in Fig. 7.5, while the probabilities of OCA for the algorithms applied to other images are given in Table D.1. The probabilities of OCA for the GFRIS algorithm were much better (overall 35.9% and 41.6% for the eight images) than those for the FCM and PCM algorithms, which represent far better agreement between the number of objects in the segmented and the corresponding reference regions.
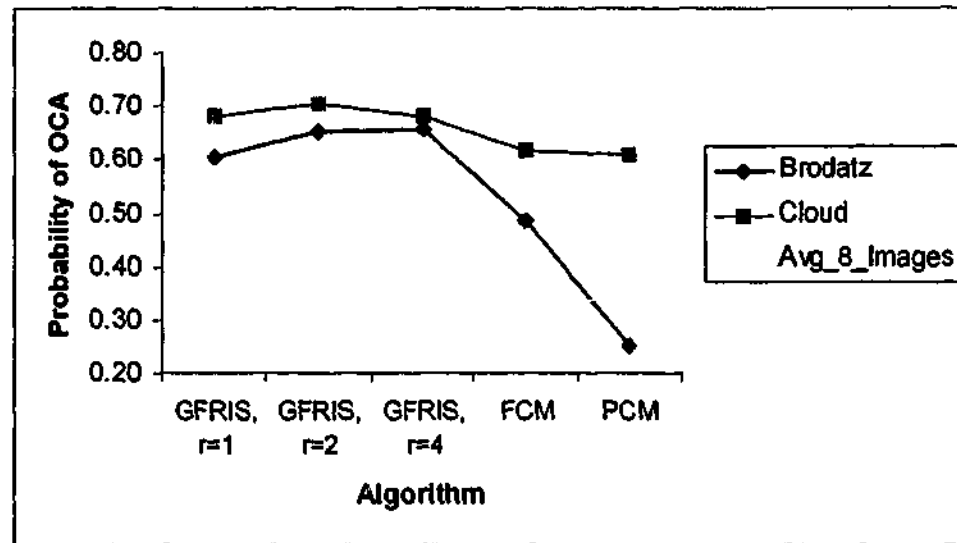
Fig. 7.5: Probability of object-count-agreement (OCA) for GFRIS, FCM, and PCM for the Fig. 7.1(a) and 7.1(c), and an average of the eight image segmentations.

Table 7.3: The overall results of the statistical significance test, *sign test* for the cloud image in Fig. 7.1(a).

Algorithm	Ref. Algorithm	Percentage of + Pixels	Percentage of - Pixels	Z Value	Significance Level
GFRIS r=1	FCM	10.715	1.039	-34.610	Beyond 0.0001
GFRIS r=2	FCM	13.393	3.013	-35.459	Beyond 0.0001
GFRIS r=4	FCM	13.483	4.327	-32.950	Beyond 0.0001
PCM	FCM	0.553	0.288	-5.661	Beyond 0.0001
GFRIS r=1	PCM	10.250	0.838	-34.106	Beyond 0.0001
GFRIS r=2	PCM	12.936	2.821	-34.929	Beyond 0.0001
GFRIS r=4	PCM	12.986	4.094	-32.398	Beyond 0.0001
FCM	PCM	0.288	0.553	-5.661	Beyond 0.0001
GFRIS r=1 with FRIS	GFRIS r=1	3.285	0.000	-14.248	Beyond 0.0001
GFRIS r=2 with FRIS	GFRIS r=2	3.654	0.000	-15.033	Beyond 0.0001
GFRIS r=4 with FRIS	GFRIS r=4	2.772	0.000	-13.077	Beyond 0.0001
FCM with FRIS	FCM	3.032	0.000	-13.893	Beyond 0.0001
PCM with FRIS	PCM	3.220	0.008	-14.037	Beyond 0.0001
FRIST r=1	GFRIS r=1	6.426	1.758	-7.131	Beyond 0.0001
FRIST r=2	GFRIS r=2	8.542	3.721	-1.345	0.0893
FRIST r=4	GFRIS r=4	9.792	2.742	-7.951	Beyond 0.0001

A further quantitative evaluation was conducted using the statistical significance test called the *sign test*. The results of this test are presented in Tables 7.3 and 7.4, which again demonstrate that GFRIS accomplished significant progress over both FCM and PCM for both images at a significance level beyond 0.0001, that is 0.01%, which is a very high significance indeed.

Table 7.4: The overall results of the statistical significance test, *sign test* for the Brodatz image in Fig. 7.1(c).

Algorithm	Ref. Algorithm	Percentage of + Pixels	Percentage of - Pixels	Z Value	Significance Level
GFRIS $r=1$	FCM	9.911	5.316	-12.467	Beyond 0.0001
GFRIS $r=2$	FCM	16.080	4.684	-26.504	Beyond 0.0001
GFRIS $r=4$	FCM	15.680	3.227	-30.356	Beyond 0.0001
PCM	FCM	8.533	40.062	-47.958	Beyond 0.0001
GFRIS $r=1$	PCM	43.911	7.787	-53.276	Beyond 0.0001
GFRIS $r=2$	PCM	50.018	7.093	-60.232	Beyond 0.0001
GFRIS $r=4$	PCM	50.782	6.800	-61.464	Beyond 0.0001
FCM	PCM	40.062	8.533	-47.958	Beyond 0.0001
GFRIS $r=1$ with FRIS	GFRIS $r=1$	6.640	0.089	-26.750	Beyond 0.0001
GFRIS $r=2$ with FRIS	GFRIS $r=2$	8.969	0.000	-31.733	Beyond 0.0001
GFRIS $r=4$ with FRIS	GFRIS $r=4$	7.964	0.044	-29.650	Beyond 0.0001
FCM with FRIS	FCM	7.467	0.000	-28.948	Beyond 0.0001
PCM with FRIS	PCM	0.400	0.089	-4.585	Beyond 0.0001
FRIST $r=1$	GFRIS $r=1$	13.591	0.667	-36.280	Beyond 0.0001
FRIST $r=2$	GFRIS $r=2$	6.356	0.569	-23.289	Beyond 0.0001
FRIST $r=4$	GFRIS $r=4$	5.431	0.000	-24.678	Beyond 0.0001
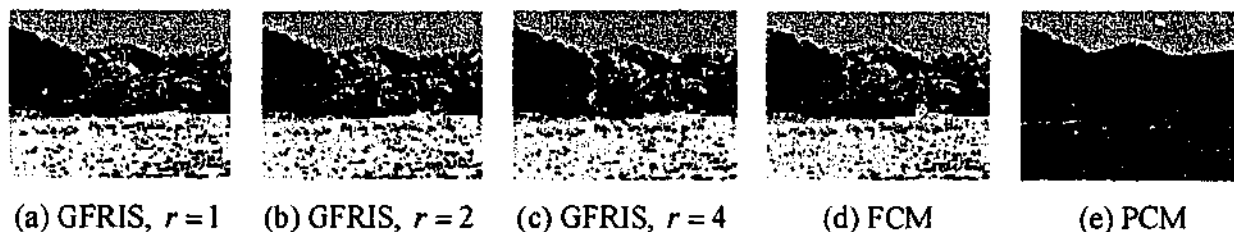
(a) GFRIS, $r=1$ (b) GFRIS, $r=2$ (c) GFRIS, $r=4$ (d) FCM   (e) PCM

Fig. 7.6: The segmented results of the forest image in Fig. 7.1(e) into three regions using the GFRIS, FCM, and PCM algorithms.

(a) GFRIS, $r=1$ (b) GFRIS, $r=2$ (c) GFRIS, $r=4$ (d) FCM   (e) PCM
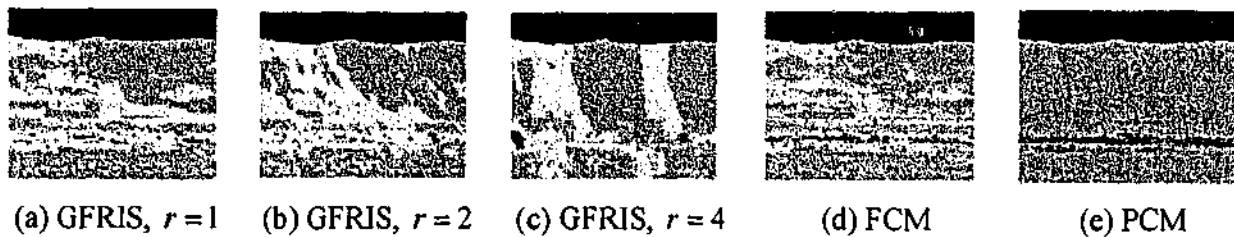
Fig. 7.7: The segmented results of the hill image in Fig. 7.1(g) into three regions using the GFRIS, FCM, and PCM algorithms.

A second series of experiments were performed using the six natural images containing three different objects shown in Fig. 7.1(e), 7.1(g), and B.2. The forest and hill images in Fig. 7.1(e) and 7.1(g) comprise three distinct regions, namely forest (R_1), sky (R_2), and water (R_3) and sky (R_1),

hill (R_2), and field (R_3) respectively. The segmentation performance for the three regions using GFRIS, FCM, and PCM is presented in Fig. 7.6, 7.7, and C.2.

Table 7.5: Error percentages for the forest and hill image segmentations respectively using the GFRIS, FCM, and PCM algorithms.

Algorithm	Forest (Fig. 7.1(e))			Hill (Fig. 7.1(g))		
	Region	Type I	Type II	Region	Type I	Type II
GFRIS r=1	Forest (R_1)	▓▓	6.398	Sky (R_1)	0.475	▓▓
	Sky (R_2)	1.430	▓▓	Hill (R_2)	43.411	34.646
	Water (R_3)	▓▓	▓▓	Field (R_3)	▓▓	▓▓
GFRIS r=2	Forest (R_1)	▓▓	6.433	Sky (R_1)	0.475	▓▓
	Sky (R_2)	1.415	▓▓	Hill (R_2)	45.663	▓▓
	Water (R_3)	▓▓	▓▓	Field (R_3)	▓▓	33.463
GFRIS r=4	Forest (R_1)	▓▓	▓▓	Sky (R_1)	0.475	▓▓
	Sky (R_2)	1.415	▓▓	Hill (R_2)	37.961	35.488
	Water (R_3)	▓▓	▓▓	Field (R_3)	56.891	▓▓
FCM	Forest (R_1)	25.353	5.526	Sky (R_1)	0.440	1.680
	Sky (R_2)	0.730	3.539	Hill (R_2)	44.836	33.233
	Water (R_3)	15.761	16.485	Field (R_3)	54.720	32.799
PCM	Forest (R_1)	3.578	49.464	Sky (R_1)	0.387	3.484
	Sky (R_2)	1.141	2.254	Hill (R_2)	5.317	58.497
	Water (R_3)	83.008	2.206	Field (R_3)	97.338	3.420

It was visually apparent again that the GFRIS algorithm produced more distinctive regions in both images for all values of the neighbourhood radius r and hence considerably outperformed both FCM and PCM. PCM could not separate the water (R_3) (Fig. 7.6(e)) and field (R_3) (Fig. 7.7(e)) regions from the forest and hill images respectively because it was unable to distinguish between regions exhibiting a poor gray level contrast. In Fig. 7.7(a)-Fig. 7.7(c) GFRIS provided better results for the hill image compared with FCM and PCM, even though it could not separate the hill (R_2) and field (R_3) regions well because as mentioned earlier, they are very similar in gray level and exhibit strong spatial correlation, which means they perceptually appear almost the same.

The error rates for the segmentation of the forest, hill, and additional four images compared with the manually segmented reference images are given in Tables 7.5 and D.2 respectively. Again

the shaded entries in Table 7.5 highlight the best GFRIS results. Overall, GFRIS obtained improved results especially for all regions and the sky (R_1) and field (R_2) regions of the forest and hill images respectively because there exists good continuation among the spatially correlated pixels of these regions.

The mean error rates shown in Fig. 7.8 of GFRIS for the forest, hill, and the average of the six images containing three regions were considerably lower than for both FCM and PCM, while the error was the highest for the PCM for all cases. As mentioned before, this was due to PCM being unable to segment poorly contrasted regions. GFRIS achieved 14.8% and 31.2% of the overall error improvements over FCM and PCM respectively for the six images.
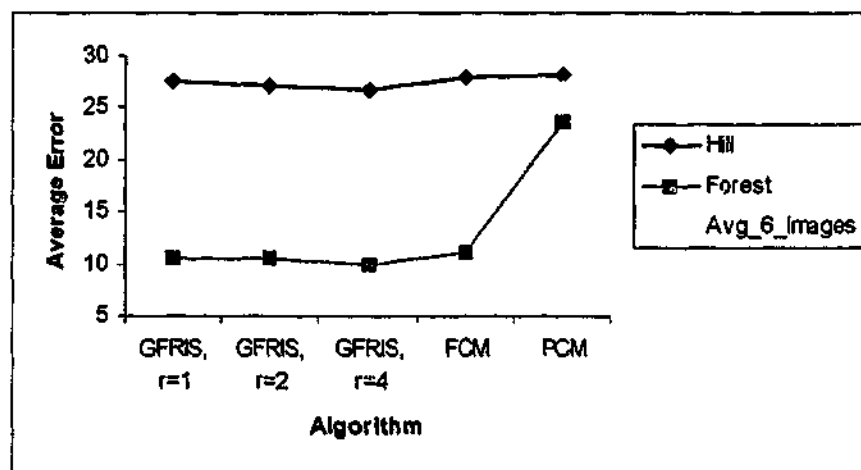
Fig. 7.8: Average percentages of error rates of GFRIS, FCM, and PCM for the Fig. 7.1(e), 7.1(g), and average of the six image segmentations.

Fig. 7.9 shows better probability of object-count-agreement for GFRIS for all the sample images. The best probability was obtained for GFRIS using neighbourhood radius $r = 4$ because the higher order spatial relationship reduces the scattering regions therefore keeping the spatially correlated pixels together. Overall GFRIS provided significant improvements (34% and 50.6% over FCM and PCM respectively for the six images) for all values of r and both forest and hill images at a significance level greater than 0.0001 as shown in Tables 7.6 and 7.7.
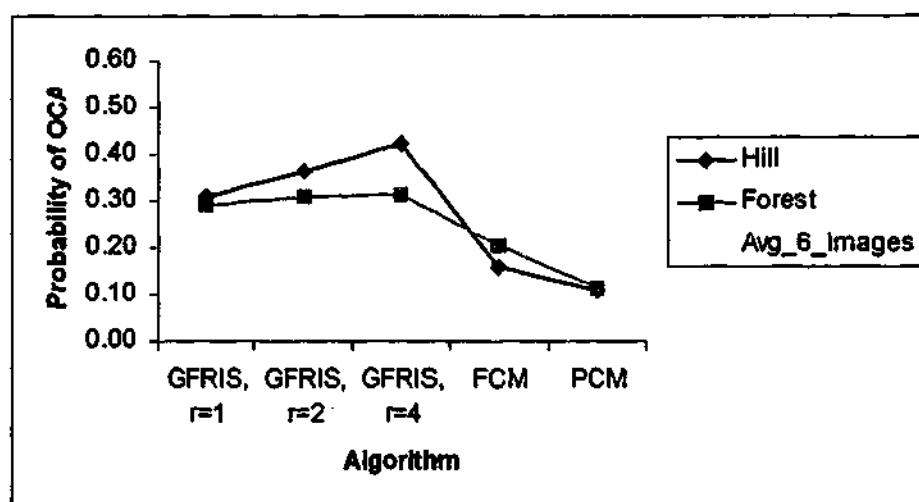
Fig. 7.9: Probability of object-count-agreement (OCA) for GFRIS, FCM, and PCM for the Fig. 7.1(e), 7.1(g), and average of the six image segmentations.

Table 7.6: The overall results of the statistical significance test, *sign test* for the forest image in Fig. 7.1(e).

Algorithm	Ref. Algorithm	Percentage of + Pixels	Percentage of - Pixels	Z Value	Significance Level
GFRIS r=1	FCM	2.398	1.369	-11.297	Beyond 0.0001
GFRIS r=2	FCM	2.649	1.768	-8.998	Beyond 0.0001
GFRIS r=4	FCM	3.073	1.514	-14.427	Beyond 0.0001
PCM	FCM	7.258	22.553	-46.585	Beyond 0.0001
GFRIS r=1	PCM	22.903	6.579	-50.964	Beyond 0.0001
GFRIS r=2	PCM	22.867	6.691	-50.347	Beyond 0.0001
GFRIS r=4	PCM	23.527	6.673	-52.044	Beyond 0.0001
FCM	PCM	22.553	7.258	-46.585	Beyond 0.0001
GFRIS r=1 with FRIS	GFRIS r=1	3.375	0.013	-33.408	Beyond 0.0001
GFRIS r=2 with FRIS	GFRIS r=2	4.029	0.008	-37.068	Beyond 0.0001
GFRIS r=4 with FRIS	GFRIS r=4	3.691	0.013	-35.540	Beyond 0.0001
FCM with FRIS	FCM	9.358	0.011	-58.095	Beyond 0.0001
PCM with FRIS	PCM	0.176	0.247	-1.762	0.0392
FRIST r=1	GFRIS r=1	0.564	0.021	-13.567	Beyond 0.0001
FRIST r=2	GFRIS r=2	0.611	0.000	-14.697	Beyond 0.0001
FRIST r=4	GFRIS r=4	0.543	0.000	-14.000	Beyond 0.0001

In the above experiments, the number of segmented regions was constrained to either two or three. In order to examine the full discriminating potential of the GFRIS algorithm for a larger number of regions, a comparison was made with the FCM and PCM algorithms on the image in Fig. 7.1(i) that possessed five regions [6]. The regions were: - egg (R_1), glass of milk (R_2), curtain

(R_3), cheese (R_4), and table (R_5). Fig. 7.10 shows the respective segmentation performance of the GFRIS, FCM, and PCM algorithms.

Table 7.7: The overall results of the statistical significance test, *sign test* for the hill image in Fig. 7.1(g).

Algorithm	Ref. Algorithm	Percentage of + Pixels	Percentage of - Pixels	Z Value	Significance Level
GFRIS r=1	FCM	4.792	4.194	-4.393	Beyond 0.0001
GFRIS r=2	FCM	7.871	6.805	-3.814	Beyond 0.0001
GFRIS r=4	FCM	13.269	11.713	-8.472	Beyond 0.0001
PCM	FCM	15.628	16.643	-15.060	Beyond 0.0001
GFRIS r=1	PCM	16.228	14.614	-13.051	Beyond 0.0001
GFRIS r=2	PCM	17.179	15.098	-12.484	Beyond 0.0001
GFRIS r=4	PCM	15.087	12.515	-8.209	Beyond 0.0001
FCM	PCM	16.643	15.628	-15.060	Beyond 0.0001
GFRIS r=1 with FRIS	GFRIS r=1	0.934	0.060	-17.718	Beyond 0.0001
GFRIS r=2 with FRIS	GFRIS r=2	0.512	0.256	-7.430	Beyond 0.0001
GFRIS r=4 with FRIS	GFRIS r=4	0.752	0.006	-15.202	Beyond 0.0001
FCM with FRIS	FCM	1.205	0.000	-23.324	Beyond 0.0001
PCM with FRIS	PCM	0.074	0.000	-5.570	Beyond 0.0001
FRIST r=1	GFRIS r=1	18.710	9.910	-20.339	Beyond 0.0001
FRIST r=2	GFRIS r=2	20.779	8.980	-28.974	Beyond 0.0001
FRIST r=4	GFRIS r=4	14.113	17.591	-14.543	Beyond 0.0001

(a) GFRIS, $r=1$ (b) GFRIS, $r=2$ (c) GFRIS, $r=4$ (d) FCM   (e) PCM
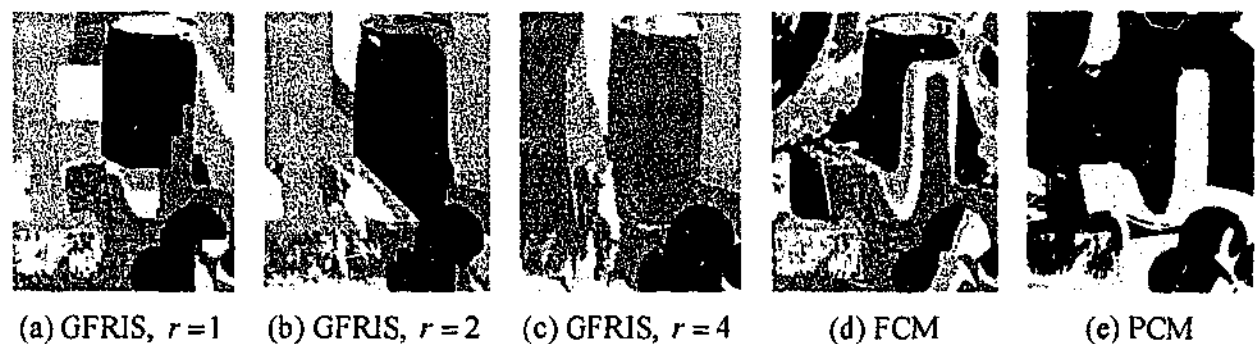
Fig. 7.10: The segmented results of the food image in Fig. 7.1(i) into five regions using the GFRIS, FCM, and PCM algorithms.

From Fig. 7.10(d)-7.10(e), it is clear that both FCM and PCM arbitrarily divided the image into five regions without considering any semantic meaning of the data. The results produced by GFRIS for r=1 and r=2, in Fig. 7.10(a) and 7.10(b) showed much greater consistency with the information derived from the manually segmented regions. There are some regions such as egg (R_1) and milk (R_2), curtain (R_3) and cheese (R_4), which overlap with each other because their gray level pixel intensities are very similar. The most promising results in Fig. 7.10(c) were obtained for GFRIS

using $r=4$, with the exception of region cheese (R_4), which partially merged with region milk (R_2) because cheese (R_4) and milk (R_2) possess almost exactly the same gray level intensities. Again the GFRIS algorithm considered the underlying meaning of data far better than both the FCM and PCM algorithms when compared with the manually segmented results.

Table 7.8: Error percentages for the food image segmentation in Fig. 7.1(i).

Algorithm	Egg (R_1) Error Type		Milk (R_2) Error Type		Curtain (R_3) Error Type		Cheese (R_4) Error Type		Table (R_5) Error Type	
	I	II	I	II	I	II	I	II	I	II
GFRIS $r=1$			82.05	18.38					69.86	2.77
GFRIS $r=2$			91.35	9.46		19.91	81.04	12.02		2.15
GFRIS $r=4$				33.21			81.43	11.22		3.02
FCM	53.90	27.79	78.17	17.57	57.73	19.38	73.68	18.32	64.17	1.67
PCM	24.58	59.36	97.22	3.85	98.21	1.10	61.25	30.53	100.00	2.33

The numerical evaluations of the image segmentation given in Table 7.8, reveal that the mean errors for the egg (R_1), curtain (R_3), and cheese (R_4), egg (R_1), curtain (R_3), and table (R_5), and egg (R_1), milk (R_2), curtain (R_3), and table (R_5) regions were appreciably lower using GFRIS with $r=1$, $r=2$, and $r=4$ respectively than for either FCM or PCM. In general, the results confirm that a significant improvement was achieved for all regions using GFRIS with neighbourhood radius $r=4$, except for the cheese (R_4) region, for the reason alluded above.

The average error rates and the probabilities of object-count-agreement (OCA) for each algorithm in the food image segmentation are shown in Fig. 7.11 and 7.12 respectively. These show lower average errors and better object-count-agreement for GFRIS for all values of neighbourhood radius r over both the FCM and PCM algorithms. GFRIS obtained 17.9% and 29.2% improved overall errors and 203.9% and 2127.4% (!) better overall probability of OCA than FCM and PCM respectively. The inordinately high improvement over PCM for overall probability of OCA is due to the very poor performance of PCM highlighted in both Fig. 7.10(e) and Fig. 7.12 caused by the poorly contrasted regions in the food image (Fig. 7.1(i)). This five region example confirms that just as with FCM and PCM, the GFRIS algorithm can be extended to separate an arbitrary number

of regions (objects) in an image, though there will be a commensurate increase in the computational complexity.
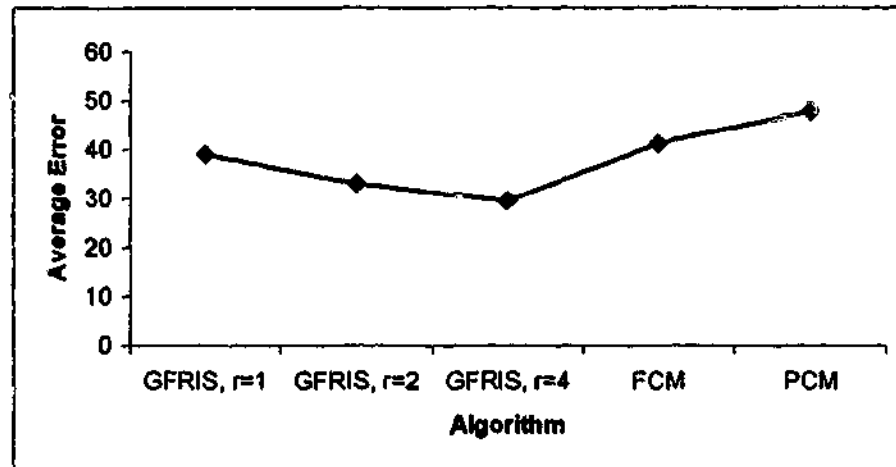
Fig. 7.11: Average percentages of error rates of GFRIS, FCM, and PCM for the Fig. 7.1(i) image segmentation.
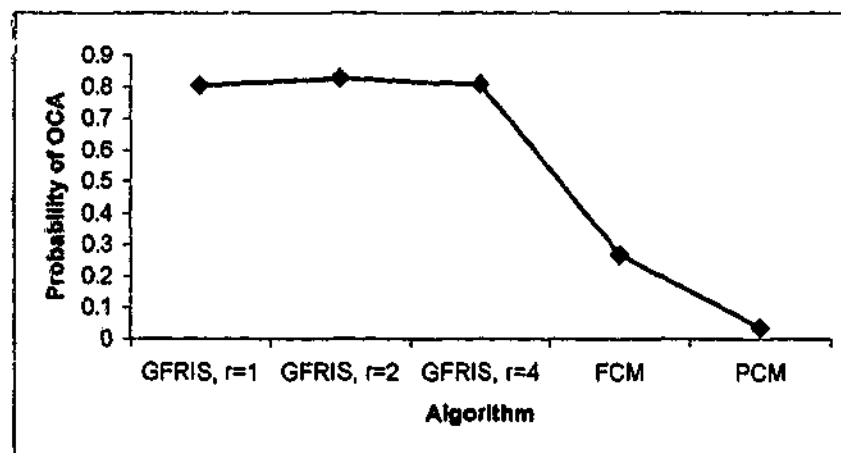

Fig. 7.12: Probability of object-count-agreement (OCA) for GFRIS, FCM, and PCM for the Fig. 7.1(i) image segmentation.

The results of the *sign test* in Table 7.9 also support the significantly improved results of the GFRIS algorithm over both the FCM and PCM algorithms at a significance level greater than 0.0001.

In comparison with both FCM and PCM, GFRIS provided significantly superior results for a variety of different image types, including image examples having multiple regions. Its performance in considering the underlying meaning of data was also better when the results were compared with the manually segmented reference regions. However, it proved ineffective for image regions characterised by either being non-homogeneous or possessing sharp variations in pixel intensity (see urban scene (R_2) in Fig. 7.2(a)-(c) and Brodatz texture d8 (R_1) and d94 (R_2) in Fig. 7.3(a)-(c) regions). To address these disadvantages, new refining rules have been developed for integration into the integrated fuzzy rule-based image segmentation framework (Fig. 1.1), by utilizing a combination of an object's connectedness, surroundedness, uniformity, and contrast properties. These refinement rules have been fully explained in Chapter 4 and the performance analysis of the FRIS algorithm will now be discussed.

Table 7.9: The overall results of the statistical significance test, *sign test* for the food image in Fig. 7.1(i).

Algorithm	Ref. Algorithm	Percentage of + Pixels	Percentage of - Pixels	Z Value	Significance Level
GFRIS $r=1$	FCM	15.597	7.502	-72.576	Beyond 0.0001
GFRIS $r=2$	FCM	24.504	11.292	-89.370	Beyond 0.0001
GFRIS $r=4$	FCM	34.821	8.833	-176.214	Beyond 0.0001
PCM	FCM	13.326	24.046	-122.966	Beyond 0.0001
GFRIS $r=1$	PCM	27.364	8.549	-177.769	Beyond 0.0001
GFRIS $r=2$	PCM	30.967	7.036	-203.151	Beyond 0.0001
GFRIS $r=4$	PCM	41.865	5.157	-269.828	Beyond 0.0001
FCM	PCM	24.046	13.326	-122.966	Beyond 0.0001

7.6 Performance Analysis of the FRIS Algorithm

Since FRIS (Block 2 in Fig. 1.1) is a refinement algorithm, GFRIS will be used together with FCM and PCM in order to initially segment an image. The refinement process will be applied to all three algorithms and the performance correspondingly evaluated. The segmentation results of the cloud (Fig. 7.1(a)), Brodatz texture (Fig. 7.1(c)), and the other six images (Fig. B.1) comprising the two regions are shown in Fig. 7.13, 7.14, and C.3 respectively for FCM, PCM, and GFRIS.

It is visually apparent that the segmentation results especially for the urban scene (R_2) and d8(R_1) and d94 (R_2) of the cloud and Brodatz texture regions respectively (Fig. 7.2(a) - 7.2(e) and 7.3(a) - 7.3(e)) produced by FCM, PCM, and GFRIS algorithms, without applying FRIS contain a

large number of misclassified pixels from the other region. This is because in all cases they possess very sharp variations in pixel intensity. Nearly all the misclassified pixels of all regions, except the text caption for cloud and the misclassified pixels by PCM for Brodatz texture were correctly classified when the refinement rules of FRIS were incorporated into GFRIS, FCM, and PCM (Fig. 7.13(a) - 7.13(e) and 7.14(a) - 7.14(d)). FRIS improved very little for PCM for the Brodatz texture image (Fig. 7.14(e)) because the initial PCM segmentation could not separate the texture regions at all for this image. This reiterates the point that FRIS refines effectively an initial segmentation, but is unable to improve a very poor initial segmentation.
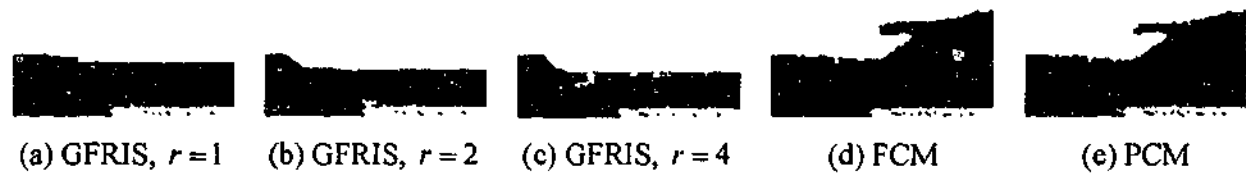
   (a) GFRIS, $r = 1$ (b) GFRIS, $r = 2$ (c) GFRIS, $r = 4$ (d) FCM   (e) PCM

Fig. 7.13: The segmented results of the cloud image in Fig. 7.1(a) into two regions using FRIS with the GFRIS, FCM, and PCM algorithms.

   (a) GFRIS, $r = 1$ (b) GFRIS, $r = 2$ (c) GFRIS, $r = 4$ (d) FCM   (e) PCM
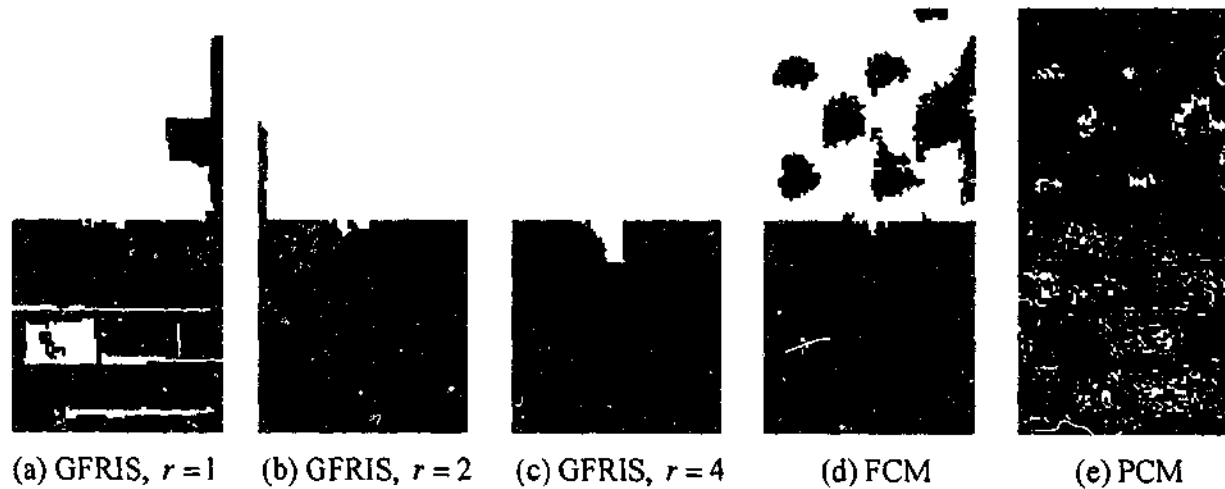
Fig. 7.14: The segmented results of the Brodatz texture image (d8 and d94) in Fig. 7.1(c) into two regions using FRIS with the GFRIS, FCM, and PCM algorithms.

The numerical segmentation results of the cloud, Brodatz texture, and supplementary six image segmentations with respect to the manually segmented reference images (Fig. 7.1 and B.1) using the *discrepancy based on the number of mis-segmented pixels* method are shown in Tables 7.10 and

D.3 respectively. In Table 7.10, only the error rates for the cloud (R_1) and Brodatz texture d8 (R_1) regions are shown. The improvements achieved using FRIS are highlighted in Table 7.10.

Table 7.10: Error percentages for the cloud and Brodatz texture d8 regions of the cloud (Fig. 7.1(a)) and Brodatz texture (Fig. 7.1(c)) image segmentations respectively using FRIS with the GFRIS, FCM, and PCM algorithms.

Algorithm	Cloud (R_1) Region		Brodatz Texture d8 (R_1) Region	
	Type I	Type II	Type I	Type II
GFRIS $r=1$	7.3333			
GFRIS $r=2$	1.7273			
GFRIS $r=4$	1.803			
FCM				
PCM				
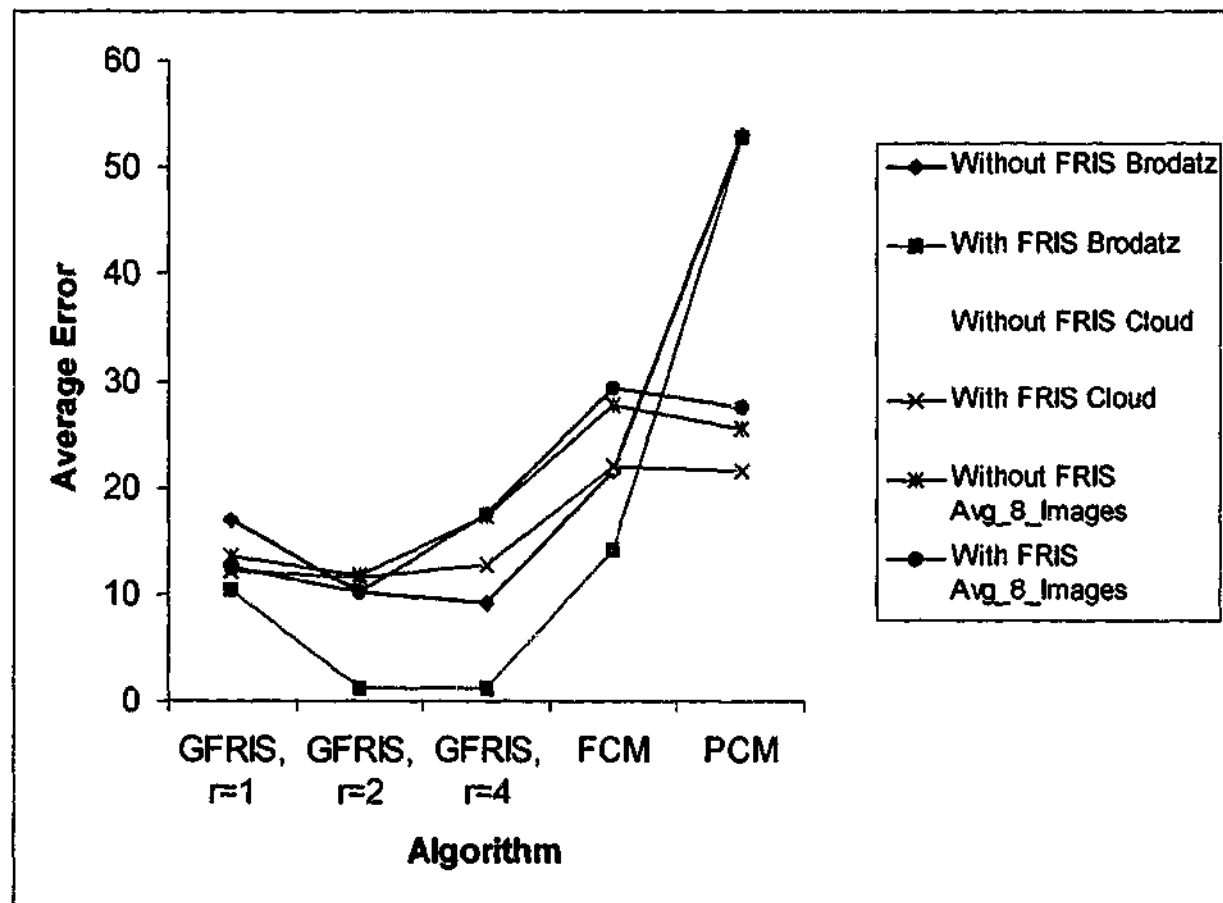
Fig. 7.15: Average percentages of error rates of GFRIS, FCM, and PCM with and without using FRIS for the Fig. 7.1(a) and 7.1(c), and average of the eight image segmentations.

The average error rates for all three algorithms with and without using FRIS are plotted in Fig. 7.15. This reveals very promising results for all algorithms for all images including the average results of the eight images when FRIS was integrated within these algorithms. The exception was PCM for the Brodatz texture, which as mentioned above failed because PCM could not segment the Brodatz texture d8 (R_1) region at all. 48.4%, 37.2%, and 20.7% improvements of the overall errors were obtained for the GFRIS, FCM, and PCM algorithms respectively for the eight images, again emphasising the merit of incorporating the refinement rules.

The probabilities of object-count-agreement (OCA) for all algorithms with and without using FRIS are shown in Fig. 7.16 and reveal considerable improved probabilities of OCA for the refinement algorithm than those for all algorithms without FRIS. The GFRIS, FCM, and PCM algorithms produced 45.5%, 123.5%, and 48.9% higher probabilities of OCA for the eight images.
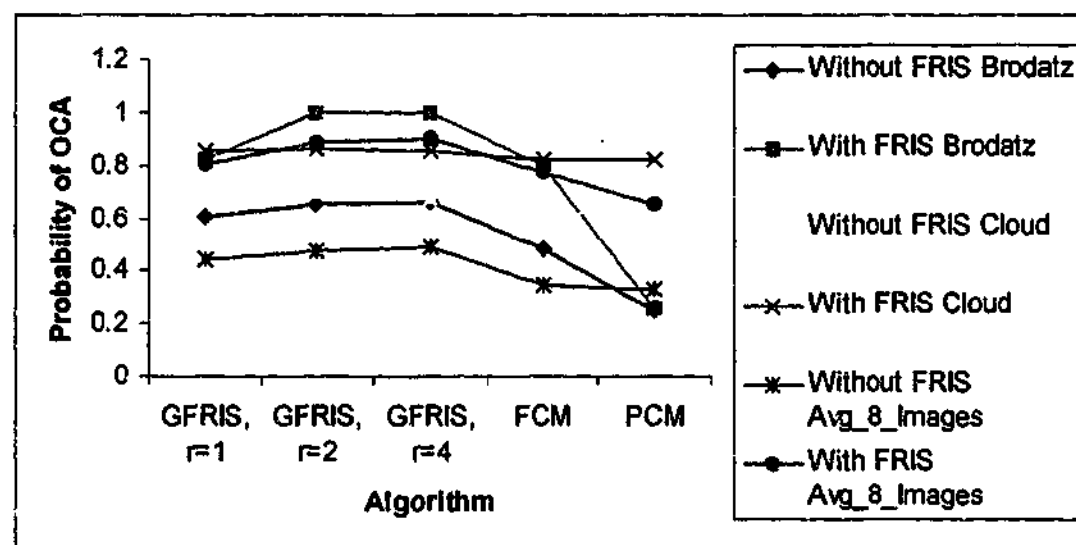
Fig. 7.16: Probability of object-count-agreement (OCA) for GFRIS, FCM, and PCM with and without using FRIS for the Fig. 7.1(a) and 7.1(c), and average of the eight image segmentations.

The results of the statistical significance test *(sign test)* in Tables 7.3 and 7.4 show that all of the algorithms incorporating FRIS exhibited significant improvement at the significant level beyond 0.0001 for the cloud and Brodatz texture image segmentations.

The segmented results of GFRIS, FCM, and PCM integrating FRIS for the forest (Fig. 7.1(e)), hill (Fig. 7.1(g)), and the remaining four images (Fig. B.2) containing three regions are shown in Fig. 7.17, 7.18, and C.2 respectively. The results for the forest image (Fig. 7.17(a) -7.17(d)) exhibit the perceptually improved regions for all algorithms, except PCM, by applying the FRIS algorithm.

It is important to emphasise that FRIS is a refinement algorithm, so its performance depends very much on the initial segmentation algorithm and for PCM the improvement is negligible because PCM could not initially separate the water (R_3) region from the forest (R_1) region in Fig. 7.17(e). The best improvement achieved for the FCM algorithm is shown in Fig. 7.17(d), where almost all three regions have been completely separated.

The segmentation potential of the FRIS algorithm was tested again using the hill image (Fig. 7.1(g)), which contains extremely poor contrast regions, namely the hill (R_2) and field (R_3) shown in Fig. 7.1(g). If the results produced by the original initial algorithms (Fig. 7.7(a) - 7.7(e)) are compared with the results (Fig. 7.18(a)- 7.18(e)) after applying FRIS, it can be seen that the latter ensures better results, even though the initial segmentation for these two regions was not promising (see Fig. 7.7). The numerical results using the FRIS algorithm, shown in Table 7.11, prove that FRIS accomplished better results for all regions of the forest and most of the regions in the hill image for all algorithms, except in the case of the hill (R_2) region for GFRIS, $r = 2$ and $r = 4$ and PCM because of poor initial segmentation. The numerical results for the remaining four images are given in Table D.4.
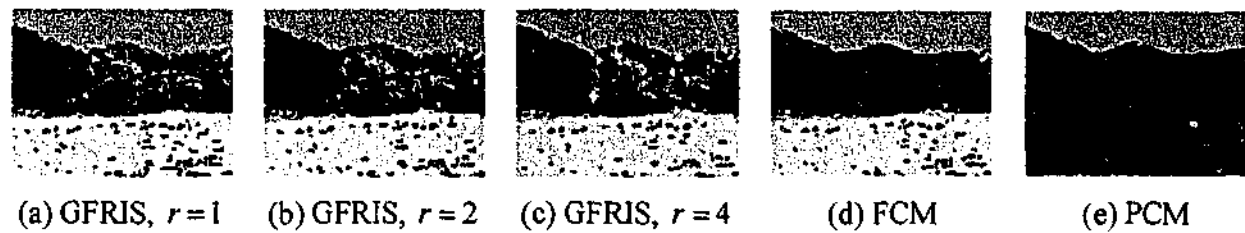
(a) GFRIS, $r = 1$ (b) GFRIS, $r = 2$ (c) GFRIS, $r = 4$ (d) FCM   (e) PCM

Fig. 7.17: The segmented results of the forest image in Fig. 7.1(e) into three regions using FRIS with the GFRIS, FCM, and PCM algorithms.

(a) GFRIS, $r = 1$ (b) GFRIS, $r = 2$ (c) GFRIS, $r = 4$ (d) FCM   (e) PCM
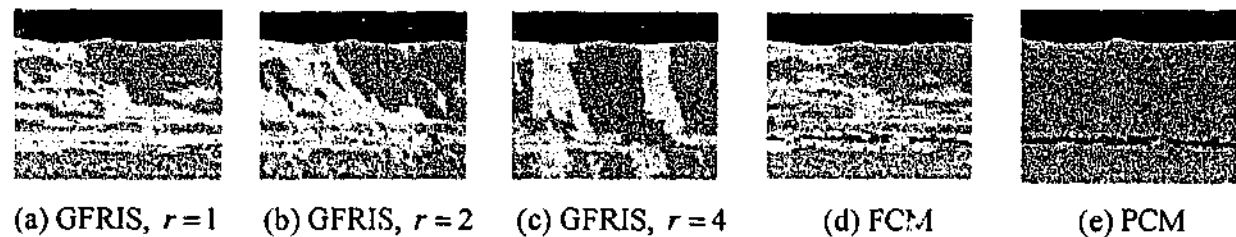
Fig. 7. 18: The segmented results of the hill image in Fig. 7.1(g) into three regions using FRIS with the GFRIS, FCM, and PCM algorithms.

The overall improvement in all three algorithms compared with obtained by using the FRIS algorithm in terms of both the average error percentage and the probability of object-count-agreement are shown in Fig. 7.19 and 7.20 respectively. Fig. 7.19 shows that FRIS obtained slight better overall errors for the hill image for all initial algorithms because of the inferior initial segmentation, but it achieved much higher probability of object-count-agreement for the hill image as shown in Fig. 7.20, since it reduced the scatter parts of some of the segmented regions of this image. The average error percentages and probability of object-count-agreements for the forest, the hill, and the six natural images containing three different regions clearly emphasise the improved performance of the FRIS algorithm. The overall error improvements obtained were 15.2%, 16.2%, and 9.3% for the GFRIS, FCM, and PCM algorithms respectively, whereas the respective gains for the probabilities of OCA were 27.7%, 58.5%, and 14% for the six images.

Table 7.11: Error percentages for the forest and hill image segmentations respectively using FRIS with the GFRIS, FCM, and PCM algorithms.

Initial Algorithm	Forest Image (Fig. 7.1(e))			Hill Image (Fig. 7.1(g))		
	Region	Type I	Type II	Region	Type I	Type II
GFRIS r=1	Forest (R_1)			Sky (R_1)	0.475	
	Sky (R_2)			Hill (R_2)		
	Water (R_3)			Field (R_3)		
GFRIS r=2	Forest (R_1)			Sky (R_1)	0.475	
	Sky (R_2)			Hill (R_2)		32.766
	Water (R_3)			Field (R_3)	51.001	
GFRIS r=4	Forest (R_1)			Sky (R_1)	0.475	
	Sky (R_2)			Hill (R_2)	37.961	35.562
	Water (R_3)			Field (R_3)		27.838
FCM	Forest (R_1)			Sky (R_1)	0.44	
	Sky (R_2)			Hill (R_2)		
	Water (R_3)			Field (R_3)		
PCM	Forest (R_1)		51.189	Sky (R_1)	0.387	
	Sky (R_2)			Hill (R_2)		59.843
	Water (R_3)			Field (R_3)		3.443
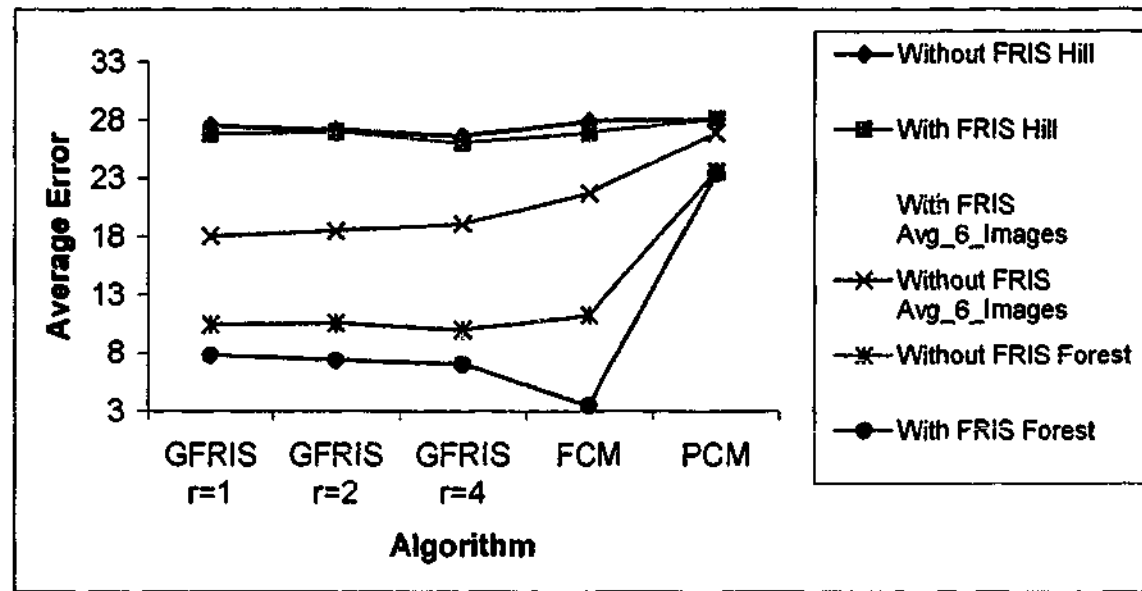
Fig. 7.19: Average percentages of error rates of GFRIS, FCM, and PCM with and without using FRIS for the Fig. 7.1(e), 7.1(g), and average of the six image segmentations.
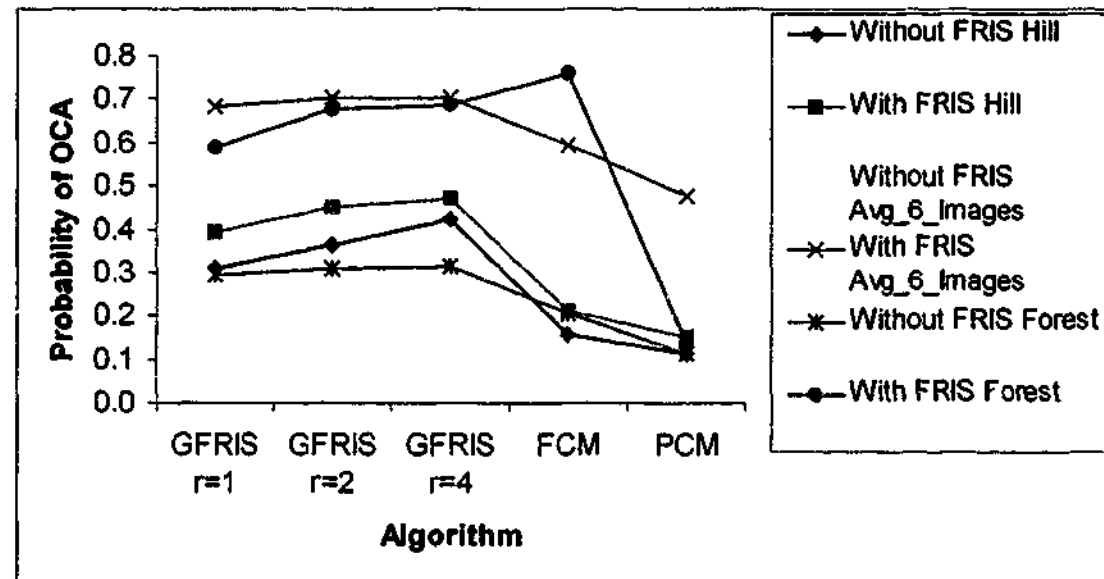

Fig. 7.20: Probability of object-count-agreement (OCA) for GFRIS, FCM, and PCM with and without using FRIS for the Fig. 7.1(e), 7.1(g), and average of the six image segmentations.

The *sign test* also confirmed these improvements for all algorithms using the refinement rules except PCM for the forest image at a significance level greater than 0.0001 shown in Tables 7.6 and 7.7. Table 7.6 illustrates that the significance level of improvement for PCM for the forest image

was 0.0392 i.e. 3.92% significance level of improvement, which means that this achievement is also noteworthy since it is more significant than the usual 5-10% significant levels.

From the analysis of the experimental results it has been proven that the FRIS algorithm has certainly enhanced segmentation of all algorithms, however, its potentiality depends on the performance of the initial segmentation algorithm. In this context, this demands improvement in the basic GFRIS algorithm. Note, that it was mentioned in Section 3.5 that the GFRIS algorithm did not generate good results for regions that contain irregular texture. The next section will describe the performance of the FRIST algorithm (**Block 3** in Fig. 1.1), which incorporates membership functions to consider texture features.

7.7 Performance Analysis of the FRIST Algorithm

The results of segmenting the cloud, Brodatz texture, and the additional six images into two regions using the FRIST algorithm, articulated in Chapter 5, are shown in Fig. 7.21, 7.22, and C.5 respectively. Fig. 7.21 and 7.22 demonstrate that a considerable number of the misclassified pixels of the urban scene (R_2) in Fig. 7.2 and the Brodatz texture d94 (R_2) in Fig. 7.3 produced by the GFRIS algorithm have been correctly classified by the FRIST algorithm for all images. Note, also that the FRIST algorithm correctly classified all most the entirely text caption of the cloud image (Fig. 7.21), which was not accomplished even by the FRIS algorithm (Fig. 7.13) because these two regions contain a number of sharp variations in the pixel intensity. As mentioned in Chapter 5, these sharp variations directly oppose the spatial relationships between the pixels, which is the basis of the GFRIS algorithm, however, the merit of the strategy adopted by FRIST to relax the condition upon the variance of spatial relations (see (5.5) and (5.6)) is fully vindicated by the results in Fig. 7.21 and 7.22.
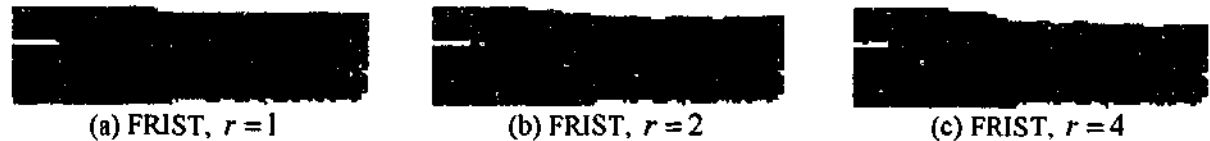
(a) FRIST, $r = 1$ (b) FRIST, $r = 2$ (c) FRIST, $r = 4$

Fig. 7.21: The segmented results of the cloud image in Fig. 7.1(a) into two regions using the FRIST algorithm.

(a) FRIST, $r = 1$ (b) FRIST, $r = 2$ (c) FRIST, $r = 4$
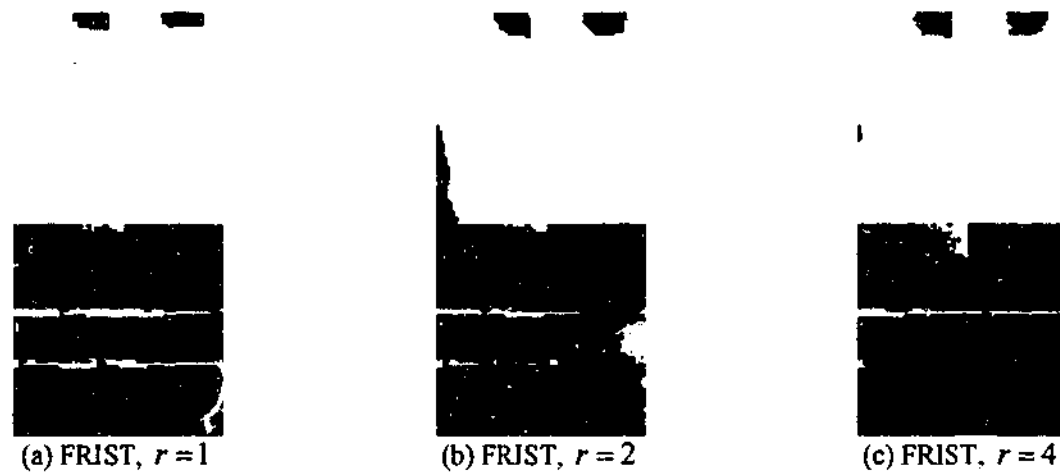
Fig. 7.22: The segmented results of the Brodatz texture image (d8 and d94) in Fig. 7.1(c) into two regions using the FRIST algorithm.

The numerical segmentation results of the cloud and Brodatz texture images together with the other six image segmentations with respect to manually segmented reference images are shown in Tables 7.12 and D.5 respectively. FRIST achieved improved Type II error and Type I and II errors for the cloud and Brodatz texture images respectively, especially for the regions that contain textures i.e. the urban scene (R_2) and d94 (R_2) regions of the cloud and Brodatz texture respectively.

Table 7.12: Error percentages for the cloud and Brodatz texture (d8) regions of the cloud (Fig. 7.1(a)) and Brodatz texture (Fig. 7.1(c)) image segmentations respectively using the FRIST algorithm.

Algorithm	Cloud (R_1) Region		Brodatz Texture d8 (R_1) Region	
	Type I	Type II	Type I	Type II
FRIST $r=1$	10.560			
FRIST $r=2$	9.106		6.169	
FRIST $r=4$	7.287			

The average error rates and probability of object-count-agreement (OCA) for the FRIST and GFRIS algorithms for the cloud, Brodatz texture, and average of the eight images are graphically shown in Fig. 7.23 and 7.24 respectively. From Fig. 7.23 and 7.24, it is clear that FRIST achieved considerable improvements over GFRIS. The best performance was obtained for the Brodatz texture image, because both its regions contain textures. The average over the eight images also illustrates the potential performance (25.5% and 15.3% improvements of the overall average error and probabilities of OCA respectively over GFRIS) of the FRIST algorithm.
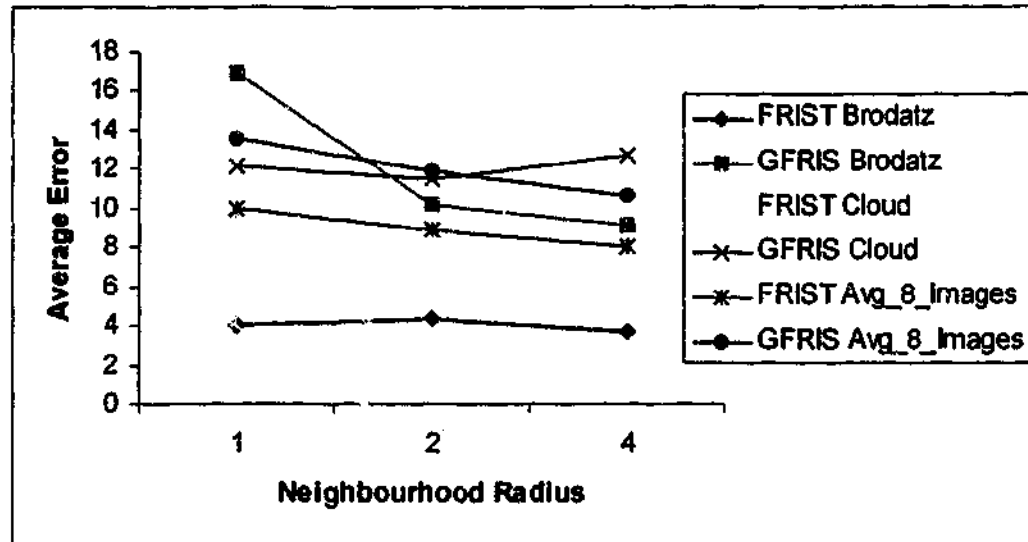
Fig. 7.23: Average percentages of error rates of FRIST and GFRIS for the Fig. 7.1(a) and 7.1 (c), and average of the eight image segmentations.
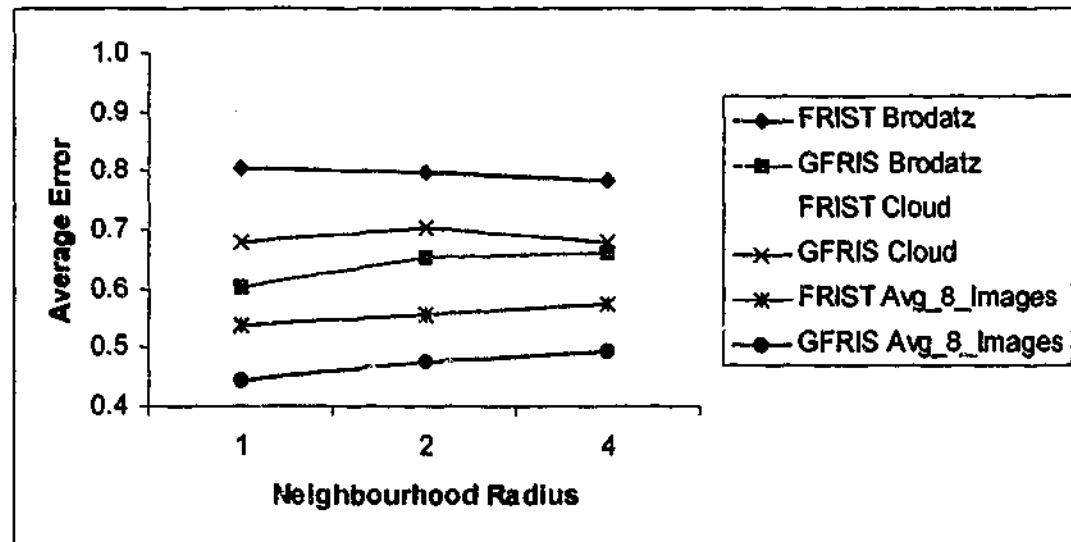
Fig. 7.24: Probability of object-count-agreement (OCA) of the FRIST and GFRIS algorithms for the Fig. 7.1(a) and 7.1 (c), and average of the eight image segmentations.

The significance levels of the improvement for the cloud and Brodatz image segmentations for the FRIST algorithm compared with GFRIS were greater than 0.0001 (Tables 7.3 and 7.4) except for the case of $r = 2$ for the cloud image, which provided a significance level of 0.0893. This was because FRIST could not segment the entire cloud (R_1) region as GFRIS did for $r = 2$. The reason for this is that there is no distinct boundary between the cloud (R_1) and urban scene (R_2) regions, so, GFRIS interpreted some sections of the urban scene (R_2) as cloud (R_1) for higher order spatial

relations. FRIST, because it is specifically designed to consider texture, relaxes the condition for good continuation and so prevents this misclassification thereby improving the segmentation performance and justifying the integration of this algorithm into the framework. This is also a significant improvement since the significance level of 0.0893 i.e. 8.93% is less than the standard significance level of 10%.
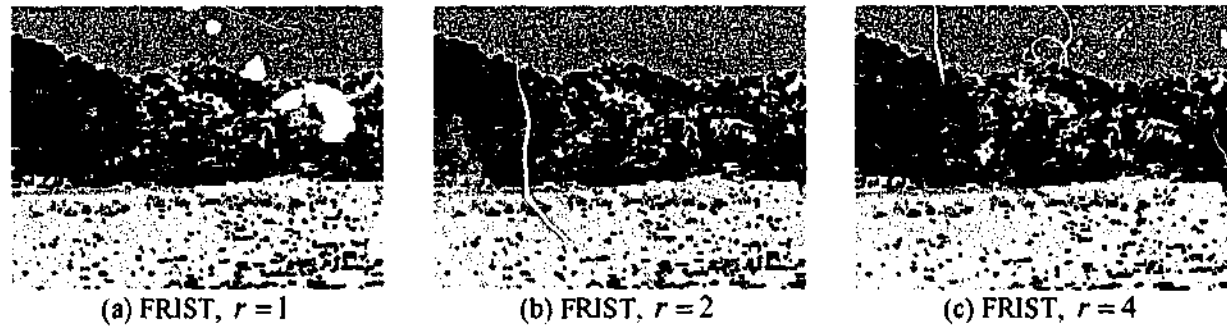
(a) FRIST, $r = 1$　　　　　　　(b) FRIST, $r = 2$　　　　　　(c) FRIST, $r = 4$

Fig. 7.25: The segmented results of the forest image in Fig. 7.1(e) into three regions using the FRIST algorithm.

(a) FRIST, $r = 1$　　　　　　　(b) FRIST, $r = 2$　　　　　　(c) FRIST, $r = 4$
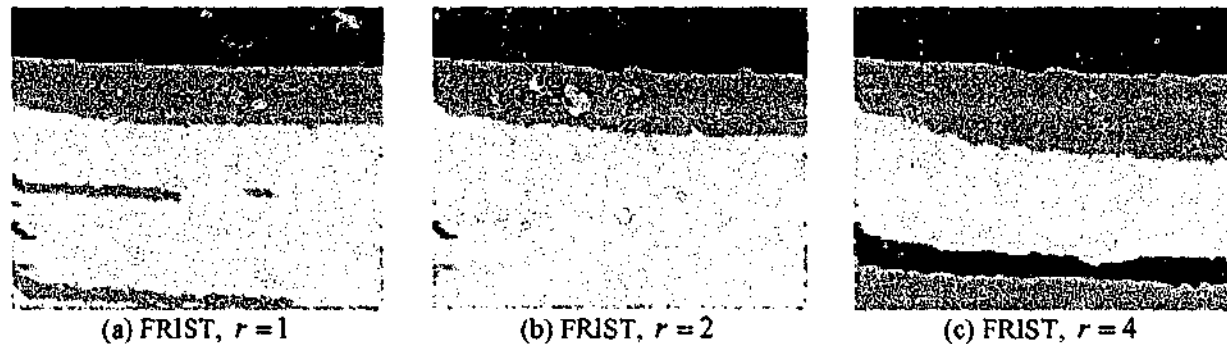
Fig. 7.26: The segmented results of the hill image in Fig. 7.1(g) into three regions using the FRIST algorithm.

The segmentation results of the forest (Fig. 7.1(e)), hill (Fig. 7.1(g)), and four supplementary images (Fig. B.2) into three regions produced by FRIST are shown in Fig. 7.25, 7.26, and C.6 respectively. If the segmented results of FRIST (Fig. 7.25 and 7.26) are compared with the corresponding segmented results of GFRIS (Fig. 7.6 and 7.7), the improvement of the FRIST algorithm is perceptually better despite the example of $r = 4$ for the hill image. This case misclassified some portions of the field (R_3) region into sky (R_1) and hill (R_2) because a portion of the field (R_3) has a similar gray level intensity to the sky (R_1). In addition the hill (R_2) and field (R_3) regions exhibit very poor contrast, are spatially correlated, and have the same surface

characteristic i.e. texture. The highest improvement was obtained using FRIST, $r = 2$ for the hill image (Fig. 7.26(b)), which completely separated the three regions except a small portion of the hill (R_2) region, which was misclassified into the field (R_3) region.

The numerical error rates of the misclassified pixels of the forest, hill, and additional four image segmentations with respect to the manually segmented reference regions (Fig. 7.1 and B.2) are given in Tables 7.13 and D.6 respectively. FRIST improved for all regions of the forest and the hill (R_2) and field (R_3) regions of the hill images except $r = 4$. For such high order spatial relationship FRIST clearly identified the three regions (Fig. 7.26(c)) of the hill image but as mentioned previously, a part of the field (R_3) region is very similar to the sky (R_1) region, which resulted in it being misclassified as the sky, which is shown by the erroneous narrow *blue band* in the field (R_3) region in Fig. 7.26(c).

The comparative values of the average of error percentages and the probabilities of the object-count-agreement for the segmentation of the forest (Fig. 7.1(e)), hill (Fig. 7.1(g)), and the average of the six images (Fig. B.2) are plotted in Fig. 7.27 and 7.28 respectively. These illustrate that FRIST provided better performance compared with GFRIS except as mentioned above for the case of $r = 4$. The average error (5.9% of overall error improvement) and probabilities of OCA (17.6% of overall probabilities of OCA) for the six image segmentations confirm both the potentiality and improvement of integrating these additional texture-based membership functions in the overall segmentation framework.

Table 7.13: Error percentages for the forest and hill image segmentations using the FRIST algorithm.

Initial	Forest Image (Fig. 7.1(e))			Hill Image (Fig. 7.1(g))		
Algorithm	Region	Type I	Type II	Region	Type I	Type II
FRIST $r=1$	Forest (R_1)			Sky (R_1)	1.408	1.246
	Sky (R_2)	1.43		Hill (R_2)	57.479	
	Water (R_3)			Field (R_3)		40.862
FRIST $r=2$	Forest (R_1)			Sky (R_1)	0.686	2.812
	Sky (R_2)			Hill (R_2)	58.649	
	Water (R_3)			Field (R_3)		39.802
FRIST $r=4$	Forest (R_1)			Sky (R_1)	0.651	11.965
	Sky (R_2)			Hill (R_2)	48.277	
	Water (R_3)			Field (R_3)		32

The *sign test* also confirmed significant improvement of FRIST algorithm over GFRIS algorithm at a significance level greater than 0.0001, except for $r = 4$ (Tables 7.6 and 7.7).
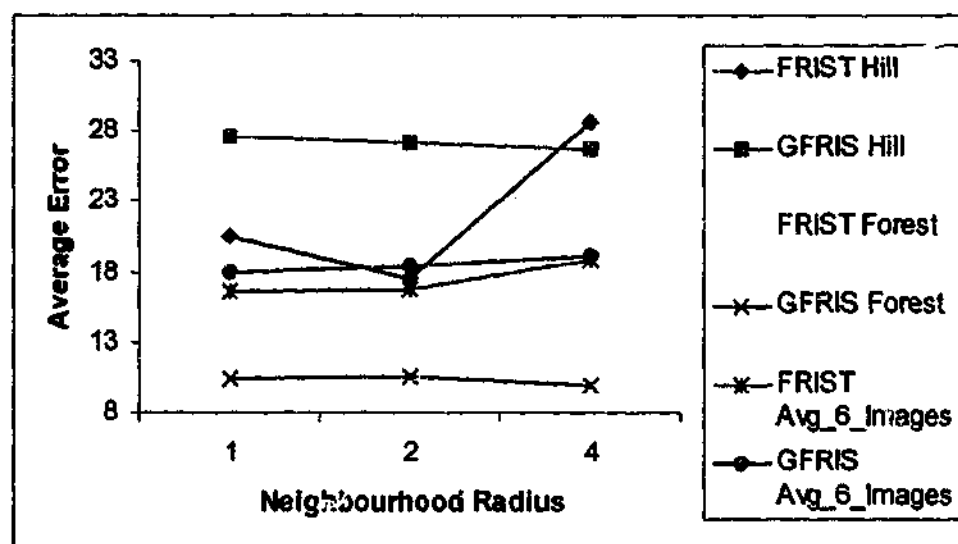

Fig. 7.27: Average percentages of error rates of FRIST and GFRIS for the Fig. 7.1(e), 7.1(g), and average of the six image segmentations.
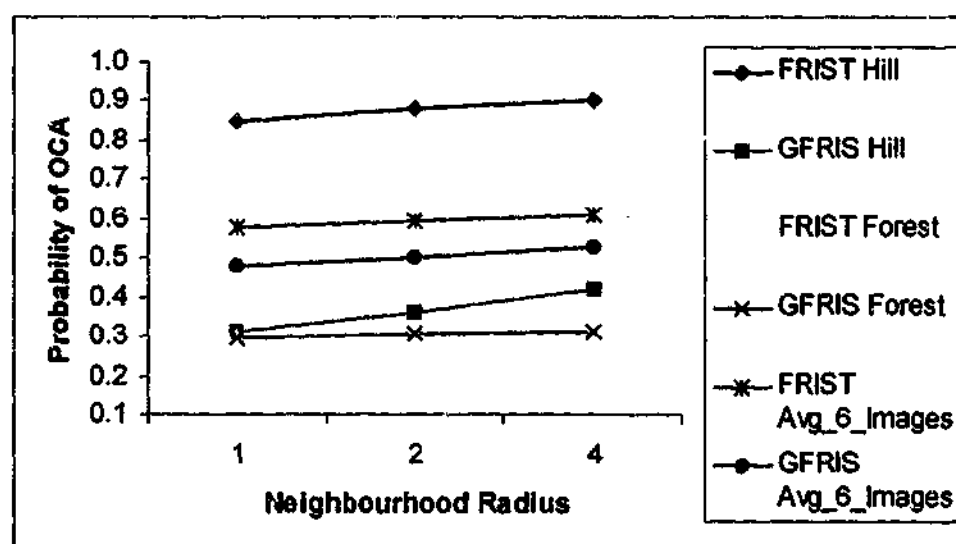

Fig. 7.28: Probability of object-count-agreement (OCA) of the FRIST and GFRIS algorithms for the Fig. 7.1(e), 7.1(g), and average of the six image segmentations.

So far, the segmentation of only gray level images have been considered for all algorithms, however, colour is the most important attribute of an object. It provides additional information in addition to the gray level, which can assist the segmentation of an object from an image. The next

section will provide the effectiveness of the fuzzy rule-based colour image segmentation (FRCIS) algorithm (**Block 4** in Fig. 1.1), which has been analysed in Chapter 6.

7.8 Performance Analysis of the FRCIS Algorithm

In this section, colour image segmentation performance using FRCIS, FCM, and PCM based on the HSV and RGB colour models will be described. The detailed underlying theory of the FRCIS algorithm and the motivations for choosing the HSV and RGB colour models have been presented in Chapter 6 and Section 2.4 respectively. The results produced by the FRCIS, FCM, and PCM algorithms for the cloud (Fig. 7.1(a)) and crocodile (Fig. 7.1(m)) images based on the HSV and RGB colour models are presented in Fig. 7.29 and 7.30 and Fig. 7.31 and 7.32 respectively. FRCIS provided better results than FCM and PCM when the segmented results of the FRCIS are visually compared with the respective results of FCM and PCM.

(a) FRCIS, $r=1$ (b) FRCIS, $r=2$ (c) FRCIS, $r=4$ (d) FCM (e) PCM
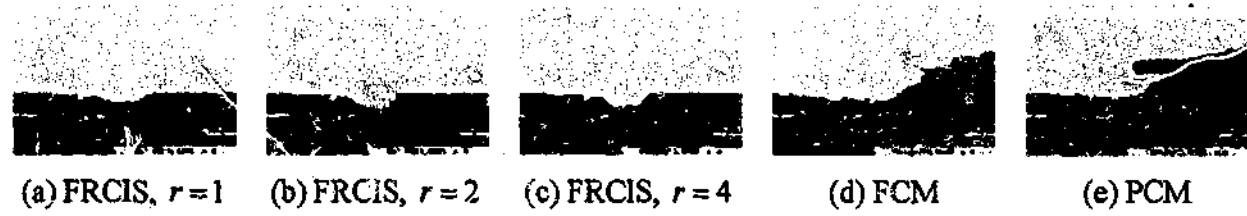
Fig. 7.29: The segmented results of the cloud image in Fig. 7.1(a) into two regions for the HSV colour model using the FRCIS, FCM, and PCM algorithms.

(a) FRCIS, $r=1$ (b) FRCIS, $r=2$ (c) FRCIS, $r=4$ (d) FCM (e) PCM
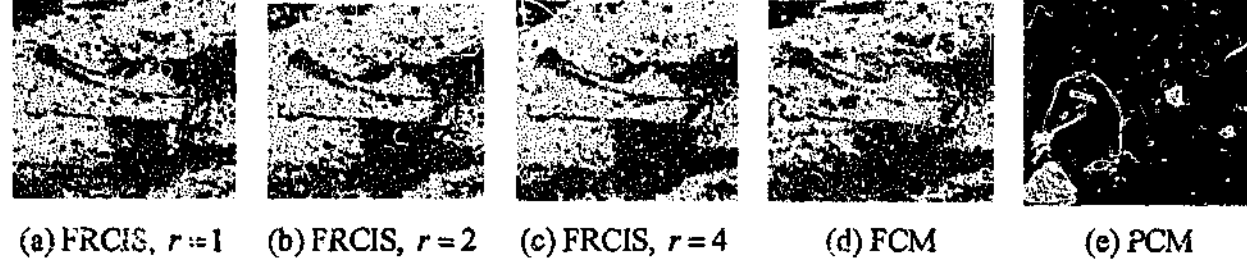
Fig. 7.30: The segmented results of the crocodile image in Fig. 7.1(m) into two regions for the HSV colour model using the FRCIS, FCM, and PCM algorithms.

The results produced using the HSV colour model (Fig. 7.29 and 7.30) outperformed those obtained utilising the RGB colour model (Fig. 7.31 and 7.32) for all images and algorithms except PCM for the crocodile image (Fig. 7.30(e) and 7.32(e)), which was totally unable to separate the background (R_2) region from crocodile (R_1). This is because the background (R_2) and the

crocodile (R_1) regions are very poor in contrast and PCM could not separate regions in such circumstances. The main reason for the superiority of the HSV colour model compared with the RGB model for colour image segmentation is that HSV is a perceptual colour model i.e. humans can recognise the basic attributes of the colour: H (hue), S (saturation), and V (value), while conversely RGB is a non-uniform colour model [136].
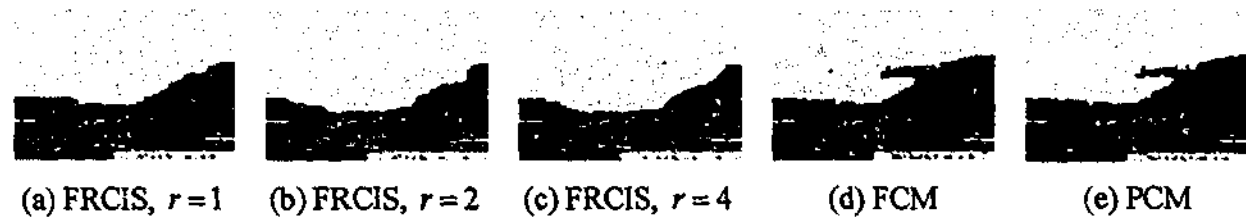
(a) FRCIS, $r=1$ (b) FRCIS, $r=2$ (c) FRCIS, $r=4$ (d) FCM   (e) PCM

Fig. 7.31:   The segmented results of the cloud image in Fig. 7.1(a) into two regions for the RGB colour model using the FRCIS, FCM, and PCM algorithms.

(a) FRCIS, $r=1$ (b) FRCIS, $r=2$ (c) FRCIS, $r=4$ (d) FCM   (e) PCM
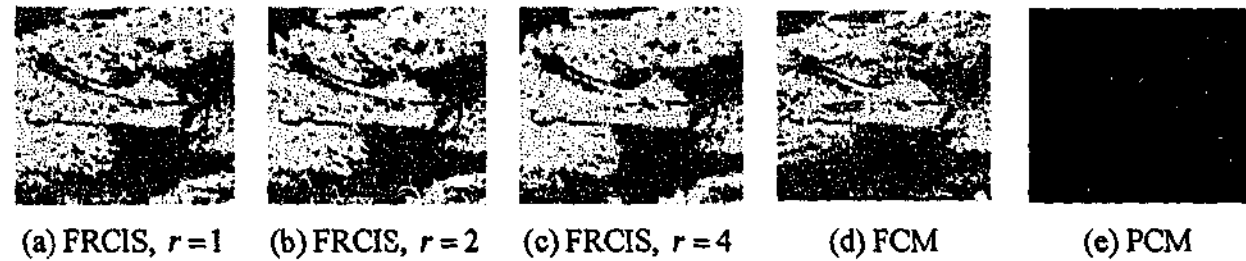
Fig. 7.32:   The segmented results of the crocodile image in Fig. 7.1(m) into two regions for the HSV colour model using the FRCIS, FCM, and PCM algorithms.

Table 7.14: Error percentages for the cloud (R_1) and crocodile (R_1) regions of the cloud (Fig. 7.1(a)) and crocodile (Fig. 7.1(m)) image segmentations respectively for the HSV and RGB colour models using the FRCIS, FCM, and PCM algorithms.

Algorithm	HSV Colour Model				RGB Colour Model			
	Cloud Region		Crocodile Region		Cloud Region		Crocodile Region	
	Type I	Type II	Type I	Type II	Type I	Type II	Type I	Type II
FRCIS, r=1				33.37		16.96		
FRCIS, r=2				35.53		17.37	57.80	
FRCIS, r=4				33.79		16.83	59.41	
FCM	21.12	13.24	57.00	32.88	21.12	14.97	56.63	46.43
PCM	28.33	10.67	0.00	99.89	28.33	15.80	0.00	100.00

The error percentages for the cloud (R_1) and crocodile (R_1) regions of the image in Fig. 7.1(a) and 7.1(m) respectively using the HSV and RGB colour models, and the FRCIS, FCM, and PCM

algorithms are tabulated in Table 7.14. It can be seen that the error rates of FRCIS for all values of r are better than both FCM and PCM using both the HSV and RGB colour models.
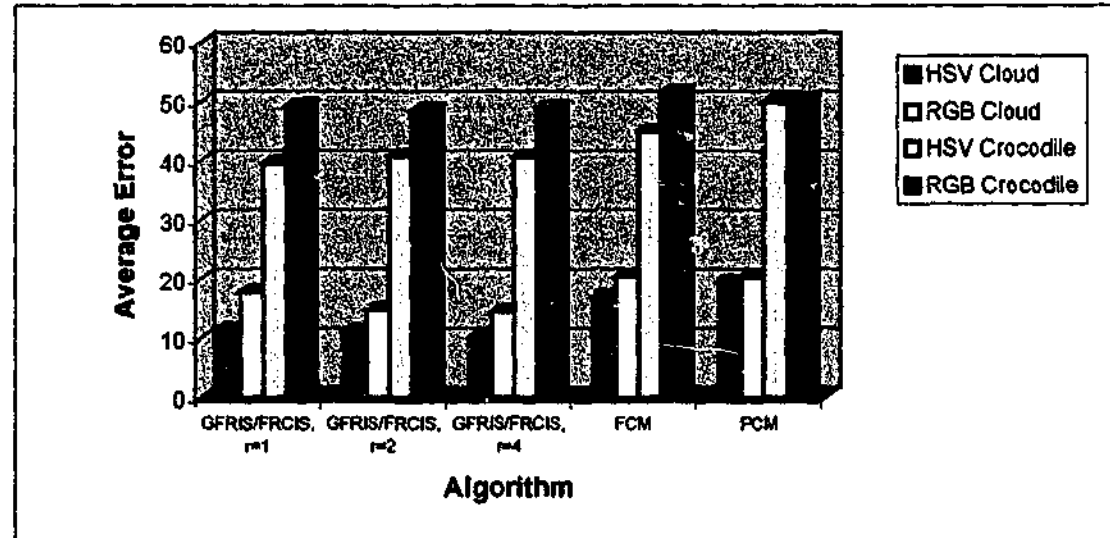
Fig. 7.33: Average error rates of the FRCIS, FCM, and PCM algorithms using the HSV and RGB colour models for the Fig. 7.1(a) and 7.1(m).

Table 7.15: The overall results of the statistical significance test, *sign test* for the cloud image in Fig. 7.1(a) using the HSV colour model.

Algorithm	Ref. Algorithm	Percentage of + Pixels	Percentage of - Pixels	Z Value	Significance Level
FRCIS $r=1$	FCM	6.242	0.720	-24.015	Beyond 0.0001
FRCIS $r=2$	FCM	6.523	0.667	-25.060	Beyond 0.0001
FRCIS $r=4$	FCM	6.864	0.492	-26.957	Beyond 0.0001
PCM	FCM	0.606	3.606	-16.752	Beyond 0.0001
FRCIS $r=1$	PCM	9.220	0.697	-31.067	Beyond 0.0001
FRCIS $r=2$	PCM	9.545	0.689	-31.777	Beyond 0.0001
FRCIS $r=4$	PCM	9.697	0.326	-33.981	Beyond 0.0001
FCM	PCM	3.606	0.606	-16.752	Beyond 0.0001

Table 7.16: The overall results of the statistical significance test, *sign test* for the cloud image in Fig. 7.1(a) using the RGB colour model.

Algorithm	Ref. Algorithm	Percentage of + Pixels	Percentage of - Pixels	Z Value	Significance Level
FRCIS $r=1$	FCM	3.856	0.720	-16.805	Beyond 0.0001
FRCIS $r=2$	FCM	6.803	0.644	-25.899	Beyond 0.0001
FRCIS $r=4$	FCM	6.962	0.545	-26.874	Beyond 0.0001
PCM	FCM	0.515	0.197	-4.229	Beyond 0.0001
FRCIS $r=1$	PCM	3.455	0.636	-15.965	Beyond 0.0001
FRCIS $r=2$	PCM	6.371	0.530	-25.511	Beyond 0.0001
FRCIS $r=4$	PCM	6.545	0.447	-26.464	Beyond 0.0001
FCM	PCM	0.197	0.515	-4.229	Beyond 0.0001

Table 7.17: The overall results of the statistical significance test, *sign test* for the crocodile image in Fig. 7.1(m) using the HSV colour model.

Algorithm	Ref. Algorithm	Percentage of + Pixels	Percentage of - Pixels	Z Value	Significance Level
FRCIS $r=1$	FCM	11.671	6.689	-23.289	Beyond 0.0001
FRCIS $r=2$	FCM	11.519	9.015	-11.066	Beyond 0.0001
FRCIS $r=4$	FCM	11.865	8.153	-16.616	Beyond 0.0001
PCM	FCM	28.493	74.584	-90.982	Beyond 0.0001
FRCIS $r=1$	PCM	74.042	22.969	-103.921	Beyond 0.0001
FRCIS $r=2$	PCM	71.647	23.051	-100.080	Beyond 0.0001
FRCIS $r=4$	PCM	73.576	23.773	-101.161	Beyond 0.0001
FCM	PCM	74.584	28.493	-90.982	Beyond 0.0001

Table 7.18: The overall results of the statistical significance test, *sign test* for the crocodile image in Fig. 7.1(m) using the RGB colour model.

Algorithm	Ref. Algorithm	Percentage of + Pixels	Percentage of - Pixels	Z Value	Significance Level
FRCIS $r=1$	FCM	9.351	4.967	-23.208	Beyond 0.0001
FRCIS $r=2$	FCM	12.856	5.512	-34.333	Beyond 0.0001
FRCIS $r=4$	FCM	14.422	7.035	-31.948	Beyond 0.0001
PCM	FCM	28.316	59.632	-66.920	Beyond 0.0001
FRCIS $r=1$	PCM	63.546	27.846	-74.839	Beyond 0.0001
FRCIS $r=2$	PCM	67.559	28.899	-78.887	Beyond 0.0001
FRCIS $r=4$	PCM	68.405	29.703	-78.307	Beyond 0.0001
FCM	PCM	59.632	28.316	-66.920	Beyond 0.0001

A comparison of the average error rates between the algorithms using the HSV and RGB models for the cloud and crocodile images are displayed in Fig. 7.33. The average error rates of the FRCIS algorithm for both images using the HSV and RGB models are lower than those of FCM and PCM algorithms. The overall error improvements of FRCIS over FCM and PCM for the cloud and crocodile images were 17.4% and 26.2% using the HSV colour model respectively, while the corresponding values for the RGB colour model were 10.1% and 8%, which again confirms the superiority of HSV for colour image segmentation since it is a perceptual colour model. The results of statistical significant test (Tables 7.15-7.18) prove that FRCIS produced significant better results compared with FCM and PCM for both the cloud and crocodile images for both the HSV and RGB colour models at a significance level greater than 0.0001.

Further experiments were conducted using the gorilla (Fig. 7.1(k)) and fish (7.1(o)) images consisting of three distinct regions. The gorilla (Fig. 7.1(k)) image has background (R_1), gorilla (R_2), and field (R_3) regions, while the fish (7.1(o)) image comprises water (R_1), ground and trees (R_2), and fish (R_3) regions. The segmented results of these two images produced by the FRCIS, FCM, and PCM algorithms using the HSV and RGB colour models are presented in Fig. 7.34 and

7.35 and Fig. 7.36 and 7.37 respectively. Fig. 7.34 clearly illustrates that FRCIS separated gorilla (Fig. 7.34(a) - 7.34(c)) better for the HSV colour model and all values of r than FCM and PCM (Fig. 7.34(d) and 7.34(e)). For this, FRCIS provided improved results for all values of r especially for gorilla region than both FCM and PCM (Fig. 7.34(d)-(e)). FRCIS also outperformed both FCM and PCM especially for ground and trees (R_2) and fish (R_3) regions for the fish image (Fig. 7.35 and 7.37) for both the HSV and RGB colour models. PCM could not separate at all the fish (R_3) from ground and trees (R_2) region shown in Fig. 7.35(e) and 7.37(e).
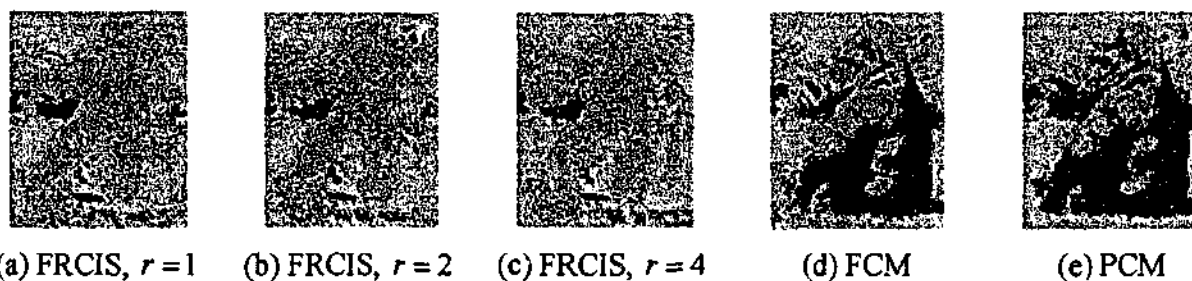
(a) FRCIS, $r = 1$ (b) FRCIS, $r = 2$ (c) FRCIS, $r = 4$ (d) FCM   (e) PCM

Fig. 7.34: The segmented results of the gorilla image in Fig. 7.1(k) into two regions for the HSV colour model using the FRCIS, FCM, and PCM algorithms.

(a) FRCIS, $r = 1$ (b) FRCIS, $r = 2$ (c) FRCIS, $r = 4$ (d) FCM   (e) PCM

Fig. 7.35: The segmented results of the fish image in Fig. 7.1(o) into two regions for the HSV colour model using the FRCIS, FCM, and PCM algorithms.

(a) FRCIS, $r = 1$ (b) FRCIS, $r = 2$ (c) FRCIS, $r = 4$ (d) FCM   (e) PCM
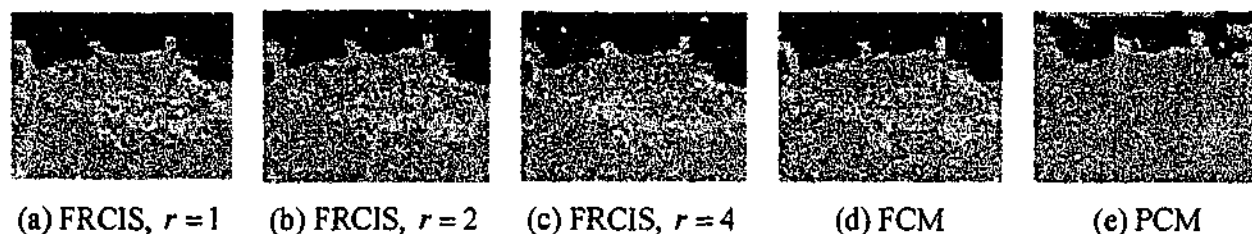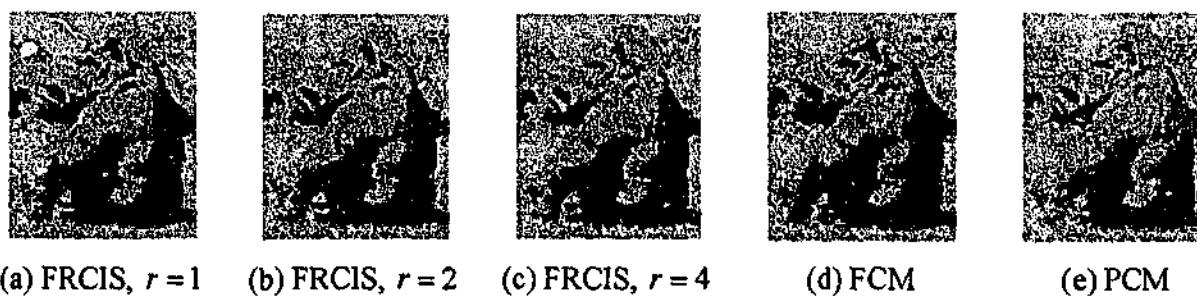
Fig. 7.36: The segmented results of the gorilla image in Fig. 7.1(k) into two regions for the RGB colour model using the FRCIS, FCM, and PCM algorithms.

(a) FRCIS, $r = 1$ (b) FRCIS, $r = 2$ (c) FRCIS, $r = 4$ (d) FCM   (e) PCM

Fig. 7.37: The segmented results of the fish image in Fig. 7.1(o) into two regions for the RGB colour model using the FRCIS, FCM, and PCM algorithms.

Table 7.19: Error percentages for the gorilla and fish image segmentations for the HSV colour model using the FRCIS, FCM, and PCM algorithms.

Algorithm	Gorilla Image (Fig. 7.1(k))			Fish Image (Fig. 7.1(o))		
	Region	Type I	Type II	Region	Type I	Type II
FRCIS, $r=1$	Background (R_1)	46.058	36.982	Water (R_1)	2.057	2.618
	Gorilla (R_2)	45.555	30.008	Ground (R_2)	24.161	20.050
	Field (R_3)	27.525	2.850	Fish (R_3)	35.592	12.593
FRCIS, $r=2$	Background (R_1)	54.850	35.854	Water (R_1)	0.434	3.557
	Gorilla (R_2)	43.072	33.701	Ground (R_2)	25.386	20.343
	Field (R_3)	39.471	5.972	Fish (R_3)	38.179	12.744
FRCIS, $r=4$	Background (R_1)	61.565	36.184	Water (R_1)	0.468	3.966
	Gorilla (R_2)	42.566	36.589	Ground (R_2)	26.145	19.939
	Field (R_3)	42.145	6.784	Fish (R_3)	37.834	12.931
FCM	Background (R_1)	88.712	39.985	Water (R_1)	1.014	1.597
	Gorilla (R_2)	55.752	19.240	Ground (R_2)	34.294	19.099
	Field (R_3)	7.576	24.905	Fish (R_3)	33.283	18.903
PCM	Background (R_1)	85.259	44.563	Water (R_1)	36.098	0.002
	Gorilla (R_2)	65.117	8.558	Ground (R_2)	0.990	71.810
	Field (R_3)	3.066	30.963	Fish (R_3)	97.588	0.578

In all these three region examples, it is clear again that the HSV colour model has consistently provided improved results over the RGB model from a segmentation perspective.

The numerical results of the gorilla and fish image segmentation using the FRCIS, FCM, and PCM algorithms for the HSV and RGB colour models are shown in the Table 7.19 and 7.20 respectively. The results using the HSV colour model shown in Table 7.19 exhibit that FRCIS provided better results for both images than both FCM and PCM, which was confirmed by the

comparative average error rates presented in Fig. 7.38. The FRCIS algorithm obtained 4.9% and 26.3% of the overall error improvements over FCM and PCM respectively for the gorilla and fish images using the HSV colour model, compared with corresponding values of 2.4% and 12.5% for the RGB colour model.

For the RGB colour model, FRCIS gave improved performance over FCM for all values of neighbourhood radius r, for the gorilla (Fig. 7.1(k)) and $r = 1$ and $r = 2$ for the fish (Fig. 7.1(o)) images. FRCIS also produced better average errors than PCM for all values of r for fish image only (Fig. 7.38).

Table 7.20: Error percentages for the gorilla and fish image segmentations for the RGB colour model using FRCIS, FCM, and PCM algorithms.

Algorithm	Region	Gorilla Image (Fig. 7.1(k))		Region	Fish Image (Fig. 7.1(o))	
		Type I	Type II		Type I	Type II
FRCIS, r=1	Background (R_1)	91.840	1.279	Water (R_1)	1.995	2.467
	Gorilla (R_2)	42.867	27.646	Ground (R_2)	24.495	19.459
	Field (R_3)	17.320	47.631	Fish (R_3)	34.372	12.821
FRCIS, r=2	Background (R_1)	92.701	1.128	Water (R_1)	2.023	2.711
	Gorilla (R_2)	42.890	28.190	Ground (R_2)	25.533	19.154
	Field (R_3)	18.348	47.998	Fish (R_3)	33.876	13.176
FRCIS, r=4	Background (R_1)	93.078	0.915	Water (R_1)	1.820	2.827
	Gorilla (R_2)	41.910	28.912	Ground (R_2)	24.348	20.106
	Field (R_3)	20.837	47.820	Fish (R_3)	35.763	12.404
FCM	Background (R_1)	83.363	42.795	Water (R_1)	2.186	0.890
	Gorilla (R_2)	61.095	27.165	Ground (R_2)	34.482	20.700
	Field (R_3)	22.769	22.395	Fish (R_3)	35.053	19.755
PCM	Background (R_1)	89.371	33.110	Water (R_1)	14.757	0.147
	Gorilla (R_2)	49.963	27.640	Ground (R_2)	3.936	60.211
	Field (R_3)	17.139	24.344	Fish (R_3)	93.041	2.159

For the HSV colour model, FRCIS produced significantly superior results to FCM and PCM for both the gorilla and fish images (Table 7.21 and 7.23), whereas for the RGB colour model, it provided significant improved results with respect to FCM, for all values of r (Table 7.22) and $r = 2$ and $r = 4$ (Table 7.24) for the gorilla and fish images respectively. FRCIS also showed

significant improvements over PCM for the fish image for the RGB colour model at a significance level beyond 0.0001 (Table 7.24).
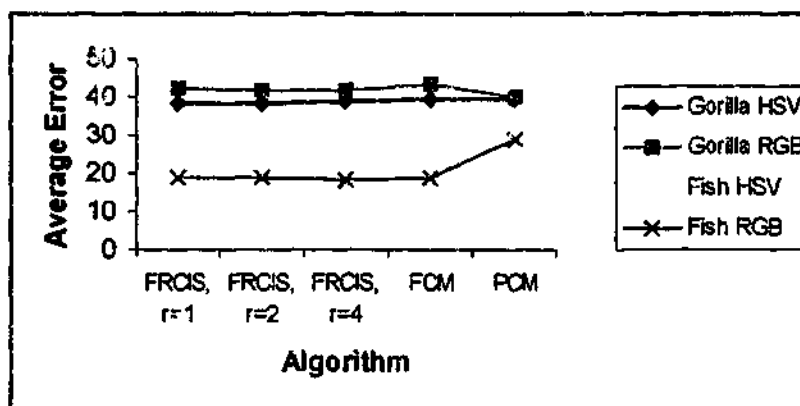
Fig. 7.38: Average percentages of error rates of the FRCIS, FCM, and PCM algorithms for the Fig. 7.1(k) and 7.1(o) image segmentations using the HSV and RGB colour models.

Table 7.21: The overall results of the statistical significance test, *sign test* for the gorilla image in Fig. 7.1(k) using the HSV colour model.

Algorithm	Ref. Algorithm	Percentage of + Pixels	Percentage of - Pixels	Z Value	Significance Level
FRCIS r=1	FCM	11.671	6.689	-23.289	Beyond 0.0001
FRCIS r=2	FCM	11.519	9.015	-11.066	Beyond 0.0001
FRCIS r=4	FCM	11.865	8.153	-16.616	Beyond 0.0001
PCM	FCM	28.493	74.584	-90.982	Beyond 0.0001
FRCIS r=1	PCM	74.042	22.969	-103.921	Beyond 0.0001
FRCIS r=2	PCM	71.647	23.051	-100.080	Beyond 0.0001
FRCIS r=4	PCM	73.576	23.773	-101.161	Beyond 0.0001
FCM	PCM	74.584	28.493	-90.982	Beyond 0 0001

Table 7.22: The overall results of the statistical significance test, *sign test* for the gorilla image in Fig. 7.1(k) using the RGB colour model.

Algorithm	Ref. Algorithm	Percentage of + Pixels	Percentage of - Pixels	Z Value	Significance Level
FRCIS r=1	FCM	3.868	2.196	-21.926	Beyond 0.0001
FRCIS r=2	FCM	5.406	2.814	-29.202	Beyond 0.0001
FRCIS r=4	FCM	5.980	2.691	-36.092	Beyond 0.0001
PCM	FCM	8.157	2.931	-50.713	Beyond 0.0001
FRCIS r=1	PCM	2.858	6.412	-37.723	Beyond 0.0001
FRCIS r=2	PCM	2.396	5.031	-31.233	Beyond 0.0001
FRCIS r=4	PCM	2.578	4.515	-23.491	Beyond 0.0001
FCM	PCM	2.931	8.157	-50.713	Beyond 0.0001

Table 7.23: The overall results of the statistical significance test, *sign test* for the fish image in Fig. 7.1(o) using the HSV colour model.

Algorithm	Ref. Algorithm	Percentage of + Pixels	Percentage of - Pixels	Z Value	Significance Level
FRCIS $r=1$	FCM	8.478	4.686	-24.104	Beyond 0.0001
FRCIS $r=2$	FCM	8.499	4.977	-22.124	Beyond 0.0001
FRCIS $r=4$	FCM	8.303	5.026	-20.702	Beyond 0.0001
PCM	FCM	15.724	41.387	-78.352	Beyond 0.0001
FRCIS $r=1$	PCM	41.062	11.607	-93.646	Beyond 0.0001
FRCIS $r=2$	PCM	41.214	12.030	-92.284	Beyond 0.0001
FRCIS $r=4$	PCM	40.480	11.539	-92.583	Beyond 0.0001
FCM	PCM	41.387	15.724	-78.352	Beyond 0.0001

Table 7.24: The overall results of the statistical significance test, *sign test* for the fish image Fig. 7.1(o) using the RGB colour model.

Algorithm	Ref. Algorithm	Percentage of + Pixels	Percentage of - Pixels	Z Value	Significance Level
FRCIS $r=1$	FCM	5.597	5.214	-2.676	0.00375
FRCIS $r=2$	FCM	5.450	5.197	-1.780	0.0375
FRCIS $r=4$	FCM	5.794	5.296	-3.436	0.0003
PCM	FCM	14.430	30.982	-56.670	Beyond 0.0001
FRCIS $r=1$	PCM	29.303	12.368	-60.529	Beyond 0.0001
FRCIS $r=2$	PCM	29.363	12.557	-59.887	Beyond 0.0001
FRCIS $r=4$	PCM	29.675	12.625	-60.484	Beyond 0.0001
FCM	PCM	30.982	14.430	-56.670	Beyond 0.0001

Overall, the FRCIS algorithm produced improved results for the FCM and PCM algorithms for both the HSV and RGB colour models, while the HSV colour model proved its superiority to the RGB colour model for image segmentation particularly that involving object-based segmentation. This is because, as mentioned before, HSV is a perceptual colour model.

7.9 General Framework Issues

To conclude this chapter we briefly discuss some broader issues relating to the fuzzy rule-based framework. One of the key advantages of the framework is its inherent flexibility, that is its ability to integrate any type of image attribute in any special application, which has been experimentally proven by integration of the texture features into the FRIST algorithm. Possible examples for further extending the framework include text and video object segmentation, which will be briefly explored in the future work section of Chapter 8.

One requirement that is enforced it that the actual number of regions $\Re$ to be separated needs to be stipulated prior to the segmentation, however, possible solutions to automate this will also be discussed in the future work in section.

There are also domain specific issues that cognisance must be made of, such as that segmentation may be ineffective in separating regions, which are adjacent and have similar colours or exhibit very strong spatially correlation, which has been highlighted in Fig. 7.10 for the food image segmentation, where certain regions were not able to be completely segmented. This is however a fundamental challenge for any image segmentation system.

Finally, from a computational perspective, since all the membership functions are independent of each other, every algorithm except FRIS, in the framework possess a high degree of inherent concurrency, which could be exploited by a parallel implementation, with a dedicated processor being used for each membership function.

7.10 Summary

A full evaluation of the performance and the potential capability of the proposed four (GFRIS, FRIS, FRIST, and FRCIS) algorithms for object-based image segmentation have been examined using an image database comprising 18 different natural images consisting of two, three, and five objects (regions). The images were selected considering natural objects as regions and possessing diverse characteristics including homogeneous, non-homogeneous, very poor contrast, perceptually distinct, and natural textured regions. All the results have been numerically evaluated, statistically tested for significant improvements, and contrasted with the standard fuzzy image segmentation clustering algorithms, namely FCM and PCM. The methods of numerical evaluations and the statistical significant test have also been described in this chapter.

The generic fuzzy rule-based segmented algorithm (GFRIS) has showed promising performance for the regions (objects) that are homogenous i.e. having proximity and good continuation relation (spatial relation) and some Brodatz texture images compared with FCM and PCM. The segmentation refinement algorithm (FRIS) has provided significant improved results than all of the original initial algorithms (GFRIS, FCM, and PCM) except some cases for PCM. Since it is a refinement algorithm, its performance crucially depends on the initial algorithm and for this reason FRIS could not always provide good results for PCM. The algorithm incorporating texture features based on image domain specific information (FRIST) achieved superior results to GFRIS for the selected Brodatz texture as well as the natural images, especially for images that

have texture to some degree. The GFRIS algorithm has been extended to colour image segmentation with an algorithm for calculating the average of the hue components of the HSV colour model and named as FRCIS. The FRCIS algorithm has produced enhanced results over FCM and PCM for both in the HSV and RGB colour models. FRCIS provided better results for the HSV colour model than the RGB.

The numerical evaluations have been conducted based on two powerful objective and quantitative segmentation evaluation methods, namely *discrepancy based on the number of mis-segmented pixels* and *discrepancy based on the number of objects in the image*. A statistical significant test called *sign test* has also been implemented. Almost all of the algorithms for all images achieved an overall significant improvement at a significance level greater than 0.0001.

Conclusions and Future Work

8.1 Conclusions

Image segmentation particularly that involving object-based segmentation, is very complex and demands fuzzy image processing due to the imprecise nature of the data involved. It is also necessary to incorporate human expert and/or domain specific knowledge. Fuzzy rule-based techniques afford the potential of integrating such knowledge into a segmentation system, however, such techniques are very much application domain and image dependent. The structures of the membership functions are perceptually defined and their corresponding parameters are either manually or automatically derived.

This thesis has directly addressed these issues, by presenting the development and implementation of a novel, flexible, general-purpose integrated fuzzy rule-based image segmentation (object-based) framework. The framework considers all possible general attributes of the perceptual grouping so that users can incorporate their own application specific information in order to obtain perceptually meaningful segments. In pursuit of this aim, four dedicated fuzzy rule-based image segmentation algorithms have been developed for the framework.

The first of these is a *generic fuzzy rule-based image segmentation (GFRIS)* algorithm, which is both image and application independent and also exploits inter-pixel spatial relationships. GFRIS has three membership functions, which considers the principles of similarity based on a region's pixel distribution and gray level pixel intensity, together with proximity and good continuation. The algorithm automatically approximates both the key weighting factor and threshold value in the definitions of the fuzzy rule and neighbourhood system respectively. The performance of GFRIS has proven very effective, outperforming both FCM and PCM in segmenting many image types with no increase in the order of computational complexity, which is $O(n)$ for an image containing n pixels. One issue identified within the GFRIS algorithm was that it was not so effective in segmenting regions characterised by non-homogeneity or possessing sharp variations in pixel

143

intensity. This lead to the second major algorithm in the framework, which is a refinement algorithm called *fuzzy rules for image segmentation (FRIS)*.

FRIS is mainly based on region *splitting and merging* techniques and utilises the principles of connectedness, surroundedness, uniformity, and contrast properties amongst an objects' pixels. A series of mutually exclusive rules covering the *growth, prevention,* and *merger* of objects were developed to help FRIS provide significant improvements to the initial segmentations produced by algorithms such as GFRIS, FCM, and PCM. The computational complexity of this algorithm is $O(n\log(n))$, which is however higher than FCM and PCM. The performance of FRIS also depends on the initial segmentation and in this context, meant that the basic GFRIS algorithm needed to be enhanced, since it does not directly consider texture.

The third algorithm, called *fuzzy rules for image segmentation incorporating texture features (FRIST)*, integrates the fractal dimension and contrast features of texture together with image domain specific information within the GFRIS algorithm. This new algorithm exhibited significantly better results than the original GFRIS algorithm, however, it incurs an additional computational cost for integrating these membership functions, though the order of the computational complexity remains the same at $O(n)$.

Finally, as all three framework algorithms (GFRIS, FRIS, and FRIST) have been developed for gray level images, the fourth algorithm deals with colour segmentation. Colour often provides additional information and in many cases makes it easier to separate an object from an image. A new *fuzzy rule-based colour image segmentation (FRCIS)* algorithm has been presented by extending the original gray level GFRIS algorithm to process colour model components including RGB and HSV. A special algorithm has been developed to calculate the average of the hue components in the perceptual HSV colour model. The FRCIS algorithm significantly outperformed the FCM and PCM algorithms for both the HSV and RGB colour models and importantly it also does not alter the order of the computational complexity, which remains at $O(n)$.

All framework algorithms have been both quantitatively and qualitatively evaluated using a database containing 18 different types of real images having two, three, and five objects. A statistical significance test called *sign test* has also been conducted. The overall conclusion being that all four algorithms in the framework produced significantly improved segmentation performance. One additional major advantage of the framework is its flexibility, with the potential for integrating new membership functions into this system for high-level semantics of an object for object-based image segmentation.

8.2 Future Work

There are a number of potential areas where this research may be fruitfully extended within the framework in Fig. 1.1. Some of them are summarised as follows: -

1. The framework currently requires the number of regions to be segmented to be pre-defined prior to the segmentation. All the proposed algorithms except FRIS, could be extended in order to automatically estimate the explicit number of regions in an image possibly using histogram analysis or mountain clustering techniques [95]. This is however one of the most difficult and challenging tasks in object-based image segmentation.

2. Since the framework is fuzzy rule-based, it is capable of incorporating any type of attribute of any special application domain. For example, algorithms could be introduced to segment objects in video sequences, text or particular medical imaging applications by incorporating domain specific information. For instance, in the case of video, object motion in the form of motion vectors and motion compensation could be exploited as feasible membership functions. Again the flexibility of the framework means that application specific information from medical experts could be incorporated to assist in identifying for instance, abnormalities in MRI, X-ray, and CAT scans for detecting brain tumours and skin cancers. Dedicated membership functions could be defined based upon expert knowledge from medical practitioners.

3. It is important to state that while the research focus has been on segmenting images, the flexibility of the framework means that it can equally be applied to audio segmentation for example, by incorporating membership functions relevant to audio features such as pitch and frequency content.

4. The FRCIS algorithm could be developed by intuitively defining fuzzy colour model exploiting human visual perception. The fuzzy colour model could be defined by quantising and combining the components of existing colour models [141] and the membership value estimated from the predefined fuzzy colour.

Bibliography

[1] G. C. Karmakar, L. Dooley, and S. M. Rahman, "A survey of fuzzy rule based image segmentation techniques," In the Proceedings of the First IEEE Pacific-Rim Conference on Multimedia, Sydney, NSW, Australia, pp. 350-353, 2000.

[2] G. C. Karmakar, L. Dooley, and S. M. Rahman, "Review on fuzzy image segmentation techniques," in *Design and Management of Multimedia Information Systems: Opportunities and Challenges*: Idea Group Publishing, USA, pp. 282 -313, ISBN 1-930708-00-9, 2001 (a Book Chapter).

[3] G. C. Karmakar and L. Dooley, "Generic fuzzy rule based technique for image segmentation," In the Proceedings of IEEE International Conference on Acoustics, Speech, and Signal Processing, (ICASSP'2001), Salt Lake City, Utah, vol. 3, pp. 1577-1580, 2001.

[4] G. C. Karmakar and L. S. Dooley, "Analysis of fuzzy clustering and a generic fuzzy rule based image segmentation technique," presented at International Conference on Intelligent Multimedia and Distance Education, Fargo, North Dakota, USA, pp. 68-75, 2001.

[5] G. C. Karmakar and L. S. Dooley, "Extended fuzzy rules for image segmentation," In the Proceedings of IEEE International Conference on Image Processing (ICIP2001), Thessaloniki, Greece, vol. 3, pp. 1099-1102, 2001.

[6] G. C. Karmakar and L. S. Dooley, "A Generic fuzzy rule based image segmentation algorithm," *Pattern Recognition Letters*, vol. 23, pp. 1215-1227, 2002.

[7] G. C. Karmakar, L. S. Dooley, and M. Murshed, "New fuzzy rules for improved image segmentation," In the Proceedings of IEEE International Conference on Acoustics, Speech, and Signal Processing (ICASSP2002), Orlando, Florida, USA, vol. 4, pp. 4192-4192, 2002.

[8] G. C. Karmakar, L. S. Dooley, and M. M. Murshed, "Fuzzy rules for image segmentation incorporating texture features," In the Proceedings of IEEE 2002 International Conference on

Image Processing (ICIP2002), Rochester, New York, vol. 4, pp. 797-800, 2002.

[9]   G. C. Karmakar, L. S. Dooley, and M. Murshed, "Image segmentation using modified extended fuzzy rules," In the Proceedings of 6th International Conference on Signal Processing (ICSP'02), Beijing, China, vol. 2, pp.941-944, 2002.

[10] G. C. Karmakar, "Shape and texture based feature   extraction for object ranking using neural networks," in *Gippsland School of Computing and Information Technology*. Melbourne, Australia: Monash University, 1998.

[11] G. A. Baxes, *Digital Image Processing: Principles and Applications*, John Wiley & Sons, Inc., New York, USA, 1994.

[12] R. M. Haralick and L. G. Shapiro, "Survey, Image segmentation techniques," *Computer Vision, Graphics, and Image Processing*, vol. 29, pp. 100-132, 1985.

[13] D. L. Pham and J. L. Prince, "An adaptive fuzzy c-means algorithm for image segmentation in the presence of intensity inhomogeneities," *Pattern Recognition Letters*, vol. 20, pp. 57-68, 1999.

[14] N. R. Pal and S. K. Pal, "A review on image segmentation techniques," *Pattern Recognition*, vol. 26, pp. 1277-1294, 1993.

[15] J. Liu, K. Bowyer, D. Goldgof, and S. Sarkar, "A comparative study of texture measures for human skin treatment," In the Proceedings of International Conference on Information, Communications and Signal Processing (ICICS '97), Singapore, pp. 170-174, 1997.

[16] D. H. Barallard and C. Brown, *Computer Vision*: Prentice Hall, 1982.

[17] A. Chakrabotry, L. H. Staib, and J. S. Duncan, "Deformable boundary finding influenced by region homogeneity," Department of Electrical Engineering and Diagnostic Radiology, Yale University, 333 Cedar Street, New Haven CT 06520-8042, 1994.

[18] M. Kass, A. Witkin, and D. Terzopoulos, "Snakes: Active contour models," *Int'l J. Computer Vision*, pp. 321-331, 1988.

[19] L. D. Cohen and I. Cohen, "Finite-element methods for active contour models and balloons for 2D and 3D images," *IEEE Transactions on Pattern Analysis and Machine Intelligence*, vol. 15, pp. 1131-1147, 1993.

[20] R. Ronald, "Region-based strategies for active contour models," *Int'l J. Computer Vision*, vol. 13, pp. 229-251, 1994.

[21] V. Caselles, R. Kimmel, and G. Sapiro, "Geodesic active contours," In the Proceedings of

IEEE ICCV-95, pp. 840-845, 1995.

[22] R. P. Grzeszczuk and L. D.N., "Brownian strings: Segmenting images with stochastically deformable contours," *IEEE Transactions on Pattern Analysis and Machine Intelligence*, vol. 19, pp. 1100-1114, 1997.

[23] R. Grzeszczuk and L. D.N., "Segmenting images by stochastic contour optimization," In the Proceedings of Soc. Magnetic Resonance in Medicine, vol. 1, pp. 508-, 1993.

[24] R. M. Haralic and L. G. Shapiro, "Survey: image segmentation techniques," *Computer, Vision, and Image Processing*, vol. 29, pp. 100-132, 1985.

[25] C. K. Chow and T. 'Kaneko, "Boundary detection of radiographic images by thresholding method," *Frontiers of Pattern Recognition*, pp. 61-82, 1972.

[26] R. Kohler, "A segmentation system based on thresholding," *Comput. Graphics Image Process.*, vol. 15, pp. 319-338, 1981.

[27] M. Goldberg and S. Shlien, "A clustering scheme for multispectral image," *IEEE Transactions on Systems, Man, and Cybernetis*, vol. SMC-8, pp. 86-92, 1978.

[28] M. Goldberg and S. Shilen, "A four-dimensional histogram approach to the clustering of LANDSAT data, in machine processing of remotely sensed data," Purdue University, West Lafayette, Indiana IEEE CH 1218-7 MPRSD, 21-23 June 1977.

[29] J. Bryant, "On the clustering of multidimensional pictorial data," *Pattern Recognition*, vol. 11, pp. 115-125, 1979.

[30] R. M. Haralick and I. Dinstein, "A spatial clustering procedure for multi-image data," *IEEE Transactions on Circuits and Systems*, vol. CAS-22, pp. 440-450, 1975.

[31] M. D. Levine and J. Leemet, "A method for non-purposive picture segmentation," In the Proceedings of Third International Joint Conference on Pattern Recognition, 1976.

[32] R. L. Kettig and D. A. Landgrebe, "Computer classification of multispectral image data by extraction and classification of homogeneous objects," The Laboratory for Application of Remote Sensing, Purdue University, West Lafayete, Indiana LARS Information Note 050975, 1975.

[33] P. J. Brut, T. H. Hong, and A. Rosenfeld, "Segmentation and estimation of image region properties through cooperative hierarchical computation," *IEEE Transaction on Systems, Man, and Cybernetics*, vol. SMC-11, 1981.

[34] L. G. Minor and J. Sklansky, "The detection and segmentation of blobs in infrared images," *IEEE Transaction on Systems, Man, and Cybernetics*, vol. SMC-11, pp. 194-201, 1981.

[35] R. M. Haralick and G. L. Kelly, "Pattern recognition with measurement space and spatial clustering for multiple image," In the Proceedings of IEEE 57, pp. 654-665, 1969.

[36] Y. Fukada, "Spatial clustering procedure for region analysis," *Pattern Recognition*, vol. 12, pp. 395-403, 1980.

[37] J. D. Browning and S. L. Tanimoto, "Segmentation of pictures into regions with a tile by tile method," *Pattern Recognition*, vol. 15, pp. 1-10, 1982.

[38] S. L. Horowitz and T. Pavlidis, "Picture segmentation by a tree traversal algorithms," *J. Assoc. Comput. Mach.*, vol. 23, pp. 368-388, 1976.

[39] A. Klinger, "Data structures and pattern recognition," In the Proceedings of First International Joint Conference on Pattern Recognition, Washington, D.C., pp. 497-498, 1976.

[40] M. M. Reid, R. J. Millar, and N. D. Black, "Second - generation image coding: An overview," *ACM Computing Survey*, vol. 29, pp. 3-29, 1997.

[41] A. Moghaddamzadeh and N. Bourbakis, "A fuzzy region growing approach for segmentation of color images," *Pattern Recognition*, vol. 30, pp. 867-881, 1997.

[42] H. Samet, *Application of Spatial Data Structures*, First Edition ed: Addison-Wesley, Reading, MA, 1989a.

[43] F. R. Hansen and H. Elliott, "Image segmentation using simple Markov random field models," *Comput. Graphics Image Process*, vol. 20, pp. 101-132, 1984.

[44] H. Derin and H. Elliott, "Modeling and segmentation of noisy and textured images using Gibbs random fields," *IEEE Transactions on Pattern Analysis and Machine Intelligence*, vol. 9, pp. 39-55, 1987.

[45] H. Derin, H. Elliott, R. Cristi, and D. Geman, "Byes something algorithms for segmentation of binary images modeled by Markov random fields," *IEEE Transactions on Pattern Analysis and Machine Intelligence*, vol. 6, pp. 707-720, 1984.

[46] S. Geman and D. Geman, "Stochastic relaxation, Gibbs distribution, and the Byesian restoration of images," *IEEE Transactions on Pattern Analysis and Machine Intelligence*, vol. 6, pp. 721-74, 1984.

[47] N. Otsu, "A threshold selection method from gray-level histograms," *IEEE Transactions on Systems, Man, and Cybernatics*, vol. 9, pp. 62-66, 1979.

[48] S. D. Yanowitz and M. A. Bruckstein, "A new method for image segmentation," *Computer Vision Graphics Image Process.*, vol. 46, pp. 82-95, 1989.

[49] T. Taxt, P. J. Flynn, and A. K. Jain, "Segmentation of document images," *IEEE Transactions on Pattern Analysis and Machine Intelligence*, vol. 11, pp. 1322-1329, 1989.

[50] S. Peleg, "A new probablistic relaxation scheme," *IEEE Transactions on Pattern Analysis and Machine Intelligence*, vol. 2, pp. 362-369, 1980.

[51] S. Geman and D. Geman, "Stochastic relaxation, Gibbs distributions, and the Bayesian restoration of images," *IEEE Transactions on Pattern Analysis and Machine Intelligence*, vol. 6, pp. 721-741, 1984.

[52] P. Andrey and P. Tarroux, "Unsupervised segmentation of Markov random field modeled textured images using selectionist relaxation," *IEEE Transactions on Pattern Analysis and Machine Intelligence*, vol. 20, pp. 252-262, 1998.

[53] A. Rosenfeld, R. A. Hummel, and S. W. Zucker, "Scene labeling by relaxation operators," *IEEE Transactions on Systems, Man, and Cybernetics*, vol. SMC-6, pp. 420-433, 1976.

[54] X. Liu and D. L. Wang, "Range image segmentation using relaxation oscillator network," *IEEE Transactions on Neural Networks*, vol. 10, pp. 564-573, 1999.

[55] P. Andrey, "Selectionist relaxation: genetic algorithms applied to image segmentation," *Image and Vision Computing*, vol. 17, pp. 175-187, 1999.

[56] H. Elliot, H. Derin, R. Cristi, and D. Geman, "Appication of the Gibbs distribution to image segmentation," In the Proceedings of IEEE International Conference on Acoustics, Speech, and Signal Processing, Sandiego, California, 1984.

[57] A. Gosh, N. R. Pal, and S. K. Pal, "Object background classification using Hopefield type neural network," *Int. J. Pattern Recognition Artif. Intell.*, vol. 6, pp. 989-1008, 1992.

[58] A. Gosh, N. R. Pal, and S. K. Pal, "Self-organization for object extraction using multilayer neural networks and fuzziness measure," *IEEE Transactions on Fuzzy Systems*, vol. 1, pp. 54-68, 1993.

[59] C. T. Chen, E. C. Tsao, and W. C. Lin, "Medical image segmentation by a constraint satisfaction neural networks," *IEEE Transactions on Nucl. Sci.*, vol. 38, pp. 678-686, 1991.

[60] P. C. Besl and R. C. Jain, "Segmentation using variable surface fitting," *IEEE Transactions on Pattern Analysis and Machine Intelligence*, vol. 10, pp. 167-192, 1988.

[61]   N. Yokoya and M. D. Levine, "Range image segmentation based on differential geometry: a hybrid approach," *IEEE Transactions on Pattern Analysis and Machine Intelligence,* vol. 11, pp. 643-694, 1989.

[62]   R. D. Rimey and F. S. Cohen, "A maximum-likelyhood approach to segmenting range data," *IEEE J. Robotics Automn,* vol. 4, pp. 277-286, 1988.

[63]   R. D. Overheim and D. L. Wanger, *Light and color:* Wiley, New York, 1982.

[64]   Y. Ohta, T. Kanade, and T. Sakai, "Color infonnation for region segmentation," *Comput. Graphics Image Process,* vol. 13, pp. 224-138, 1980.

[65]   J. Kittler, J. Eggleton, J. Illingworth, and K. Paler, "An average edge detector," *Pattern Recognition Letters,* vol. 6, pp. 27-32, 1987.

[66]   J. F. Canny, "A computational approach to edge detection," *IEEE Transactions on Pattern Analysis and Machine Intelligence,* vol. 8, pp. 679-698, 1986.

[67]   J. F. Haddon, "Generalised threshold selection for edge detection," *Pattern Recognition,* vol. 21, pp. 195-203, 1988.

[68]   M. Gokmen and C. C. Li, "Edge detection with iteratively refined regularization," In the Proceedings of 10th ICPR, pp. 690-693, 1990.

[69]   S. Cagnoni, A. B. Dobrzeniecki, and J. C. Yanch, "Genetic algorithm-based interactive segmentation of 3D medical images," *Image and Vision Computing,* vol. 17, pp. 881-, 1999.

[70]   B. Bhanu, S. Lee, and J. Ming, "Adaptive image segmentation using a genetic algorithm," *IEEE Transactions on Systems, Man, and Cybernatics,* vol. 25, pp. 1543-, 1995.

[71]   P. Andrey and P. Tarroux, "Unsupervised image segmentation using a distributed genetic algorithm," *Pattern Recognition,* vol. 27, pp. 659-, 1994.

[72]   J. Yen, "Fuzzy logic- A modern perspective," *IEEE Transactions on Knowledge and Data Engineering,* vol. 11, 1999.

[73]   J. M. Prewitt, *Object Enhancement and Extraction:* New York: Academics, 1970.

[74]   S. Medasani, R. Krishnapuram, and J. Keller, "Are fuzzy definitions of basic attributes of image objects really usefull?," *IEEE Transactions on Systems, Man, and Cybernetics-Part A: Systems and Humans,* vol. 29, pp. 378-386, 1999.

[75]   H. R. Tizhoosh, "Fuzzy Image Processing," Springer, http://watfast.uwaterloo.ca/ tizhoosh/fip.htm, 1997.

[76] J. Richard, S. Jost, and E. Gose, *Pattern Recognition and Image Analysis*. NJ 07458: Upper Saddle River, Prentice Hall PTR, 1996.

[77] Z. Chi, H. Yan, and T. Pham, *Fuzzy Algorithms: With Applications to Image processing and Pattern Recognition*: World Scientific Publishing Co. Pte. Ltd., Singapore, 1996.

[78] J. C. Bezdek, R. J. Hathaway, M. J. Sabin, and W. T. Tucker, "Covergence theory for fuzzy c-means: counterexaples and repairs," *IEEE Transactions on Systems, Man, and Cybernatics*, vol. SMC-17, pp. 873-877, 1987.

[79] J. C. Bezdek, *Pattern Recognition with Fuzzy Objective Function Algorithms*: Plenum, New York, 1981.

[80] J. C. Bezdek, "Fuzzy mathematics in pattern classification," Cornell University, Ithaca, New York, 1973.

[81] R. Krishnapuram and J. M. Keller, "Fuzzy and possibilistic clustering methods for computer vision," in *Neural and Fuzzy Systems: The Emerging Science of Intelligent Computing*, S. Mitra, M. M. Gupta, and W. F. Kraske, Eds. Bellingham, Washington: SPIE- The International Society for Optical Engineering, 1994.

[82] R. Krishnapuram and J. Keller, "A possibilistic approach to clustering," *IEEE Transactions on Fuzzy Systems*, vol. 1, pp. 98-110, 1993.

[83] R. Krishnapuram and J. M. Keller, "The possibilistic c-means algorithm: insight and recommendations," *IEEE Transactions on Fuzzy Systems*, vol. 4, pp. 385-393, 1996.

[84] R. C. Gonzalez and R. E. Woods, *Digital Image Processing*, third edition ed.: Addison-Wesley Publishing Company, Inc., 1992.

[85] A. Rosenfeld, "The fuzzy geometry of image subsets," *Pattern Recognition Letters*, vol. 2, pp. 311-317, 1984.

[86] A. Rosenfeld, "Fuzzy geometry: an overview," In the Proceedings of International Conference on Fuzzy Systems, Sandiego, California, pp. 113-118, 1992.

[87] D. Dubois and M. C. Jaulent, "A general approach to parameter evaluation in fuzzy digital pictures," *Pattern Recognition Letters*, vol. 6, pp. 251-259, 1987.

[88] S. K. Pal and A. Gosh, "Index of area coverage of fuzzy image subsets and object extraction," *Pattern Recognition Letters*, vol. 11, pp. 831-841, 1990.

[89] S. K. Pal and A. Rosenfeld, "Image enhancement and thresholding by optimization of fuzzy compactness," *Pattern Recognition Letters*, vol. 7, pp. 77-86, 1998.

[90]   S. K. Pal and A. Gosh, "Fuzzy geometry in image analysis," *Fuzzy Sets and Systems*, vol. 48, pp. 23-40, 1992.

[91]   S. K. Pal and R. A. King, "Automatic grey level thresholding through index of fuzziness and entropy," *Pattern Recognition Letters*, vol. 1, pp. 141-146, 1983.

[92]   L. K. Huang and M. J. Wang, "Image thresholding by minimzing the measure of fuzziness," *Pattern Recognition*, vol. 28, pp. 41-51, 1995.

[93]   J. M. Keller, H. Qiu, and H. Tahani, "Fuzzy integral and image segmentation," In the Proceedings of North American Fuzzy Information Processing Society, New Orleans, pp. 334-338, 1986.

[94]   H. Tahani and J. M. Keller, "Information fusion in computer vision using the fuzzy integral," *IEEE Transactions on Systems, Man, and Cybernatics*, vol. 20, pp. 733-741, 1990.

[95]   T. D. Pham and H. Yan, "Color image segmentation using fuzzy integral and mountain clustering," *Fuzzy Sets and Systems*, vol. 107, pp. 121-130, 1999.

[96]   L. A. Zadeh, *Roles of soft computing and fuzzy logic in the conception, design, and deployment of information/intelligent system.*: Springger, 1998.

[97]   L. O. Hall, B. Ozyurt, and J. C. Bezdek, "Clustering with genetically optimised approach," http://morden.csee.usf.edu/~hall/galong.pdf, 1999.

[98]   H. Ishibuchi and T. Murata, "Minimizing the fuzzy rule base and maximizing its performance by a multi-objective genetic algorithm," In the Proceedings of FUZZ-IEEE'97, vol. 1, pp. 259-264, 1997.

[99]   B. Karayiannis and P. Pai, "Segmentation of magnetic resonance images using fuzzy algorithms for linear vector quantisation," *IEEE Transactions on Medical Imaging*, vol. 18, pp. 172-180, 1999.

[100] J. Yen and L. Wang, "Simplifying fuzzy rule-based models using orthogonal transformation," *IEEE Transactions on Systems, Man, and Cybernetics-Part B: Cybernetics*, vol. 29, pp. 13-23, 1999.

[101] W. Park, E. A. Hoffman, and M. Sonka, "Segmentation of intrathoracic airway trees: a fuzzy logic approach," *IEEE Transactions on Medical Imaging*, vol. 17, pp. 489-497, 1998.

[102] Y. Q. Shi and H. Sun, *Image and Video Compression for Multimedia Engineering: Fundamentals, Algorithms, and Standards:* New Jersey: CRC Press, New York, 2000.

[103] --------, "MPEG-7: context and objective (version-10)," ISO/IEC JTC1/SC29/WG11, Atlantic City, USA N2460, October 1998.

[104] D. Ruan and E. E. Kerre, "Fuzzy IF-THEN Rules in Computational Intelligence: Theory and Applications," Norwell, Massachusetts: Kluwer Academic Publishers, 2000.

[105] R. Beichel, R. Bolter, and A. Pinz, "Fuzzy clustering of a land sat TM scene," In the Proceedings of IGARSS'99, Hamburg, Germany, 1999.

[106] J. C. Dunn, "A fuzzy relative of the ISODATA process and its use in detecting compact well-separated clusters," *Journal of Cybernatics*, vol. 3, pp. 32-57, 1973.

[107] Y. A. Tolias and S. M. Panas, "Image segmentation by a fuzzy clustering algorithm using adaptive spatially constrained membership functions," *IEEE Transactions on Systems, Man, and Cybernetics-Part A: System and Humans*, vol. 28, pp. 359-369, 1998.

[108] M. Barni, V. Cappellini, and A. Mecocci, "Comments on a possibilistic approach to clustering," *IEEE Transactions on Fuzzy Systems*, vol. 4, pp. 393-396, 1996.

[109] C.-W. Chang, H. Ying, G. R. Hillman, T. A. Kent, and J. Yen, "A rule-based fuzzy segmentation system with automatic generation of membership functions for pathological brain MR images," *Computers and Biomedical Research*, 1998.

[110] G. L. Vernazz, B. S. Serpico, and S. G. Dellepiane, "A knowledge-based system for biomedical image processing and recognition," *IEEE Transactions on Circuits Systems*, vol. CS-34, pp. 1399-1416, 1987.

[111] --------, "Fuzzy Logic Toolbox for USE with Mathlab, User's Guide," Third ed., 24 Prime Park Way, Natick, MA 01760-1500: The MathWorks, Inc., 1998.

[112] Z. Chi and H. Yan, "Segmentation of geographic map images using fuzzy rules," In the Proceedings of Digital Image Computing, Techniques and applications (DICTA-93), Australian Pattern Recognition Soc., Broadway, NSW, Australia, vol. 1, pp. 95-101, 1993.

[113] L. Wang and J. M. Mendel, "Generating fuzzy rules by learning from examples," In the Proceedings of IEEE International Symposium on Intelligent Control, Arlington, Virginia, USA, pp. 263-268, 1991.

[114] Z. Chi, J. Wu, and H. Yan, "Handwritten numeral recognition using self organizing maps and fuzzy rules," *Pattern Recognition*, vol. 28, pp. 59-66, 1995.

[115] L. O. Hall and A. Namasivayam, "Using adaptive fuzzy rules for image segmentation," In the Proceedings of FUZZ-IEEE'98, 1998.

[116] J. S. Weszka and A. Rosenfeld, "Histogram modification for threshold selection," *IEEE Transactions on Systems, Man, and Cybernatics*, vol. 9, pp. 38-52, 1979.

[117] A. M. Bensaid and L. O. H. e. al., "Partially supervised clustering for image segmentation," *Pattern Recognition*, vol. 29, pp. 859-871, 1996.

[118] T. Kapur, "Segmentation of brain tissue from magnetic resonance images," MIT AI laboratory, Technical Report AITR-1566, 1995.

[119] L. A. Zadeh, "Fuzzy Sets," *Information Control*, vol. 8, pp. 338-353, 1965.

[120] T. Sasaki, Y. Hata, Y. Ando, M. Ishikawa, and H. Ishikawa, "Fuzzy rule based approach to segment the menisci region from MR images," In the Proceedings of SPIE Medical Imaging, San Diego, California, USA, vol. 3661, pp. 258-, 1999.

[121] ---------, "Computed Tomography Imaging (CT Scan, CAT Scan)," Imaginis Corporation, 2000, http://www.imaginis.com/ct-scan/.

[122] M. Sonka, W. Park, and E. A. Hoffman, "Rule-based detection of intrathoracic airway trees," *IEEE Transactions on Medical Imaging*, vol. 15, pp. 314-326, 1996.

[123] E. A. Hoffman, D. Gnanaprakasam, K. B. Gupta, J. D. Hoford, S. D. Kugelmass, and R. S. Kulawiec, "VIDA: An environment for multidimensional image display and analysis," In the Proceedings of SPIE, Bellingham, WA: SPIE, vol. 1660, pp. 694-711, 1992.

[124] E. A. Hoffman, L. J. Sinak, R. A. Robb, and E. L. Ritman, "Noninvasive quantitative imaging of shape and volume of lungs," *J. Appl. Physiol.*, vol. 54, pp. 1414-1421, 1983.

[125] S. Wood, J. Hoford, E. Zerhouni, E. Hoffman, and W. Mitzner, "Quantitative 3-D reconstruction of airway and pulmonary vascular trees using HRCT," In the Proceedings of Biomedical Image Processing and Biomedical Visulisation, Bellingham, WA: SPIE, vol. 1905, pp. 316-323, 1993.

[126] S. Wood, E. Zerhouni, E. A. Hoffman, and W. Mitzner, "Measurement of three-dimensional lung tree structures using computed tomography," *J. Appl. Physiol.*, vol. 79, pp. 1687-1697, 1995.

[127] M. Sonka, V. Hlavac, and R. Boyle, *Image Processing, Analysis, and Machine Vision*, 2nd edition,Boston ed: London, U.K.: Chapman and Hall, 1993.

[128] E. Cox, *The Fuzzy Systems Handbook*. Cambridge: MA: AP professional, 1994.

[129] H. J. Zimmermann, *Fuzzy Sets, Decision Making and Expert Systems*. Boston: MA: Kluwer, 1987.

[130] S. P. Raya and J. K. Udupa, "Shape-based interpolation of multidimensional objects," *IEEE Transactions on Medical Imaging*, vol. 9, pp. 22-32, 1990.

[131] B. B. Chaudhuri and N. Sarkar, "Texture segmentation using fractal dimension," *IEEE Transactions on Pattern Analysis and Machine Intelligence*, vol. 17, pp. 72-77, 1995.

[132] M. Sharma, M. Markou, and S. Singh, "Evalution of texture methods for image analysis," http://citeseer.nj.nec.com/sharma80evaluation.html, 1980.

[133] J. Zhang and T. Tan, "Brief review of invariant texture analysis methods," *Pattern Recognition*, vol. 35, pp. 735-747, 2002.

[134] N. Sarkar and B. B. Chaudhuri, "An efficient approach to estimate fractal dimension of textural images," *Pattern Recognition*, vol. 25, pp. 1035-1041, 1992.

[135] J. K. Geuseberk, R. V. D. Boomgaard, and A. W. M. Smeulders, "Color and scale: The spatial structure of color image," ISIS technical report series, Vol. 18, 2000.

[136] S. J. Sangwine and R. E. N. Horne, "The colour Image Processing Handbook," first edition ed.: Chapman & Hall, 1998.

[137] J. D. Foley, A. Dam, S. K. Feiner, J. F. Hughes, and R. L. Phillips, *Introduction to Computer Graphics*: Addison-Wesley Publishing Company, Inc., 1994.

[138] H. D. Cheng, X. H. Jiang, Y. Sun, and J. L. Wang, "Color Image Segmentation: Advances and Prospects," *Pattern Recognition Letters*, vol. 11, pp. 2259-2281, 2001.

[139] Y. W. Lim and S. U. Lee, "On the color image segmentation algorithm based on the thresholding and the fuzzy c-means techniques," *Pattern Recognition Letters*, vol. 23, pp. 935-952, 1990.

[140] A. Moghaddamzadesh and N. Bourbakis, "A fuzzy region growing approach for segmentation of color images," *Pattern Recognition Letters*, vol. 30, pp. 935-952, 1997.

[141] B. C. Chien and M. C. Cheng, "A colour image segmentation approach based on fuzzy similarity measure," presented at FUZZ-IEEE'02, 2002.

[142] H. D. Cheng, X. H. Jiang, and J. Wang, "Color image segmentation based on homogram thresholding and region merging," *Pattern Recognition Letters*, vol. 35, pp. 373-393, 2002.

[143] M. Wertheimer, "Laws of organization in perceptual forms," *Pshychologische Forschung*, vol. 6, 1923.

[144] E. Gose et al., *Pattern Recognition and Image Analysis*. NJ 07458: Prentice Hall PTR Upper Saddle River, 1996.

[145] C. B. Kellogg, F. Zhao, and K. Yip, "Spatial aggregation: language and applications," In the Proceedings of AAAI-96, 1996.

[146] K. Yip and F. Zhao, "Spatial aggregation: theory and applications," *Jour. of Artificial Intelligence Research*, vol. 5, pp. 1-26, 1996.

[147] M. Tuceryan, "Computational geometry," http:// klingon.cs.iupui.edu/~tuceryan, 2000.

[148] S. Geman and D. Geman, *Stochas*. NJ 07458: Prentice Hall River, 1984.

[149] S. M. H. Zaman, K. Rahim, and M. Howlader, *Simple Lesson From Biometry*. Joydebpur, Dhaka, Bangladesh.: Bangladesh Rice Research Institute, 1982.

[150] H. Lamehamedi, D. Kebbal, E. Talbi, A. Bensaid, and A. Benllaachia, "Adaptive programming: application to a semi supervised point prototype clustering algorithm," presented at International Conference on Parallel and Distributed Techniques and Applications (PDPTA'99), Lasvegas, Nevada, 1999.

[151] P. F. Preparata and I. M. Shamos, *Computational Geometry*, 2nd ed: Springer - Verlag New York Inc., 1985.

[152] P. Rapant, "Topological representation of input data for DTM," http://www.geogr.muni.cz/lgc/gis98/proceed/rapant.htm, 1998.

[153] V. Robins, J. D. Mesis, and E. Bradley, "Computing Connectedness: an exercise in computational topology," *Nonlinearity*, vol. 11, pp. 913-922, 1998.

[154] E. Horch, "Basic Priciples of Imaging Science II," Lecture Notes 8, http://www.cis.rit.edu/class/simg712/lectures/lect_08/lect_08.pdf, 2001.

[155] A. Wardhani and R. Gonzalez, "Image structure analysis for CBIR," In the Proceedings of the Multimedia Systems Conference, Austin, Texas, 1998.

[156] Bruce and P. R. Green, *Visual Perception: Physiology, Psychology and Ecology*, 2nd Edition ed. Hove and London: Lawrence Erlbaum Association, 1990.

[157] J. K. Udupa, "Go digital, go fuzzy," In the Proceedings of DGCI 2000, LNCS 1953, pp. 284-295, 2000.

[158] P. K. Sahoo, S. Soltani, and A. K. C. Wong, "A survey of Thresholding Techniques," *Computer Vision, Graphics, and Image Processing*, vol. 41, pp. 233-260, 1988.

[159] H. Tamura, S. Mori, and T. Yamawaki, "Textural features corresponding to visual perception," *IEEE Transactions on Systems, Man, and Cybernetics*, vol. SMC-8, pp. 460-473, 1978.

[160] M. B. Dillencourt, H. Samet, and M. Tamminen, "A general approach to connected-component labeling for arbitrary image representations," *Journal of the ACM*, vol. 39, pp. 253-280, 1992.

[161] B. B. Mandelbrot, *Fractal Geometry of Nature*: Freeman San Francisco, 1982.

[162] A. Conci and C. B. Proenca, "A fractal image analysis system for fabric inspection based on a box-counting method," wysiwyg://275/http://www.geocities.com/ResearchTriangle/2743/www.html, 2001.

[163] L. Luccehese and S. K. Mitra, "An algorithm for fast segmentation of color images," In the Proceedings of IEEE 10th Tyrrhenian Workshop on Digital Communication, Ischia, Italy, pp. 110-119, 1998.

[164] D. Cardani, "Adventures in HSV Space," http://www.buena.com/articles/hsvspace.pdf, 2002.

[165] Y. J. Zhang, "A survey on evaluation methods for image segmentation," *Pattern Recognition*, vol. 29, pp. 1335-1346, 1996.

[166] W. A. Yasnoff, J. K. Mui, and J. W. Bacus, "Error measures for scene segmentation," *Pattern Recognition*, vol. 9, pp. 217-231, 1977.

[167] W. A. Yasnoff and J. W. Bacus, "Scene segmentation algorithm development using error measures," *Analytical and Qantiritative Cytology and Histology (AOCH)*, vol. 6, pp. 45-48, 1984.

[168] W. J. Popham and K. A. Sirotnik, *Educational Statistics Use and Interpretation*, second edition ed. New York: Harper & Row, Publishers, 1973.

Publications

During the PhD research, the following selected papers have been published from the thesis.

1 Refereed International Journal

[1] G. C. Karmakar and L. S. Dooley, "A Generic fuzzy rule based image segmentation algorithm," *Pattern Recognition Letters*, vol. 23, pp. 1215-1227, 2002.

2 Book Chapter

[2] G. C. Karmakar, L. Dooley, and S. M. Rahman, "Review on fuzzy image segmentation techniques," in *Design and Management of Multimedia Information Systems: Opportunities and Challenges*: Idea Group Publishing, USA, pp. 282 -313, ISBN 1-930708-00-9, 2001.

3 Refereed International Conferences

[1] G. C. Karmakar, L. Dooley, and S. M. Rahman, "A survey of fuzzy rule based image segmentation techniques," In the Proceedings of the First IEEE Pacific-Rim Conference on Multimedia, Sydney, NSW, Australia, pp. 350-353, 2000.

[2] G. C. Karmakar and L. Dooley, "Generic fuzzy rule based technique for image segmentation," In the Proceedings of IEEE International Conference on Acoustics, Speech, and Signal Processing, (ICASSP'2001), Salt Lake City, Utah, vol. 3, pp. 1577-1580, 2001.

[3] G. C. Karmakar and L. S. Dooley, "Analysis of fuzzy clustering and a generic fuzzy rule based image segmentation technique," presented at International Conference on Intelligent Multimedia and Distance Education, Fargo, North Dakota, USA, pp. 68-75, 2001.

[4] G. C. Karmakar and L. S. Dooley, "Extended fuzzy rules for image segmentation," In the Proceedings of IEEE International Conference on Image Processing (ICIP2001), Thessaloniki, Greece, vol. 3, pp. 1099-1102, 2001.

[5] G. C. Karmakar, L. S. Dooley, and M. Murshed, "New fuzzy rules for improved image segmentation," In the Proceedings of IEEE International Conference on Acoustics, Speech, and Signal Processing (ICASSP2002), Orlando, Florida, USA, vol. 4, pp. 4192-4192, 2002.

[6] G. C. Karmakar, L. S. Dooley, and M. M. Murshed, "Fuzzy rules for image segmentation incorporating texture features," In the Proceedings of IEEE 2002 International Conference on Image Processing (ICIP2002), Rochester, New York, vol. 4, pp. 797-800, 2002.

[7] G. C. Karmakar, L. S. Dooley, and M. Murshed, "Image segmentation using modified extended fuzzy rules," In the Proceedings of 6th International Conference on Signal Processing (ICSP'02), Beijing, China, vol. 2, pp.941-944, 2002.

A generic fuzzy rule based image segmentation algorithm

Gour C. Karmakar *, Laurence S. Dooley

Gippsland School of Computing and Information Technology, Monash University, Churchill, Vic. 3842, Australia

Received 7 May 2001; received in revised form 1 November 2001

Abstract

Fuzzy rule based image segmentation techniques tend in general, to be application dependent with the structure of the membership functions being predefined and in certain cases, the corresponding parameters being manually determined. The net result is that the overall performance of the segmentation technique is very sensitive to parameter value selections. This paper addresses these issues by introducing a generic fuzzy rule based image segmentation (GFRIS) algorithm, which is both application independent and exploits inter-pixel spatial relationships. The GFRIS algorithm automatically approximates both the key weighting factor and threshold value in the definitions of the fuzzy rule and neighbourhood system, respectively. A quantitative evaluation is presented between the segmentation results obtained using GFRIS and the popular fuzzy c-means (FCM) and possibilistic c-means (PCM) algorithms. The results demonstrate that GFRIS exhibits a considerable improvement in performance compared to both FCM and PCM, for many different image types. © 2002 Elsevier Science B.V. All rights reserved.

Keywords: Generic fuzzy rules; Image segmentation; Spatial information; Fuzzy clustering

1. Introduction

Classical, so-called "crisp" image segmentation techniques, while effective for images containing well-defined structures such as edges, do not perform as well in the presence of ill-defined data. In such circumstances, the processing of images that possess ambiguities is better performed using fuzzy segmentation techniques, which are more adept at dealing with imprecise data. Fuzzy techniques may be broadly classified into five main categories: fuzzy clustering, fuzzy rule based, fuzzy geometry, fuzzy thresholding, and fuzzy integral based segmentation techniques (Tizhoosh, 1998). Of these, the most widely used are fuzzy clustering and fuzzy rule based segmentation.

The two most popular fuzzy clustering techniques are the fuzzy c-means (FCM) (Bezdek, 1981; Chi et al., 1996) and possibilistic c-means (PCM) algorithms (Krishnapuram and Keller, 1993). While both these methods have been applied extensively, neither integrates human expert knowledge nor includes information about pixel spatial relations. Image segmentation which relies upon only feature based information without considering inter-pixel relationships, does not generally

* Corresponding author. Tel.: +51-223-884; fax: +99-026-842.

E-mail addresses: Gour.Karmakar@infotech.monash.edu.au (G.C. Karmakar), Laurence.Dooley@infotech.monash.edu.au (L.S. Dooley).

produce good results, because there are usually a large number of overlapping pixel values between different regions.

In contrast, fuzzy rule based image segmentation techniques are able to integrate expert knowledge and are less computationally expensive compared with fuzzy clustering. They are also able to interpret linguistic as well as numeric variables (Chang et al., 1998). The performance of fuzzy rule based segmentation in many applications however, is sensitive to both the structure of the membership functions and associated parameters used in each membership function. For example, the fuzzy rule based segmentation technique proposed by Chi and Yan (1993) for geographic map images, intuitively defined the structure of the membership functions with the related parameters being automatically determined, while Hall and Namasivayam (1998) and Chang et al. (1998) used a different approach for segmenting magnetic resonance images (MRI) of the brain. They predefined the membership functions so the corresponding parameters could be automatically derived. Another approach (Sasaki et al., 1999) was used for segmenting the menisci region from MRI slices, with the structure of the membership functions defined from the anatomical knowledge of the knee and the parameters being taken from actual MRI device data. A different strategy was proposed by Park et al. (1998) who used perceptually selected structures and parameters for the membership functions, in the segmentation of intrathoracic airways trees in computer tomography (CT) images.

Karmakar et al. (2000) presented a contemporary review of fuzzy rule based image segmentation techniques, and confirmed that despite being used in a wide range of applications, both the structure of membership functions and derivation of their relevant parameters were still very much application domain and image dependent.

This paper presents a new generic fuzzy rule based image segmentation (GFRIS) algorithm, which addresses a number of the aforementioned issues, most crucially by incorporating spatial pixel information and automatically data-mining both the key fuzzy rule weighting factor and its threshold (Karmakar and Dooley, 2001). The

paper is organised as follows: In Section 2, the three membership functions used in the GFRIS algorithm are defined. The fuzzy rule definition and underlying theory, together with the data-mining algorithm for obtaining both the key weighting factor and threshold are presented in Sections 3 and 4, respectively. Section 5 details the full GFRIS algorithm, while Section 6 discusses the experimental results and performance of this new segmentation technique when applied to a range of different images. All the results are quantitatively evaluated using the empirical objective segmentation assessing method (Zhang, 1996), "*discrepancy based on the number of mis-segmented pixels*". Finally, Section 7 concludes the paper.

2. Definition of membership functions

The definition of the membership function lies at the heart of any fuzzy logic system and the capability of fuzzy rule based techniques significantly depend upon it. The eminent psychologist Gestalt, discovered that visual elements may be perceptually grouped together based on the principles of: proximity, similarity, common fate, good continuation, surroundedness, closure, relative size and symmetry (Wertheimer, 1923). In this section, three membership function types are defined to respectively represent the: (i) region pixel distributions, (ii) closeness to a region's centre, and (iii) pixel spatial relations. The second membership function for instance, characterises similarity based on gray level pixel intensity, while the third reflects the characteristics of proximity and good continuation. Each membership function has a corresponding membership value for every region, which indicates the degree of belonging to that region.

2.1. Membership function for region pixel distributions

In gray level images, every region has a distinctive pixel distribution, which characterises to some extent that region's properties. The approach adopted here is to automatically define the membership function including its structure from the

pixel distribution of that particular region. This is achieved in three steps:

1. Segment the original image into a desired number of regions by applying a clustering algorithm such as FCM.
2. Generate the gray level pixel intensity histogram for every region and normalise the frequency for each gray level into the range [0 1].
3. Use a polynomial representation to approximate each region. The polynomial value of a region, for every gray level pixel corresponds to the membership value of that pixel in that region, with the actual gray level intensity values being the parameters of the membership function.

As an example, the reference image shown in Fig. 1(a) is classified into two separate regions, namely R_1 (cloud) and R_2 (urban scene) using the standard FCM algorithm. The respective pixel distribution of each region is used to produce the corresponding membership function and a gray level intensity histogram (*gray level histogram*) is generated for both regions, with the frequencies of occurrence being normalised. A polynomial then approximates the histogram of each region. As an example, a 3rd order polynomial is given by

$$f(x) = a_0 + a_1 x + a_2 x^2 + a_3 x^3, \tag{1}$$

where x is an independent variable, which in this example is the 8-bit gray level pixel intensity.

The coefficients a_0, a_1, a_2, and a_3 are computed by applying a least squares (LS) fit to the histogram for each region. The values of $f(x)$ are con-

strained between 0 and 1, and represent the membership value of each gray level pixel. The 3rd order polynomials for the segmented regions R_1 and R_2 in the example image, are shown in Fig. 1(b) and (c), respectively.

The degree of belonging to a region of a candidate pixel, that is the pixel to be classified, is determined from the respective membership function. Hence, for a pixel having a gray level value of 150, the membership values for regions R_1 and R_2 can be easily determined from the respective polynomials as 0.425 and 0.125, respectively. Considering the general case of a pixel with a gray level value of $P_{s,t}$ at location (s, t), then the two membership functions $\mu_{DR_1}(P_{s,t})$ and $\mu_{DR_2}(P_{s,t})$ for the pixel distribution of regions R_1 and R_2, respectively, are expressed as:

$$\mu_{DR_1}(P_{s,t}) = f_{R_1}(P_{s,t}) \tag{2}$$

and

$$\mu_{DR_2}(P_{s,t}) = f_{R_2}(P_{s,t}), \tag{3}$$

where $f_{R_1}(P_{s,t})$ and $f_{R_2}(P_{s,t})$ are the respective polynomials of regions R_1 and R_2.

2.2. Membership function to measure the closeness of a region

This membership function represents the similarity between a candidate pixel and the centre of a region based on gray level pixel intensity and is measured using the *city block distance*. A pixel must always be closer to the belonging region than any other region and the degree of *belongingness* of a candidate pixel to a region is determined from


(a)   (b)   (c)
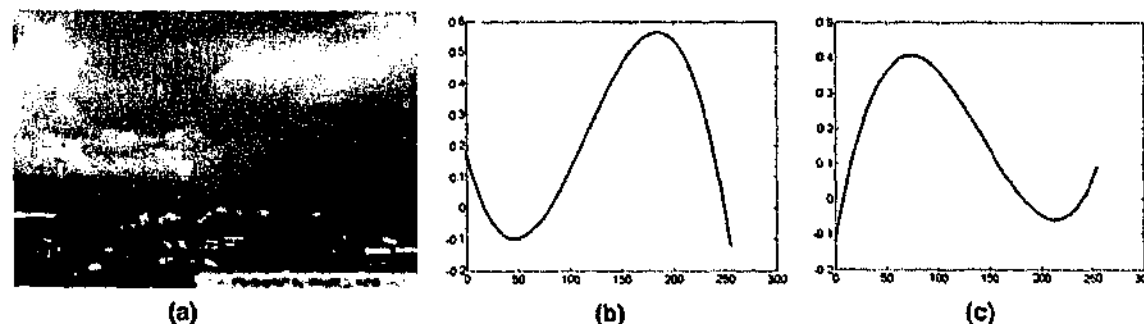
Fig. 1. Reference image and its membership function for each region: (a) original image, (b) membership function for R_1, (c) membership function for R_2.

the k-means clustering algorithm (Gose et al., 1996). When a candidate pixel joins its nearest region, the centre of that particular region is recomputed. The centroid of a region R_j is defined as

$$C(R_j) = \frac{1}{N_j} \sum_{i=1}^{N_j} P_j(i), \tag{4}$$

where N_j is the number of pixels and $P_j(i)$ represents the ith pixel gray level intensity in the jth region.

A membership function should reflect the axiom that "*the closer a pixel is to a region, the larger the membership value that pixel should have*". Hence, the membership function $\mu_{CR_j}(P_{s,t})$, which determines the degree of belongingness of a candidate pixel $P_{s,t}$ at location (s,t), to a region R_j is defined as

$$\mu_{CR_j}(P_{s,t}) = 1 - \frac{|C(R_j) - P_{s,t}|}{D}, \tag{5}$$

where D is a constant equal to the difference between the maximum and minimum gray level intensity values in an image, so using an 8-bit gray scale, $D = 255$.

Theorem 1. *The maximum value of the membership function $\mu_{CR_j}(P_{s,t})$ will always be at the centre of the region and the structure of the function will be symmetrical about a vertical line that passes through the centre of the region.*

Proof. For positive values of D,

$$\frac{|C(R_j) - P_{s,t}|}{D} \geqslant 0.$$

The function $\mu_{CR_j}(P_{s,t})$ will therefore be a maximum whenever $|C(R_j) - P_{s,t}| = 0$, i.e. when $C(R_j) = P_{s,t}$, so the maximum always occurs at $C(R_j)$, which is the centre of region R_j.

To prove the membership function is symmetrical about $C(R_j)$, consider the values of $\mu_{CR_j}(P_{s,t})$ for $P_{s,t} = C(R_j) + \delta$ and $P_{s,t} = C(R_j) - \delta$, where δ is an arbitrary constant.

$$\mu_{CR_j}(C(R_j) + \delta) = 1 - \frac{|C(R_j) - C(R_j) - \delta|}{D}$$
$$= 1 - \frac{|\delta|}{D},$$

$$\mu_{CR_j}(C(R_j) - \delta) = 1 - \frac{|C(R_j) - C(R_j) + \delta|}{D}$$
$$= 1 - \frac{|\delta|}{D}.$$

Since $\mu_{CR_j}(C(R_j) + \delta) = \mu_{CR_j}(C(R_j) - \delta)$, $\mu_{CR_j}(P_{s,t})$ is also symmetrical about a vertical line passing through the centre of region R_j. $\square$

2.3. Membership function for spatial relations

The principles of proximity and good continuation are used to define this particular membership function. Wherever pixels are close together and exhibit relatively smooth variations, there is an obvious expectation that strong spatial relationships will exist between neighbouring pixels within that region. In the preceding sections, the respective membership functions have been constructed using only feature values, i.e. gray level pixel intensities. Spatial relations between pixels within an identified region have not been considered, yet are vital since they characterise the geometric features of a region as any spatial object contains two descriptors: feature and geometric (Kellogg et al., 1996; Yip and Zhao, 1996).

In many natural images, there are a large number of overlapping pixels between regions, so that effective segmentation cannot be expected unless these overlapping pixels are taken into account. By considering the neighbourhood relationship between the candidate pixel and the pixels of a region that surround it, a large number of overlapping pixels can be reduced. Based on the neighbourhood relations, the candidate pixel can then be assigned to the appropriate region.

Many approaches exist to define neighbourhood relations (Tuceryan, 2000), such as minimum spanning tree, fixed size neighbourhoods, and Voronoi tessellation. This paper concentrates upon only fixed size neighbourhoods around the candidate pixel, since the number of pixels and their distances from a candidate pixel has to be calculated.

The neighbourhood pixel configurations for $r = 1$, $r = 2$, and $r = 4$ are shown in the Fig. 2(a)–(c), respectively, (Geman and Geman, 1984) where $r \geqslant 1$ denotes the neighbourhood radius, while o and # represent the candidate and neighbourhood

```
                    #  #  #  #  #
    #        #  #  #    #  #  #  #  #
 #  O  #     #  O  #    #  #  O  #  #
    #        #  #  #    #  #  #  #  #
                    #  #  #  #  #
  (a) r=1      (b) r=2       (c) r=4
```
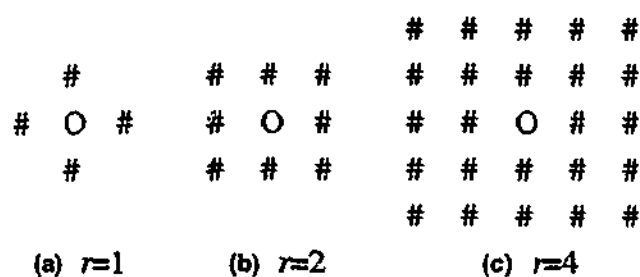
Fig. 2. Neighbourhood configurations.

pixels, respectively. The number of neighbours will be $(r+1)^2$ for $r = 1$ and $(r+1)^2 - 1$ otherwise.

As previously mentioned, the principles of proximity and good continuation imply that pixels, which are close together and have smooth variations should be part of the same region, that is, segmented regions are homogeneous and mutually exclusive. It is thus assumed that the variation of neighbouring pixels in a region is limited to some threshold T, and the neighbourhood system of a region based on this premise is defined as

Definition 1 (*Neighbourhood system*). A neighbourhood system $\zeta(P_{s,t}, r)$ with radius r, of a candidate pixel $P_{s,t}$ is the set of all pixels $P_{x,y}$ such that $\zeta(P_{s,t}, r) = \{P_{x,y} | (d(P_{x,y}, P_{s,t}) \leqslant r) \wedge ((P_{x,y} \sim P_{s,t}) \leqslant T)\}$ where the distance, $d(P_{x,y}, P_{s,t}) = |x - s| + |y - t|$, $P_{x,y}$ is the gray level value of the pixel at Cartesian coordinates (x, y), $(P_{x,y} \sim P_{s,t})$ is the absolute value of the difference between the gray level values of the pixels $P_{x,y}$ and $P_{s,t}$, and T is the threshold.

To construct a membership function, the number of neighbourhood pixels and their distances from the candidate pixel must be considered. The membership function μ should possess the following properties:

1. $\mu \propto N$ where N is the number of neighbours.
2. $\mu \propto (1/d(P_{x,y}, P_{s,t}))$,

where $d(P_{x,y}, P_{s,t})$ is the distance between pixels $P_{x,y}$ and $P_{s,t}$.

The summation of inverse distances of a region R_j is

$$G_{R_j} = \sum_{i=1}^{N_j} \frac{1}{d_i(P_{x,y}, P_{s,t})}, \qquad (6)$$

where $N_j = |\zeta(P_{s,t}, r)|$ is the number of neighbourhood pixels of the candidate pixel $P_{s,t}$ in the region R_j and $d_i(P_{x,y}, P_{s,t})$ is the distance between the ith pixel $P_{x,y}$ of region R_j and the candidate pixel $P_{s,t}$.

By considering the number of neighbours N_j and the sum of their inverse distances G_{R_j} from the candidate pixel $P_{s,t}$, the membership function $\mu_{NR_j}(P_{s,t}, r)$ of the region R_j becomes

$$\mu_{NR_j}(P_{s,t}, r) = \frac{N_j \times G_{R_j}}{\sum_{j=1}^{\Re} (N_j \times G_{R_j})}, \qquad (7)$$

where $\Re$ is the number of segmented image regions. Eq. (7) shows that the greater the number of neighbours in a region, the larger the membership function value will be for that region. Hence, if all neighbours fall into a single region, the corresponding membership function value will be one for that region, since the sum of the membership function values for all regions always equals unity.

3. Fuzzy rule definition

The definition of the fuzzy rule is the single most important and challenging aspect of fuzzy rule based image segmentation, as its effectiveness is vital to the overall performance. In this paper, the fuzzy rule is heuristically defined using the three membership functions defined in Section 2, in combination with the widely used fuzzy IF–THEN rule structure.

The overall membership value $\mu_{AR_j}(P_{s,t})$ of a pixel $P_{s,t}$ for region R_j represents the overall degree of belonging to that region, and is defined by the weighted average of the three individual membership function values $\mu_{DR_j}(P_{s,t})$, $\mu_{CR_j}(P_{s,t})$ and $\mu_{NR_j}(P_{s,t})$, which are given in Eqs. (2), (5) and (7), respectively.

$$\mu_{AR_j}(P_{s,t}) = \frac{W_1 \mu_{DR_j}(P_{s,t}) + W_2 \mu_{CR_j}(P_{s,t}) + W_3 \mu_{NR_j}(P_{s,t})}{W_1 + W_2 + W_3}. \qquad (8)$$

W_1, W_2, and W_3 are the weightings of the membership values for pixel distribution, closeness to the cluster centres, and neighbourhood relations, respectively. The overall membership value

$\mu_{AR_j}(P_{s,t})$ is used in the antecedent condition of the fuzzy IF–THEN rule.

Definition 2 (*Rule*). IF $\mu_{AR_j}(P_{s,t})$ supports region R_j THEN pixel $P_{s,t}$ belongs to region R_j.

$\mu_{AR_j}(P_{s,t})$ will give support to the region R_j if $\mu_{AR_j}(P_{s,t}) = \max\{\mu_{AR_1}(P_{s,t}), \mu_{AR_2}(P_{s,t}), \ldots, \mu_{AR_{\Re}}(P_{s,t})\}$. This rule is deliberately generic so that it can be applied to any image type thus adhering to one of the key objectives that the GFRIS algorithm should be both image and application independent.

4. Determination of weighting factors and the threshold

The threshold value T introduced in Section 2.3, plays a major role in defining the spatial relationship between pixels in any region, because it regulates the level of variation between the candidate pixel and its neighbours. The greater the variation between a candidate pixel and its neighbours, the larger the standard deviation will be, which pro rata results in poor continuation. Two issues need to be considered in determining the threshold value:

1. The degree to which pixels of one region overlap with those of another region.
2. The pixel standard deviations in each region.

The approximate threshold T_a is computed using 1, by considering the centres of the initially segmented regions, while the status of this approximate threshold as to whether it is actually an overestimation of the final threshold value, is determined using 2. Estimation of both the status and final threshold value is detailed in the algorithm below. If the centre of a particular region is two standard deviations away from the boundary of another region and the pixels in that region are normally distributed, there is at best a 5% probability that the pixels of that region will overlap with the other. The procedure to determine the approximate threshold T_a for two regions may be formalised as follows

Theorem 2. *If two regions with centres c_1 and c_2 have pixels that are normally distributed, then for at least 5% levels of significance, the approximate threshold will be bounded by $T_a \leqslant |c_1 - c_2|/4$.*

Proof. Assuming that the pixels are normally distributed, then in a region having a centre c_1 and standard deviation σ_1, the 5% level of significance means the probability of pixels falling outside $c_1 \pm 2\sigma_1$ will be 0.05 (Zaman et al., 1982). The same is also true for other region, which has a centre c_2 and standard deviation σ_2. Thus, for at least 5% levels of significance,

$$2(\sigma_1 + \sigma_2) \leqslant |c_1 - c_2|.$$

Since the threshold is considered the same for both regions, it may be written as $T_a = (\sigma_1 + \sigma_2/2)$ such that

$$4T_a \leqslant |c_1 - c_2| \Rightarrow T_a \leqslant \frac{|c_1 - c_2|}{4}. \quad \square$$

This theory may be extended to an arbitrary number of regions for determining the weight and the threshold values. If the approximate threshold is overestimated, the minimum value between the standard deviations and the approximate threshold is used as the final threshold. This is conditional on the value not being either zero or very small (less than some arbitrary percentage of T_a), so ensuring that some spatial relationship exists. The weight W_1 in Eq. (8) governs the importance assigned to region pixel distributions, and empirical observations reveal that the resultant segmentation results are not very sensitive to variations in this particular parameter.

The important weighting factors are W_2 and W_3, as their values represent a trade-off between the gray level pixel intensity and spatial relationship. Prominence was initially given to the former, because it contributed more to the human visual perception and for this reason, following empirical evaluation; W_2 was set equal to 1.8, with the other two weighting factors being set to one. If the standard deviation in a number of regions is high with respect to the approximate threshold, then the spatial relationship will be ineffective and greater emphasis needs to be given to W_2 by increasing its value. In all other instances, impor-

tance should be given to the pixel spatial relationships so that the value of W_2 should be reduced. The following details the various stages of the algorithm to automatically determine this key weighting factor and its threshold.

1. Set the initial values for the three weighting factors as $W_1 = 1$; $W_2 = 1.8$; $W_3 = 1$.
2. Define a set of all regions (R) and a set of centre pairs of all regions (V)

$$R = \{R_i | (1 \leqslant i \leqslant \Re)\},$$

$$V = \{(C(R_i), C(R_j)) | (\forall i, j R_i, R_j \in R) \wedge (i \neq j)\}.$$

3. Compute the absolute sum of differences $(sofd)$ between the elements of all pairs

$$sofd = \sum_{i=1}^{nc2} |V_i(1) - V_i(2)|,$$

where $nc2$ is the number of combination pairs of all regions.
4. Determine the approximate threshold T_a using Theorem 2

$$T_a = \frac{sofd}{nc2 \times 4}.$$

5. Calculate the average sum of differences $(arstd)$ between the various standard deviations and approximate threshold

$$arstd = \frac{\sum_{i=1}^{\Re} (rstd_i - T_a)}{\Re},$$

where $rstd_i$ is the standard deviation of the ith region.
6. If the approximate threshold is overestimated, $(arstd < 0)$, then the minimum of the standard deviation and T_a is taken as the final threshold value T, provided this value is neither too small (less than $K\%$ of T_a, where K is an arbitrary constant) nor zero. If this condition is invalid, then T_a becomes the final threshold.
7. Normalise the average sum of differences between the standard deviation and approximate threshold

$$narstd = \frac{arstd}{\max(rstd_i, T_a)}.$$

8. Adjust the weight W_2 accordingly

$$W_2 = W_2 + narstd.$$

This algorithm has been experimentally tested upon various different image types and as results will prove in Section 6, the automatic data mining of the key weighting factor and threshold value is a significant reason for the superior performance of the GFRIS algorithm.

5. The GFRIS algorithm

The detailed stages involved in the GFRIS algorithm can now be formalised as follows:

1. Classify the pixels of an image into a desired number of regions using any appropriate clustering algorithm.
2. Derive the key weight and threshold value by applying the data-mining algorithm in Section 4, and the membership function for each pixel distribution from the theory given in Section 2.1.
3. Initialise the centre of all regions required to define the membership function in Section 2.2, with the respective centres produced by the clustering algorithm in step 1.
4. Sequentially select an unclassified pixel from the image and calculate each membership function value in each region for that pixel.
5. Classify the pixel into a region applying the fuzzy rule defined in Section 3.
6. Return to step 4 until every pixel is classified.

6. Discussion of experimental results

The GFRIS algorithm, FCM, and PCM were all implemented using MATLAB version 6.0. In order to evaluate the performance of the new GFRIS algorithm, a variety of different image types were applied possessing diverse characteristics, including homogeneous and non-homogeneous regions, low pixel contrast regions and perceptually distinct regions. Three images in particular, Figs. 1(a), 5(a) and 6(a), were used for demonstration and numerical evaluation.

All quantitative evaluations were performed using the powerful empirical discrepancy method (Zhang, 1996) *discrepancy based on the number of*

mis-segmented pixels. The confusion matrix C is a $\mathfrak{R} \times \mathfrak{R}$ square matrix, where C_{ij} denotes the number of jth region pixels wrongly classified in the ith region by the segmentation algorithm. Two error measures Type I, $errorI_i$ and Type II $errorII_i$, were defined as performance measures:

$$errorI_i = \frac{\left(\sum_{j=1}^{\mathfrak{R}} C_{ji} - C_{ii}\right)}{\sum_{j=1}^{\mathfrak{R}} C_{ji}} \times 100, \tag{9}$$

$$errorII_i = \frac{\left(\sum_{j=1}^{\mathfrak{R}} C_{ij} - C_{ii}\right)}{\left(\sum_{i=1}^{\mathfrak{R}} \sum_{j=1}^{\mathfrak{R}} C_{ij} - \sum_{j=1}^{\mathfrak{R}} C_{ji}\right)} \times 100. \tag{10}$$

Type I, $errorI_i$ represents the percentage error of all ith region pixels that are not classified in the ith region, whereas Type II, $errorII_i$ is the percentage error of all other region pixels wrongly classified in the ith region. The two manually segmented reference regions of the image in Fig. 1(a) used in the evaluation, are shown in Fig. 3.

For FCM, initialisation of the centre of the regions was performed randomly. The maximum number of iterations, the minimum level of improvement and the value of the fuzzifier (m) were empirically selected as 100, 0.00001 and 2, respectively.

For PCM, initialisation of the centre of the regions utilised the output of FCM. The value of the scale parameter η_i (Krishnapuram and Keller, 1993), was taken as the variance of the region i produced by FCM. The maximum number of iterations, minimum level of improvement and value of fuzzifier (m) were empirically chosen as 200, 0.00001 and 1.5, respectively.

For the GFRIS algorithm, the membership function defined in Section 2.1 was constructed using the regions produced by FCM, with their centre values used to initialise the centre of the regions required to define the membership function (Section 2.2). The respective weighting and threshold values were automatically data mined using the algorithm described in Section 4, with the constant $K = 0.25$. The segmented results of

(a)	(b)

Fig. 3. Manually segmented reference regions of Fig. 1(a): (a) cloud, (b) urban scene.

(a) R_1	(b) R_2

(c) R_1	(d) R_2

(e) R_1, $r=1$	(f) R_2, $r=1$

(g) R_1, $r=2$	(h) R_2, $r=2$

(i) R_1, $r=4$	(j) R_2, $r=4$
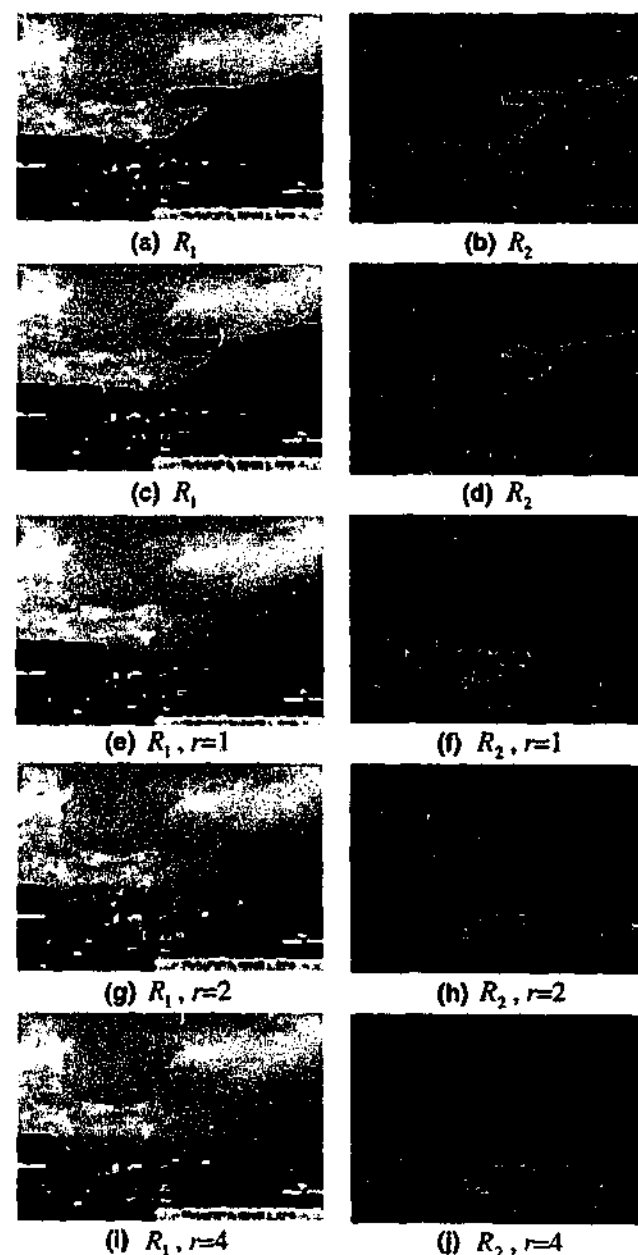
Fig. 4. Automatic segmentation of Fig. 1(a) into two regions using FCM (a)–(b), PCM (c)–(d), and GFRIS (e)–(j).

Table 1
Error percentages for the cloud region (R_1) segmentation in Fig. 1(a)

Algorithm	Error		
	Type I	Type II	Mean
FCM	28.0000	15.7372	21.8686
PCM	26.8939	16.3141	21.6040
GFRIS $r = 1$	7.3333	17.0513	12.1923
GFRIS $r = 2$	1.7273	21.2500	11.4887
GFRIS $r = 4$	1.8030	23.6218	12.7124

the image Fig. 1(a) for the two regions, cloud (R_1) and urban scene (R_2) produced by FCM, PCM and GFRIS, respectively are shown in Fig. 4.

The results confirmed that GFRIS separated almost the entire cloud region from the urban scene and produced significantly better results than both FCM and PCM. FCM and PCM gave approximately equal performance since as alluded earlier, both algorithms do not consider the spatial
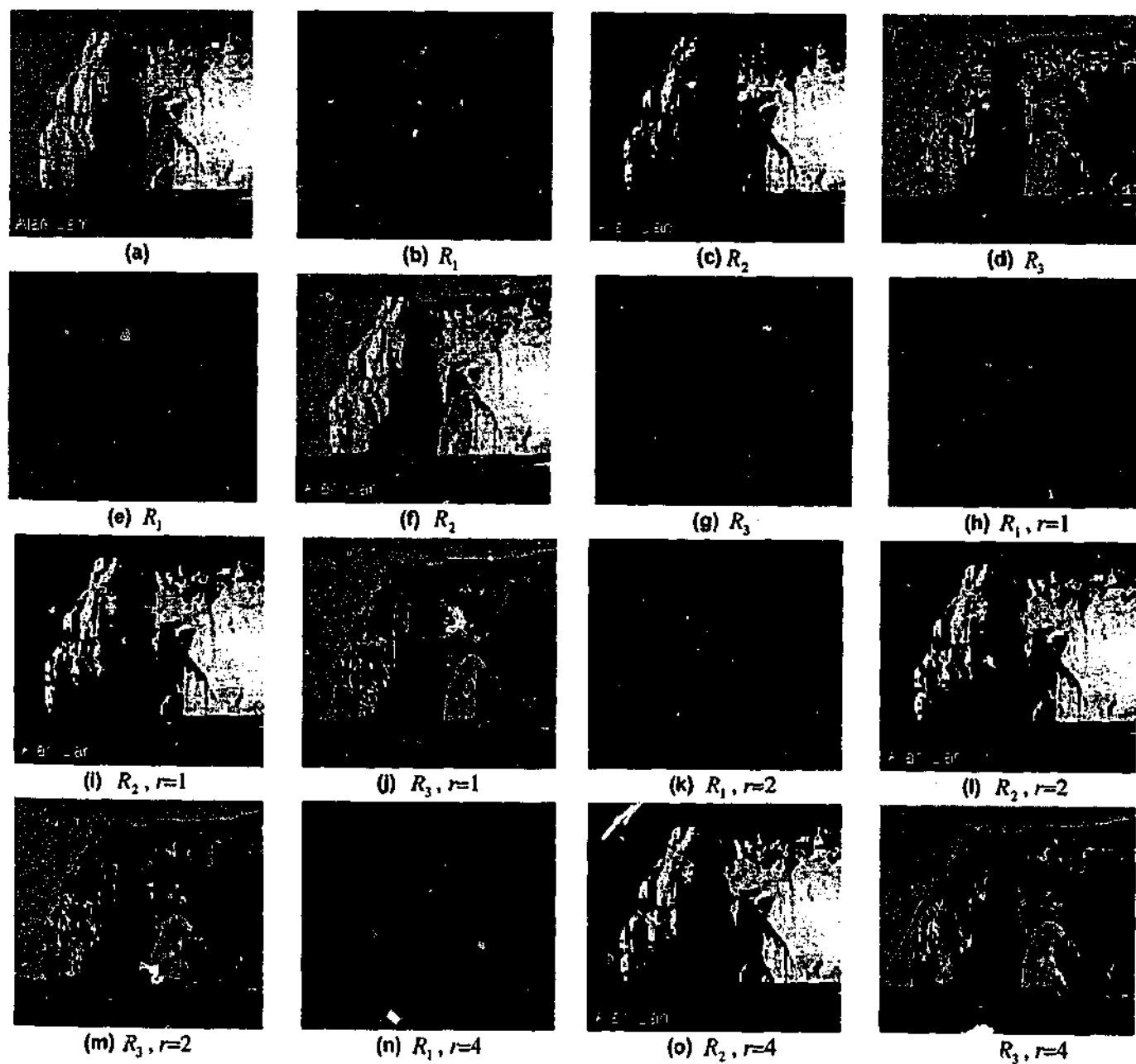
Fig. 5. Original iceberg image (a), and the segmented results for three regions produced by FCM (b)–(d), PCM (e)–(g), and GFRIS (h)–(p).

relationships between the pixels in each region. GFRIS also exhibited better results for larger values of neighbourhood radius r, since the pixels of region R_1 (cloud) are homogeneous and possess strong spatial correlation. Evaluation of the segmentation results for the cloud image, compared with the manually segmented reference images in Figs. 3(a) and (b), are shown in Table 1, where the final column is the average of the Type I and Type II errors. Note that only the error rates for the segmented cloud region are displayed in Table 1, because only two regions were identified, and the error rate of one region would be the reverse of that of the other region. The values given in italics correspond to the best GFRIS results.

The average GFRIS error rates for Fig. 1(a) were significantly better than those of both FCM and PCM for each value of the neighbourhood radius r. While GFRIS provided particularly good performance in segmenting the cloud region (R_1), it is worth noting that the error rates of GFRIS for the type II error were higher than those for both PCM and FCM. This was because not all the pixels in this region possessed good continuation due to the abrupt changes in the urban scene, which did not constitute a single object and so opposed the necessary condition for good inter-pixel relationships.

A second series of experiments were performed using the image in Fig. 5(a), which comprised three distinct regions, namely water (R_1), iceberg (R_2), and sky (R_3). The segmentation performance for the three regions using FCM, PCM and GFRIS is presented in Figs. 5(b)–(p).

It was visually apparent again that the GFRIS algorithm produced more distinctive regions for all values of neighbourhood radius r and hence considerably outperformed both FCM and PCM. PCM divided the iceberg image into only two regions (Figs. 5(e) and (f)) instead of three, because it was unable to distinguish between regions having a poor gray level contrast. The error rates for the segmentation of the iceberg image compared with the manually segmented reference images are given in Table 2.

The mean error rates of GFRIS for the iceberg and sky regions were considerably lower than for both FCM and PCM, while the error was slightly

Table 2
Error percentages for the iceberg image segmentation in Fig. 5(a)

Algorithm	Region	Error		
		Type I	Type II	Mean
FCM	Water	7.2228	20.7483	13.9856
	Iceberg	62.5797	0.8486	31.7141
	Sky	1.0421	24.3015	12.6718
PCM	Water	8.9581	19.1153	14.0367
	Iceberg	28.3612	59.5832	43.9722
	Sky	100.0000	0.0000	50.0000
GFRIS $r = 1$	Water	7.4898	21.3213	14.4055
	Iceberg	51.5495	0.9331	*26.2413*
	Sky	1.1869	15.8559	*8.5214*
GFRIS $r = 2$	Water	7.0449	22.2586	14.6517
	Iceberg	51.8344	0.9299	*26.3822*
	Sky	1.3027	14.9659	*8.1343*
GFRIS $r = 4$	Water	9.1435	21.4849	15.3142
	Iceberg	51.7933	0.9006	*26.3470*
	Sky	1.1406	16.3272	*8.7339*

higher for the water region. This was due to floating ice on the water, which was classified as water in the manually segmented reference region but was misclassified as sky using GFRIS.

In the above experiments, the number of segmented regions was constrained to two and three, respectively. In order to examine the discriminating potential of the GFRIS algorithm for a larger number of regions, a comparison was made with FCM and PCM algorithms on the image in Fig. 6(a) that possessed five regions. These were: egg (R_1), glass of milk (R_2), curtain (R_3), cheese (R_4) and table (R_5). Fig. 6 shows the segmentation performance of all three algorithms.

From Fig. 6(b)–(k), it is clear that both FCM and PCM arbitrarily divided the image into five regions without considering any semantic meaning of the data. The results produced by GFRIS for $r = 1$ and $r = 2$, in Figs. 6(l)–(u) showed more typical information of the regions. There are some regions such as egg and milk, curtain and cheese, which overlap with each other because their gray level pixel intensities are very similar. The most

Fig. 6. Original food image (a), and its segmented results for five regions produced by FCM (b)–(f), PCM (g)–(k), and GFRIS (l)–(z).

promising results in Fig. 6(v)–(z) were obtained for GFRIS using $r = 4$, with the exception of region R_4 (cheese) in Fig. 6(y), which partially merged with region R_2 (milk) as shown in Fig. 6(w). Again the GFRIS algorithm considered the underlying meaning of data far better than both the FCM and PCM techniques when compared with the manually segmented results.

Table 3
Error percentages for the food image segmentation in Fig. 6(a)

Algorithm	Region	Error		
		Type I	Type II	Mean
FCM	Egg	53.8987	27.7937	40.8462
	Milk	78.1723	17.5717	47.8720
	Curtain	57.7310	19.3766	38.5538
	Cheese	73.6814	18.3165	45.9990
	Table	64.1724	1.6680	32.9202
PCM	Egg	24.5806	59.3575	41.9690
	Milk	97.2167	3.8489	50.5328
	Curtain	98.2103	1.0998	49.6551
	Cheese	61.2456	30.5258	45.8857
	Table	100.0000	2.3314	51.1657
GFRIS $r = 1$	Egg	27.5875	19.8809	23.7342
	Milk	82.0478	18.3831	50.2155
	Curtain	34.9451	15.1914	25.0683
	Cheese	72.7393	18.4654	45.6024
	Table	69.8608	2.7701	36.3155
GFRIS $r = 2$	Egg	21.2948	25.2192	23.2570
	Milk	91.3547	9.4606	50.4077
	Curtain	16.2273	19.9142	18.0708
	Cheese	81.0402	12.0240	46.5321
	Table	51.6803	2.1541	26.9172
GFRIS $r = 4$	Egg	5.8837	0.2062	3.0450
	Milk	14.8141	33.2056	24.0099
	Curtain	49.5865	6.2929	27.9397
	Cheese	81.4295	11.2236	46.3266
	Table	46.0001	3.0249	24.5125

The numerical evaluations of the image segmentation given in Table 3, revealed that the mean error rates for the egg, curtain and cheese, egg, curtain and table, and egg, milk, curtain and table regions were appreciably lower using GFRIS with $r = 1$, $r = 2$, and $r = 4$, respectively than for either FCM or PCM. Overall the results confirmed that a significant improvement was achieved for all regions using GFRIS with neighbourhood radius $r = 4$, except for the cheese (R_4) region, for the reason alluded to above.

7. Conclusions

This paper has presented a new generic fuzzy rule based image segmentation (GFRIS) algorithm, which crucially has incorporated spatial relationships between pixels. It has been experimentally shown that in comparison with both FCM and PCM, GFRIS provided significantly superior results for a variety of different image types, including image examples having multiple regions. Its performance in considering the underlying meaning of data was also better when the results were compared with the manually segmented reference regions.

A single fuzzy rule was defined in order to classify the pixels, and three weighting factors W_1, W_2, and W_3 applied to stress the importance attached to feature based and spatial information in the image. Another important advantage of the GFRIS algorithm was that the structure of the membership functions and associated parameters were automatically derived and a new data-mining algorithm presented to determine both the key weighting factor and threshold value. The vital role of the threshold to the performance of GFRIS in controlling the maximum permitted pixel intensity variation between neighbouring and candidate pixels was highlighted.

From a computational perspective, since the three membership functions are independent of each other, the GFRIS algorithm possesses a high degree of inherent concurrency, which could be exploited by a parallel implementation, with a dedicated processor being used for each function.

Finally, as GFRIS is fuzzy rule based, the algorithm has the capability of incorporating any type of image attribute in any special application, by simply defining new membership functions, so making this solution both image and application independent.

References

Bezdek, J.C., 1981. Pattern Recognition With Fuzzy Objective Function Algorithms. Plenum, New York.

Chang, C.W., Ying, H., Hillman, G.R., Kent, T.A., Yen, J., 1998. A rule-based fuzzy segmentation system with automatic generation of membership functions for pathological brain MR images. Computers and Biomedical Research. Available from http://gopher.cs.tamu.edu/yen/publications/index.html.

Chi, Z., Yan, H., 1993. Segmentation of geographic map images using fuzzy rules. In: Conf. Proc. DICTA-93, Digital Image Computing, Techniques and Applications, Vol. 1. Australian Pattern Recognition Society, Broadway, NSW, Australia, pp. 95–101.

Chi, Z., Yan, H., Pham, T., 1996. Fuzzy Algorithms: With Applications to Image Processing and Pattern Recognition. World Scientific, Singapore.

Geman, S., Geman, D., 1984. Stochas. Prentice Hall River, NJ.

Gose, E., Johnsonbaugh, R., Jost, S., 1996. Pattern Recognition and Image Analysis. Prentice Hall River, NJ.

Hall, L.O., Namasivayam, A., 1998. Using adaptive fuzzy rules for image segmentation. FUZZ-IEEE'98. Available from http://modern.csee.usf.edu/~hall/adrules/segment.html.

Karmakar, G.C., Dooley, L., 2001. Generic fuzzy rule based technique for image segmentation. In: IEEE Internat. Conf. on Acoustics, Speech, and Signal Process., (ICASSP'2001), Salt Lake City, Utah, ISBN 0-7803-7043-0.

Karmakar, G.C., Dooley, L., Rahman, S.M., 2000. A survey of fuzzy rule based image segmentation techniques. In: 1st IEEE Pacific-Rim Conf. on Multimedia, Sydney, Australia, pp. 350–353.

Kellogg, C.B., Zhao, F., Yip, K., 1996. Spatial aggregation: language and applications. In: Proc. AAAI-96. Available from http://www.cis.ohio-state.edu/insight/pubs.html.

Krishnapuram, R., Keller, J., 1993. A possibilistic approach to clustering. IEEE Trans. Fuzzy Syst. 1, 98–110.

Park, W., Hoffman, E.A., Sonka, M., 1998. Segmentation of intrathoracic airway trees: a fuzzy logic approach. IEEE Trans. Med. Imaging 17 (4), 489–497.

Sasaki, T., Hata, Y., Ando, Y., Ishikawa, M., Ishikawa, H., 1999. Fuzzy rule based approach to segment the menisci region from MR images. In: Proc. SPIE Medical Imaging, San Diego, CA, USA, Vol. 3661, p. 258.

Tizhoosh, H.R., 1998. Fuzzy image processing. Available from http://pmt05.et.uni-magdeburg.de/~hamid/-segment.html.

Tuceryan, M., 2000. Computational geometry. Available from http://klingon.cs.iupui.edu/~tuceryan.

Wertheimer, M., 1923. Laws of organization in perceptual forms. Pshychol. Forsch. 6.

Yip, K., Zhao, F., 1996. Spatial aggregation: theory and applications. J. Artif. Intell. Res. 5, 1–26.

Zaman, S.M.H., Rahim, K., Howlader, M., 1982. Simple Lesson From Biometry. Bangladesh Rice Research Institute, Joydebpur, Dhaka, Bangladesh.

Zhang, Y.J., 1996. A survey on evaluation algorithms for image segmentation. Pattern Recognition 29 (8), 1335–1346.

Chapter XIV

Review of Fuzzy Image Segmentation Techniques

Gour C. Karmakar and Laurence Dooley
Monash University, Australia

Mahbubur Rahman Syed
Minnesota State University, Mankato, MN, USA

This chapter provides a comprehensive overview of various methods of fuzzy logic-based image segmentation techniques. Fuzzy image segmentation techniques outperform conventional techniques, as they are able to evaluate imprecise data as well as being more robust in noisy environment. Fuzzy clustering methods need to set the number of clusters prior to segmentation and are sensitive to the initialization of cluster centers. Fuzzy rule-based segmentation techniques can incorporate the domain expert knowledge and manipulate numerical as well as linguistic data. It is also capable of drawing partial inference using fuzzy IF-THEN rules. It has been also intensively applied in medical imaging. These rules are, however, application-domain specific and very difficult to acquire either manually or automatically that can complete the segmentation alone. Fuzzy geometry and thresholding-based image segmentation techniques are suitable only for bimodal images and can be applied in multimodal images, but they don't produce a good result for the images that contain a significant amount of overlapping pixels between background and foreground regions. A few techniques on image segmentation based on fuzzy integral and soft computing techniques have been published and appear to offer considerable promise.

INTRODUCTION

The usage of digital images is increasing rapidly due to quick development of Internet and multimedia technologies, so the recent research interests are being directed towards the fields of digital image processing. There are various types of digital images, as they are generated from the diverse fields of application. Most commonly used are light intensity (LI) images, range images (RI), computed tomography (CT) images, thermal images and

magnetic resonance image (MRI). Image segmentation can be defined as the process for separating the mutually exclusive homogeneous interested region(s) from other regions of an image. Image segmentation is becoming an active and promising field of research since it is the most challenging and difficult task of image processing and computer vision systems. Much research to date has been done in this field, but it is highly dependent on the type of image, its dimension and its applications. None of them is suitable for all types of images. Image segmentations are being extensively used in the various types of applications such as automatic car assembly in robotic vision, airport identification from aerial photographs, object-based image identification and retrieval, object recognition, second-generation image coding, criminal investigation, computer graphic and medical science (cancerous cell detection, segmentation of brain images and intrathoracic airway trees, etc.) (Phan and Prinle, 1999; Pal and Pal, 1993).

Image segmentation may be achieved in a large variety of ways. Generally it is divided into two approaches: region-based approach and boundary or contour-based approach (Ballard and Brown, 1982; Chakrabotry, Staib and Duncan, 1994). The first one uses the homogeneity of the pixel or features while the later one finds the contour or the boundary of the interested region. The two types of contours mainly used are: active contours (Kass, Witkin and Terzopoulos, 1988; Cohen and Cohen, 1993; Ronald, 1994; Caselles, Kimmel and Shapiro, 1995), and deformable contours (Chakrabory et al., 1994; Grzeszczuk and Levin, 1997; Grzeszczuk and Levin, 1993).

Haralic (1985) divided the image segmentation techniques into four classes: measurement space guided spatial clustering, region growing (single linkage, hybrid linkage and centroid linkage region growing approaches), spatial clustering, and split and merge. Measurement space guided spatial clustering assigns each pixel a label of a cluster of the measurement space in which it feels right. The pixels bearing the same label are treated as the connected component and in the same class. Generally clustering and histogram mode-seeking techniques are used in this approach. This method does not work well when the gray label intensity of an object in the interest of segmentation varies extensively and the background is not uniform. In region growing the image is divided into some regions. The gray level intensity variation of all the pixels of a region lies within the limit of the specified threshold. The region is grown by taking a pixel as a starting point and then adding all pixels into the region whose gray level intensity variation lies within the selected threshold (Reid, Millar and Black, 1997). This technique is expensive in terms of computation and memory (Moghaddamzadeh and Bourbakis, 1997). The single linkage region growing approach uses the graph theory to segment the image. Each vertex of the graph represents each pixel of the image. Pixels containing similar characteristics are connected by the links of the graph. This approach suffers from the problem of chaining. If the chain cuts, it loses all the pixels of the other part. Hybrid linkage region growing approach allocates a property vector to each pixel, which is a function of its kxk neighborhood values. One of the hybrid linkage approaches used information on the edges to connect the link, but this depends on the edge detection method used. In the centroid linkage region growing approach, the image is first scanned and then a region is formed by comparing the pixel value with the mean of that region. Pixels are added into the region if they are close enough and then update the mean of the region. The similar regions (if any) are merged. The effectiveness of this approach depends on the combing criteria. The spatial clustering approach forms the cluster by considering both the measurement space as well as spatial space between the parent pixels and their neighbors. Initially, split and merge approach assumes the image as one segment and then divides the image into some subdivisions (number of subdivision$=4^n$ where

n=1,2,3...) based on quadtree (Samet, 1989a; Reid et al., 1997). Adjacent regions are merged if they are sufficiently homogenous, but if the quadrants are not sufficiently homogeneous they will again be subdivided.

Pal and Pal (1993) stated that the image segmentation approaches could be generally classified into two approaches: classical and fuzzy mathematical approaches. The classical approach includes histogram thresholding, edge detection, and semantic and syntactic approaches. Fuzzy mathematical approaches are categorized as edge detection, thresholding and relaxation. They also mentioned that there are some other approaches (Hansen and Elliott; Derin and Elliott, 1987; Derin, Elliott, Cristi and Geman, 1984; Geman and Geman, 1984) that are not classified into either of the above mentioned classes. They described all image segmentation approaches in seven sections: gray level thresholding, iterative pixel classification (relaxation, MRF-based techniques and neural network-based-approaches), surface-based segmentation, segmentation of color images, edge detection and methods based on fuzzy set theory (fuzzy thresholding and fuzzy edge detection). Although they described the fuzzy segmentation approaches, they did not include the fuzzy segmentation approaches on fuzzy rule, fuzzy integral, genetic algorithm-based approaches and soft computing approaches. Genetic algorithm-based image segmentation approaches are described in Cognoni, Dobrzeniecki and Yanch (1999), Bhanu, Lee and Ming (1995) and Andrey and Tarroux (1994). Zadeh first introduced the term soft computing in the early 1990s and it includes all of the approaches that are a synergistic combination of neural networks, fuzzy logic, genetic algorithms and probabilistic computing (Yen, 1999).].

Image segmentation is one of the most complicated tasks in image processing and computer vision due to a lot of factors, some of which are summarized below (Pal and Pal, 1993; Chakrabotry et al., 1994; Haralic and Shapiro, 1985).

- The image processing system possesses some inborn constraints, so the resulting image is not perfect and will contain artifacts.
- The image data can be susceptible and ambiguous. For example, SPECT imaging often deforms the high frequency information of the image data and produces fuzzy and non-reliable edges.
- The shape of the same object can differ from image to image. The structures of the object are not well defined for most natural images and very difficult to find the accurate contour of an object.
- The gray level pixel values and their distributions of the same object are not the same for all images. Even in the same image, the pixels belonging to the same class may differ in their pixel intensities and distributions.
- The object(s) to be segmented are highly domain and application dependent.
- The properties of an object used in image segmentation differ in the way of representations, the types of the images and their domains. It also needs a trade off between the desired properties. For example, gray level distribution follows the Poisson distribution for some visual images, but this is not a valid case for MRI and RI images. So segmentation techniques need semantic and prior information on the type of image in addition to other properties.

From the above-mentioned problems, it is obvious that an image itself contains a lot of ambiguities. For example, it is not possible to define precisely the contour of an object in an image, region, the relationship between the regions, edge, surface and corner, etc. Pal and Pal (1993) mentioned that LI images contain ambiguity because of their multi-valued gray level pixel intensity. This ambiguity may be defined in two ways: grayness and spatial. Grayness ambiguity represents the whiteness or blackness of a pixel, while spatial

ambiguity deals with the shape and geometry of a region contained in an image. In classical methods, each is taken as a crisp or hard decision. Hard decision is not suitable for image processing because of its ill-defined data. It is of paramount importance that an image processing system need a recognition strategy, which can handle any type of uncertainty arising in any level of the processing steps. Prewitt (1990) recognized this when he introduced image segmentation by exploiting fuzzy regions.

In a fuzzy system each image is considered as a number of fuzzy regions, such as $R_1...R_n$ where n denotes the number of regions (Medasani, Krishnapuram and Kelleer, 1999). Each region contains a set of pixels, and each pixel is assigned a grade (a degree of membership value), which measures the possibility of a pixel belonging to a region. The membership function maps each of the feature values f(x,y) of a pixel I(x,y) of an image I in coordinate (x,y) into a range of value from 0 to 1. The membership function of pixels for image I can be defined as

$$\mu \left(f(x,y) \right) : \Omega \rightarrow [0,1] \qquad (1)$$

where Ω represents a universal set of all feature values for all pixels contained in image I.

It is evident that a fuzzy approach can handle many uncertainties well and use the membership value (varying grade) to define the imprecise or ill-defined property of an image. It was mentioned that membership value denotes the possibility of belonging to a region or more than one regions which contrasts the fuzzy approach with the classical approach (hard decision-based approach). Fuzzy approach can also interpret linguistic variables such as VERY BRIGHT, BRIGHT and BLACK, etc., very well. Medasani, Krishnapuram and Keller, J. (1999) measured geometric (area, perimeter, height and length) and non-geometric (average pixel intensity, entropy and homogeneity) properties for both real and artificial images using both fuzzy and crisp approaches. Experimental results showed that fuzzy approach give more accurate and better values in both cases than crisp approach. They also calculated those properties by adding different levels of noise for both approaches. It was shown that the fuzzy approach produced more improved estimates than the crisp approach for both properties even in the noisy image. They also showed that there was no need for noise removal during measuring of fuzzy properties, which is especially useful in overcoming some of the difficulties raised in eliminating noise especially for texture images.

Fuzzy rule-based modeling is a very interesting and promising field of research. It is widely used in various fields of industrial applications such as robotic, control engineering, medical imaging and complex nonlinear system recognition. The advantages of this approach are given below Yen, 1999; Yen and Wang, 1999).

- Potential capability to represent the knowledge explicitly using IF-THEN rule and capture the knowledge from imprecise information of linguistic as well as numerical terms.
- The ability of partial reasoning in human understandable terms. It determines the degree of similarity based on the degree of condition satisfied in the antecedent clause of the rule.
- Approximating potency of complex nonlinear system.

This chapter will examine the different methods used for fuzzy image segmentation. The types of fuzzy image segmentation approaches developed so far will be described in the next section, while a detailed description of each approach is then presented. Finally a conclusion is provided.

TYPES OF FUZZY IMAGE SEGMENTATION

Fuzzy image segmentation is increasing in popularity because of the rapid extension of fuzzy set theory, the development of various fuzzy set theory-based mathematical modeling, synergistic combination of fuzzy, genetic algorithm and neural networks, and its successful and practical application in image processing, pattern recognition and computer vision system. One may classify fuzzy image segmentation in a variety of ways, however they may be broadly classified as Tizhoosh (1998).

- Fuzzy clustering-Based Image Segmentation
- Fuzzy Rule-Based Image Segmentation
- Fuzzy Geometry-Based Image Segmentation
- Fuzzy Thresholding-Based Image Segmentation
- Fuzzy Integral-Based Image Segmentation
- Soft Computing-Based Image Segmentation

A review of the different techniques available in each category will now be provided.

FUZZY CLUSTERING-BASED IMAGE SEGMENTATION

Clustering means unsupervised grouping of data based on similarity measure (Chi, Yan and Pham, 1996). There are mainly two types of clustering: hard clustering and fuzzy clustering. In hard clustering, data is clearly classified into only one group, i.e., the groups are mutually exclusive. But in fuzzy clustering a membership value is assigned to data, which supports the group(s) into which it belongs. One data may belong to more than one group. Fuzzy clustering techniques can be classified into the following.

- Fuzzy C-Means Algorithm (FCM)
- Possibilistic C-Means Algorithm (PCM).
- Adaptive Fuzzy C-Means Algorithm (AFCM).

Fuzzy C-Means Algorithm (FCM)

FCM is the oldest and most popular fuzzy-based clustering technique. It was developed by Bezdek (1981) and is still being used in image segmentation. It performs classification based on the iterative minimization of the following objective function and constraints (Chi, Yan and Pham, 1996).

$$f_m(\mu, V, X) = \sum_{i=1}^{c} \sum_{j=1}^{n} \left(\mu_{ij}\right)^m d(x_j, v_i)^2 \tag{2}$$

$$0 \leq \mu_{ij} \leq 1 \qquad i \in \{1..c\} \text{ and } j \in \{1..n\} \tag{3}$$

$$\sum_{i=1}^{c} \mu_{ij} = 1 \quad j \in \{1..n\} \tag{4}$$

$$0 < \sum_{j=1}^{n} \mu_{ij} < n \quad i \in \{1..c\} \tag{5}$$

Where c and n are the number of cluster and data respectively, μ is a fuzzy partition matrix containing membership values [μ_{ij}]. V is a prototype vector containing the values of cluster centers [v_i], m is the fuzzifier ($1<m\leq\infty$), d is the distance between x_j, v_i and X is a data vector. The next two equations are derived after minimization of function $f_m(\mu$, V, X) in equation (2) with respect to μ and V.

$$\mu_{ij} = \frac{1}{\sum_{k=1}^{c}\left(\frac{d(x_j,v_i)}{d(x_j,v_k)}\right)^{2/(m-1)}} \quad (6)$$

$$v_i = \frac{\sum_{j=1}^{n}\left(\mu_{ij}\right)^m x_j}{\sum_{j=1}^{n}\left(\mu_{ij}\right)^m} \quad (7)$$

The set of cluster centers is initialized randomly or by an approximation method. The membership values and cluster centers are updated through an iterative process until the maximum change in μ_{ij} becomes less or equal to a specified threshold.

The number of clusters, the fuzzifier (m), and the threshold are needed to set up empirically in FCM. Equations (6) and (7) are not sufficient to achieve the local minimum of $f_m(\mu$, V, X) (Tolias and Panas, 1998). The selection of the value of m is also important, as if it is equal to 1; FCM produces crisp partition instead of fuzzy patron. If any of the values of the distances ($d(x_j, v_i)$) is zero, the equation (6) will be undefined. FCM strongly supports probability as it has set the constraint in (4), which prevents the trivial solution $\mu=0$.

Possibilistic C-Means Algorithm (PCM)

FCM arbitrarily divides the data set based on the selected number of clusters. The membership values generated by FCM represent the degrees of sharing. In order to eliminate the constraints in equation (4), Krishnapuram and Keller first introduced PCM whose membership values represent the degrees of typicality, instead of degrees of sharing, and clusters are independent of each other (Krishnapuram and Kelleer, 1993; 1994. They modified the FCM objective function and defined the PCM objective function as:

$$f_m\left(\mu,V,X\right) = \sum_{i=1}^{c}\sum_{j=1}^{n}\left(\mu_{ij}\right)^m d^2\left(x_j,v_i\right) + \sum_{i=1}^{c} \eta_i \sum_{j=1}^{n}\left(1-\mu_{ij}\right)^m \quad (8)$$

and the constraints are:

$$0\leq M_{ij}\leq 1 \quad i\in\{1..c\} \text{ and } j\in\{1..n\} \quad (9)$$

$$0 < \sum_{j=1}^{n}\mu_{ij} < n \quad i\in\{1..c\} \quad (10)$$

$$\max \mu_{ij} > 0 \quad j\in\{1..n\} \quad (11)$$

where η_i is the scale parameter, which determines the zone of influence of a point, and other parameters are as defined previously. The following are obtained after minimizing the function $f_m(\mu, V, X)$.

$$\mu_{ij} = \frac{1}{1 + \left(\frac{d^2\left(x_j, v_i\right)}{\eta_i}\right)^{\frac{1}{(m-1)}}} \qquad (12)$$

$$v_i = \frac{\sum_{j=1}^{n}\left(\mu_{ij}\right)^m x_j}{\sum_{j=1}^{n}\left(\mu_{ij}\right)^m} \qquad (13)$$

The membership value (μ_{ij}) and prototype center (v_i) are updated using the equations (12) and (13) through an iterative process. When fuzzifier m=1, PCM produces crisp partition. PCM gives promising results in the presence of noise but it is highly dependent on initialization and estimation of the scale parameters. The output of FCM can be used for initialization and scale estimation, but FCM is very sensitive to noise. Barni also mentioned that PCM achieves local minimum but it can't minimize $f_m(\mu, V, X)$ globally (Barni, Cappellini and Mecocci, 1996).

Adaptive Fuzzy C-Means Algorithm (AFCM)

Image data are intrinsically correlated. It is essential for segmentation techniques to adapt themselves to local features of an image, which is the important disadvantage of both FCM and PCM. In FCM and PCM, the prototype vectors don't vary spatially and inter-pixel correlation and intensity inhomogeneities are not considered. The adaptive fuzzy C-means algorithm in which prototype vectors are varied along the image have been described in Pham and Prince (1993) and Tolias and Panas (1998). Inter-pixel correlation and intensity inhomogeneities are taken into account in Pham and Prince (1993) and Tolias and Panas (1998) respectively.

Both algorithms degenerate into crisp clustering as m tends to one. The selection of as optimum number of cluster automatically remains unsolved, which is the crucial problem of clustering algorithms. Some of the parameters especially for Pham and Prince (1993) are selected empirically.

FUZZY RULE-BASED IMAGE SEGMENTATION

This is a promising field of research. Initially fuzzy IF-THEN rules were extensivel used in control engineering problems but now the application of fuzzy IF-THEN rules i image segmentation is increasing. Their advantages in image segmentation are mainly i the following (Chang et al., 1998).
- Human can easily understand the problems due to linguistic representation ' numeric variables.

- It is computationally less expensive than fuzzy clustering methods.
- It has the potential ability to integrate the domain expert knowledge.

The general format of fuzzy IF-THEN rule can be defined as follows.

IF antecedent-condition THEN consequence

The consequence is measured based on the quantity satisfied in the antecedent condition. Generally fuzzy rule-based image segmentation has been applied to three image types: LI, MR and CT images. These are described in the following subsections.

Fuzzy Rule-Based LI Image Segmentation

Chi and Yan utilized the fuzzy IF-THEN rules in the segmentation (separation of background and foreground pixels) of 8 bits (256 gray scales) geographic map images containing strings, streets, roads, boundaries, etc., that are considered foreground pixels of the images (Chi, Yan and Pham, 1996; Chi and Yan, 1993). The main processing steps of this approach are described in the following.

Features used in segmentation

Three features, difference between pixel intensity (DI), local standard deviation (SD) and local contrast of darker pixel (CD), are used in segmentation and they are defined as:

$$DI(x,y) = PI(x,y) - LA(x,y) \tag{14}$$

$$SD(x,y) = \sqrt{\frac{\sum_{i=x-3}^{x+3} \sum_{j=y-3}^{y+3} (PI(i,j) - LA(i,j))^2}{49}} \tag{15}$$

$$CD(x,y) = \frac{\max(0, RB(x,y))\operatorname{sgn}(CI(x,y))}{LA(x,y)} \tag{16}$$

Where PI(x,y) is pixel intensity in the location (x,y), LA(x,y) local average pixel intensity in 7x7 window, sgn (CI(x,y)) is sign operator and it is -1 when CI(x,y) $\leq$0 otherwise it is 1. CI(x,y) is the difference of pixel intensity in location (x,y) and the average of its neighbours and can be defined as:

$$CI(x,y) = \frac{1}{8}[PI(x-3,y) + PI(x-2,y) + PI(x+2,y) + PI(x+3,y) + PI(x,y-3) + PI(x,y-2) + PI(x,y+2)$$
$$+ PI(x,y+3)] - PI(x,y) \tag{17}$$

BR(x,y) is the average of relative brighter pixels and is defined as:

$$BR(x,y) = \frac{1}{N} \sum_{\substack{x-4 \leq i \leq x+4 \\ y-4 \leq j \leq y+4 \\ CI(i,j) \leq 0}} PI(i,j) \tag{18}$$

where N indicates the number of brighter pixels contained in 9x9 window.

Membership functions

The input and output domains are divided into five fuzzy regions named as L2, L1, M, H1 and H2 and two fuzzy regions such as background and foreground respectively. Triangular membership functions are utilized for input regions. The input and output membership functions are shown in Figures 1(a) and 1(b) respectively.

Figure 1: Input and output membership functions

(a): Input membership functions

(b): Output membership functions

Development of fuzzy rules

Fuzzy rules are developed by learning from examples as outlined by Wang (Wang and Mendel, 1991). The input and output domains are divided into fuzzy regions that are shown in Figure 1. The membership values of all regions for each input are calculated and each input is assigned to the region of the maximum membership values. So a pair of rules is generated for each training sample. An example of such rule would be

> IF DI is L1 AND SD is H1 AND CD is H2 THEN it is a foreground pixel
> IF DI is H1 AND SD is M AND CD is L1 THEN it is a background pixel

A learning set produced by this method may contain a larger number of rules including repeated and conflict rules. To avoid these the rules are selected that are supported by a large number of examples. Each rule is kept in a fuzzy rule bank and is shown in Figure 2.

Defuzzification

The centroid defuzzication method used to calculate the output for each input pixel is defined as:

$$C_P = \frac{\sum_{i=1}^{n} M_p^i C_i}{\sum_{i=1}^{n} M_p^i} \tag{19}$$

Figure 2: Fuzzy Rule Bank for Geographic Map Image Segmentation.

where C_i is the class produced by the ith rule. n is the number of rules and M_p^i is the matching degree of the antecedent of ith rule for pth pattern. If $C_p \leq 0.5$, the input pixel is categorized as background pixel, otherwise it is categorized as foreground pixel.

Concluding remarks

This system is faster than neural network techniques. It was found that some parts of characters of the maps are missed for standard triangular function (Chi, Yan, and Phan, 1996). This is because the selecting of the shape and parameters of the membership functions was done intuitively. For this they used an automatic method using fuzzy C-means clustering (extension factor = 3.0 and merging threshold=0.08) to determine the parameters of the membership functions. But there still exists the problem of manual determination of the shape of the membership function. Heuristic rules are not used in this method.

Fuzzy Rule-Based MR Image Segmentation

Magnetic resonance images are the most important and complicated images used in medical imaging. Magnetic resonance images are extensively used in the various types of disease diagnostic tasks. Medical experts generally draw the conclusion in regard to the disease by manually scanning the images (Chang, Ying, Hillman, Kent, and Yeu, 1998), which is both a tedious and time-consuming task. Analysis, especially segmentation of MR images using automated computer techniques, saves the time and helps the doctor to detect irregularity in diagnosis. The fuzzy rule-based MRI image segmentation methods may be broadly classified into two classes: hybrid fuzzy rule-based MRI segmentation and conventional fuzzy rule-based MRI segmentation. Both of the methods are described in the following sections.

Hybrid fuzzy rule-based MRI segmentation

Hybrid fuzzy rule-based segmentation system consists of fuzzy rule-based and fuzzy C-means clustering algorithm. Clustering is computational expensive, does not incorporate human expert knowledge and thus does not produce appropriate class (Hall and Namasivayam, 1998). For these reasons, a set of fuzzy rules is applied to classify the pixels/voxels. It is very difficult to define fuzzy rules that cover all pixels/voxels. So fuzzy C-means algorithm is used to classify the remaining pixels/voxels, and the pixels/voxels classified by the fuzzy rules are used to initialize the centers of the clusters during clustering. Hybrid fuzzy rule-based image segmentation systems are faster than clustering and are described in Chang et al. (1998) and Hall and Namasivayam (1998).

The techniques (Hall and Namasivayam, 1998) utilizing adapting fuzzy rules for segmenting the brain tissue into six classes—white matter (WM), gray matter (GM), cerebrospinal fluid (CSF), pathology, skull tissues and background—are described in the following.

Database and features

105 axial brain slices, 5 mm thick from 15 persons (39 normal slices from 8 persons and 66 abnormal slices from 7 patients) are used for experimental purposes. Relative pixel intensities of T1, T2 and PD weighted images are used as features.

292 Karmakar, Dooley, Syed

Figure 3: Membership functions (Source ref: Hall & Namasivayam, 1998)
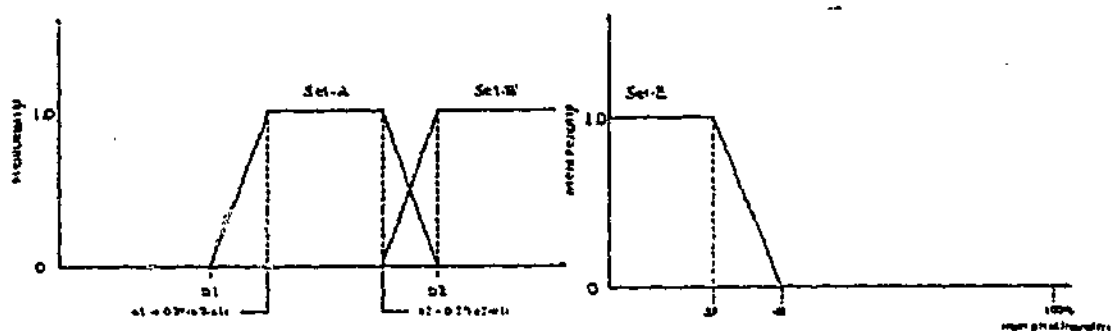
(a): Membership Functions for T1 weighted Image
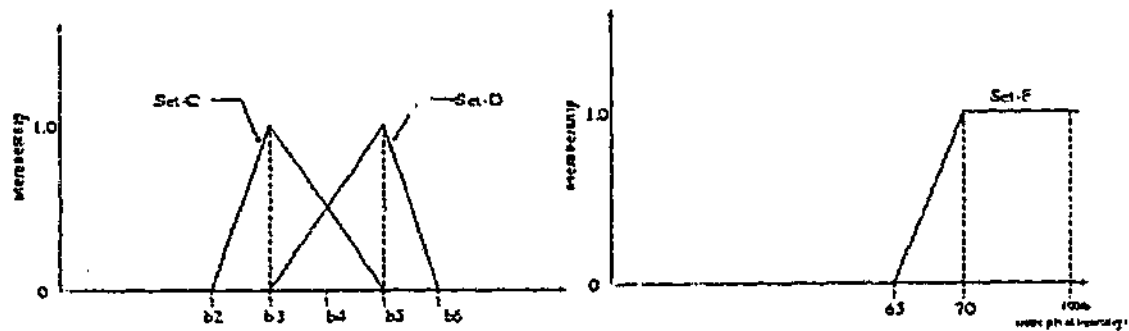
(b): Membership Function for T1 weighted Image (c): Membership Function for T2 weighted Image

Figure 4: Histograms with Turning Points (Source ref: Hall & Namasivayam, 1998)
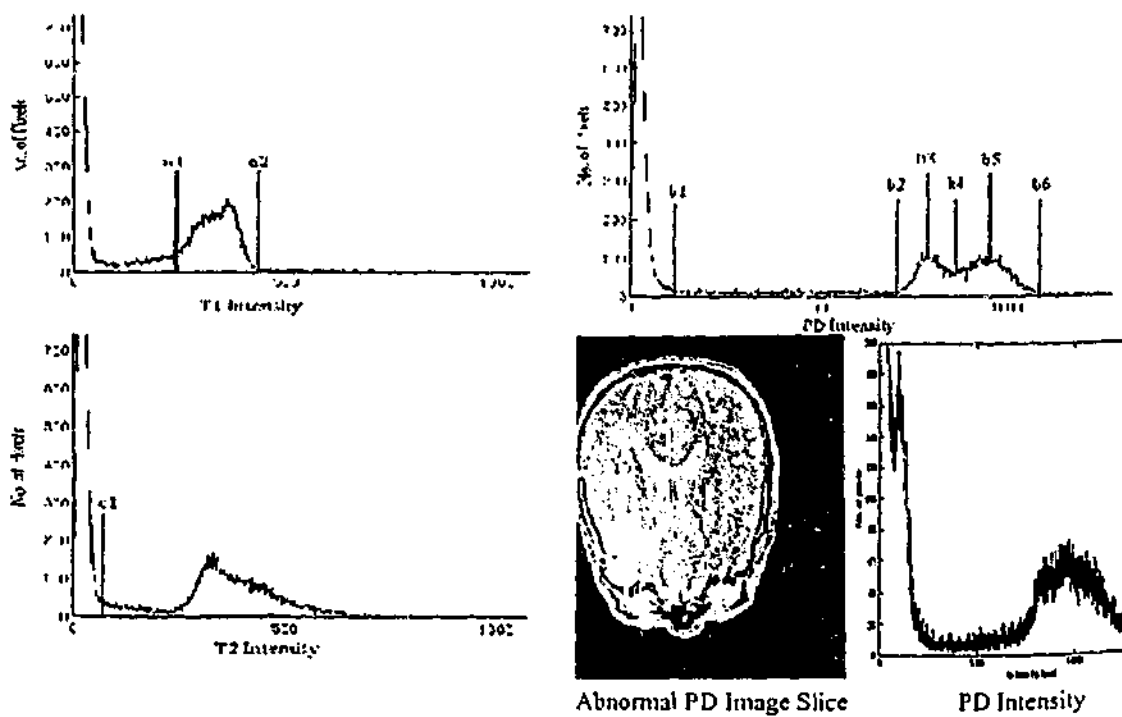
Abnormal PD Image Slice   PD Intensity

Membership Functions

Triangular and trapezoidal membership functions used in the experiment are shown in Figure 3.

The parameters of the membership functions (a1, a2, b1, b2, b3, b4, b5 and b6) are calculated by determining the turning points of intensity histograms based on a training set consisting of 6 normal and 4 abnormal slices and suggestions from expert radiologists. The turning points are regarded as peaks, valleys or the starting point of the histogram and indicate the estimated boundary of the tissue types. The turning points of the histograms are shown in Figure 4.

Patients having brain tumors usually get treatment with radiation and chemotherapy. For this the PD histogram of the patient with brain tumor becomes like the PD histogram for abnormal slice shown in Figure 4 due to the change of properties of gray and white matter. The turning points of this histogram are obscure and difficult to select. An edge detection technique (Weszka and Rosenfeld, 1979) was used in order to sharpen the boundary between gray and white matter and utilized a suitable threshold to detect the peaks. The initial value of threshold is chosen as 5 and increase by 5 until two peaks are found. If peaks are not found, two peaks are assumed at 1/3 and 2/3 of the region between b1 and b2.

Rules generation

The turning points of three histograms (T1,T2 and PD histograms) are used to separate the tissue into white matter, gray matter, cerebrospinal fluid (csf), pathology, background (air) and other skull tissues. The heuristics used here to generate the rules are 'all voxels between b2 and b4 are usually white matter, below b1 are air in PD histogram, and between a1 and a2 are the mixture of white and gray matter in T1 weighted histogram'. A set of rules used to classify the brain tissue is described as follows:

IF voxel in T1 in Set-E AND voxel in T2 in Set-F THEN voxel is CSF
IF voxel in PD is Set-C AND voxel in T1 in Set-A THEN voxel is White matter
IF voxel in PD is Set-D AND voxel in T1 in Set-A AND NOT (voxel in T2 is Set-F AND voxel in T1 is Set-E) THEN voxel is Gray matter
IF voxel in T1 is Set-B AND voxel in T2 is Set-F THEN voxel is Pathology
IF voxel in T1 is Set-B AND NOT (voxel in T2 is Set-F) THEN voxel is Other
IF PD voxel intensity < b1 AND T2 voxel intensity < c1 THEN voxel is Background

Rules are adapted themselves to each slice during processing as they are generated from the turning points of the histograms.

Classification techniques

Voxels are classified into six classes by applying the above rules. The unclassified voxels and isolated voxels (voxels whose membership values are 1 but no neighborhoods) for each class are assigned the membership values with the average membership values of their neighborhoods and zero respectively. Finally the voxel membership values are normalized (0 to 1) using the following equation:

$$\mu_i = \frac{\mu_i(v)}{\sum_j \mu_j(v)} \tag{20}$$

where i and j represent each of the six classes and v is a voxel. The incorrect classified voxels (voxels whose membership values is less than and equal to 0.80) are classified using semi-supervised clustering algorithm (Bensaid et al., 1996). The correctly classified voxels are used as training set and weighted by 100.

Concluding remarks

This system is faster than FCM and the parameters of the membership functions are adjusted automatically during the processing of each slice, but it does not produce better results than FCM. Rules are generated based on turning points of the histogram, but the turning points are sufficient to distinguish the voxels if there is a significant amount of overlapping voxels. The spatial information is not well considered as it is taken into account for only unclassified voxels. The threshold and approximate peaks (when there are no peaks in PD histogram) are chosen empirically, and extra cranial tissues are not removed before classification.

Another hybrid fuzzy rule-based brain MR image segmentation technique (Chang et al., 1998) used to separate WM, GM, CSF and CMV lesion from the brain is as follows.

Database

A set of T1, T2 and PD weighted images containing 12 normal images and 3 abnormal images with lesions are used for experimental purposes. GE Signa 1.5T MRI and a Technicare 0.6T instruments are used to access these images.

Preprocessing

Preprocessing stage comprises image registration and selection of region of interest (ROI). Image registration makes the same pixels' coordinates for the same pixels contained in two different images by the method of shifting of coordinates. For example, if the two images T2 and PD are not matched, the coordinates of PD image are shifted to match with T2 image. The shifted coordinates of PD image are recorded, and T2 and shifted PD images are regarded as registered image.

Intracranial region of the brain is selected as ROI. It is needed to separate the intracranial region from the skull and scalp. The intracranial region is anatomically

Figure 5: Membership Function for T2 Weighted Images
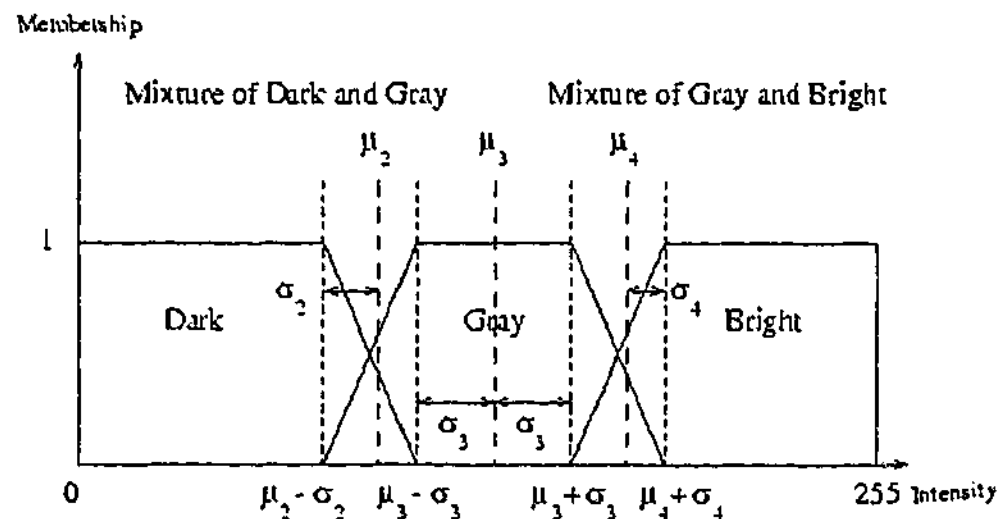
separated from the scalp and skull by a layer of CSF, except there are a few connections where the layer of CSF is thin. To separate the intracranial region, the image is first thresholded and then a region growing technique is applied to grow empty space surrounding the intracranial region. The problems for the connections between brain and scalp are solved by applying the morphological operators erosion and dilation (Kapur, 1995).

Determination of parameters of the membership functions

The membership functions are identified perceptually. Three different types of tissue such as WM, GM and CSF were identified for T2 images. T2 image as well as its edges that are determined by Cohen's edge detection method described in Gonzalez and Woods (1992) are classified into five classes WM, GM, CSF, WM-GM and GM-CSF using standard FCM algorithm. The mean intensities (M_i) and variance (O_i) of ith class are used to calculate the parameters of the membership function for ith class. The membership functions for T2 images are shown in Figure 5.

The PD weighted image and its edge values are given to FCM, which classifies them into four classes. The class containing highest pixel intensity is discarded in order to eliminate the high edge values on the boundary of the brain. The techniques used to generate the membership function for PD weighted images are the same as T2 weighted images. The membership function for PD weighted images is shown in Figure 6.

PD weighted abnormal images contain periventricular hyperintensity which have higher pixel intensities in brighter class than other pixels in the same class. So the membership function for PD weighted abnormal image is presented in Figure 7.

A membership function to represent the closeness of a pixel from the center of the brain as the ventricle is considered a major connected CSF area adjacent to the center of the brain. This membership function is used to discover the periventricular hyperintensity which represents the lesions of the PD weighted images. The membership function to measure the closeness to the ventricle is given in Figure 8.

Development of fuzzy rule-based segmentation

Two groups of fuzzy rules have been developed. The first and the second group are used to segment the T2 weighted images and to recognize the CMV lesions.

Figure 6: Membership function for PD weighted images
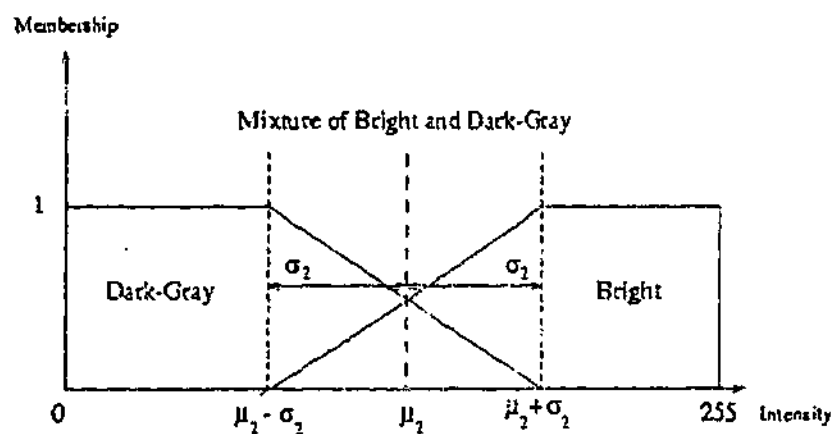
Figure 7: Membership function for PD weighted abnormal images

First Group:
IF pixel in T2 is Dark THEN pixel is White Matter
IF pixel in T2 is Grey THEN pixel is Grey Matter
IF pixel in T2 is Bright THEN pixel is CSF

The second group is formulated by splitting the last rule of the first group into three new rules that discriminate CSF and CMV lesions.

Second Group:
IF pixel in T2 is Dark THEN pixel is White Matter
IF pixel in T2 is Grey THEN pixel is Grey Matter
IF pixel in T2 is Bright AND pixel in PD is Dark-Grey THEN pixel is CSF
IF pixel in T2 is Bright AND pixel in PD is Very Bright AND pixel is not close to the ventricle THEN pixel is CSF
IF pixel in T2 is Bright AND pixel in PD is Very Bright AND pixel is close to the ventricle THEN pixel is CMV lesion

Figure 8: Membership function to represent the closeness to ventricle
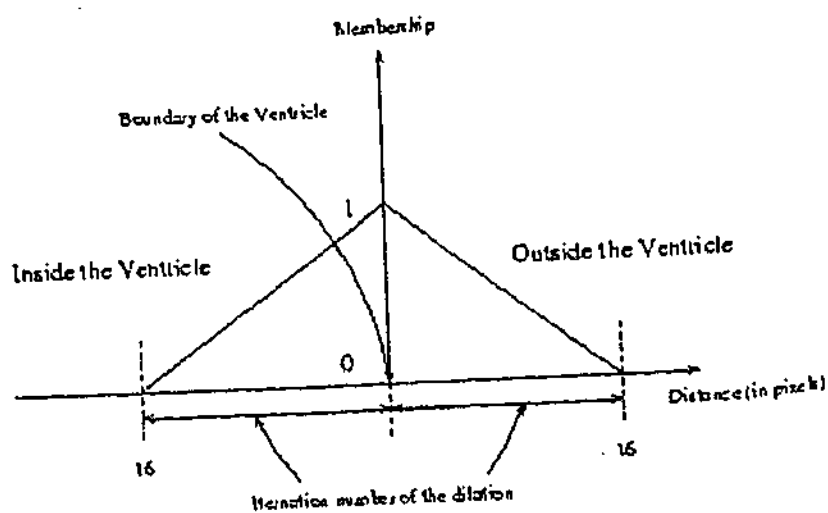
AND operator is evaluated by applying the fuzzy logic minimum operator (Zadeh, 1965). All pixels are classified using the rules described above. The pixels whose membership values are less than 0.5 and the pixel having two maximum membership values are declared as unclassified pixels.

Modified FCM segmentation

The initial value of each cluster center is derived from the average value of each respective classified class. All unclassified pixels are classified using FCM with the derived initial cluster centers. If the number of classified pixels in CMV lesion is very small (from 10 to 20), they are reclassified as CSF.

Concluding remarks

This system is 10 to 20 times faster than FCM, and produces better results for abnormal images containing lesions but it has not given promising result compared to FCM for normal images. The parameters of the membership functions have been derived automatically, but the structure of the membership functions have been defined according to the knowledge of medical experts. Although anatomical position of the lesion has been taken into account, the inter-pixel correlation has not been considered. Some other criteria may be included in addition to gradient and pixel intensity in order to define the membership functions' parameters.

Conventional fuzzy rule-based MRI segmentation

Conventional fuzzy rule-based segmentation uses only fuzzy rules to segment the MR image and does not apply FCM in addition to the fuzzy rules. Sasaki et. al. introduced such a fuzzy rule-based method to segment the menisci region from MR images (Sasaki et al., 1999).

Figure 9: Anatomical location of menisci region (Source ref: Sasaki et al., 1999)
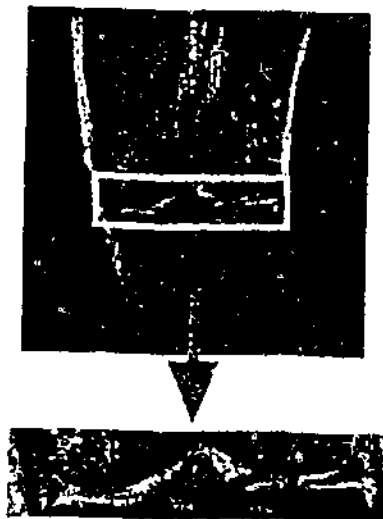
(a) MRI and enlarged Image   *(b) Anatomical location of knee*
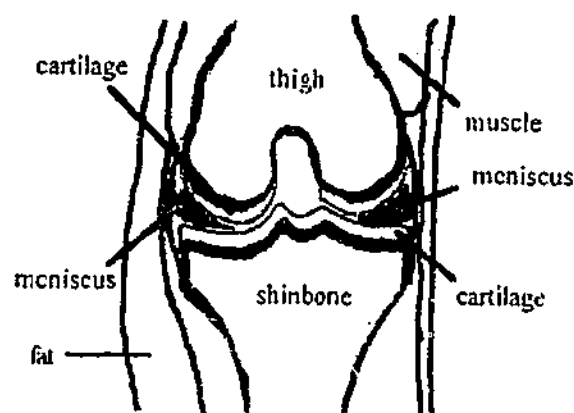
Database

Five normal MR data sets consisting of three normal and two injured knees are used in the experiments. T1 weighted 3D SPGR with TR=100 msec, TE=15 msec and flip angle=30 degrees image are acquired with Genesis Sigma 1.5 Tesla MRI scanner. Each image contains 60 separate 1.5 mm thick slices.

Knowledge used to segment the menisci region

The anatomical position of the menisci region is shown in Figure 9. Knowledge is used to generate the fuzzy rules.

1. Voxel intensities of cartilage regions are high.
2. The menisci region lies in between the thigh and shinbone.
3. The cartilage regions are adjacent to the center of the gravity of the knees.
4. The menisci are automatically located near the cartilage.
5. The voxel intensities of the menisci regions are coherent.

Fuzzy rules generation and segmentation

Two different sets of fuzzy rules are developed as the segmentation is performed in two stages. Firstly the candidate region of the menisci are segmented whereas the menisci are extracted from the candidate region in the second stage. Candidate region can be defined as the region between the cartilages as menisci are located between the cartilages. A set of voxels represented by straight contiguous two-dimensional data (x,z) is called unit (x,z). Two types of units, A and B, are defined to segment the candidate region. Unit A contains the candidate region while unit B does not contain any candidate region voxels. Figure 10 shows the model of candidate region and representation of the smallest unit.

D and d denote the constant distance of the most distance unit and distance of the interested unit from the center. Units A and B are shown if Figure11.

Figure 10: A model of candidate region and representation of the smallest unit (Source
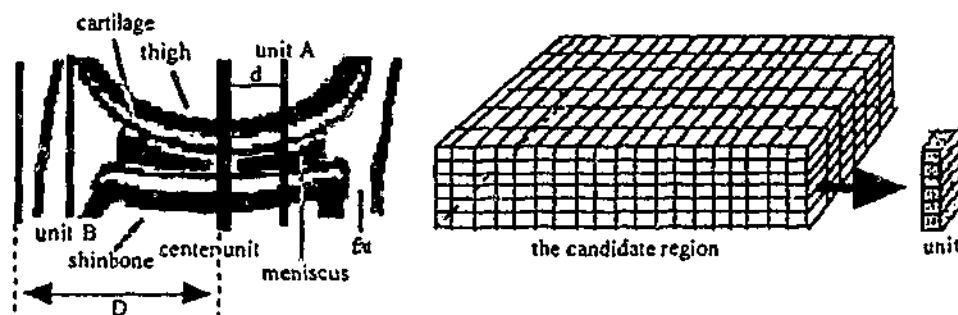
Figure 11: Unit A and unit B (Source ref: Sasaki et al., 1999)
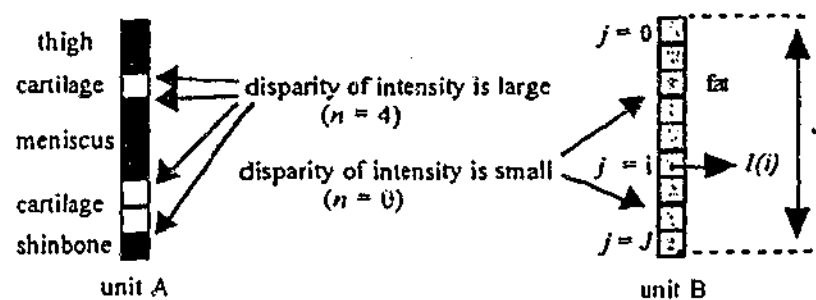
The number of disparities between two adjacent voxel intensities on a unit is defined as

$$n = \sum_{j=0}^{J-1} C(j) \tag{21}$$

where C(j) is calculated as

$$C(j) = \begin{cases} 1 & for \; |v(j)-v(j+1)| > T \\ 0 & otherwise \end{cases} \tag{22}$$

and J is the range of candidate region, v(j) is the voxel intensity at coordinate j and T is the threshold.

The membership functions of distance and disparity to measure the values of linguistic variables, small and large, are shown in Figure 12.

From the knowledge, 1, 2 and 3, the following rules are defined using the membership functions described above in order to segment the candidate region:

IF d is small AND n is large THEN degree of belonging to unit A is large
IF d is large AND n is small THEN degree of belonging to unit B is large

The degree of belonging to unit A and B are calculated using the following equations:

$$gradeA = w1 \; udsmall(d) + w2 \; unl \arg e(n) \tag{23}$$

$$gradeB = w1 \; udl \arg e(d) + w2 \; unsmall(n) \tag{24}$$

where w1 and w2 are weights. The unit is classified into unit A if gradeA > gradeB, otherwise unit is classified into unit B.

Figure 12: Membership functions for distance and disparity of intensity (Source ref:Sasaki et al.. 1999)

Figure 13: Membership functions for segmenting menisci from cartilage region (Source ref: Sasaki et al., 1999)

(a) Distance from cartilage for   (b) Membership functions   (c) Membership functions
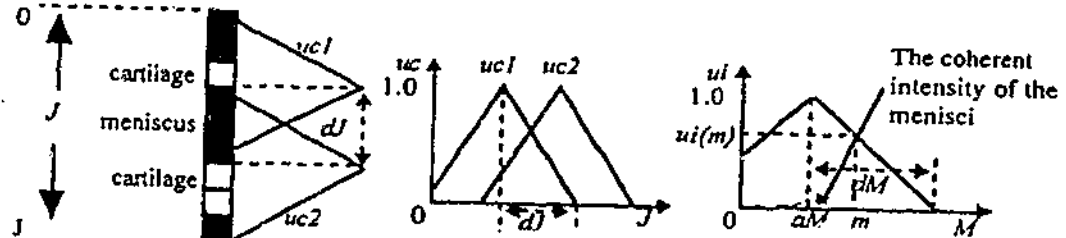
From knowledge 4 and 5, two membership functions uc and ui shown in Figure 13 are derived for segmenting the menisci from the candidate region. Figure 13(a) shows that the menisci exist near the cartilage. uc and ui map the distance of a voxel from the cartilage region and the voxel intensity into degree of belonginess to menisci respectively. The parameters dj and dM used in the membership functions, shown in Figure 13(b) and 13(c) respectively, are widths of the one side of the triangles, whereas aM is the coherent intensity.

The calculation of uc for two cartilages is defined:

$$uc(j) = \begin{cases} uc1(j) + uc2(j) & for \ uc1(j) + uc2(j) < 1 \\ 1 & otherwise \end{cases} \quad (25)$$

For one cartilage:

$$uc(j) = uc1(j) \quad (26)$$

The following two rules are developed from knowledge 4 and 5.

IF a voxel is anatomically adjacent to the cartilage THEN the degree of menisci voxel for uc is high

IF the intensity of the voxel is same as coherent intensity of the menisci voxel THEN the degree for ui is high

The total degree, $gradeM = w3uc(j) + w4ui(m)$ (27)

where w3 and w4 are the weights. If gradeM > Th then the voxel is classified as a menisci voxel. Where Th is a threshold.

Concluding remarks

3D construction and display of menisci has been performed for both normal and injured knees. This method can successfully identify cartilage tears. The rules have been defined based on anatomical position and coherent intensity of the menisci voxels. The structure of the membership function is predefined. The parameters used in the membership functions are taken from the MR device parameters.

Fuzzy Rule-Based CT Image Segmentation

CT imaging is also known as Computed Axial Tomography (CAT) scanning (CT 2000). CT is one of the most important medical imaging techniques and is used in various types of disease and wound diagnosis. A fuzzy rule-based segmentation of intrathoracic airway trees on CT image has been described in Park and Hoffman (1998).

Database

Five canine data sets are scanned using EBCT scanner from five anesthetized dogs. Each data set contains 40 slices of 3mm thick. 40 slices, 8 per data set are randomly selected and their airways are perceptually determined by an expert in order to determine both the training and test sets.

Steps of airway tree segmentation

Segmentation technique consists of the following five steps.
- Separation of lungs from the volumetric data set

- Definition of primary airway tree
- Preprocessing of all individual image slices
- Fuzzy rule-based identification of airways in all image slices
- Construction of airway tree using 3-D connectivity.

The techniques used for steps 1, 2, and 3 are described in Park and Hoffman (1998) and Sonka, Park and Hoffman (1996). Primary airway tree contains the major branches of the tree and is defined as the 3-D connected components of the image voxels below a threshold, which is formed by 3-D seeded region growing approach. The main task of the preprocessing step is to identify the background and all possible locations of airways and vessels for each slice. The regions having from 55 to 110 gray level intensities are considered background. The regions darker and brighter than background are treated as candidate airways and vessels respectively.

Fuzzy rule-based identification of airways in all image slices

The following anatomical information is used to determine the airways.

1. Airways are generally dark
2. Airways are encompassed by airways wall
3. Airways are near to airway vessels

The anatomical position of airways and their vessels are shown in Figure 14.

The following three features are defined according to a region adjacency graph properties (Sonka, Hlavac and Boyle, 1993).

- BRIGHTNESS: Uses minimum and maximum grey level regions to represent the airways and vessels candidate regions respectively.
- ADJACENCY: Represents the grey level of the brightest adjacent region.
- DEGREE OF WALL EXISTENCE: It determines the existence of the wall. The degree of wall existence is determined by the ratio of the total number of concentric rays possessed dark-bright-dark profile and the total number of concentric rays directed from the center of the candidate region.

Figure 14: Anatomical position of airways (Source ref: Park and Hoffman, 1998)

(a) Airways detection principles (b) Assessment of wall evidence
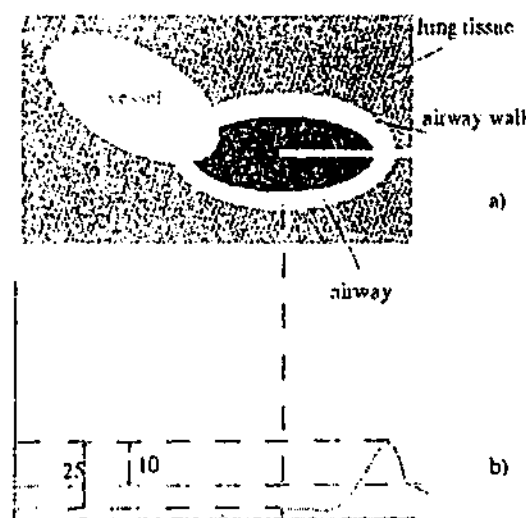
Figure 15: Membership Functions for BRIGHTNESS, ADJACENCY and DEGREE_WALL_EXISTENCE
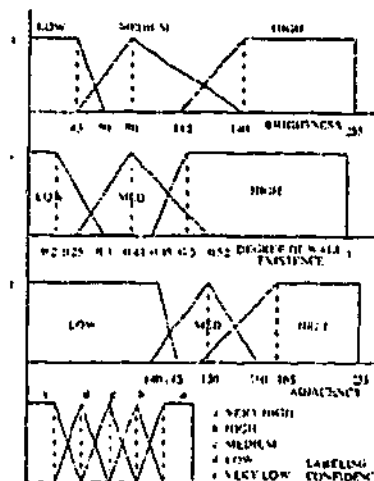
The membership functions for BRIGHTNESS, ADJACENCY and DEGREE_OF_WALL _EXISTENCE, including their linguistic variables, are shown in Figure 15.

The parameters of the membership function are determined from a manually tracking training set containing eight randomly selected slices of a single volumetric data set. The conflicts arising among membership functions are solved manually in order to obtain optimum classification results.

The rule banks developed for the segmentation are represented in the tabular form and shown in Figure 16.

The value of each cell indicates the confidence level of airway. For example of a rule,
IF BRIGHTNESS is LOW AND ADJACENCY is LOW AND DEGREE_OF_WALL_EXISTENCE is HIGH THEN region is airway with MEDIUM confidence

Finally a defuzzification method, namely, centroid defuzzification is applied in order to get numerical confidence level for each region, which indicates the possibility that the region belongs to airway.

Figure 16: Fuzzy Rule Banks to Determine the Confidence Level of Airway

BRIGHTNESS	DEGREE_OF_WALL_EXISTENCE		
	LOW	MED	HIGH
LOW	MED	HIGH	VERY HIGH
MED	LOW	MED	HIGH
HIGH	VERY LOW	LOW	MED

ADJACENCY=HIGH

BRIGHTNESS	DEGREE_OF_WALL_EXISTENCE		
	LOW	MED	HIGH
LOW	LOW	MED	HIGH
MED	VERY LOW	LOW	MED
HIGH	VERY LOW	VERY LOW	LOW

ADJACENCY=MED

BRIGHTNESS	DEGREE_OF_WALL_EXISTENCE		
	LOW	MED	HIGH
LOW	VERY LOW	LOW	MED
MED	VERY LOW	VERY LOW	LOW
HIGH	VERY LOW	VERY LOW	VERY LOW

ADJACENCY=LOW

Construction of airway tree using 3D connectivity

Airway tree named C-tree is constructed by stacking all the regions whose airway confidence level is more than 73% utilizing shape-based interpolation along z-axis. From C-tree, A tree and B-tree are created. A-tree is defined as a 3D connected region and subset of C-tree, which contains the airway-tree root. B-tree is the combination of A-tree and disconnected airway tree branches of C-tree that contains above threshold volume.

Concluding remarks

This method has constructed three trees named A-tree, B-tree and C-tree. The medical specialist may use any of the trees according to his need. The parameters of the membership function have not been derived fully automatically.

FUZZY GEOMETRY-BASED IMAGE SEGMENTATION

Geometrical properties such as perimeter, area, length, width, extrinsic diameter, intrinsic diameter, index of area coverage (IOAC) and compactness of an object can be used to describe an object (Rosenfeld, 1984; 1992; Dubois and Jaulent, 1987; Pal and Gosh, 1990). Such geometrical properties of an object can be derived using fuzzy membership values without segmenting the object from the image, and they are dependent on fuzzy membership function (μ). Segmentation is achieved through the utilization of minimum values of compactness or IOAC (Pal and Gosh, 1990; 1992; Pal and Rosenfeld, 1988). Geometrical properties of an object in an image are determined using fuzzy membership in the following ways (Rosenfeld, 1984; Pal and Gosh, 1990).

Area

The equation to calculate the area of fuzzy subset μ is expressed as:

$$a(\mu) = \int \mu \tag{28}$$

where integration covers the region whose outside $\mu=0$. The equation of area for piecewise or digital image is defined as:

$$a(\mu) = \sum_{x=1}^{w} \sum_{y=1}^{h} \mu(x,y) \tag{29}$$

where w and h are the width and height of the image respectively.

Perimeter

The equation of perimeter for piecewise constant function μ is expressed as:

$$p(\mu) = \sum_{i,j,k} |\mu(i) - \mu(j)| |A(i,j,k)| \tag{30}$$

where A(i,j,k) is the kth common arc length between m(i) and m(j) meet. The common arc length between neighboring pixels of digital image is one. So the equation (30) for digital image is defined as:

$$p(\mu) = \sum_{i,j} |\mu(i) - \mu(j)| \tag{31}$$

304 Karmakar, Dooley, Syed

Height

The height of μ is defined as:

$$h(\mu) = \int \max_x [\mu(x,y)] \, dy \qquad (32)$$

For digital image,

$$h(\mu) = \sum_y \max_x [\mu(x,y)] \qquad (33)$$

Width

The width of μ is defined as:

$$w(\mu) = \int \max_y [\mu(x,y)] \, dx \qquad (34)$$

For digital image,

$$w(\mu) = \sum_x \max_y [\mu(x,y)] \qquad (35)$$

Length

The length of fuzzy subset μ is defined as:

$$l(\mu) = \max_x \left[\int \mu(x,y) \, dy \right] \qquad (36)$$

For digital image,

$$l(\mu) = \max_x \left[\sum_y \mu(x,y) \right] \qquad (37)$$

Breadth

The breadth of fuzzy subset μ is defined as:

$$b(\mu) = \max_y \left[\int \mu(x,y) \, dx \right] \qquad (38)$$

For digital image,

$$b(\mu) = \max_y \left[\sum_x \mu(x,y) \right] \qquad (39)$$

Compactness

The compactness of fuzzy subset μ means the portion of maximum area covered by the object and is defined as:

$$c(\mu) = \frac{a(\mu)}{p(\mu)^2} \qquad (40)$$

where $a(\mu)$ and $p(\mu)$ denote the area and perimeter of fuzzy subset μ respectively.

Index of Area Coverage (IOAC)

The IOAC of fuzzy subset μ is defined as:

$$IOAC(\mu) = \frac{a(\mu)}{l(\mu) \times b(\mu)} \tag{41}$$

where $a(\mu)$, $l(\mu)$ and $b(\mu)$ are area, length and breath of μ respectively.

Techniques of Segmentation Using IOAC

The techniques used in segmentation are described in detail in Pal and Gosh (1990). The input pixels are fuzzified using standard S or Z (1-S) type membership function for bright or dark object pixels respectively and then the crossover point is calculated. In the crossover point, the value of the membership function is 0.5 and it is below or above 0.5 in below or above of the crossover point. The IOAC is calculated using equation (41). IOAC and compactness measures decrease for increasing μ and are lowest for a crisp one. The crossover point is adjusted in order to get the minimum value of IOAC. The μ plane obtained for minimum value of IOAC is used for segmentation. For image containing multiple objects, multiple optimum μ planes can be used.

Concluding remarks

The optimum value of IOAC has been calculated considering the predefined membership function, namely, standard S type membership function. The IOAC has been calculated using area, length and breadth of an object. It is very difficult to calculate the accurate area, length and breadth of an object with wide range of gray level pixel variations and the result of segmentation will not be good if there exists a significant amount of overlapping pixels. It is computationally expensive, as it needs to calculate the value of the membership function for each pixel everytime the crossover point is adjusted.

FUZZY THRESHOLDING-BASED IMAGE SEGMENTATION

Thresholding-based image segmentation is one of the oldest and most well-known techniques. Its main function is background and foreground separation. It is very difficult to produce appropriate threshold since the real image is itself ambiguous and there is overlap between background and foreground pixels. Fuzzy thresholding-based image segmentation is potential as it can handle imprecise data (Chi, Yan and Pham, 1996). So far there are the following two ways to calculate the optimal threshold in the fuzzy system:

- Techniques based on minimum values of index of fuzziness and entropy (Pal and King, 1983).
- Fuzzy image thresholding based on minimization of fuzziness using histogram (Chi, Yan and Pham, 1996; Huang and Wang, 1995).

In the first technique the optimal threshold is determined by adjusting the cross over point so that optimal (minimum) values of index of fuzziness and entropy are achieved. The segmentation based on index of fuzziness and entropy is described in the following.

Segmentation based on index of fuzziness and entropy

The input image is fuzzified using the standard S-function in the following ways.

$$\mu_X(f(i,j)) = S(f(i,j), a, b, c) = \begin{cases} 0 & if\, f(i,j) \le a \\ 2\{(f(i,j)-a)/(c-a)\}^2 & if\, a \le f(i,j) \le b \\ 1-2\{(f(i,j)-c)/(c-a)\}^2 & if\, b \le f(i,j) \le c \\ 1 & otherwise \end{cases} \quad (42)$$

Where f(i,j) is the grey level pixel intensity at (i,j) location, X is the fuzzy property plane of image f(i,j), $b = \frac{1}{2}(a+c)$ is the crossover point where the value of the membership function is 0.50 and $\Delta b = b-a = c-b$ is the bandwidth.

The linear and quadratic index of fuzziness measure the distance between property plane X and its nearest ordinary plane X. The linear index of fuzziness is defined as:

$$I_l(X) = \frac{2}{wh} \sum_{i=0}^{w-1} \sum_{j=0}^{h-1} \left| \mu_X(f(i,j)) - \mu'_X(f(i,j)) \right| \quad (43a)$$

$$= \frac{2}{wh} \sum_{i=0}^{w-1} \sum_{j=0}^{h-1} \mu_{X \cap \bar{X}}(f(i,j)) \quad (43b)$$

where w and h are the width and height of the image respectively and $\bar{X}$ is the complement set of X.

The quadratic index of fuzziness is defined as:

$$I_q(X) = \frac{2}{\sqrt{wh}} \left(\sum_{i=0}^{w-1} \sum_{j=0}^{h-1} \left\{ \mu'_X(f(i,j)) - \mu_X(f(i,j)) \right\}^2 \right)^{\frac{1}{2}} \quad (44)$$

The entropy is defined as:

$$E(X) = \frac{1}{wh \ln 2} \sum_{i=0}^{w-1} \sum_{j=0}^{h-1} Sn(\mu_X(f(i,j))) \quad (45)$$

where $Sn(\mu_X(f(i,j))) = -\mu_X(f(i,j))\ln \mu_X(f(i,j)) - (1 - \mu_X(f(i,j)))\ln (1 - \mu_X(f(i,j)))$.

The crossover point is adjusted so that optimum (minimum) values of I(X) and E(X) are achieved. The crossover point corresponding to the minimum values of I(X) and E(X) represents the optimum threshold, which provides the appropriate segmentation of the object and background. This technique may be applied to the segmentation of an image contains more than two regions or multiple objects by obtaining each local minimum of I(X) and E(X) for each optimum threshold value.

This method needs to compute the membership values for each pixel for all possible values of crossover point in order to calculate the optimum values of I(X) and V(X). For this the computational cost increases rapidly with the increase of the size of the image (Chi, Yan and Pham, 1996).

Segmentation based on minimization of fuzziness using histogram

In this method the image is segmented using the threshold, which is determined by

computing the minimum value of fuzziness between the regions, i.e., object and background for bimodal images (Huang and Wang, 1995). The techniques used in this method are described in the following.

Calculating expected values of background and object regions

For a given threshold T, the expected values of background (μ_0) and object (μ_1) are defined as:

$$\mu'_0 = \frac{\sum_{p=0}^{T} ph(p)}{\sum_{p=0}^{T} h(p)} \tag{46}$$

$$\mu'_1 = \frac{\sum_{p=T+1}^{L-1} ph(p)}{\sum_{p=T+1}^{L-1} h(p)} \tag{47}$$

where h(p) denotes the frequency of gray level p and 0..L-1 is the range of the gray level intensity of the image.

Calculation of membership function

The value of membership function is calculated by considering the notion that each pixel should be classified into its nearest region, i.e., the less distance between the pixel and its belonging region, the more value of the membership function. The membership function is defined as:

$$\mu'_X(f(x,y)) = \begin{cases} \dfrac{1}{1 + |f(x,y) - \mu'_0|\big/ D} & \text{if } f(x,y) \leq T \\[4mm] \dfrac{1}{1 + |f(x,y) - \mu'_1|\big/ D} & \text{if } f(x,y) > T \end{cases} \tag{48}$$

where f(x,y) is the gray level pixel intensity at the position (x,y) and D is chosen in such a way that $0.5 \leq ?_X(f(x,y)) \leq 1$ is achieved. The usual value of D is taken as the absolute difference between the maximum and minimum gray level values.

Entropy and Yager's fuzziness measure

The entropy has already been defined in equation (45) and using the histogram it is defined as:

$$E(X) = \frac{1}{wh \ln 2} \sum_{p=0}^{L-1} Sn(\mu'_X(p))h(p) \tag{49}$$

Yager (1979) defined the measure of fuzziness of a set as its lack of distinction from its complement set. The fuzziness between fuzzy image set X and its complement set $\overline{X}$ is defined as:

$$\mu_e(X) = 1 - \frac{D_e\left(X,\overline{X}\right)}{|X|^e} = 1 - \frac{D_e(X,\overline{X})}{(w,h)^e} \qquad (50)$$

where $D_e(X,\overline{X})$ is the distance between X and $\overline{X}$ and it is defined as:

$$D_e(X,\overline{X}) = \left(\sum_{x=0}^{w-1}\sum_{y=0}^{h-1} \left| \mu_X(f(x,y)) - \mu_{\overline{X}}(f(x,y)) \right|^e \right)^{\frac{1}{e}} \qquad (51)$$

using histogram:

$$D_e(X,\overline{X}) = \left(\sum_p \left| \mu_X(p) - \mu_{\overline{X}}(p) \right|^e \right)^{\frac{1}{e}} h(p) \qquad (52)$$

where p=0, 1,...,L-1 and e is 1 for Hamming distance and 2 for Euclidean distance.

Determination of optimum threshold

The fuzziness of an image is calculated using equation (48 and 49) or (52) considering all gray level pixel intensity, i.e., for all values from 0 to L-1. The optimum threshold is regarded as one of the gray level pixel intensities for which the fuzziness is a minimum value. Sometimes this optimum threshold does not locate in the deepest valley between the peaks. A fuzzy range (R) is defined in the following way in order to make sure that the optimum threshold falls in the real valley.

R=minf+(maxf-minf)×α%   (53)

where minf and maxf are the minimum and maximum measure of fuzziness respectively and the value of α is between 0 and 100 inclusive. The optimum threshold is determined by minimizing h(p-1)+h(p)+h(p+1) where p∈R. It is possible to calculate the multilevel threshold using this method.

Concluding remarks

Thresholding is not a good solution for the image segmentation if there is a significant overlap between the background and the object pixels.

FUZZY INTEGRAL-BASED IMAGE SEGMENTATION

A few techniques on image segmentation based on the fuzzy integral have been published so far. Fuzzy integral has been used in image segmentation (Keller, Qiu and Tahani, 1986) and classifier fusion (Chi, Yan and Pham, 1996; Tahani and Keller, 1990). Recently segmentation of color image using fuzzy integral had been done (Pham and Yan, 1999). The techniques used in color image segmentation of this method contain the following two steps.

- Determination of number of clusters and the initial values of the cluster centers using mountain clustering and fuzzy integral respectively.
- FCM classification of color image pixels by measuring the similarity between a color image pixel and cluster centers using fuzzy integral.

Determination of number of clusters and the initial values of the cluster centers using mountain clustering and fuzzy integral

The image space is divided into a specific number of grid points that are initially considered possible cluster centers and denoted by c_i where $i=1,...,M$ and M is the number of grid points. The correct number of clusters and their centers are determined using the mountain function, which has been described in Phan and Yan (1999). The mountain function $M_f(c_i)$ for grid point c_i is defined as:

$$M_f(c_i) = \sum_{j=1}^{n} e^{-\alpha d(p_j, c_i)} \tag{54}$$

where α is a constant, n is the number of pixels, p_j is the jth pixel and $d(p_j, c_i)$ is the distance between jth pixel p_j and c_i grid point using fuzzy integral is defined as:

$$d(p_j, c_i) = 1 - S(p_j, c_i) \tag{55}$$

and $S(p_j, c_i)$ the similarity between pixel p_j and cluster center c_i using Choquet integral is defined as:

$$S(p_j, c_i) = \sum_{k=1}^{3} \{f(x_k) - f(x_{k-1})\} g(A) \tag{56}$$

where $f(x)$ is extended π-membership function, which was introduced by Zadeh (1976),

$f(x_0)=0$, $x_1 = p_{j_R}, x_2 = p_{j_G}, x_3 = p_{j_B}$, $A = \left\{ x_1 = c_{i_R}, x_2 = c_{i_G}, x_3 = c_{i_B} \right\}$ and $g(A)$ is fuzzy density measure, which is measured by scaling the individual color component of all pixels using the following exponential equation as the R, G and B component of each pixel is in the range [0,1]:

$$x = b_0 + b(1 - e^{-x/a}) \tag{57}$$

where $b_0=0.2$, $b=1$ and $a=1$ for this particular problem. The techniques used in fuzzy measure are described in Tahani and Keller, (1990). In the first step the grid point, which achieves the largest mountain value, is regarded as the first cluster center. The next cluster center is identified by setting the previous cluster to zero and utilizing a specified threshold T instead of adopting subtractive techniques used in mountain clustering. If the fuzzy integral similarity values between a grid point having largest mountain value and all previously identified clusters are less than threshold, T is treated as the next cluster center. This also ensures that there exists some dissimilarity between cluster centers.

FCM classification of color image pixels by measuring the similarity between a color image pixel and cluster centers using fuzzy integral

In this method the distance between RGB color components of a pixel and cluster center is determined using the fuzzy integral in equation (55) instead of using traditional distance measure method during FCM classification of the color image pixels.

Concluding remarks

This method has solved the two main drawbacks of fuzzy clustering—the number of cluster centers and their initial values utilizing mountain algorithm. But there exists a trade off between the number of grid points and computational cost, especially for a large image. The potential of this method also depends on the value of threshold T used in mountain algorithm.

SOFT COMPUTING-BASED IMAGE SEGMENTATION

Soft computing is an integrated method, which is a synergistic combination of fuzzy logic (FL), neurocomputing (NC), genetic computing (GC) and probabilistic computing (PC) (Zadeh, 1998). Each part has distinguished capability to solve the problem that enables soft computing to manipulate imprecision, uncertainty and partial truth in a better way than compared to traditional approaches, and yields low cost and promising results.

Image segme.itation based on fuzzy-genetic computing has been presented in Hall, Ozyurt and Bezdek (1999) and Ishibuchi and Murata (1997). In Hall, Ozyurt and Bezdek (1999) the objective function of FCM algorithm is optimized using a genetic algorithm. Ishibuchi et.al. classified the high dimensional patterns by genetically selecting the minimum number of fuzzy rules that maximize the classification performance. A method of MRI segmentation based on neuro-fuzzy computing has been described in Karayiannhis and Pai (1999). In this method the MR image of the brain was segmented using a fuzzy algorithm for unsupervised linear vector quantization neural network.

CONCLUSION

This chapter has outlined some of the existing fuzzy image segmentation techniques, which have been shown to perform better than conventional techniques as well as coping with the noise. The most difficult task of fuzzy image segmentation is to determine the shape and parameters of the membership functions. Some of the methods have calculated the parameters of the membership functions automatically, but all of the methods have applied the predefined structures of the membership functions.

The leading techniques for fuzzy image segmentation are fuzzy clustering and rule-based techniques. The main two drawbacks of the former are to select the appropriate number of clusters and their initial values. Fuzzy rule-based image segmentation techniques seem promising, but they are very much application specific and very difficult to define and select fuzzy rules that cover all voxels/pixels. They can incorporate domain expert knowledge, process the linguistic variables and draw partial inference. For this fuzzy rule-based segmentation, techniques have been extensively applied to medical imaging. Fuzzy geometry and thresholding-based image segmentations are suitable for bimodal images and don't produce a good result if there exists a significant amount of overlapping pixels between the background and foreground regions. The literature on fuzzy integral and soft computing-based image segmentation techniques is not so rich. The fuzzy integral is good for integrating the results produced from different sources. Soft computing-based techniques are very promising for future research in the field of image segmentation.

REFERENCE

Andrey, P. and Tarroux, P. (1994). Unsupervised image segmentation using a distributed genetic algorithm. *Pattern Recognition*, 27(5), 659.

Barallard, D.H. and Brown, C. (1982). *Computer Vision*. Prentice Hall.

Barni, M., Cappellini, V. and Mecocci, A. (1996). Comments on "a possibilistic approach to clustering". *IEEE Transactions on Fuzzy Systems*, 4(3), 393-396.

Bensaid, A.M. and L.O.H. et al. (1996). Partially supervised clustering for image segmentation. *Pattern Recognition*, 29(5), 859-871.

Bezdek, J.C. (1981). *Pattern Recognition with Fuzzy Objective Function Algorithms*. New York: Plenum.

Bhanu, B., Lee, S. and Ming, J. (1995). Adaptive image segmentation using a genetic algorithm. *IEEE Transactions on Systems, Man, and Cybernatics*, 25(12), 1543-.

Cagnoni, S., Dobrzeniecki, A.B. and Yanch, J.C. (1999). Genetic algorithm-based interactive segmentation of 3D medical images. *Image and Vision Computing*, 17(12), 881.

Caselles, V., Kimmel, R. and Sapiro, G. (1995). Geodesic active contours. In the *Proceedings of IEEE ICCV-95*, 840-845.

Chakrabotry, A., Staib, L.H. and Duncan, J.S. (1994). Deformable boundary finding influenced by region homogeneity. Department of Electrical Engineering and Diagnostic Radiology, Yale University, New Haven, CT. http://noodle.med.yale.edu/alums/chakrab/pap1/pap1.html.

Chang, C-W., Ying, H., Hillman, G.R., Kent, T.A. and Yen, J. (1998). A rule-based fuzzy segmentation system with automatic generation of membership functions for pathological brain MR images. *Computers and Biomedical Research*, http://gopher.cs.tamu.edu/faculty/yen/publications/index.html .

Chi, Z. and Yan, H. (1993). Segmentation of geographic map images using fuzzy rules. *Conference Proceedings DICTA-93, Digital Image Computing, Techniques and applications, Australian Pattern Recognition Soc.*, 1, 95-101, Broadway, NSW, Australia.

Chi, Z., Yan, H. and Pham, T. (1996). *Fuzzy Algorithms: With Applications to Image Processing and Pattern Recognition*. Singapore: World Scientific Publishing Co. Pte. Ltd.

Cohen, L.D. and Cohen, I. (1993). Finite-element methods for active contour models and balloons for 2D and 3D images. *IEEE Transactions on Pattern Analysis and Machine Intelligence*, 15(11), 1131-1147.

CT(2000). Computed Tomography Imaging (CT Scan, CAT Scan), http://www.imaginis.net/ct-scan

Derin, H. and Elliott, H. (1987). Modeling and segmentation of noisy and textured images using Gibbs random fields. *IEEE Transactions on Pattern Analysis and Machine Intelligence*, 9(1), 39-55.

Derin, H., Elliott, H., Cristi, R. and Geman, D. (1984). Byes something algorithms for segmentation of binary images modeled by Markov random fields. *IEEE Transactions on Pattern Analysis and Machine Intelligence*, 6, 707-720.

Dubois, D. and Jaulent, M.C. (1987). A general approach to parameter evaluation in fuzzy digital pictures. *Pattern Recognition Letters*, 6, 251-259, North-Holland.

Geman, S. and Geman, D. (1984). Stochastic relaxation, Gibbs distribution, and the Byesian restoration of images. *IEEE Transactions on Pattern Analysis and Machine Intelligence*, 6, 721-74.

Gonzalez, R.C. and Woods, R.C. (1992). *Digital Image Processing*. Reading, MA: Addison-Wesley.

Grzeszczuk, R.P. and Levin, D.N. (1997). Brownian strings: Segmenting images with stochastically deformable contours. *IEEE Transactions on Pattern Analysis and Machine Intelligence*, 19(10), 1100-1114.

Grzeszczuk, R. and Levin D.N. (1993). Segmenting images by stochastic contour optimization. In the *Proceedings of Soc. Magnetic Resonance in Medicine*, 1, 508-.

Hall, L.O. and Namasivayam, A. (1998). Using adaptive fuzzy rules for image segmentation. *FUZZ-IEEE'98*. http://modern.csee.usf.edu/~hall/adrules/segment.html

Hall, L.O., Ozyurt, B. and Bezdek, J.C. (1999). Clustering with genetically optimized approach. http://morden.csee.usf.edu/~hall/galong.pdf.

Hansen, F.R. and Elliott, H. (1984). Image segmentation using simple Markov random field models. *Comput. Graphics Image Process*, 20, 101-132.

Haralic R.M. and Shapiro L.G. (1985). Survey: Image segmentation Techniques. *Computer, Vision, and Image Processing* , 29, 100-132.

Huang, L.K. and Wang, M.J. (1995). Image thresholding by minimzing the measure of fuzziness. *Pattern Recognition*, 28, 41-51.

Ishibuchi, H. and Murata, T. (1997). Minimizing the fuzzy rule base and maximizing its performance by a multi-objective genetic algorithm. *FUZZ-IEEE'97*, 1, 259-264.

Kapur, T. (1995). Segmentation of brain tissue from magnetic resonance images. MIT AI laboratory, *Technical Report No. AITR-1566*.

Karayiannis, B. and Pai, P. (1999). Segmentation of magnetic resonance images using fuzzy algorithms for linear vector quantization. *IEEE Transactions on Medical Imaging*, 18(2), 172-180.

Kass, M., Witkin, A. and Terzopoulos, D. (1988). Snakes: Active contour models. *International Journal on Computer Vision*, 321-331.

Keller, J., Qiu, H. and Tahani, H. (1986). Fuzzy integral and image segmentation. In the *Proceedings of North American Fuzzy Information Processing Society*, New Orleans, 334-338.

Krishnapuram, R. and Keller, J. (1993). A possibilistic approach to clustering. *IEEE Transactions on Fuzzy Systems*, 1, 98-110.

Krishnapuram, R. and Keller, J.M. (1996). The possibilistic c-means algorithm: insight and recommendations. *IEEE Transactions on Fuzzy Systems*, 4(3), 385-393.

Medasani, S., Krishnapuram, R. and Keller, J. (1999). Are fuzzy definitions of basic attributes of image objects really usefull?. *IEEE Transactions on Systems, Man, and Cybernetics-Part A: Systems and Humans*, 29(4), 378-386.

Moghaddamzadeh, A. and Bourbakis, N. (1997). A fuzzy region growing approach for segmentation of color images. *Pattern Recognition*, 30(6), 867-881

Pham, D.L. and Prince, J.L. (1999). An adaptive fuzzy C-means algorithm for image segmentation in the presence of intensity inhomogeneities. *Pattern Recognition Letters*, 20(1), 57-68.

Pal, N.R. and Pal, S.K. (1993). A review on image segmentation techniques. *Pattern Recognition*, 26(9), 1277-1294.

Pal, S.K. and Gosh, A. (1990). Index of area coverage of fuzzy image subsets and object extraction. *Pattern Recognition Letters*, 11, 831-841, North-Holland.

Pal, S.K. and Rosenfeld, A. (1988). Image enhancement and thresholding by optimization of fuzzy compactness . *Pattern Recognition Letters*, 7, 77-86.

Pal, S.K. and King, R.A. (1983). Automatic grey level thresholding through index of fuzziness and entropy. *Pattern Recognition Letters*, 1, 141-146.

Pal, S.K. and Gosh, A. (1992). Fuzzy geometry in image analysis. *Fuzzy Sets and Systems*, 48, 23-40.

Park, W. and Hoffman, E.A. (1998). Segmentation of intrathoracic airway trees: a fuzzy logic approach. *IEEE Transactions on Medical Imaging*, 17(4), 489-497.

Pham, T.D. and Yan, H. (1999). Color image segmentation using fuzzy integral and mountain clustering. *Fuzzy Sets and Systems*, 107, 121-130.

Prewitt, J.M. (1970). *Object Enhancement and Extraction*. New York: Academics, 75-149.

Reid, M.M., Millar, R.J. and Black, N.D. (1997). Second-generation image coding: An overview. *ACM Computing Survey*, 29(1), 3-29.

Ronald, R. (1994). Region-based strategies for active contour models. *International Journal on Computer Vision*, 13, 229-251.

Rosenfeld A. (1984). The fuzzy geometry of image subsets. *Pattern Recognition Letters*, 2, 311-317, North-Holland.

Rosenfeld A. (1992). Fuzzy geometry: An overview. In the *Proceedings of International Conference on Fuzzy Systems*, 113-118, San Diego, CA.

Samet, H. (1989a). *Application of Spatial Data Structures* (First edition). Reading, MA: Addison-Wesley.

Sasaki, T., Hata, Y., Ando, Y., Ishikawa, M. and Ishikawa, H. (1999). Fuzzy rule-based approach to segment the menisci region from MR images. In *Proceedings of SPIE Medical Imaging*, 3661, 258-, San Diego, CA.

Sonka, M., Park, W. and Hoffman, E. A. (1996). Rule-based detection of intrathoracic airway trees. *IEEE Transactions on Medical Imaging*, 15, 314-326.

Sonka, M., Hlavac, V. and Boyle, R. (1993). *Image Processing, Analysis, and Machine Vision*. London, U.K.: Chapman and Hall, 2nd edition, Boston.

Tahani, H. and Keller, J. (1990). Information fusion in computer vision using the fuzzy integral. *IEEE Transactions on Systems, Man, and Cybernatics*, 20(3), 733-741.

Tizhoosh, H.R. (1998). Fuzzy image processing. http://pmt05.et.uni-magdeburg.de/~hamid/segment.html.

Tolias, Y. A. and Panas, S. M. (1998): Image segmentation by a fuzzy clustering algorithm using adaptive spatially constrained membership functions. *IEEE Transactions on Systems, Man, and Cybernetics-Part A: System and Humans*, 28(3), 359-369.

Wang, L. and Mendel, J.M. (1991). Generating fuzzy rules by learning from examples. In *Proceedings of the IEEE International Symposium on Intelligent Control*, 263-268, Arlington, VA.

Weszka, J.S. and Rosenfeld, A. (1979). Histogram modification for threshold selection. *IEEE Transactions on Systems, Man, and Cybernatics*, 9(1), 38-52.

Yager, R.R. (1979). On the measure of fuzziness and negation. Part I: Membership in the unit interval. *International Journal on Gen. Systems*, 5, 221-229.

Yen, J. (1999). Fuzzy logic- A modern perspective. *IEEE Transactions on Knowledge and Data Engineering*, 11(1). http://gopher.cs.tamu.edu/faculty/yen/publications/index.html.

Yen, J. and Wang, L. (1999). Simplifying fuzzy rule-based models using orthogonal transformation. *IEEE Transactions on Systems, Man, and Cybernetics-Part B: Cybernetics*, 29(1), 13-23.

Zadeh, L.A. (1965). Fuzzy Sets. *Information Control*, 8, 338-353.

Zadeh, L.A. (1976). A fuzzy-algorithmic approach to the definition of complex or imprecise concepts. *International Journal of Man-Machine Studies*, 8, 249-291.

Zadeh, L.A. (1998). Roles of soft computing and fuzzy logic in the conception, design, and deployment of information/intelligent system. *Computational Intelligence: Soft Computing and Fuzzy-Neuro Integration with Applications*, Springer.

A SURVEY OF FUZZY RULE BASED IMAGE SEGMENTATION TECHNIQUES

Gour C Karmakar, Laurence Dooley and Syed Mahbubur Rahman
Email: {gourk+lsdooley}@mail1.monash.edu.au, mahbubur.syed@mankato.msus.edu
Gippsland School of Computing and Information Technology, Monash University, Australia

ABSTRACT

This paper describes the various fuzzy rule based techniques for image segmentation. Fuzzy rule based segmentation techniques can incorporate the domain expert knowledge and manipulate numerical as well as linguistic data. They are also capable of drawing partial inference using fuzzy IF-THEN rules. For these reasons they have been intensively applied in medical imaging. But these rules are application domain specific and it is very difficult to define the rules either manually or automatically so that the segmentation can be achieved successfully.

1   INTRODUCTION

Prewitt first stated that image segmentation should produce fuzzy regions [1]. Fuzzy image segmentation techniques are advantageous over classical methods as they are capable of handling imprecise data and they may be broadly classified in five classes [2]: fuzzy clustering, fuzzy rule, fuzzy geometry, fuzzy thresholding, and fuzzy integral. Initially fuzzy IF-THEN rules were extensively used in control engineering problems but now they are being increasingly applied in image segmentation. The advantages of the fuzzy rules based image segmentation over other methods are mainly [3] that humans can more easily understand the problems due to linguistic representation of numeric variables, it is computationally less expensive than fuzzy clustering methods, and it has the potential ability to integrate the domain expert knowledge. Generally fuzzy rule-based image segmentation has been applied in three types of images: light intensity (LI), magnetic resonance (MR), and computed tomography (CT) images and they are described in the sections 2, 3 and 4 respectively. Section 5 provides the conclusion.

2   FUZZY RULE BASED LI IMAGE SEGMENTATION

Chi and Yan utilized the fuzzy IF-THEN rules in the segmentation (separation of background and foreground pixels) of 256 gray scale geographic map images containing strings, streets, roads, boundaries etc. that are considered foreground pixels of the images [4-5]. Three features such as difference intensity (DI), local standard deviation (SD) and local contrast of darker pixel (CD) are used in segmentation. The input and output domains are divided into five fuzzy regions named as L2, L1, M, H1 & H2 and two fuzzy regions such as background & foreground respectively.   Triangular membership functions shown are utilized for input regions. Fuzzy rules are generated by learning from examples. A pair of rules shown below is generated for each training sample.

IF DI is L1 AND SD is H1 AND CD is H2 THEN it is a foreground pixel
IF DI is H1 AND SD is M AND CD is L1 THEN it is a background pixel

To avoid repeated and conflict rules, the rules selected are supported by a large number of examples. If the centroid defuzzification value $C_p <= 0.5$, the input pixel is categorized as background pixel otherwise it is categorized as foreground pixel. This system is faster than neural network techniques and superior to the adaptive thresholding techniques. It was found that some parts of characters are missed for standard triangular function [4]. This is because of selecting the shape and parameters of the membership functions was done intuitively.   For this they used an automatic method using fuzzy C-means clustering (FCM) to determine the parameters of the membership functions. The shapes of the membership functions have been determined manually and heuristics rules are not used in this method.

3   FUZZY RULE BASED MR IMAGE SEGMENTATION

The fuzzy rule based MRI image segmentation methods may be broadly classified into two classes: Hybrid and conventional fuzzy rule based MRI segmentation.

3.1   HYBRID FUZZY RULE BASED MRI SEGMENTATION

Hybrid fuzzy rule based segmentation system consists of fuzzy rule based and FCM. Clustering is computational expensive and does not produce appropriate class alone due to inability of incorporating human expert knowledge [6]. For these reasons, a set of fuzzy rules is applied to classify the pixels/voxels. It is very difficult to define fuzzy rules that cover all pixels/voxels. So the classified pixels/voxels are used to initialize the cluster centers and FCM is used to classify the remaining unclassified pixels/voxels. Hybrid fuzzy rule based

image segmentation systems are faster than clustering and are described in [3][6].

The method using adapting fuzzy rules for segmenting the brain tissue into six classes: white matter (WM), gray matter (GM), cerebro-spinal fluid (CSF), pathology, skull tissues and background is described in [6]. In this method 105 axial brain slices, 5 mm thick from 15 persons (39 normal slices from 8 persons and 66 abnormal slices from 7 patients) are used for experimental purposes. Relative voxel intensities of T1, T2 and PD weighted intensity images are used as feature. The shapes of the membership functions are triangular and trapezoidal. The parameters of the membership functions (a1, a2, b1, b2, b3, b4, b5 and b6) are calculated by determining the turning points (peaks, valleys or the starting point of the histogram) of intensity histograms of T1, T2 and PD images using a training set consisting of 6 normal & 4 abnormal slices and suggestions of expert radiologists. The PD histogram of the patient with brain tumor become like the PD histogram for abnormal slice due to the change of properties of gray and white matter. The turning points of this histogram are obscure and difficult to select. They used an edge detection technique in order to sharpen the boundary between gray & white matter utilizing a suitable threshold to detect the peaks. The initial value of threshold is chosen as 5 and increased by 5 until two peaks are found. If peaks are not found, two peaks are assumed at 1/3 and 2/3 of the region between b1 and b2. The Set-A, Set-B, Set-C, Set-D, Set-E, and Set-F are defined from the membership functions. A set of the following fuzzy rules are defined heuristically.

IF voxel in T1 in Set-E AND voxel in T2 in Set-F THEN voxel is CSF
IF voxel in PD is Set-C AND voxel in T1 in Set-A THEN voxel is White matter
IF voxel in PD is Set-D AND voxel in T1 in Set-A AND NOT (voxel in T2 is Set-F AND voxel in T1 is Set-E) THEN voxel is Gray matter
IF voxel in T1 is Set-B AND voxel in T2 is Set-F THEN voxel is Pathology
IF voxel in T1 is Set-B AND NOT (voxel in T2 is Set-F) THEN voxel is Other
IF PD voxel intensity < b1 AND T2 voxel intensity < c1 THEN voxel is Bcakground

Rules adapt themselves for each slice during processing. After classification using fuzzy rules the unclassified voxels and isolated voxels for each class are assigned the membership values with the average membership values of their neighbors and zero respectively. Finally the voxel membership values are normalized (0 to 1). The incorrect classified voxels (voxels whose membership value <= 0.80) are classified using semi-supervised clustering algorithm [7]. The correctly classified voxels are used as training set for the clustering algorithm. This system is faster than FCM. Rules are generated based on turning points of the histograms that are not sufficient enough to distinguish the brain tissues containing a significant amount of overlapping voxels. The threshold and approximate peaks (when there are no peaks in the PD histogram) are chosen empirically.

Another hybrid fuzzy rule based brain MR image segmentation method, which separates WM, GM, CSF and CMV lesion from the brain is described in [3]. In this method a set of T1, T2 & PD weighted images containing 12 normal images and 3 abnormal images with lesions are used for experimental purposes. Preprocessing step consists of two sub-steps: Image registration and selection of region of interest (ROI). Image registration makes the same pixel coordinates for the same pixels contained in two different images by the method of shifting of coordinates. Intracranial region of the brain is selected as ROI. The shapes of the membership functions are identified perceptually. Three different types of tissue such as WM, GM and CSF were identified for T2 images. T2 image as well as its edges that are determined by Cohen's edge detection method [8] are classified into five classes WM, GM, CSF, WM-GM and GM-CSF using standard FCM algorithm. The mean intensities (μ_i) and variance (σ_i) of ith class are used to calculate the parameters of the membership function for ith class. The PD weighted image and its edge values are given to FCM, which classifies them into four classes. The class containing highest pixel intensity is discarded in order to eliminate the high edge values on the boundary of the brain. The techniques used to generate the membership function for PD weighted images are same as T2 weighted images. For PD weighted abnormal images contain periventricular hyperintensity which have higher pixel intensities in brighter class than other pixels in the same class. So another membership function for PD weighted abnormal image is generated. A membership function is used to represent the closeness of a pixel from the center of the brain as the ventricle is considered a major connected CSF areas adjacent to the center of the brain. This membership function is used to discover the periventricular hyperintensity, which represents the lesions of the PD weighted images. Two groups of fuzzy rules have been developed. First and the second group are used to segment the T2 weighted images and to recognize the CMV lesions respectively. The first group is shown below.

IF pixel in T2 is Dark THEN pixel is White Matter
IF pixel in T2 is Grey THEN pixel is Grey Matter
IF pixel in T2 is Bright THEN pixel is CSF

Second group shown below is formulated by splitting the last rule of the first group into three new rules that discriminate CSF and CMV lesions.

IF pixel in T2 is Dark THEN pixel is White Matter
IF pixel in T2 is Grey THEN pixel is Grey Matter

IF pixel in T2 is Bright AND pixel in PD is Dark-Grey
THEN pixel is CSF
IF pixel in T2 is Bright AND pixel in PD is Very Bright
AND pixel is not close to the ventricle
THEN pixel is CSF
IF pixel in T2 is Bright AND pixel in PD is Very Bright
AND pixel is close to the ventricle
THEN pixel is CMV lesion

All pixels are classified using the rules described above. The pixels whose membership values are less than 0.5 and the pixel having two maximum membership values are declared as unclassified pixels. The initial value of each cluster center is derived from the average value of each respective classified class. All unclassified pixels are classified using FCM. If the number of classified pixels in CMV lesion is very small (from 10 to 20), they are reclassified as CSF. This system is 10 to 20 times faster than FCM and gives better result for abnormal images containing lesions. The structures of the membership functions have been defined according to the knowledge of medical experts.

3.2 CONVENTIONAL FUZZY RULE BASED MRI SEGMENTATION

Conventional fuzzy rule based segmentation uses only fuzzy rules to segment the MR image. Sasaki et. al. introduced such a fuzzy rule based method to segment the menisci region from MR images [9]. Five T1 weighted images (three normal and two injured knees), each contains 60 separate 1.5 mm thick slices are used in the experiments. The knowledge used to generate the fuzzy rules is : voxel intensities of cartilage regions are high, the menisci region lies in between the thigh and shinbone, the cartilage regions are adjacent to the center of the gravity of the knees, the menisci are automatically located near the cartilage, and the voxel intensities of the menisci regions are coherent . Two different sets of fuzzy rules are developed as the segmentation is performed in two stages. In first the candidate region of the menisci are segmented whereas the menisci are extracted from the candidate region in the second stage. Candidate region can be defined as the region between the cartilages as menisci are always located between the cartilages. A set of voxels represented by straight contiguous two dimensional data(x,z) is called unit(x,z). Two types of units such as unit A and unit B are defined to segment the candidate region. Unit A contains the candidate region while unit B does not contain any candidate region voxels. From the knowledge, 1, 2 and 3, the following rules are defined functions in order to segment the candidate region.

IF d is small AND n is large THEN degree of belonging to unit A is large
IF d is large AND n is small THEN degree of belonging to unit B is large

Where d and n denote distance of the interested unit from the center, and the number of disparity of voxel intensity on a unit respectively. The membership functions for distance and disparity to measure the values of linguistic variables, small and large are defined intuitively. The degree of belonging to unit A and B are calculated using equations: gradeA=w1 udsmall(d)+w2 unlarge(n) and gradeB=w1 unlarge(d)+w2 unsmall(n) where w1 and w2 are weights. The unit is classified into unit A if gradeA > gradeB, otherwise the unit is classified into unit B. From knowledge 4 and 5, two membership functions uc & ui, and the following two fuzzy rules are derived to segment the menisci from the candidate region.

IF voxel is anatomically adjacent to the cartilage THEN the degree of menisci voxel for uc is high
IF the intensity of the voxel is same as coherent intensity of the menisci voxel THEN the degree for ui is high

The total degree, gradeM=w3uc(i)+w4ui(m) where w3 and w4 are the weights. If gradeM > T, the voxel is classified as menisci voxels where T is the threshold. This method can successfully identify the tears. The rules have been defined based on anatomical position and coherent intensity of the menisci voxels. The structure of the membership function is defined from the knowledge of the expert. The parameters used in membership function are taken from the MR device parameters.

4 FUZZY RULE BASED CT IMAGE SEGMENTATION

A fuzzy rule based automatic segmentation of intrathoracic airway trees on CT image has been described in [10]. Five canine data sets, each contains 40 slices of 3mm thick are scanned from five anesthetized dogs. 40 slices, 8 per data set are randomly selected and their airways are perceptually determined by an expert in order to determine the training and test sets. Segmentation consists of the following five steps: separation of lungs from the volumetric data set, definition of primary airway tree, preprocessing of all individual image slices, fuzzy rule based identification of airways in all image slices, and construction of airway tree using 3-D connectivity. The techniques used for steps 1, 2, and 3 are described in [10-11]. Primary airway tree contains the major branches of the tree and is defined as the 3-D connected components of the image voxels below a threshold, which is formed by 3-D seeded region growing approach. The main task of preprocessing step is to identify the background and all possible locations of airways and vessels for each slice. The pixels (55 to 110 gray level intensities) are considered background pixels. The voxels darker and brighter than background are treated as candidate airways and vessels respectively. The anatomical

information used to determine the airways is: airways are generally dark, airways are encompassed by airways wall, and airways are near to airway vessels. The following three features are defined according to a region adjacency graph properties [12].

- BRIGHTNESS: Uses minimum and maximum grey level regions to represent the airways and vessels candidate regions respectively.
- ADJACENCY: Represents the grey level of the brightest adjacent region.
- DEGREE OF WALL EXISTENCE: It determines the existence of the wall. The degree of wall existence is determined by the ratio of the total number of concentric rays possessed dark-bright-dark profile and the total number of concentric rays directed from the center of the candidate region.

The membership functions for BRIGHTNESS, ADJACENCY and DEGREE_OF_WALL _EXISTENCE including their linguistic variables are determined perceptually. The parameters of the membership function are determined from a manually tracking training set containing eight randomly selected slices of a single volumetric data set. The conflicts arisen among membership functions are solved manually in order to get optimum classification results. The rule banks are developed for the segmentation. For example, a rule of the rule bank,

IF BRIGHTNESS is LOW AND ADJACENCY is LOW AND DEGREE_OF_WALL_EXISTENCE is HIGH THEN region is airway with MEDIUM confidence

Centroid defuzzification is applied to get numerical confidence level for each region, which indicates the possibility that the region belongs to airway. Airway tree named C-tree is constructed by stacking of all the regions whose airway confidence level is more than 73% utilizing shape based interpolation along z-axis. From C- tree, A tree and B-tree are created. A-tree is defined as a 3-D connected region and subset of C-tree, which contains the airway-tree root. B-tree is the combination of A-tree and disconnected airway tree branches of C-tree that contains above threshold volume. This method has constructed three trees: A-tree, B-tree and C-tree and is not fully automatic.

5 CONCLUSION

This paper describes some of the existing fuzzy rule based image segmentation techniques. The most difficult task of fuzzy image segmentation is to determine the shape and parameters of the membership functions. Some of the methods have calculated the parameters of the membership functions automatically but all of the methods have applied the predefined structures of the membership functions. It has been seen from the

literature that fuzzy rule based image segmentation techniques seem promising but they are very much application specific and very difficult to define and select fuzzy rules that cover all voxels/pixels. Fuzzy rule based techniques are capable of incorporating expert knowledge, processing the linguistic variables and drawing partial inferences.

REFERENCE

[1] Prewitt, J.M. (1970). Object Enhancement and Extraction. New York: Academics, 75-149.

[2] Tizhoosh, H.R. (1998). Fuzzy image processing, http://pmt05.et.unimagdeburg.de/~hamid/segment .html

[3] Chang, C.-W.; Ying, H.; Hillman, G.R.; Kent, T.A. and Yen, J. (1998). A rule-based fuzzy segmentation system with automatic generation of membership functions for pathological brain MR images. Computers and Biomedical Research, http://gopher.cs.tamu.edu/faculty/yen/publications /index.html

[4] Chi, Z.; Yan, H. and Pham, T.(1996). Fuzzy Algorithms: With Applications to Image Processing and Pattern Recognition. World Scientific Publishing Co. Pte. Ltd. Singapore.

[5] Chi, Z. and Yan, H. (1993). Segmentation of geographic map images using fuzzy rules. Conference Proceedings DICTA-93, Digital Image Computing, Techniques and applications, Australian Pattern Recognition Soc., 1, 95-101, Broadway, NSW, Australia.

[6] Hall, L.O. and Namasivayam, A.(1998). Using adaptive fuzzy rules for image segmentation. FUZZ-IEEE'98, http://modern.csee.usf.edu/~hall /addrules/segment.html

[7] Bensaid, A.M. and L.O.H. et al.(1996). Partially supervised clustering for image segmentation. Pattern Recognition, 29(5), 859-871.

[8] Gonzalez, R.C. and Woods, R.C.(1992). Digital Image Processing, Reading, Mass., Addison-Wesley, 1992.

[9] Sasaki, T.; Hata, Y.; Ando, Y.; Ishikawa, M. and Ishikawa, H.(1999). Fuzzy rule based approach to segment the menisci region from MR images. In Proceedings of SPIE Medical Imaging, 3661, 258-, San Diego, California, USA.

[10] Park, W.; Hoffman, E. A. and Sonka, M.(1998). Segmentation of intrathoracic airway trees: a fuzzy logic approach. IEEE Transactions on Medical Imaging, 17(4), 489-497.

[11] Sonka, M.; Park, W. and Hoffman, E. A.(1996). Rule-based detection of intrathoracic airway trees. IEEE Transactions on Medical Imaging, 15, 314-326.

[12] Sonka, M.; Hlavac, V. and Boyle, R.(1993). Image Processing, Analysis, and Machine Vision. U.K.: Chapman and Hall, 2nd edition, Boston.

A GENERIC FUZZY RULE BASED TECHNIQUE FOR IMAGE SEGMENTATION

Gour Chandra Karmakar and Laurence Dooley
Email:{ gourk, lsdooley}mail1.monash.edu.au
Gippsland School of Computing and Information Technology
Monash University, Churchill, Victoria, Australia - 3842

ABSTRACT

Many fuzzy clustering based techniques do not incorporate spatial relationships of the pixels, while all fuzzy rule-based image segmentation techniques tend to be very much application dependent. In most techniques, the structure of the membership functions are predefined and their parameters are either automatically or manually determined. This paper addresses the aforementioned problems by introducing a general fuzzy rule based image segmentation technique, which is application independent and can also incorporate the spatial relationships of the pixels. It also proposes the automatic defining of the structure of the membership functions. A qualitative comparison is made between the segmentation results using this method and the popular fuzzy c-means (FCM) applied to two types of images: light intensity (LI) and X-ray of human vocal tract. The results clear show that this method exhibits significant improvements over FCM for both types of images.

1. INTRODUCTION

Classical so-called "crisp", image segmentation techniques while effective when an image contains well-defined structures, such as edges and regular shapes, do not perform nearly so well in the presence of ill-defined data. In such circumstances, the processing of such images that possess ambiguities produces fuzzy regions. Fuzzy image segmentation techniques can cope with the imprecise data well and they can be classified into five classes: fuzzy clustering, fuzzy rule based, fuzzy geometry, fuzzy thresholding, and fuzzy integral based image segmentation techniques [1] but among them the most dominant are fuzzy clustering and fuzzy rule based segmentation techniques. The most popular and extensively used fuzzy clustering techniques are: fuzzy c-means (FCM) [2-3] and possibilistic c-means (PCM) algorithms [4]. These clustering techniques however cannot incorporate human expert knowledge and spatial relation information. Image segmentation without considering the spatial relationships among pixels does not produce good result, as there is a huge amount of overlapping pixel values between different regions. Fuzzy rule based image segmentation techniques can incorporate human expert knowledge, are less computational expensive than fuzzy clustering and able to interpret linguistic as well as numeric variables [5]. But they are very much application dependent and very difficulty to define fuzzy rules that cover all of the pixels. In most techniques, the structures of the membership functions are predefined and their parameters are either manually or

automatically determined [5-9]. In addition to the above-mentioned advantages, a fuzzy rule based image segmentation technique should be both application and image independent, be capable of incorporating spatial information of the regions and be able to define the membership functions and their parameters automatically.

This paper explores a new approach in the development of such a type of fuzzy rule based image segmentation techniques. Section 2 explores the technique used to define the membership function, while the underlying theoretical concepts and fuzzy rule definition and the experimental results are presented in sections 3 and 4 respectively. Finally the discussions and conclusion are provided in section 5.

2. DEFINITION OF MEMBERSHIP FUNCTIONS

In this section three types of membership functions are automatically defined to represent respectively the region pixel distributions, the closeness to their centers and their spatial relations. Each membership function possesses a membership value for each region, which indicates the degree of belonging to that particular region. The techniques used to automatically define the structures of the membership functions and hence the membership functions from the region pixel distributions are described in the following subsection

2.1. Membership Function for Region Pixel Distributions

In this subsection an attempt is made to automatically define the membership function including its structure from the region pixel distributions. The steps needed to define the membership function are: classification of the sample or the image to be segmented into desired number of regions using manual segmentation or automatically by applying any of the fuzzy clustering algorithms, generation of the gray level pixel intensity histogram for each region and map the frequency for each gray level into {0 1}, and approximation of the polynomial for each region. This polynomial represents the membership function for that particular region and the value of the polynomial for each gray level denotes the membership value of that particular gray level value. The cloud image shown in figure 1(a) is divided into two regions namely cloud (R_1) and urban scene (R_2) using FCM. The membership functions shown in figures 1(b)-1(c) of these two regions are determined from respective region pixel distributions using third order polynomial approximation.

(a): Cloud image   (b): Membership function for R_1 (c): Membership function for R_2
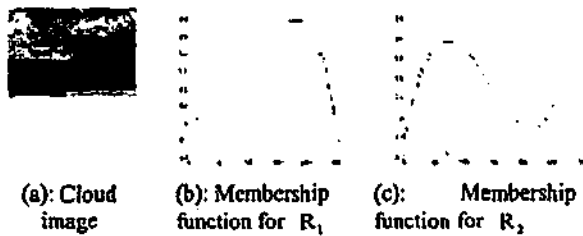
Figure 1: Cloud image and its region membership functions

The degree of belonging of a candidate pixel (the pixel to be classified) to a region is determined from the respective membership function. The structures of the membership functions are automatically generated from the region pixels and hence relieve us from manually defining the structure and parameters of the membership function for each region. The membership function $\mu_{DR_j}(P_{s,t})$ of the region R_j for the pixel distribution can be defined as

$$\mu_{DR_j}(P_{s,t}) = f_{R_j}(P_{s,t}) \tag{1}$$

Where $f_{R_j}(P_{s,t})$ and $P_{s,t}$ are the polynomial of the region R_j and the pixel value at the position (s,t) respectively.

2.2. Membership Function to Measure the Closeness of the Region

Each pixel should be more compact i.e. more close to the belonging region than other regions. The degree of belongingness of a candidate pixel to a region is determined by following the strategy of k-means clustering algorithm. Candidate pixel joins in its nearest region and after joining the center of that region is recomputed. The centroid of a region R_j can be defined as

$$C(R_j) = \frac{1}{N_j} \sum_{i=1}^{N_j} P_j(i) \tag{2}$$

Where N_j and $P_j(i)$ represent the number of pixels and the ith pixel gray level intensity of the jth region respectively.

The membership function should reflect the relation "the more close to a region the larger membership value the pixel should have". So the membership function $\mu_{CR_j}(P_{s,t})$, which determines the degree of belongingness of a candidate pixel $P_{s,t}$ at a location (s,t) to a region R_j can be defined as

$$\mu_{CR_j}(P_{s,t}) = 1 - \frac{|C(R_j) - P_{s,t}|}{D} \tag{3}$$

Where the constant D can be defined as difference of maximum and minimum gray level intensity values of an image i.e. here D equals to 255. The maximum value of the membership function will be always at the center of the region and the structure of the membership function will be symmetrical around the vertical line passes through the center of the region.

2.3. Membership Functions for Spatial Relation

In the previous two sections the membership functions have been developed only based on the feature values i.e. gray level pixel intensities of an image. They don't consider any spatial relationships of the pixels of a region, but there exists strong spatial relations between the pixels of a region. Spatial relations also represents the geometric features of a region and a spatial object contains two descriptors- feature and geometric [11]. There is a large amount of overlapping pixels between the regions. Segmentation does not produce good result without taking into account of these overlapping pixels. The number of overlapping pixels can be trim downed by considering the neighborhood relation among a candidate pixel and the classified pixels of the regions i.e. once we get the some region pixels we can easily calculate the neighborhood relation between the candidate pixel and the region pixels. Based on the neighborhood relation the candidate pixel can be assigned to the appropriate cluster or group. The neighborhood relation can mainly be defined using the three techniques- fixed size neighborhoods around candidate pixel, minimum spanning tree and Voronoi tessellation even though there are many ways to define a neighborhood relation [12]. We are interested in fixed size neighborhoods around a candidate pixel, as we need to calculate the number of pixels and their distances from the candidate pixels inside the neighborhood area. The neighborhood configurations of the pixels for r=1, r=2 and r=4 are shown in the figures 2(a), 2(b) and 2(c) respectively [13] where O, # and r represent the candidate pixel, neighborhood pixels and neighborhood radius respectively.

(a): r=1   (b): r=2   (c): r=4
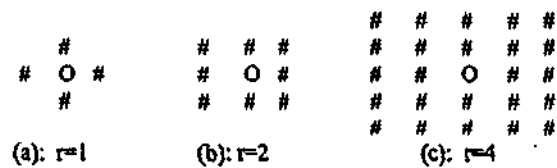
Figure 2: Neighborhood configuration

The number of neighbors would be $(r+1)^2$ for r=1 otherwise $(r+1)^2 - 1$. The main task of the segmentation is to divide the image into desired number of mutually exclusive homogeneous regions. It is thus assumed that the variation of the pixel intensities of a region is in a limited extent but there is a sharp variation of the pixel intensities on the boundaries of the regions that divides the image into some regions. We are interested in determining the spatial relationships among the pixels of a region. So the neighborhood system of a region can be defined as,

Definition 1 (Neighborhood system) A neighborhood system with radius r, $\zeta(P_{s,t}, r)$ of a candidate pixel $P_{s,t}$ is a set of all pixels $P_{x,y}$ such that $\zeta(P_{s,t}, r) = \{P_{x,y} \mid (d(P_{x,y}, P_{s,t}) \subseteq r) \wedge ((P_{x,y} \sim P_{s,t}) \leq T)\}$ where distance $d(P_{x,y}, P_{s,t}) = |x - s| + |y - t|$. $P_{x,y}$ is a 2D image pixel at Cartesian coordinate (x,y), and T is

1578

the threshold, which denotes the maximum pixel intensity variation of a region.

Now it is needed to define a membership function, which considers the number of neighborhood pixels and the distances between the neighbors and candidate pixel. A membership function μ of the spatial relation should possess two characteristics: $\mu \propto N$ where N denotes the number of neighbors and $\mu \propto \dfrac{1}{d(P_{x,y}, P_{s,t})}$.

The summation of inverse distances of a region R_j can be defined as

$$G_{R_j} = \sum_{i=1}^{N_j} \frac{1}{d_i(P_{x,y}, P_{s,t})} \tag{4}$$

Where $N_j = \left| \zeta(P_{s,t}, r) \right|$ = the number of neighborhood pixels of the candidate pixel $P_{s,t}$ in the region R_j and $d_i(P_{x,y}, P_{s,t})$ is the distance between the ith pixel $P_{x,y}$ of the region R_j & the candidate pixel $P_{s,t}$.

So considering the number of neighbors (N_j) and their sum of inverse distances (G_{R_j}) from the candidate pixel ($P_{s,t}$), the membership function $\mu_{NR_j}(P_{s,t}, r)$ of the region R_j can defined as

$$\mu_{NR_j}(P_{s,t}, r) = \frac{N_j \times G_{R_j}}{\sum_{j=1}^{\Re}(N_j \times G_{R_j})} \tag{5}$$

Where $\Re$ is the desired number of regions of an image.

3. FUZZY RULE DEFINITION

The effectiveness of the fuzzy rule plays the vital role for the segmentation result. In this paper, a fuzzy rule is heuristically defined using the three membership functions defined in section 2 and the most wide used fuzzy IF-THEN rule structure.

The overall membership value $\mu_{AR_j}(P_{s,t})$ of a pixel $P_{s,t}$ for the region R_j, which represent the overall degree of belonging to the region R_j, can be defined by the weighted average of the values of the membership functions $\mu_{DR_j}(P_{s,t})$, $\mu_{CR_j}(P_{s,t})$ and $\mu_{NR_j}(P_{s,t})$.

$$\mu_{AR_j}(P_{s,t}) = \frac{W_1\mu_{DR_j}(P_{s,t}) + W_2\mu_{CR_j}(P_{s,t}) + W_3\mu_{NR_j}(P_{s,t})}{W_1 + W_2 + W_3} \tag{6}$$

Where W_1, W_2 and W_3 represent the weight of the membership values for the pixel distribution, closeness to the cluster centers and neighbor relation respectively. The overall membership value $\mu_{AR_j}(P_{S,T})$ is used in the antecedent condition of IF THEN RULE and the rule can be defined as,

Definition 2 (Rule) IF $\mu_{AR_j}(P_{s,t})$ *supports region* R_j *THEN pixel* $P_{s,t}$ *belongs to region* R_j.

$\mu_{AR_j}(P_{s,t})$ will give support to the region R_j if

$$\mu_{AR_j}(P_{s,t}) = \max\{\mu_{AR_1}(P_{s,t}), \quad \mu_{AR_2}(P_{s,t}),...,\mu_{AR_{\Re}}(P_{s,t})\}$$

where $\Re$ indicates the number of region. As this is the only rule, it is generalized one and can be applied in any type of image.

4. EXPERIMENTS

The proposed system and FCM had been implemented using MATLAB 5.3.1 (The Mathworks, Inc.). Two types of images such as light intensity (LI) shown in figure 1 (a) and X-ray image of the human vocal tract shown in figure 4(a) were used in the experiments. For FCM, the initialization of the cluster center was done randomly. The maximum number of iterations, minimum amount of improvement and the value of the fuzzifier (m) were taken as 100, 0.00001 and 2 respectively. For our proposed system, GFRIS the membership function defined in section 2.1 was developed using the clusters produced by FCM and their center values were used to initialize the centers of the clusters required to define the membership function described in section 2.2. The values of weights and the threshold were determined empirically and taken as $W_1 = 1$, $W_2 = 2$, $W_3 = 1$, T=25, and $W_1 = 1$, $W_2 = 1.5$, $W_3 = 1$, T=30 for cloud and X-ray image of the human vocal tract respectively. The segmented results of the original cloud image (figure 1(a)) for two regions namely cloud (R_1) and urban scene (R_2) produced by FCM and GFRIS are graphically displayed in the figure 3.

(a): FCM for R_1	(b): FCM for R_2	(C): GFRIS for R_1 for r=1	(f):GFRIS for R_2 for r=1
(g): GFRIS for R_1 for r=2	(h): GFRIS for R_2 for r=2	(e): GFRIS for R_1 for r=4	(f): GFRIS for R_2 for r=4
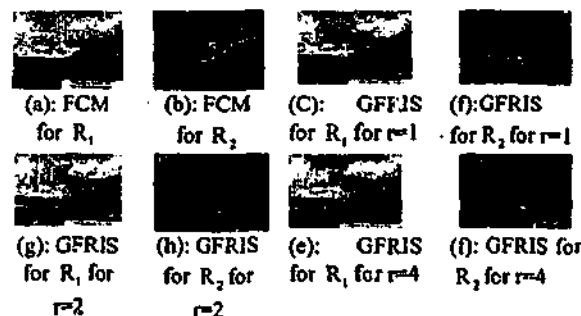
Figure 3: The segmented results of the cloud image into two regions produced by FCM and GFRIS

From the results it is visually shown that GFRIS separated almost the whole cloud from the image and produced significantly better results than FCM because FCM did not consider the spatial relationships among the pixels of a region. GFRIS also showed better results for larger values of neighborhood radius r, because the pixels of R_1 (cloud) are homogeneous and very much spatially correlated.

Another experiment was performed using an X-ray image of the human vocal tract shown in figure 4(a) and its segmentation results into two regions namely human vocal tract (R_1) and background (R_2) produced by FCM and GFRIS are presented in the figures 4(b) – 4(i). It is visually evident that the proposed technique GFRIS considerably outperformed FCM. There are no isolated pixels at all in the regions produced by GFRIS

whereas the regions (figures 4(b) -4(c)) produced by FCM contain significant amount of isolated pixels.

(a): X-ray image of human vocal tract

(b): FCM for R_1

(c): FCM for R_2

(d): GFRIS for R_1 for r=1

(e): GFRIS for R_2 for r=1

(f): GFRIS for R_1 for r=2

(g): GFRIS for R_2 for r=2

(h): GFRIS for R_1 for r=4

(i): GFRIS for R_2 for r=4
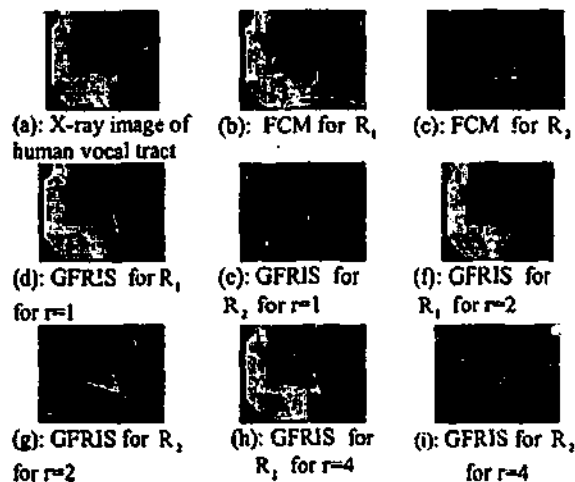
Figure 4: X-ray image of the human vocal tract and its results for two regions produced by FCM and GFRIS

This also ensures that the spatially related pixels had been classified successfully by GFRIS. The image shown in figure 3(a) contains two regions such as human vocal tract (lips, tongues, teeth) and background. The soft part of the human vocal tract is not clearly visible and has low local contrast pixels [14]. Almost the whole of the vocal tract had been successfully separated by GFRIS using r=4, which ensures the larger values of r, the better representation of the spatial relation. It also considered the underlying meaning of data better while FCM did not consider at all.

5. DISCUSSIONS AND CONCLUSION

In this paper a general fuzzy rule based image segmentation technique has been proposed. The proposed technique includes the spatial relationships among the pixels. It is also image and application independent like the standard fuzzy clustering algorithm FCM. The results have shown that it has represented the spatial relationships as well as the underlying meaning of the data better than FCM. Only one fuzzy rule is capable to classify all the pixels. The structures of the membership functions have been automatically derived and there is no need of defining the parameters. It is visually apparent that this system has shown promising result over FCM.

The values of the weighting factors W_1 & W_2, and W_3 imposes the importance of the feature based and spatial information. There is a trade-off between feature based and spatial information. It depends on the application, which one is assigned to how much importance. It is apparent that feature-based information should be given more emphasis than spatial information as it represents more human visual perspective than spatial information. Another parameter is the value of the threshold T, which represents the maximum amount of pixel intensity variation between neighbor and candidate pixels. It is intuitively determined that the suitable range of the value of W_2 and T are 1.5 to 2, and 25-30 respectively and others are 1.

It also needs more research for determining the suitable values of weighting factors and the threshold. As the proposed technique is fuzzy rule based technique, it is capable to incorporate any types of attributes of any special application. It is also possible to add membership function from the high level semantics of an object for object based image segmentation. Like FCM the proposed technique needs to provide the desired number of regions. It also needs more investigation for automatically determine the optimum number of regions.

6. REFERENCES

[1]   Tizhoosh, H.R. (1998). Fuzzy image processing, http://pmt05.et.uni-magdeburg.de/~hamid/- segment.html,.

[2]   Chi, Z.; Yan, H. and Pham, T.(1996). Fuzzy Algorithms: With Applications to Image Processing and Pattern Recognition. World Scientific Publishing Co. Pte. Ltd. Singapore.

[3]   Bezdek, J.C. (1981). Pattern Recognition with Fuzzy Objective Function Algorithms. New York: Plenum, 1981.

[4]   Krishnapuram, R. and Keller, J.(1993). A possibilistic approach to clustering. IEEE Transactions on Fuzzy Systems, 1, 98-110.

[5]   Chang, C.-W.; Ying, H.; Hillman, G.R.; Kent, T.A. and Yen, J. (1998). A rule-based fuzzy segmentation system with automatic generation of membership functions for pathological brain MR images. Computers and Biomedical Research, http://gopher.cs.tamu.edu/faculty/yen/publications/ index.html.

[6]   Chi, Z. and Yan, H. (1993). Segmentation of geographic map images using fuzzy rules. Conference Proceedings DICTA-93, Digital Image Computing, Techniques and applications, Australian Pattern Recognition Soc., 1, 95-101, Broadway, NSW, Australia.

[7]   Hall, L.O. and Namasivayam, A.(1998). Using adaptive fuzzy rules for image segmentation. FUZZ-IEEE'98, http://modem.csee.usf.edu/~hall/adrules/segment.html

[8]   Sasaki, T.; Hata, Y.; Ando, Y.; Ishikawa, M. and Ishikawa, H.(1999). Fuzzy rule based approach to segment the menisci region from MR images. In Proceedings of SPIE Medical Imaging, 3661, 258-, San Diego, California, USA

[9]   and Park, W.; Hoffman, E. A. (1998). Segmentation of intrathoracic airway trees: a fuzzy logic approach. IEEE Transactions on Medical Imaging, 17(4), 489-497.

[11]   Kellogg, C.B.; Zhao, F. and Yip, K.(1996). Spatial aggregation: language and applications. Proc. of AAAI-96. http://www.cis.ohio-state.edu/insight/pubs.html.

[12]   Tuceryan, M. Computational geometry. http://klingon.cs.iupui.edu/~tuceryan

[13]   Geman, S. and Geman, D.(1984). Stochas. Prentice Hall River, NJ 07458.

[14]   Howing, F.; Dooley, L.S. and Wermser, W.(1999). Computerized Med. Imaging and Graphics, 23, 59-67.

[15]   Karmakar, G.C. and Dooley, L.S. (2000). Generic fuzzy rule based image segmentation technique, Technical report series, August 6/2000, GSCIT, Monash University, Australia.

Analysis of Fuzzy Clustering and A Generic Fuzzy Rule Based Image Segmentation Technique

Gour C Karmakar and Laurence S Dooley
Email:{ Gour.Karmakar, Laurence.Dooley}@infotech.monash.edu.au
Gippsland School of Computing and Information Technology
Monash University, Churchill, Victoria, Australia - 3842

Abstract

Generic fuzzy rule based technique for image segmentation is a fuzzy rule based, application and image independent image segmentation technique. Fuzzy clustering algorithms are the most popular and widely used in image segmentation. This paper presents a rigorous performance analysis of fuzzy clustering algorithms and generic fuzzy rule based technique for image segmentation using light intensity and medical images. A quantitative evaluation is also conducted based on a standard segmentation evaluation technique called the empirical discrepancy method. Generic fuzzy rule based technique for image segmentation outperforms both fuzzy clustering algorithms FCM and PCM for both types of images. It also represents the underlying meaning of data better. PCM shows slightly better results and underlying structure of data than FCM.

Keywords: Fuzzy Rule, Image Segmentation, Fuzzy Clustering, and Generic.

1   Introduction

Classical so-called "crisp", image segmentation techniques while effective when an image contains well-defined structures, such as edges and regular shapes, do not perform nearly so well in the presence of ill-defined data. In such circumstances, the processing of such images that possess ambiguities produces fuzzy regions. Fuzzy image segmentation techniques can cope with the imprecise data well and they can be classified into five classes: fuzzy clustering, fuzzy rule based, fuzzy geometry, fuzzy thresholding, and fuzzy integral based image segmentation techniques [1] but among

them the most dominant are fuzzy clustering and fuzzy rule based segmentation techniques. The most popular and extensively used fuzzy clustering techniques are: fuzzy c-means (FCM) [2-3] and possibilistic c-means (PCM) algorithms [4]. Fuzzy rule based image segmentation techniques can incorporate human expert knowledge, are less computational expensive than fuzzy clustering and able to interpret linguistic as well as numeric variables [5]. But they are very much application dependent and very difficulty to define fuzzy rules that cover all of the pixels. In most techniques, the structures of the membership functions are predefined and their parameters are either manually or automatically determined [5-9]. Generic fuzzy rule based technique for image segmentation (GFRIS) is a general fuzzy rule based image segmentation technique, which is application and image independent. It also automatically derives the structures of the membership functions and incorporates the spatial relation information [10-11]. The performance evaluation of image segmentation is most critical task of computer vision system. This paper carries out an extensive comparative study of the performances of fuzzy clustering algorithms and generic fuzzy rule based technique for image segmentation. It employs the more suitable and better objectively assessing segmentation evaluation method, discrepancy based on the number of mis-segmented pixels, one of the empirical discrepancy methods [12] using two quite different types of images: light intensity and medical image (x-ray of human vocal tract).

Section 2 gives a brief of the technique of generic fuzzy rule based technique, and the underlying theoretical concepts of FCM and PCM. The techniques of evaluation and experimental results are given in section 3. Finally some conclusions are provided in section 4.

Background

A brief description on generic fuzzy rule based technique for image segmentation (GFRIS), fuzzy c-means and possibilistic c-means are given in the following sections.

Generic Fuzzy Rule Based Technique For Image Segmentation (GFRIS)

The GFRIS technique uses three types of membership functions to respectively represent the region pixel distributions, the closeness to their centres and the spatial relations among the pixels in a particular region. Each membership function possesses a membership value for every region, which indicates the degree of belonging to that particular region [10,11]. It also uses a single fuzzy rule. Details of the algorithm applied to automatically define the membership function and fuzzy rule are described in the following sections.

1.1 Membership Function for Region Pixel Distributions

This section outlines the stages used to automatically define the membership function including its structure from the region pixel distributions. The three steps required to define the membership function are: -

2 Classify the image into a desired number of regions using manual segmentation or automatically by applying any fuzzy clustering algorithms.

3 Generate the gray level pixel intensity histogram for each region and normalise the frequency for each gray level into the range [0 1].

4 Approximate the polynomial for each region. This polynomial represents the membership function for that particular region and the value of the polynomial for each gray level denotes the membership value of that particular gray level value.

The degree of belonging of a candidate pixel (the pixel to be classified) to a region is determined from the respective membership function. The membership function $\mu_{DR_j}(P_{s,t})$ of the region R_j for the pixel distribution is defined as

$$\mu_{DR_j}(P_{s,t}) = f_{R_j}(P_{s,t}) \tag{1}$$

where $f_{R_j}(P_{s,t})$ and $P_{s,t}$ are the polynomial of the region R_j and the pixel at position (s,t) respectively.

2.1.2 Membership Function to Measure the Closeness of the Region

This type of membership function represents the similarity between the candidate pixel and the centre of a region based on the gray level intensity, and is based upon a Euclidean distance measure. The degree of belongingness of a candidate pixel to a region is determined by following the strategy of k-means clustering algorithm. Candidate pixels join their nearest region and after joining, the centre of that particular region is recomputed. The centroid of a region R_j is defined as

$$C(R_j) = \frac{1}{N_j} \sum_{i=1}^{N_j} P_j(i) \tag{2}$$

where N_j and $P_j(i)$ represent the number of pixels and the ith pixel gray level intensity of the jth region respectively.

The membership function should reflect the axiom that " *the closer to a region, the larger the membership value a pixel should have*". So the membership function $\mu_{CR_j}(P_{s,t})$, which determines the degree of belongingness of a candidate pixel $P_{s,t}$ at a location (s,t) to a region R_j can be defined as

$$\mu_{CR_j}(P_{s,t}) = 1 - \frac{|C(R_j) - P_{s,t}|}{D} \tag{3}$$

where the constant D is defined as the difference between the maximum and minimum gray level intensity values of an image, so for an 8 bit gray scale image, $D=255$. The maximum value of the membership function will always be at the centre of the region and the structure of the membership function will be symmetrical about the vertical line that passes through the centre of the region.

2.1.3 Membership Functions for Spatial Relation

In the previous sections, the membership functions have been developed based only on feature values i.e. gray level intensities of a particular image, and thus did not consider any spatial relationships of the pixels within an identified region. Clearly, there is an expectation that strong spatial relationships will exist between neighbouring pixels within a region, while at the same time there also could be a considerable number of overlapping pixels between the regions. Good segmentation cannot therefore be expected unless these overlapping pixels are taken into account. By considering the neighbourhood relation between a candidate pixel and the classified pixels of the regions, the number of overlapping pixels can be reduced. Based on the neighbourhood relation the candidate pixel can be assigned to the appropriate group. In this paper, we concentrate especially on fixed size neighbourhoods around a candidate pixel. The neighbourhood configurations of the pixels for r=1, r=2 and r=4 are shown in the figures 1(a), (b) and (c) respectively, where O and # represent the candidate and neighbourhood pixels respectively.

```
        #               # # # # #
  #            # # #     # # # # #
# O #          # O #     # # O # #
  #            # # #     # # # # #
                         # # # # #

(a) r=1      (b) r=2      (c) r=4
```
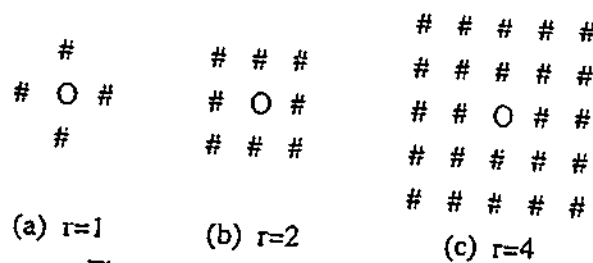
Figure 1: Neighbourhood system

The neighbourhood system of a region is defined as,

Definition 1 (Neighbourhood system) A neighbourhood system with radius r, $\zeta(P_{s,t},r)$ of a candidate pixel $P_{s,t}$ is a set of all pixels $P_{x,y}$ such that $\zeta(P_{s,t},r) = \{P_{x,y} \mid (d(P_{x,y},P_{s,t}) \le r) \wedge ((P_{x,y} \sim P_{s,t}) \le T)\}$ where distance $d(P_{x,y},P_{s,t}) = |x-s| + |y-t|$, $P_{x,y}$ is a 2D image pixel at Cartesian coordinate (x,y), r is the radius of the neighbourhood system, and T is the threshold.

The membership function $\mu_{SR_j}(P_{s,t},r)$ of the region R_j is defined as

$$\mu_{SR_j}(P_{s,t},r) = \frac{N_j \times G_{R_j}}{\sum_{j=1}^{\Re}(N_j \times G_{R_j})} \quad (4)$$

where $N_j = |\zeta(P_{s,t},r)|$ is the number of neighbourhood pixels of the candidate pixel $P_{s,t}$ in the region R_j, (G_{R_j}) is the sum of inverse pixel distances, and $\Re$ is the number of regions in an image to be segmented.

The membership function of a region defined in (4) considers the number of neighbours and their sum of inverse distances for all regions. The greater the number of neighbours in a region, the larger the value of the membership function will be for that region.

2.1.4 Fuzzy Rule Definition

The overall membership value $\mu_{AR_j}(P_{s,t})$ of a pixel $P_{s,t}$ for the region R_j, which represents the overall degree of belonging to the region R_j, can be defined by the weighted average of the values of the membership functions $\mu_{DR_j}(P_{s,t})$, $\mu_{CR_j}(P_{s,t})$ and $\mu_{SR_j}(P_{s,t})$.

$$\mu_{AR_j}(P_{s,t}) = \frac{W_1\mu_{DR_j}(P_{s,t}) + W_2\mu_{CR_j}(P_{s,t}) + W_3\mu_{SR_j}(P_{s,t})}{W_1 + W_2 + W_3} \quad (5)$$

where W_1, W_2 and W_3 are the weighting factors of the membership values for the pixel distribution, closeness to the cluster centres and neighbour relations respectively. The overall membership value $\mu_{AR_j}(P_{s,t})$ is used in the antecedent condition of the fuzzy IF-THEN rule, which is defined as,

Definition 2 (Fuzzy Rule) IF $\mu_{AR_j}(P_{s,t})$ supports region R_j THEN pixel $P_{s,t}$ belongs to region R_j

$\mu_{AR_j}(P_{s,t})$ will give support to the region R_j if $\mu_{AR_j}(P_{s,t}) = \max\{\mu_{AR_1}(P_{s,t}), \mu_{AR_2}(P_{s,t}), \ldots, \mu_{AR_\Re}(P_{s,t})\}$ where $\Re$ indicates the number of regions.

2.2 Fuzzy c-Means (FCM) Algorithm

FCM is the most popular fuzzy based clustering technique. Developed by Bezdek [3], it is still being used today in image segmentation. It performs classification based on the iterative minimization of the following objective function and associated constraints [2].

$$f_m(\mu, V, X) = \sum_{i=1}^{c} \sum_{j=1}^{n} (\mu_{ij})^m d(x_j, v_i)^2 \qquad (6)$$

$$0 \le \mu_{ij} \le 1 \quad i \in \{1..c\} \text{ and } j \in \{1..n\} \qquad (7)$$

$$\sum_{i=1}^{c} \mu_{ij} = 1 \quad j \in \{1..n\} \qquad (8)$$

$$0 < \sum_{j=1}^{n} \mu_{ij} < n \quad i \in \{1..c\} \qquad (9)$$

where c and n are the number of cluster and data respectively, μ is a fuzzy partition matrix containing membership values $[\mu_{ij}]$, V is a prototype vector containing the values of cluster centres $[v_i]$, m is the fuzzifier (1<m≤∞), d is the distance between x_j & v_i, and X is a data vector. The following two equations are derived after minimization of the function $f_m(\mu, V, X)$ in (6) with respect to μ and V.

$$\mu_{ij} = \frac{1}{\sum_{k=1}^{c} \left(\frac{d(x_j, v_i)}{d(x_j, v_k)} \right)^{2/(m-1)}} \qquad (10)$$

$$v_i = \frac{\sum_{j=1}^{n} (\mu_{ij})^m x_j}{\sum_{j=1}^{n} (\mu_{ij})^m} \qquad (11)$$

The set of cluster centres is initialised either randomly or by an approximation method. The membership values and cluster centres are updated through an iterative process until the maximum change in μ_{ij} becomes less than a predefined threshold. The selection of the value of m is important, as if m=1, then FCM produces a crisp instead of a fuzzy partitioning. Note, that if any of the distance values $d(x_j, v_i)$ is zero, then equation (11) is undefined.

2.3 Possibilistic c-Means (PCM) Algorithms

FCM arbitrarily divides the data set based on a selected number of clusters. The membership values generated by FCM represent the degrees of sharing. In order to eliminate the constraints in equation (8), Krishnapuram and Keller first introduced PCM whose membership values represent the degrees of typicality, instead of degrees of sharing and clusters are independent with each other [4,13]. They modified the FCM objective function and defined the PCM objective function as,

$$f_m(\mu, V, X) = \sum_{i=1}^{c} \sum_{j=1}^{n} (\mu_{ij})^m d^2(x_j, v_i) + \sum_{i=1}^{c} \eta_i \sum_{j=1}^{n} (1 - \mu_{ij}) \qquad (12)$$

with the constraints being

$$0 \le \mu_{ij} \le 1 \quad i \in \{1..c\} \text{ and } j \in \{1..n\} \qquad (13)$$

$$0 < \sum_{j=1}^{n} \mu_{ij} < n \quad i \in \{1..c\} \qquad (14)$$

$$\max \mu_{ij} > 0 \quad j \in \{1..n\} \qquad (15)$$

where η_i is the scale parameter, which determines the zone of influence of a point and other parameters are as defined in section 2.2. The following are obtained after minimizing the function $f_m(\mu, V, X)$.

$$\mu_{ij} = \frac{1}{1 + \left(\frac{d^2(x_j, v_i)}{\eta_i} \right)^{1/(m-1)}} \qquad (16)$$

$$v_i = \frac{\sum_{j=1}^{n} (\mu_{ij})^m x_j}{\sum_{j=1}^{n} (\mu_{ij})^m} \qquad (17)$$

The membership value (μ_{ij}) and prototype centre (v_i) are updated using the equations (16) and (17) through an iterative process. As with FCM, when fuzzifier m=1, PCM produces a crisp partition. PCM offers more promising results in presence of noise but it is highly dependent on initialisation and estimation of the scale parameters. The output of FCM can be

used for initialisation and scale estimation but FCM is very sensitive to noise. (

3 Experiments and Discussions

GFRIS, FCM, and PCM were implemented using MATLAB 5.3.1 and two different example images were used in the experiments, namely a gray scale image showing a cloud and urban scene shown in figure 2(a) and a medical X-ray image of the human vocal tract shown in figure 2(d).

(a) Cloud image   (b) Ref. image for cloud   (c) Ref. image for urban scene

(d) Human vocal tract   (e) Ref. image for vocal tract   (f) Ref. image for background
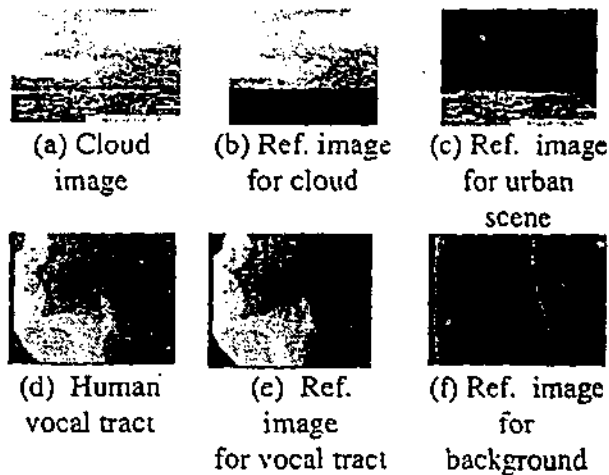
Figure 2: Original cloud and x-ray of human vocal tract and their reference images

For FCM the initialization of the cluster centre was performed randomly. The maximum number of iterations, the minimum level of improvement and the value of the fuzzifier (m) were empirically evaluated as 100, · 0.00001 and 2 respectively.

For PCM, the initialization of the cluster centres used the output of the FCM. The value of scale parameter η_i was taken as the variance of the cluster i produced by FCM [13].

For GFRIS, the membership function defined in section 2.1.1 was developed using the clusters produced by FCM and their centre values were used to initialise the centres of the clusters required to define the membership function, as described in section 2.1.2. The respective values of the weights and threshold were determined empirically as $W_1 = 1, W_2 = 2, W_3 = 1$, T=25, for the image in figure 2(a) and $W_1 = 1$, $W_2 = 1.5$, $W_3 = 1$, T=30 for the X-ray image in figure 2(d). The segmented results of the gray scale image for the two

regions (cloud, R_1 and urban scene, R_2) produced by FCM, PCM and GFRIS respectively are displayed in the figure 3.

(a) R_1 (b) R_2 (c) R_1 (d) R_2

(e) R_1 r=1   (f) R_2 r=1   (g) R_1 r=2   (h) R_2 r=2

(i) R_1 r=4   (j) R_2 r=4
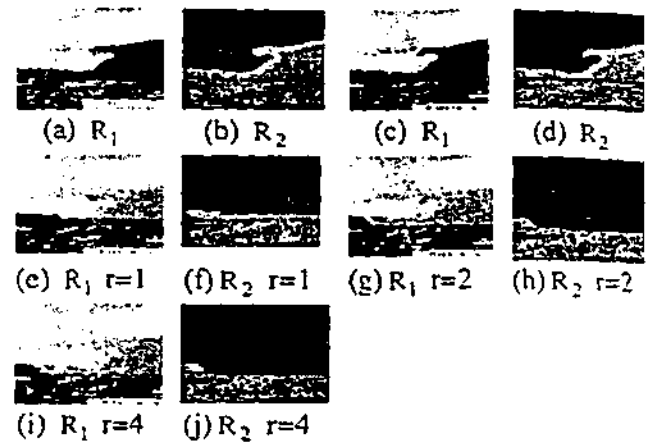
Figure 3: The segmented results of the cloud image with two regions by FCM ((a) and (b)), PCM ((c) and (d)) and GFRIS ((e) to (j))

The results clearly show that GFRIS separated almost all the cloud from the image and produced significantly better results than both FCM and PCM. FCM and PCM gave approximately equal performance since as alluded earlier, both techniques do not consider the spatial relationships between the pixels comprising each region. GFRIS also exhibited better results for larger values of neighbourhood radius r, because the pixels of region 1 (cloud) are homogeneous and possess very strong spatial correlation.

The quantitative evaluations were performed using one of the most powerful empirical discrepancy methods [12] based upon the number of wrongly segmented pixels. The confusion matrix C, is a $\Re$ by $\Re$ square matrix where $\Re$ represents the number of segmented region and C_{ij} denotes the number of jth region pixels classified as region i by segmentation. Type I error, *errorI* is defined as,

$$\text{errorI}_i = \frac{\left(\sum_{j=1}^{\Re} C_{ji} - C_{ii} \right)}{\sum_{j=1}^{\Re} C_{ji}} \times 100 \qquad (18)$$

while a Type II error, *errorII* is defined as,

$$errorII_i = \frac{\left(\sum\limits_{j=1}^{\Re} C_{ij} - C_{ii} \right)}{\left(\sum\limits_{i=1}^{\Re}\sum\limits_{j=1}^{\Re} C_{ij} - \sum\limits_{j=1}^{\Re} C_{ji} \right)} \times 100 \qquad (19)$$

The reference images in figure 2 were again used for evaluation purposes. The results of the cloud image segmentation with respect to reference images (figures 2(b) and 2(c)) are shown in Table 1.

Table 1: Percentage errors for cloud (region R_1) segmentation in figure 2(a).

Method	Error Type I	Error Type II
FCM	28.7335	17.4194
PCM	27.1375	18.3409
GFRIS r=1	8.8332	20.4783
GFRIS r=2	1.9749	21.4497
GFRIS r=4	2.0388	23.9742

In the above table, the image is segmented into two regions, so the error rates refer to incorrect segmentation for region R_1 (clouds). Since the error rate of one region will be the inverse of the error rate of other region, the results reveal that GFRIS provides superior performance for region R_1, which indicates that GFRIS successfully separated the cloud from the image and represents the underlying structure of data far better than FCM and PCM. The error rates of GFRIS for type II error are higher than for both PCM and FCM because the pixels in this region do not have good continuation i.e. they are abruptly changing, which oppose a strong spatial relation. In fact, the urban scene is not a single object. Good continuation is one of the seven properties of grouping of the visual elements [14]. The average error rates of the three techniques are shown in the figure 4.

This graph shows that the average error rates of GFRIS are much less than those of PCM and FCM. Average error rate of GFRIS for r=4 is higher than that of for r=2 because there is no sharp boundary between cloud and urban scene. For this case, GFRIS interpreted some sections of the urban scene as cloud for r=4. PCM again showed slightly better performance than FCM.
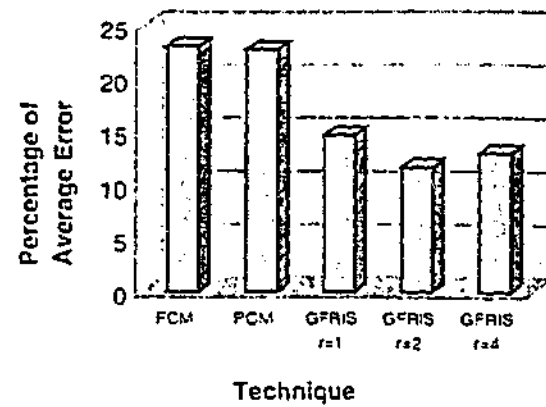
Figure 4: Average error rates of PCM. FCM and GFRIS for cloud image segmentation

A second series of experiments were performed using a medical x-ray image of the human vocal tract (figure 2(d)). The segmentation was again for two regions, namely the human vocal tract (region R_1, figure 2(e)) and general background (region R_2). The corresponding results produced by FCM, PCM and GFRIS are presented in figure 5.

(a) R_1 (b) R_2 (c) R_1 (d) R_2

(e) R_1 r=1   (f) R_2 r=1   (g) R_1 r=2   (h) R_2 r=2

(i) R_1 r=4   (j) R_2 r=4
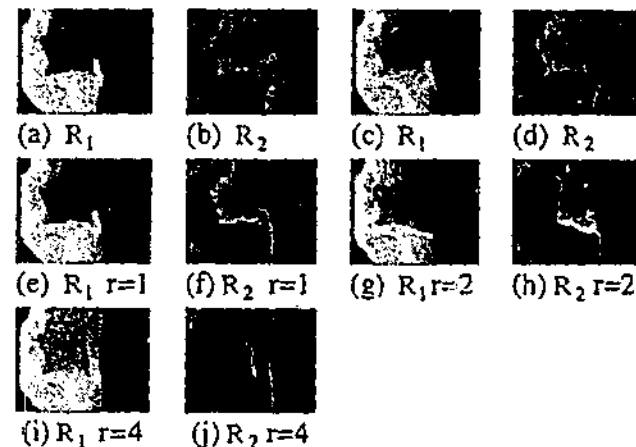
Figure 5: Segmented results of human vocal tract into two regions produced FCM ((a) and (b)), PCM ((c) and (d)) and GFRIS ((e) to (j))

It is visually evident that the proposed technique GFRIS considerably outperforms both the FCM and PCM techniques for this image type as well. The image (figure 2(d)) contains two regions, the vocal tract (comprising the lips, tongues, teeth, aural cavity) and general background. The soft part of the human vocal tract is not clearly visible and has low local contrast pixels [15]. Almost the entire vocal tract had been successfully separated by GFRIS using r=4, which confirms that the larger values of r, provide a better representation of the spatial relation.

Here PCM showed slightly better performance than FCM. The error rates of human vocal tract segmentation with respect to the reference images (figures 2(e) and 2(f)) are shown in the table 2. Both types of errors for human vocal tract segmentation are less than FCM and PCM except the error rate of error type II of GFRIS using r=4. This is caused by the fact there is good continuation of low contrast pixels of human vocal tract with the background and it takes some portion of the background as a part of human vocal tract for higher order of spatial relation i.e. r=4. The numerical results and average error rates of the human vocal tract segmentation are shown in Table 2 and figure 6 respectively.

Table 2: Error percentage for human vocal tract (region R_1) of x-ray of human vocal tract segmentation

Method	Error Type I	Error Type II
FCM	42.9797	7.5045
PCM	38.409	7.5716
GFRIS r=1	38.0529	7.477
GFRIS r=2	30.1424	7.47776
GFRIS r=4	3.903	14.5789

All the average error rates for GFRIS are less than those of FCM and PCM. The error rate is decreasing rapidly for higher orders of spatial relation, because the pixels of both regions are almost homogeneous. The error rate of FCM is higher than PCM.
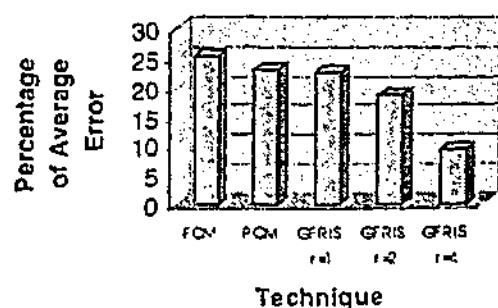
Figure 6: Average error rates of PCM, FCM and GFRIS for human vocal tract segmentation

For all of the above experiments the number of regions to be segmented was two. It is important however to use a larger number of regions in order to check the underlying meaning of data. To achieve this, another experiment was performed using the above techniques identifying three regions to be segmented. From the experimental results, it was shown that GFRIS considered the underlying meaning of data better than FCM and PCM and out performed both of them for both types of images for three regions. PCM again showed better underlying structure of the data than FCM for both types of images when three regions were to be segmented

4   Conclusions

In this paper both quantitative and qualitative performance analysis of FCM, PCM and GFRIS have been performed based on the standard segmentation evaluation method, empirical discrepancy method using two different types of images. Both results proved that generic fuzzy rule based technique for image segmentation (GFRIS) provided significantly better results than either FCM or PCM. The reasons for this are that GFRIS has considered spatial relationships very well and hence represented the underlying meaning of data better than both FCM and PCM. PCM has considered the underlying structure of data in some extent but FCM has arbitrarily divided the data into region without considering any underlying meaning of data.

The values of the weighting factors W_1, W_2, and W_3 of GFRIS were determined empirically. More research needs to be undertaken in order to determine the suitable values of both the three weighting factors as well as the threshold.

Finally, as the proposed technique is fuzzy rule-based, it is capable of incorporating any type of attribute of any special application. It is thus possible to add membership functions from the high level semantics of an object for object-based image segmentation, such as in MPEG-4 applications. Like FCM and PCM, the GFRIS technique needs to be provided with the desired number of regions to be segmented. It also needs further investigation for automatically determining the optimal number of regions.

References

[1] H.R. Tizhoosh, "Fuzzy image processing" http://pmt05.et.uni-magdeburg.de/~hamid/-segment.html, 1998.

[2] Z. Chi, H. Yan, T. Pham, "Fuzzy Algorithms: With Applications to Image Processing and Pattern Recognition" World Scientific Publishing Co. Pte. Ltd. Singapore, 1996.

[3] J.C. Bezdek, "Pattern Recognition with Fuzzy Objective Function Algorithms" New York: Plenum, 1981.

[4] R. Krishnapuram, J. Keller, "A possibilistic approach to clustering" IEEE Transactions on Fuzzy Systems, 1, 98-110,1993.

[5] C.-W. Chang, H.Ying, G.R. Hillman, T.A. Kent, J. Yen, "A rule-based fuzzy segmentation system with automatic generation of membership functions for pathological brain MR images" Computers and Biomedical Research, http://gopher.cs.tamu.edu/faculty/yen/publications/index.html, 1998.

[6] Z. Chi, H. Yan, " Segmentation of geographic map images using fuzzy rules" Conference Proceedings DICTA-93, Digital Image Computing, Techniques and applications, Australian Pattern Recognition Soc., 1, 95-101, Broadway, NSW, Australia,1993.

[7] L.O. Hall, A. Namasivayam, "Using adaptive fuzzy rules for image segmentation" FUZZ-IEEE98, http://modern.csee.usf.edu/ ~hall/adrules/segment.html, 1998.

[8] T. Sasaki, Y. Hata, Y. Ando, M. Ishikawa, H. Ishikawa."Fuzzy rule based approach to segment the menisci region from MR images" In Proceedings of SPIE Medical Imaging, 3661, 258-, San Diego, California, USA, 1999.

[9] W. Park, E. A. Hoffman, "Segmentation of intrathoracic airway trees: a fuzzy logic approach" IEEE Transactions on Medical Imaging, 17(4), 489-497, 1998.

[10] G.C. Karmakar, L.S. Dooley, "Generic fuzzy rule based image segmentation technique" Technical Report Series, August 6/2000, GSCIT, Monash University, Australia, 2000.

[11] G.C. Karmakar, L. Dooley, "Generic fuzzy rule based technique for image segmentation" IEEE International Conference on Acoustics, Speech, and Signal Processing, May 7-11, Salt Lake City, Utah, 2001, (accepted).

[12] Y.J. Zhang, "A survey on evaluation methods for image segmentation" Pattern Recognition, 29, 8, 1335-1346, 1996.

[13] R. Krishnapuram, J.M. Keller, "The possibilistic c-means algorithm: insight and recommendations" IEEE Transactions on Fuzzy Systems, 4(3), 385-393, 1996.

[14] M. Wertheimer, "Laws of organization in perceptual forms" Pshychologische Forschung, 6, 1923.

[15] F. Howing, L.S. Dooley, W. Wermser, "Tracking of non-rigid articulatory organs in X-ray image sequences" Computerized Medical Imaging and Graphics, 23, 59-67, 1999.

EXTENDED FUZZY RULES FOR IMAGE SEGMENTATION

Gour C Karmakar and Laurence S Dooley
Email:{ Gour.Karmakar, Laurence.Dooley}@infotech.monash.edu.au

Gippsland School of Computing and Information Technology

Monash University, Churchill, Victoria, Australia - 3842

ABSTRACT

The generic fuzzy rule-based image segmentation technique (GFRIS) does not produce good results for non-homogeneous regions that possess abrupt changes in pixel intensity, because it fails to consider two important properties of perceptual grouping, namely surroundedness and connectedness. In this paper a new technique called extended fuzzy rules for image segmentation (EFRIS) is proposed, which includes a second rule to that defined already in GFRIS, that incorporates both the surroundedness and connectedness properties of a region's pixels. This additional rule is based on a spilt and merge algorithm and refines the output from the GFRIS technique. Two different classes of image, namely light intensity and medical X rays are empirically used to assess the performance of the new technique. Quantitative evaluation of the performance of EFRIS is discussed and contrasted with GFRIS using one of the standard segmentation evaluation methods. Overall, EFRIS exhibits significantly improved results compared with the GFRIS approach.

1. INTRODUCTION

Image segmentation is the most important and difficult task of digital image processing and analysis systems, due to the potentially inordinate number of objects and the myriad of variations among them. The most intractable task is to define their properties for perceptual grouping, a demand that requires human expert knowledge be incorporated to achieve a superior segmentation result. Fuzzy rule-based image segmentation systems can incorporate this expert knowledge, but are very much application domain and image dependent. The structures of all of the membership functions are manually defined and their parameters are either manually or automatically derived [1-5]. Karmakar and Dooley [6-8] proposed a novel generic fuzzy rule based technique for image segmentation (GFRIS) by addressing these aforementioned problems. The technique however, does not work very well for image regions that are non-homogeneous and have sharp variations in pixel intensity. The eminent psychologist Gestalt stated that visual elements are grouped perceptually upon the principles of: proximity, closure, similarity, good continuation, common fate, surroundedness, relative size and symmetry [9]. The proximity, similarity and good continuation elements are all reflected in GFRIS. In this paper an extended fuzzy rule-based image segmentation (EFRIS) technique is proposed by integrating a rule, based upon the surroundedness and connectedness properties of region's pixels in combination with the GFRIS rule. The performance analysis of both methods is conducted by applying a superior objective segmentation evaluation technique called the "*discrepancy based on the number of mis-segmented pixels*", which is one of the powerful empirical discrepancy methods [10]. This method is subsequently applied to two different classes of image: light intensity and medical x-ray of the human vocal tract.

Section 2 provides a brief overview of the technique used to define the fuzzy rules. The processing steps of the proposed methods are presented in sections 3. The evaluation and experimental results are discussed in section 4, with conclusions provided in section 5.

2. FUZZY RULES

Two fuzzy rules are used for two different purposes. The first represents the similarity, proximity, good continuation and spatial information of a region, while the second considers the surroundedness and connectedness of a region's pixels. Both rules are described in the following sections.

2.1. First Rule

Full details of this rule and its membership functions are given in [6-8]. It uses three membership functions to represent the region pixel distribution ($\mu_{DR_j}(P_{s,t})$), closeness of a region ($\mu_{CR_j}(P_{s,t})$), and spatial information among region pixels ($\mu_{NR_j}(P_{s,t})$). Here μ, R_j, and $P_{s,t}$ are the membership function, j^{th} region and the pixel at location (s,t) respectively. The two membership functions $\mu_{DR_j}(P_{s,t})$ and $\mu_{CR_j}(P_{s,t})$ represent the similarity based on gray level pixel distribution and intensity respectively, while the third $\mu_{NR_j}(P_{s,t})$ characterizes the proximity, good continuation and spatial information of a region. The overall membership value $\mu_{AR_j}(P_{s,t})$ of a pixel $P_{s,t}$ for the region R_j, which represents the overall degree of belonging to the region R_j, is defined by the weighted average of the values of the three membership functions $\mu_{DR_j}(P_{s,t})$, $\mu_{CR_j}(P_{s,t})$, and $\mu_{NR_j}(P_{s,t})$.

$$\mu_{AR_j}(P_{s,t}) = \frac{W_1\mu_{DR_j}(P_{s,t}) + W_2\mu_{CR_j}(P_{s,t}) + W_3\mu_{NR_j}(P_{s,t})}{W_1 + W_2 + W_3} \quad (1)$$

where W_1, W_2 and W_3 represent the weightings given to the respective membership values for pixel distribution, closeness to the cluster centres and neighborhood relation. The rule is defined as:-

Definition 1 (First Rule) IF $\mu_{AR_j}(P_{s,t})$ *supports region* R_j *THEN pixel* $P_{s,t}$ *belongs to region* R_j.

$\mu_{AR_j}(P_{s,t})$ will give support to the region R_j if

$$\mu_{AR_j}(P_{s,t}) = \max\{\mu_{AR_1}(P_{s,t}), \quad \mu_{AR_2}(P_{s,t}), ..., \mu_{AR_{\Re}}(P_{s,t})\}$$

where $\Re$ indicates the number of regions.

2.2. Second Rule

The second rule deals specifically with two perceptual properties of a region, namely surroundedness and connectedness. This rule is pipelined with the above rule, so that its output is refined using the surroundedness and connectivity properties of a region based on the split and merge algorithm. If the segmented regions produced by the first rule are denoted as R_j where $j=1...\Re$, then all segmented regions (every R_j) are split into a number of objects using 4-connected neighborhood property. Following the splitting, region $R_j = \{O_{1j}, O_{2j}, ..., O_{n_j j}\}$ is a set of objects where $O_{1j} \cap O_{2j} \cap, ..., \cap O_{n_j j} = 0$ and n_j represents the number of 4-connected neighborhood objects in region R_j. The main object of a region $R_j, O_{m_j j} = O_{ij}$ for $|O_{ij}| = \max\{|O_{1j}|, |O_{2j}|, ..., |O_{n_j j}|\}$ where $| \ |$ is the cardinality of a set i.e. the number of pixels belonging to an object. The membership function for the surroundedness of an object (O_{ij}) surrounded with a main object ($O_{m_k k}$) is then defined as:-

$$\mu_{SO_{ij}}(O_{ij}, O_{m_k k}) = \frac{\eta_{ij}}{|O_{ij}|} \tag{2}$$

where η_{ij} is the number of pixels of an object O_{ij}, inside the main object $O_{m_k k}$. The contour of the main object is determined by constructing the convex hull for that object. The merging operation is performed by the following rule:-

Definition 2 (Second Rule) IF $\mu_{SO_{ij}}(O_{ij}, \underbrace{O_{m_k k}}_{i \neq m_j \wedge k \neq j}) \geq$ Th *AND*

O_{ij} *is 8-connected neighborhood with* $\underbrace{O_{m_k k}}_{i \neq m_j \wedge k \neq j}$ *THEN* O_{ij}

merges with $\underbrace{O_{m_k k}}_{i \neq m_j \wedge k \neq j}$.

Where $i \neq m_j \wedge k \neq j$ ensures that an object O_{ij} is not a main object of its region R_j and merges with a main object of another region. Th is a threshold, which defines the degree of surroundedness used in the experiments.

3. SEGMENTATION STEPS

The segmentation consists of the following steps:-

Step 1: The image is initially segmented using the first rule.

Step 2: Each segmented region is spilt into a number of objects based upon 4- connected neighborhood. The main object, which is the object that contains the maximum number of pixels of each region, is then determined.

Step 3: Objects are merged with a main object of other regions based on the second rule (see section 2.2). Once an object is merged, the merging algorithm repeats for all other objects belonging to the same region that were previously surrounded and not connected to the main region.

4. EXPERIMENTAL RESULTS

Both the new EFRIS and GFRIS systems were implemented using MATLAB 5.3.1 (The Mathworks, Inc.). Two different image types were used in the experiments, namely a light intensity gray-scale image shown in figure 1(a) which comprises one homogeneous and one non-homogeneous region, and a medical X-ray of the human vocal tract shown in figure 1(d), which contains two separate homogeneous regions.
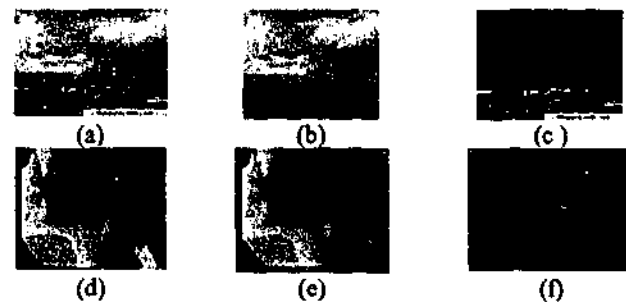
Figure 1: Original cloud scene, X-ray of the human vocal tract and their reference images: (a) Cloud image, (b) Ref: image for cloud, (c) Ref: image for urban scene, (d) Human vocal tract, (e) Ref: image for vocal tract, (f) Ref: image for the background

As alluded previously, quantitative evaluation of the segmentation process was achieved using discrepancy based on the number mis-segmented pixels [10]. The confusion matrix C, is an $\Re$ by $\Re$ square matrix where $\Re$ represents the number of segmented regions and C_{ij} denotes the number of jth region pixels classified as region i by the segmentation process. For the ith region, type I error, errorI$_i$ and type II error, errorII$_i$ are defined as:-

$$\text{errorI}_i = \frac{\left(\sum_{j=1}^{\Re} C_{ji} - C_{ii}\right)}{\sum_{j=1}^{\Re} C_{ji}} \times 100 \tag{3}$$

$$\text{errorII}_i = \frac{\left(\sum_{j=1}^{\Re} C_{ij} - C_{ii} \right)}{\left(\sum_{i=1}^{\Re} \sum_{j=1}^{\Re} C_{ij} - \sum_{j=1}^{\Re} C_{ji} \right)} \times 100 \qquad (4)$$

For both GFRIS and EFRIS, the membership function for region pixel distribution $\mu_{DR_j}(P_{s,t})$ was developed using the clusters produced by the fuzzy c-means (FCM) algorithm [11] and their centre values were used to initialize the centres of the clusters required to define the membership function for closeness of a region ($\mu_{CR_j}(P_{s,t})$). The values of weights and the threshold were empirically determined as $W_1 = 1$, $W_2 = 2$, $W_3 = 1$, T=25, and $W_1 = 1$, $W_2 = 1.5$, $W_3 = 1$, T=30 for the cloud and human vocal tract images respectively. The neighborhood radius (r) was taken as 1, 2 and 4. The threshold Th was empirically selected as 0.8. The segmented results of the cloud image (figure 1(a)) into two regions namely, the homogenous clouds (R_1) and non-homogenous urban scene (R_2) produced by GFRIS and EFRIS are shown in figure 2.

(a): R_1, r=1   (b): R_2, r=1   (c): R_1, r=2   (d): R_2, r=2

(e): R_1, r=4   (f): R_2, r=4   (g): R_1, r=1   (h): R_2, r=1

(i): R_1, r=2   (j): R_2, r=2   (k): R_1, r=4   (l): R_2, r=4
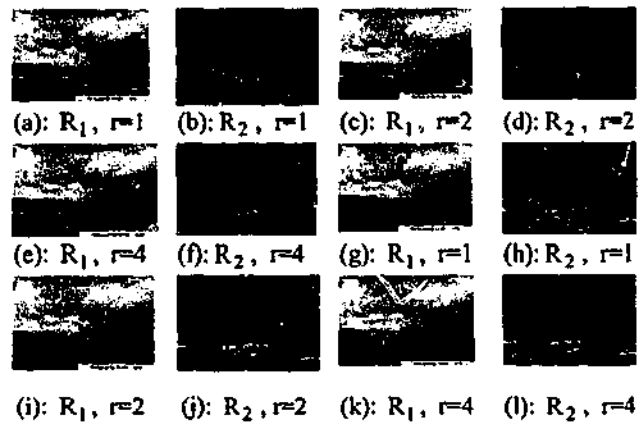
Figure 2: The segmented results of the cloud image into two regions by GFRIS (a) to (f) and EFRIS (g) to (l)

The numerical segmentation results of cloud image segmentation with respect to reference images (figures 1(b) and 1(c)) are shown in the following table 1.

Table 1: Error percentage for cloud (region R_1) of cloud image segmentation

| Method	Error I	Error II	Method	Error I	Error II
GFRIS r=1	8.8332	20.4783	EFRIS r=1	8.8332	12.9107
GFRIS r=2	1.9749	21.4497	EFRIS r=2	1.9749	13.4333
GFRIS r=4	2.0388	23.9742	EFRIS r=4	2.0308	17.7535

In table 1, only the error rates for region R_1 are shown since the error rates of the other region R_2 will simply be the reverse order of region R_1. The segmentation results for the cloud image using GFRIS show that region R_1 i.e. cloud (figures 2(a), 2(c) and 2(e)) contains a large number of misclassified pixels from region R_2, the non-homogeneous urban scene region, which has sharp variations in pixel intensity. Type II error rates for region R_1 using GFRIS (Table 1) are higher than type I error rates. Almost all of the misclassified pixels, except the text caption were correctly classified using the second rule of EFRIS (figures 2(g)-2(l)). The type I errors of region R_1 for EFRIS were caused almost exclusively by the text caption. The average error rates for both techniques are graphically shown in figure 3.
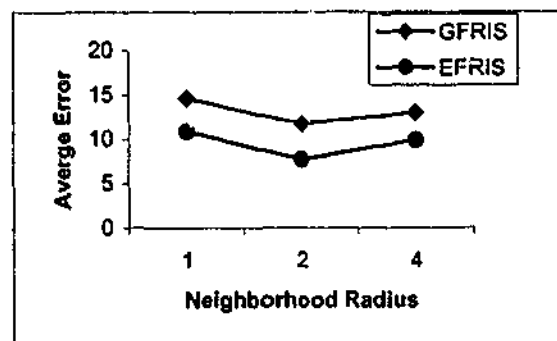
Figure 3: Average error rates of GFRIS and EFRIS for cloud image segmentation

From figures 2 and 3, it is clear that EFRIS achieved significant improvements over the GFRIS approach. The average error rates of both techniques for r=4 are higher than that for r=2 because there is no sharp boundary between cloud and urban scene. As a result, some portions of the urban scene have been interpreted as part of the cloud segment for higher orders (r=4) of spatial information.

A second series of experiments was performed using a medical X-ray image of the human vocal tract (figure 1(d)). The segmentation results for the two separate regions namely, the human vocal tract R_1, figure 1(e)) and background (R_2), produced by both GFRIS and EFRIS are given in figure 4.

(a): R_1, r=1   (b): R_2, r=1   (c): R_1, r=2   (d): R_2 r=2

(e): R_1, r=4   (f): R_2, r=4   (g): R_1, r=1   (h): R_2, r=1

(i): R_1, r=2   (j): R_2, r=2   (k): R_1, r=4   (l): R_2, r=4
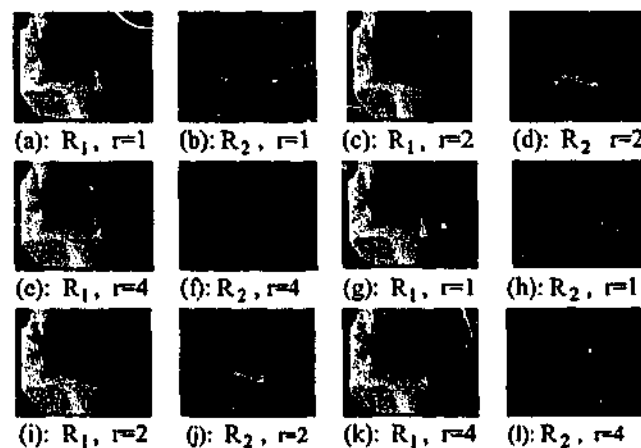
Figure 4: Segmented results of human vocal tract into two regions produced by GFRIS (a) to (f) and EFRIS (g) to (l)

The error and average error rates of human vocal tract segmentation with respect to the reference images (figures 1(e) and 1(f)) are shown in Table 2 and figure 5 respectively. The segmented results (figures 4(g)-4(j) and Table 2) using EFRIS for r=1 and r=2 are not significantly better compared with GFRIS, because there are no meaningful objects of a region that are surrounded and connected with other region and vice versa. EFRIS demonstrated superior performance compared with GFRIS for r=4, as depicted in figures 4(k), 4(l) and 5.

Table 2: Error percentage for human vocal tract (region R_1) of x-ray of human vocal tract segmentation

Method	Error I	Error II	Method	Error I	Error II
GFRIS r=1	38.0529	7.477	EFRIS r=1	37.7601	7.4734
GFRIS r=2	30.1424	7.47776	EFRIS r=2	29.7274	7.4772
GFRIS r=4	3.903	14.5789	EFRIS r=4	1.9118	14.3982

GFRIS was unable to separate a small section of the human vocal tract (figures 4(e) and 4(f)) because of the very low pixel contrast, however EFRIS was able to successfully separate the entire human vocal tract (figure 4(k)).
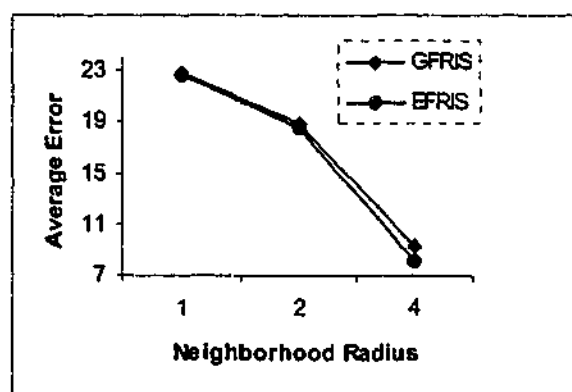
Figure 5: Average error rates of GFRIS and EFRIS for human vocal tract segmentation

Both the error and average error rates decrease rapidly for higher order of spatial information because the both regions are homogeneous.

5. CONCLUSIONS

This paper has outlined the development of a generic fuzzy rule-based image segmentation technique by incorporating two of the most important perceptual properties of region grouping namely, surroundedness and connectedness. A new technique called the extended fuzzy rules for image segmentation (EFRIS), has been proposed and both a quantitative and qualitative analysis undertaken to compare it with the generic approach (GFRIS). The experimental results have shown that EFRIS outperformed GFRIS, despite being more computationally expensive because of the additional rule integrated into the GFRIS model. The weighting factors and the thresholds were empirically determined, though a fully automated technique is currently being developed to determine these parameters. Since the proposed technique is fuzzy rule based, it is capable of incorporating any type of attribute of any special application domain. It is possible to add membership functions for high level semantics of an object for object based image segmentation. More research however is required in order to automatically determine the explicit number of regions in an image.

ACKNOWLEDGEMENT

REFERENCES

[1] C.-W. Chang, H. Ying, G.R. Hillman, T.A. Kent, and J. Yen, "A rule-based fuzzy segmentation system with automatic generation of membership functions for pathological brain MR images", Computers and Biomedical Research, 1998, http://gopher.cs.tamu.edu/faculty/yen/publications/index.html.

[2] Z. Chi, and H. Yan, "Segmentation of geographic map images using fuzzy rules", Proceedings of DICTA-93, Digital Image Computing, Techniques and applications, Australian Pattern Recognition Soc., 1, 95-101, Broadway, NSW, Australia, 1993.

[3] L.O. Hall, and A Namasivayam, "Using adaptive fuzzy rules for image segmentation", FUZZ-IEEE'98, 1998, http://modern.csee.usf.edu/~hall/adrules/segment.html

[4] T. Sasaki, Y. Hata, Y. Ando, M. Ishikawa, and H. Ishikawa, "Fuzzy rule based approach to segment the menisci region from MR images", Proceedings of SPIE Medical Imaging, 3661, 258-, San Diego, California, USA, 1999.

[5] W. Park, E. A. Hoffman, and M. Sonka, "Segmentation of intrathoracic airway trees: a fuzzy logic approach", IEEE Transactions on Medical Imaging, 17(4), 489-497, 1998.

[6] G.C Karmakar,. and L.S. Dooley, "Generic fuzzy rule based image segmentation technique", Technical report series, August 6/2000, GSCIT, Monash University, Australia, 2000.

[7] G.C. Karmakar, and L. Dooley, "Generic fuzzy rule based technique for image segmentation", IEEE International Conference on Acoustics, Speech, and Signal Processing, Salt Lake City, Utah, May 7-11, 2001. Accepted for publication.

[8] G.C. Karmakar, and L. S. Dooley, "Analysis of fuzzy clustering and a generic fuzzy rule based image segmentation technique", International Conference on Intelligent Multimedia and Distance Education, Fargo, North Dakota, USA, June 1-3, 2001. Accepted for publication.

[9] M. Wertheimer, "Laws of organization in perceptual forms", Pshychologische Forschung, 6, 1923.

[10] Y.J. Zhang, "A survey on evaluation methods for image segmentation", Pattern Recognition, 29, 8, 1335-1346, 1996.

[11] J.C. Bezdek, "Pattern Recognition with Fuzzy Objective Function Algorithms", New York: Plenum, 1981.

PHYSICAL AND LOGICAL STRUCTURE OF PRINTED BILINGUAL DICTIONARY ITEMS: LINGUISTIC REPRESENTATION AND RECOGNITION

Song Mao, University of Maryland at College Park, United States; Tapas Kanungo, IBM Almaden Research Center, United States

Parsing bilingual dictionaries is important for building cross-language retrieval systems and speech recognition algorithms. We describe a general purpose algorithm that can be easily modified to convert printed bilingual dictionaries in various layouts and language pairs into electronic/symbolic lexicons. In a previous paper [SPIE Document Recognition and Retrieval, San Jose, January 2002], we described an algorithm for segmenting the physical layout of dictionaries into columns and lines. In this paper we assume that the physical lines are given then recognize the lines that constitute a dictionary item. Furthermore, the algorithm simultaneously recognizes the logical structure within the dictionary items (head-word, pronounciation, part of speech and definition). We demonstrate our algorithm on 30 scanned Chinese-English dictionary pages which include more than 2500 lexicon items.

NEW FUZZY RULES FOR IMPROVED IMAGE SEGMENTATION

Gour Karmakar; Laurence Dooley; Manzur Murshed, Monash University, Australia

The extended fuzzy rules for image segmentation (EFRIS) algorithm initially splits all segmented regions into mutually exclusive 4-connected objects, from which the largest one in each region is designated as its main object. A drawback of this approach is that it is less effective when the main objects are relatively small and some of the minor objects are completely surrounded and connected to the main object of another region. Besides, defining insufficient merging rules, EFRIS also only considers the surrounding main objects in the original order that the regions were segmented, which is undesirable. In this paper, a new general segmentation algorithm called modified extended fuzzy rules for image segmentation (MEFRIS) is presented, which addresses these problems and whose improved segmentation performance is analysed and numerically evaluated. The results are also contrasted with both the original generic fuzzy rule-based image segmentation (GFRIS) and EFRIS algorithms.

DSP CONTROLLED LOW-VOLTAGE HIGH-CURRENT FAST-TRANSIENT VOLTAGE REGULATOR MODULE

Jaber Abu-Qahouq; Nattorn Pongratananukul; Issa Batarseh; Takis K   paris, University of Central Florida, United States

Future generation of microprocessors will require high performance Voltage Regulator Modules (VRMs) that produce tightly regulated low supply voltage with very small deviation window and able to respond very quickly to a large and continuous load transients at high output current while maintaining a high power density. On one hand, the current drawn from the VRM by the microprocessor is continuously changing since it depends at the current use of the microprocessor. On the other hand, High Frequency VRMs as any Power Electronics System is a complex combination of linear, nonlinear, and switching elements that is required to have fast dynamics. Moreover, this complex combination is also real-time system that needs to continuously and instantly monitor and respond to the load changes (the microprocessor). A high performance basic control loop is essential to follow up with such transients. Such controller design is usually complicated especially since it requires high knowledge of the converter and its behavior and accurate converter model that includes nonlinearities and parameters and components variations. DSP has many advantages over the analog circuits when it comes to applying high performance sophisticated control techniques such the simplicity in applying sophisticated control algorithms and modifying them via software revision, lower environmental and noise sensitivity, and less components count. In this paper, a DSP setup to be

FUZZY RULE FOR IMAGE SEGMENTATION INCORPORATING TEXTURE FEATURES

Gour Karmakar, Laurence Dooley, and Manzur Murshed
Email: {Gour.Karmakar, Laurence.Dooley, Manzur.Murshed}@infotech.monash.edu.au

Gippsland School of Computing and Information Technology

Monash University, Churchill, Victoria, Australia - 3842

ABSTRACT

The generic fuzzy rule-based image segmentation algorithm (GFRIS) does not produce good results for images containing non-homogeneous regions, as it does not directly consider texture. In this paper a new algorithm called fuzzy rules for image segmentation incorporating texture features (FRIST) is proposed, which includes two additional membership functions to those already defined in GFRIS. FRIST incorporates the fractal dimension and contrast features of a texture by considering image domain specific information. Quantitative evaluation of the performance of FRIST is discussed and contrasted with GFRIS using one of the standard segmentation evaluation methods. Overall, FRIST exhibits considerable improvement in the results obtained compared with the GFRIS approach for many different image types.

1. INTRODUCTION

Image segmentation is the most important and difficult task of digital image processing and analysis systems, due to the potentially inordinate number of objects and the myriad of variations among them. The most intractable task is to define their properties for perceptual grouping, a demand that requires human expert and/or domain specific knowledge to be incorporated to achieve a superior segmentation result. Fuzzy rule-based image segmentation systems can incorporate this expert knowledge, but they are very much application domain and image dependent. The structures of all of the membership functions are manually defined and their parameters are either manually or automatically derived [1]-[5]. Karmakar and Dooley [6][7] proposed a novel *generic fuzzy rule based image segmentation* (GFRIS) algorithm to address the aforementioned problems. This algorithm however, does not work well for images containing texture, which is for regions that are non-homogeneous and have sharp variations in pixel intensity. Texture is one of the most important attributes of any image that represents the structural arrangements of the surface as well as the relations among them and is widely used in image segmentation [8]. In this paper a new algorithm, *fuzzy rules for image segmentation incorporating texture features* (FRIST) is proposed by integrating two new membership functions into the set of GFRIS membership functions, based upon the texture features of fractal dimension and contrast. These additional membership functions consider the image domain specific

information. The performance analysis of both the GFRIS and FRIST is conducted by applying a superior objective segmentation evaluation technique called the *discrepancy based on the number of mis-segmented pixels* [9]. The new algorithm is subsequently applied to many different types of images.

The remainder of the paper is organized as follows. Section 2 provides a brief overview of the techniques used to define the membership functions. The definition of the fuzzy rule, and also the determination of the weighting factors and threshold used are presented in Sections 3 and 4 respectively. The evaluation and experimental results are discussed in Section 5, with conclusions provided in Section 6.

2. MEMBERSHIP FUNCTIONS

The GFRIS algorithm uses three types of membership functions to represent the region pixel distributions, the closeness to their centres and the spatial relations among the pixels in a particular region. Each membership function possesses a membership value for every region, which indicates the degree of belonging to that particular region. Full details of these membership functions are given in [6][7]. For the sake of completeness, a brief description of them is now provided.

The approach adopted for the membership function for region pixel distributions is to automatically define the membership function, including its structure from the pixel distributions of a region. This is obtained from the initial segmentation results of the respective region and a polynomial approximation of the pixel distribution of each region. The membership value of a pixel at location (s,t), having a gray level value of $P_{s,t}$ in region R_j is defined as: -

$$\mu_{DR_j}(P_{s,t}) = f_{R_j}(P_{s,t}) \tag{1}$$

where $f_{R_j}(P_{s,t})$ is the polynomial for the region R_j.

The membership function to measure the closeness of a pixel to a region represents the similarity between the pixel to be classified, called the candidate pixel, and the centre of a region based on the gray level intensity. The membership function reflects the axiom that *the closer to a region, the larger the membership value of the candidate pixel* and is defined as: -

$$\mu_{CR_j}(P_{s,t}) = 1 - \left|C(R_j) - P_{s,t}\right|/(2^b - 1) \tag{2}$$

where $C(R_j)$ is the centre of the region R_j, it is assumed that a b-bit gray scale image is used.

The membership function for spatial relations $\mu_{NR_j}(P_{s,t},r)$ of the region R_j for the neighbourhood radius r represents the spatial relations between the candidate pixel $P_{s,t}$ and its neighbours, and with a total of $\Re$ segmented image regions, is defined as: -

$$\mu_{NR_j}(P_{s,t}) = (N_j \times G_{R_j}) / \sum_{i=1}^{\Re}(N_i \times G_{R_i}) \qquad (3)$$

where N_j and G_{R_j} are the number of neighbours and the sum of their inverse distances of the region R_j from the candidate pixel $P_{s,t}$ respectively.

2.1. Membership functions for fractal dimension

Fractal dimension (FD) is used to estimate the texture in an image. There are many different models for estimating FD. One is called the differential box counting (DBC) method [10], and approximates *the fractal dimension based feature* (FDF) for developing the membership functions for fractal dimension. The notion of self-similarity is used to estimate fractal dimension. A self-similar set (A) is the union of N_r mutually exclusive copies of itself that are similar to A and scaled down by a ratio r. The FD of A can then be defined as,

$$1 = N_r r^{FD} \Rightarrow FD = \frac{\log N_r}{\log(1/r)} \qquad (4)$$

N_r is determined using the DBC method in the following way [10]. For an image of size $M \times M$ to be scaled down to a size of $x \times x$ where $2 \leq x \leq \lfloor M/2 \rfloor$, the ratio of scale down is $r = x/M$. The image is then extended to 3-D space by introducing a 3rd co-ordinate for the 8-bit gray level intensity of 256 levels. If the image is partitioned into grids of size $x \times x$, then each grid will have a column of boxes of size $x \times x \times x'$, which implies $\lfloor 256/x' \rfloor = \lfloor M/x \rfloor$. If the maximum and minimum gray level values in the (u,v)th grid are in the lth and k^{th} boxes, the thickness of the blanket covering the image surface on the grid (u,v) is: -

$$n_r(u,v) = l - k + 1 \qquad (5)$$

The contribution from all grids is defined as: -

$$N_r = \sum_{u,v} n_r(u,v) \qquad (6)$$

FD is estimated from the least square linear fit of $\log(N_r)$ against $\log(1/r)$.

To define the membership function for fractal dimension, the FDF of a candidate pixel $P_{s,t}$ is calculated on a window $W_{h,h}(s,t)$ of size $h \times h$ with its centre at (s,t) rather than the entire image and is defined as: -

$$FDF(P_{s,t}) = FD(W_{h,h}(s,t)) \qquad (7)$$

where $FD(W_{h,h}(s,t))$ denotes the FDF on $W_{h,h}(s,t)$ derived using DBC in the following manner. The bound of the box size is chosen as $2 \leq \xi \leq \lfloor h/2 \rfloor$, the scale down ratio $r = \lfloor \xi/h \rfloor$ and x' is taken as $\lfloor 256 \times \xi/height \rfloor$ in order to consider the finer

variations of the gray level values, where *height* is the height of the image. The value of $FD(W_{h,h}(s,t))$ will not be the exact fractal dimension of the window $W_{h,h}(s,t)$ because the height of the image is used rather than h, the height of the window, in calculating x'. Instead of considering log-log plot, the average value of $\log(N_r)/\log(1/r)$ is used to obtain the fractal dimension. The membership function $\mu_{FR_j}(P_{s,t})$ of fractal dimension based feature for the region R_j and the pixel $P_{s,t}$ can be formulated as: -

$$\mu_{FR_j}(P_{s,t}) = 1 - \frac{\left| FDF_{R_j}(P_{s,t}) - FDF_i(P_{s,t}) \right|}{\max\{FDF_{R_j}(P_{s,t}), FDF_i(P_{s,t})\}} \qquad (8)$$

where $FDR_{R_j}(P_{s,t})$ and $FDF_i(P_{s,t})$ are the fractal dimension-based features for the segmented region R_j and the original image respectively. This membership function considers the image specific information for segmentation. $FDF_i(P_{s,t})$ is determined from the ratio of the number of contributory and total grids during $FDF_{R_j}(P_{s,t})$ calculation for each value of r.

2.2. Membership functions for contrast

Contrast provides the measure of the texture of an image and is measured by considering the dynamic range of gray levels and the polarization of the distribution of black and white on the gray-level histogram. The contrast of a window $W_{h,h}(P_{s,t})$ in an image is calculated using the technique described in [11]. The membership function for the contrast of the region R_j and the pixel $P_{s,t}$ can be defined as: -

$$\mu_{C_t R_j}(P_{s,t}) = 1 - \frac{\left| Contrast_{R_j}(P_{s,t}) - Contrast_i(P_{s,t}) \right|}{\max(Contrast_{R_j}(P_{s,t}), Contrast_i(P_{s,t}))} \qquad (9)$$

where $Contrast_{R_j}(P_{s,t})$ and $Contrast_i(P_{s,t})$ represent the contrast of the portions of the segmented region R_j and the original image covered by the window $W_{h,h}(P_{s,t})$ respectively.

3. DEFINING FUZZY RULE

The overall membership value $\mu_{AR_j}(P_{s,t},r)$ of a pixel $P_{s,t}$ for region R_j represents the overall degree of belonging to that region, and is defined by the weighted average of the five individual membership function values $\mu_{DR_j}(P_{s,t})$, $\mu_{CR_j}(P_{s,t})$, $\mu_{NR_j}(P_{s,t},r)$, $\mu_{FR_j}(P_{s,t})$, and $\mu_{C_t R_j}(P_{s,t})$.

$$\mu_{AR_j}(P_{s,t},r) = \frac{w_1 \mu_{DR_j}(P_{s,t}) + w_2 \mu_{CR_j}(P_{s,t}) + w_3 \mu_{NR_j}(P_{s,t},r)}{\sum_{i=1}^{5} w_i} + \frac{w_4 \mu_{FR_j}(P_{s,t}) + w_5 \mu_{C_t R_j}(P_{s,t})}{\sum_{i=1}^{5} w_i} \qquad (10)$$

where w_1, w_2, w_3, w_4, and w_5 are the weightings of the membership values for pixel distribution, closeness to the cluster centres, neighbourhood relations, fractal dimension and contrast respectively.

Definition 1 (Rule) IF $\mu_{AR_j}(P_{s,t}, r) = \max_{i=1}^{n} \{\mu_{AR_i}(P_{s,t}, r)\}$ THEN pixel $P_{s,t}$ belongs to region R_j.

4. DETERMINING THE PARAMETERS

The weighting factors w_1, w_2, and w_3, and threshold T for neighbourhood system are automatically determined using the algorithm described in [7]. The other two weighting factors w_4 and w_5 are approximated based on the FD of the entire image and the standard deviations ($rstd$) of pixel intensities of the initially segmented regions, as follows:

$$w_4 = w_5 \approx (FD - 2) / \text{var}(rstd) \qquad (11)$$

Since $2 \le FD \le 3$ the topological dimension of the image (2) is deducted from the FD, thereby keeping the original contribution of the fractal within [0,1]. This ensures that the contributions of all the weights are constrained within their limits. From the observations, it was found that the regions having high texture suppressed the regions containing less texture because they produced higher FD values. Since the standard deviation approximates the texture, the weights w_4 and w_5 are normalised using the variance of the standard deviations var($rstd$) of the initially segmented regions, to minimize this effect. This has been experimentally tested upon various image types.

5. EXPERIMENTAL RESULTS

Both the new FRIST and GFRIS algorithms were implemented using MATLAB 6.0 (The Mathworks, Inc.). A number of different image types were used in the experiments, but only two are included in this paper, namely the cloud shown in Fig. 1(a), which comprises one homogeneous and one non-homogeneous region, and the Brodatz texture image shown in Fig. 1(c), which contains two separate textural regions.
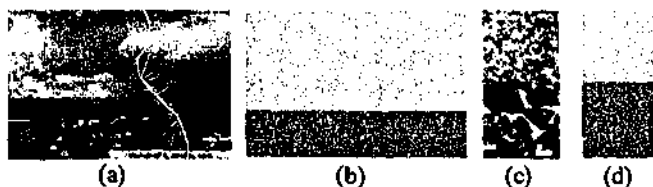

Fig. 1: (a) Cloud image, (b) Ref: images for cloud, (c) Brodatz textures, (d) Ref: images (d60 and d98) for Brodatz textures.

As alluded previously, quantitative evaluation of the segmentation process was achieved using *discrepancy based on the number mis-segmented pixels* [9]. Type I, *errorI*, represents the percentage error of all i^{th} region pixels that are not classified in the ith region, whereas Type II, *errorII_i*, is the percentage error of all other region pixels wrongly classified in the ith region.

For both GFRIS and FRIST, the membership function for region pixel distribution $\mu_{DR_j}(P_{s,t})$ was developed using the clusters produced by the initial segmentation results using the fuzzy c-means (FCM) algorithm [12]. The centre values were used to initialize the centres of the clusters required to define the membership function for the closeness of a region ($\mu_{CR_j}(P_{s,t})$).

The neighborhood radius (r) was taken as 1, 2 and 4, but only the results for the $r = 1$ and 2 cases are included in this paper, with the size of the window $W_{A,A}(s,t)$ being 4×4. The results of segmenting the cloud image (Fig. 1(a)) into two regions namely, cloud (R_1) and urban scene (R_2) using GFRIS and FRIST are shown in Fig. 2. The numerical segmentation results of the cloud image segmentation with respect to manually segmented reference images (Fig. 1(b)) are shown in Table 1.

(a) GFRIS, $r = 1$ (c) FRIST, $r = 1$

(b) GFRIS, $r = 2$ (d) FRIST, $r = 2$
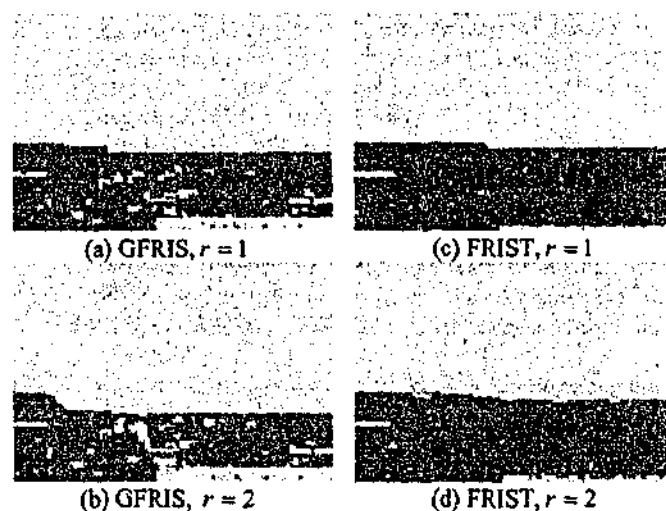
Fig. 2: The segmented results of the cloud image into two regions by GFRIS (a) to (b), and FRIST (c) to (d).

Table 1: Error percentage for region R_1 of cloud (cloud) and Brodatz (d60) image segmentations

Image	Algorithm	Error I	Error II	Algorithm	Error I	Error II
	GFRIS r=1	7.33	17.05	FRIST r=1	10.560	4.487
Cloud	GFRIS r=2	1.73	21.25	FRIST r=2	9.106	4.230
	GFRIS r=4	1.80	23.62	FRIST r=4	7.287	4.038
	GFRIS r=1	33.99	17.11	FRIST r=1	28.247	15.718
Brodatz	GFRIS r=2	33.16	19.47	FRIST r=2	25.488	18.687
	GFRIS r=4	26.65	21.96	FRIST r=4	19.97	16.269

In Table 1, only the error rates for region R_1 are shown since the error rates of the other region R_2 are simply the reverse order of R_1. The segmentation results for the cloud image using GFRIS showed that region R_1 (Fig. 2(a) and (b)) contained a large number of misclassified pixels from region R_2, which has sharp variations in pixel intensity. Type II error rates for region R_1 using GFRIS (Table 1) were higher than type I error rates. Almost all of the misclassified pixels, including the

text caption were correctly classified using FRIST (Fig. 2(c) and (d)). The average error rates for both techniques are graphically
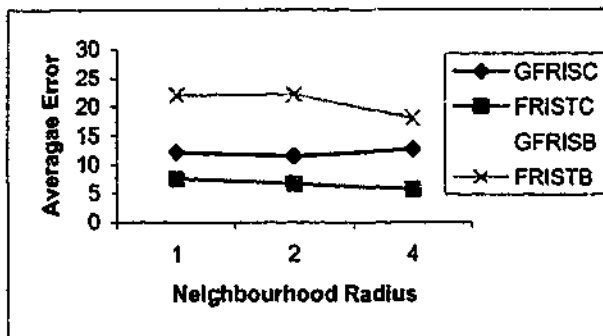
Fig. 3: Average error rates of GFRIS and FRIST for cloud (GFRISC and FRISTC) and Brodatz (GFRISB and FRISTB) images texture segmentation.

shown in Fig 3. From Fig. 2 and 3, it is clear that FRIST achieved considerable improvements over the GFRIS.

| (a) GFRIS, | (b) FRIST, | (c) GFRIS, | (d) FRIST, |
| $r = 1$ | $r = 1$ | $r = 2$ | $r = 2$ |
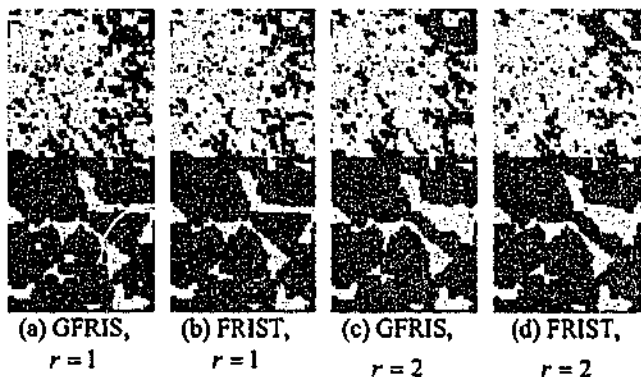
Fig. 4: Segmented results of Brodatz texture into two regions using GFRIS (a) and (c), and FRIST (b) and (d).

A second series of experiments was performed using the Bodaz texture image (Fig. 1(c)). The segmentation results for the two separate regions namely, d60 (R_1) and d98 (R_2) produced by the GFRIS and FRIST are presented in Fig. 4. The error and average error rates of d60 segmentation with respect to the manually segmented reference images (Fig. 1(d)) are shown in Table 1 and Fig. 3 respectively. The segmented results obtained using FRIST for all values of r are again considerably better than GFRIS. Note, that it was shown in [7], that GFRIS consistently provided superior results to both FCM [12] and possibilistic c-means (PCM) [13] algorithms for many different image types.

6. CONCLUSIONS

This paper has outlined the development of a new general fuzzy rule-based image segmentation technique incorporating texture based upon fractal dimension and contrast. A new algorithm titled *fuzzy rules for image segmentation incorporating texture features* (FRIST), has been proposed and both a quantitative and qualitative analysis have been undertaken to compare it with the generic approach (GFRIS). The experimental results have shown that FRIST outperformed GFRIS for many different image

types. Since the proposed technique is fuzzy rule based, it is capable of incorporating any type of attribute of any special application domain. It is possible to add membership functions for high-level semantics of an object for object based image segmentation. More research however is required in order to automatically determine the explicit number of regions in an image.

7. REFERENCES

[1] C.-W. Chang, H. Ying, G.R. Hillman, T.A. Kent, and J. Yen, "A rule-based fuzzy segmentation system with automatic generation of membership functions for pathological brain MR images", Computers and Biomedical Research, 1998, http://gopher.cs.tamu.edu/faculty/yen/publications/index.html.

[2] Z. Chi, and H. Yan, "Segmentation of geographic map images using fuzzy rules", Proceedings of DICTA-93, Digital Image Computing, Techniques and applications, Australian Pattern Recognition Soc., 1, 95-101, Broadway, NSW, Australia, 1993.

[3] L.O. Hall, and A Namasivayam, "Using adaptive fuzzy rules for image segmentation", FUZZ-IEEE'98, 1998, http://modern.csee.usf.edu/~hall/adrules/segment.html

[4] T. Sasaki, Y. Hata, Y. Ando, M. Ishikawa, and H. Ishikawa, "Fuzzy rule based approach to segment the menisci region from MR images", Proceedings of SPIE Medical Imaging, 3661, 258-, San Diego, California, USA, 1999.

[5] W. Park, E. A. Hoffman, and M. Sonka, "Segmentation of intrathoracic airway trees: a fuzzy logic approach", IEEE Transactions on Medical Imaging, 17, 4, 489-497, 1998.

[6] G.C. Karmakar and L. Dooley, "Generic fuzzy rule based technique for image segmentation", IEEE International Conference on Acoustics, Speech, and Signal Processing, Salt Lake City, Utah, 3, III-1577-III-1580, 2001.

[7] G.C. Karmakar and L.S. Dooley, "A Generic fuzzy rule based image segmentation algorithm", Pattern Recognition Letters, 23, 10, 1215-1227, 2002.

[8] B.B. Chaudhuri and N. Sarkar, "Texture segmentation using fractal dimension", IEEE Transactions on Pattern Analysis and Machine Intelligence, 17, 1, pp. 72-77, January, 1995.

[9] Y.J. Zhang, "A survey on evaluation methods for image segmentation", Pattern Recognition, 29, 8, 1335-1346, 1996.

[10] N. Sarkar and B.B. Chaudhuri, " An efficient approach to estimate fractal dimension of textural images", Pattern Recognition, 25, 9, 1035-1041, 1992.

[11] H. Tamura, S. Mori, and T. Yamawaki, "Textural features corresponding to visual perception", IEEE Transactions on Systems, Man, and Cybernetics, SMC-8, 6, 460-473, 1978.

[12] J.C. Bezdek, "Pattern Recognition with Fuzzy Objective Function Algorithms", New York: Plenum, 1981.

[13] R. Krishnapuram and J. Keller, "A possibilistic approach to clustering", IEEE Transactions on Fuzzy Systems, 1, 98-110, 1993.

IMAGE SEGMENTATION USING MODIFIED EXTENDED FUZZY RULES

Gour C. Karmakar, Laurence S. Dooley, and Manzur Murshed

Gippsland School of Computing and Information Technology. Monash University. Churchill. Vic 3842. Australia

{Gour.Karmakar,Laurence.Dooley,Manzur.Murshed}@infotech.monash.edu.au

ABSTRACT

The *extended fuzzy rules for image segmentation* (EFRIS) algorithm initially splits all segmented regions into mutually exclusive 4-connected objects, from which the largest one in each region is designated as its *main object*. A drawback of this approach is that it is less effective when the *main objects* are relatively small and some of the other objects are completely surrounded and connected to the *main object* of another region. Besides possessing insufficient merging rules, EFRIS also only considers the surrounding main objects in the original order that the regions were segmented, which is undesirable. In this paper, a new general segmentation algorithm called *modified extended fuzzy rules for image segmentation* (MEFRIS) is presented, which addresses these problems and whose improved segmentation performance is analysed and numerically evaluated. The results are also contrasted with both the original *generic fuzzy rule-based image segmentation* (GFRIS) and EFRIS algorithms.

1. INTRODUCTION

Image segmentation is one of the most important and difficult tasks of digital image processing and analysis systems, due to the potentially inordinate number of objects and the myriad of variations among them. The most intractable task is to define the properties for perceptual grouping, which requires human expert knowledge to be incorporated in order to achieve superior segmentation results. Fuzzy rule-based image segmentation techniques can incorporate such expert knowledge, but are very much application domain and image dependent, with the structure of the membership functions and the corresponding parameters having to be defined either manually or automatically [1-4]. Karmakar and Dooley [5-6] proposed a novel *generic fuzzy rule based image segmentation* (GFRIS) algorithm, which attempted to solve the aforementioned problems. The approach however, does not work effectively for image regions that were either non-homogeneous or have sharp variations in pixel intensity. Subsequently, Karmakar and Dooley [7] introduced a revised algorithm called, *extended fuzzy rules for image segmentation* (EFRIS), which incorporated the perceptual properties of surroundedness and connectedness in segmented regions. The algorithm split the regions that had already been segmented by the first rule, which was inherited from the GFRIS algorithm, into mutually exclusive 4-connected objects. The largest object in each region was designated as its *main object* and all minor objects were then tested against the two aforementioned perceptual properties, with respect to the *main objects* of other regions, for better placement through the

merging rule. This procedure has been found to be ineffective under three specific conditions: (i) when the *main object* is relatively small, (ii) when some of the minor objects are completely surrounded and connected to the *main object* of another region, and (iii) the single merging rule, which formed the fundamental basis of the EFRIS algorithm, and selected the surrounding *main objects* in the exact order that the regions were originally segmented by the first rule.

In this paper, a *modified extended fuzzy rule based image segmentation* (MEFRIS) algorithm is proposed which redefines the merging rule of the EFRIS algorithm, by incorporating new fuzzy rules for growing relatively small *main objects* and preventing similar objects from merging with other *main objects*. Additional merging rules are also defined for selecting the most suitable surrounding *main object*.

The paper is organised as follows. Section 2 provides a brief description on the initial segmentation and splitting techniques used. The underlying theory, and various membership and other functions used in MEFRIS are described in Section 3, while the fuzzy rules used in the MEFRIS algorithm are provided in Section 4. Some comparative experimental results with discussions are presented in Sections 5. Section 6 concludes the paper.

2. INITIAL SEGMENTATION AND SPLITTING TECHNIQUES

The initial image segmentation may be undertaken using any standard segmentation algorithm such as fuzzy clustering, or the GFRIS algorithm. The results of this initial phase are then refined using the fuzzy rules based on the principles of connectedness, surroundedness, uniformity and contrast criteria.

Connectivity is defined [12] as follows: -

Definition 1 (δ-connectivity) Let $N_\delta(P_2)$ denote the set of all the δ-neighbours of pixel P_2. Then pixel P_1 is considered δ-connected with pixel P_2, iff $P_1 \in N_\delta(P_2)$ where $\delta \in \{4,8\}$.

Let the initial $\Re$ segmented regions be represented by $R_j, j = 1...\Re$. Each of these regions is then split into a number of mutually exclusive objects using the 4-connected neighbourhood property. The reason for applying 4-connectedness, instead of the usual 8-connectedness in the region splitting process, is to avoid weak connections within an object and to maximize the number of possible objects in any region. Let the set of all objects in region R_j be denoted as $\{O_{1j}, O_{2j}, ..., O_{nj}\}$ where

n_j represents the number of 4-connected objects in that region. It is interesting to note that $O_{1,j} \cup O_{2,j} \cup ... \cup O_{n_j j} = R_j$ and $O_{1,j} \cap O_{2,j} \cap ... \cap O_{n_j j} = \phi$. Let object $O_{m_j j}$, where $|O_{m_j j}| = \max\{|O_{1,j}|, |O_{2,j}|, ..., |O_{n_j j}|\}$ be the *main object* of region R_j, where $|Q|$ denotes the number of pixels in object Q.

3. MEMBERSHIP AND OTHER FUNCTIONS

The surroundedness property is itself fuzzy in nature as any object may either be or not be completely surrounded by another object. This leads to the definition of a membership function for estimating the degree of surroundedness. The membership function for the surroundedness of an object (region) A by another object (region) B is defined as:-

$$\mu_s(A, B) = \frac{|A \cap B|}{|A|} \quad (1)$$

The membership function for the size of the *main object* $O_{m_k k}$ with respect to its region R_k is defined as:-

$$\mu_t(O_{m_k k}, R_k) = \frac{|O_{m_k k}|}{|R_k|} \quad (2)$$

Using membership functions (1) and (2), two other functions $large(O_{m_k k}, R_k)$ and $outer(R_k)$ can be defined as follows:-

$$large(O_{m_k k}, R_k) = \begin{cases} true, & if\ \mu_t(O_{m_k k}, R_k) \ge \lambda_1 \\ false, & otherwise \end{cases} \quad (3)$$

$$outer(R_k) = \prod_{\substack{i=1 \\ i \ne k}}^{\pi} (\mu_s(R_i, R_k) \ge \xi) \quad (4)$$

where λ_1 and ξ are prescribed thresholds.

Let us now define the function $similar(O_{m_k k}, O_{ik})$ between the *main object* $O_{m_k k}$ and its sibling O_{ik}, based on uniformity and contrast, as:-

$$similar(O_{m_k k}, O_{ik}) = \begin{pmatrix} |uniformity(O_{m_k k}) - uniformity(O_{ik})| \\ \le \tau |uniformity(O_{m_k k})| \end{pmatrix} \quad (5)$$
$$\wedge (|contrast(O_{m_k k}) - contrast(O_{ik})| \le \tau |contrast(O_{m_k k})|)$$

where τ denotes the percentage of variation, while the two functions uniformity and contrast are determined using the equations given in [9-10].

Let $MaxS(O_{ij}) = \left\{ k \left| \mu_s(O_{ij}, O_{m_k k}) = \max_{\substack{i=1 \\ i \ne j}}^{\pi} (\mu_s(O_{ij}, O_{m_l l})) \right. \right\}$

represent the set of indices of regions for which the degree of surroundedness of an object O_{ij}, by the *main objects* of those regions, is a maximum. The functions $p-connected(O_{ij}, O_{m_k k})$ and $connect_p(O_{ij})$ can then be defined as follows: -

$$p-connected(O_{ij}, O_{m_k k}) = \begin{cases} true, & if\ O_{ij}\ is\ p\text{-connected} \\ & with\ O_{m_k k} \\ false, & otherwise \end{cases} \quad (6$$

$$connect_p(O_{ij}) = \{k | k \in MaxS(O_{ij}) \wedge p-connected(O_{ij}, O_{m_k k})\} \quad (7$$

where $p \in \{4, 8\}$.

All these functions are used in defining the MEFRIS fuzzy rules in the following section.

4. FUZZY RULES

Three different types of fuzzy rules are now defined for three totally different purposes. The first type comprises only one rule known as the *growing up rule*, and is used simply to grow small *main objects*, while the second type, namely the *preventive rule* seeks to block objects similar to their *main object* from merging with any other *main object*. The final type represents a group of mutually exclusive *merging rules* that are applied to join together suitable objects with the *main objects* of other region based on the principles of connectedness and surroundedness. These fuzzy rules are formalised as follows, where it is assumed throughout that $k \ne j$ to ensure that object O_{ij} merges with the *main object* $O_{m_k k}$ of another region and λ_2 is a threshold value: -

Definition 2 (Growing Up Rule) IF NOT $large(O_{m_k k}, R_k)$ AND NOT $outer(R_k)$ AND $similar(O_{m_k k}, O_{ik})$ THEN merge O_{ik} with $O_{m_k k}$.

Definition 3 (Preventive Rule) IF $similar(O_{m_k k}, O_{ik})$ AND $\lambda_1 < \mu_t(O_{m_k k}, R_k) \le \lambda_2$ AND NOT $outer(R_k)$ THEN prevent O_{ik} from merging.

Definition 4 (Merging Rule 1) IF $|MaxS| = 1$ AND $\mu_s(O_{ij}, O_{m_k k}) \ge \xi$ AND $8-connected(O_{ij}, O_{m_k k})$ THEN merge O_{ij} with $O_{m_k k}$.

Definition 5 (Merging Rule 2) IF $|MaxS| > 1$ AND $\mu_s(O_{ij}, O_{m_k k}) \ge \xi$ AND $4-connected(O_{ij}, O_{m_k k})$ THEN merge O_{ij} with $O_{m_k k}$ such that $\min_{k \in connect_4(O_{ij})} \{\mu_t(O_{m_k k}, R_k)\}$.

Definition 6 (Merging Rule 3) IF $|MaxS| > 1$ AND $\mu_s(O_{ij}, O_{m_k k}) \ge \xi$ AND $8-connected(O_{ij}, O_{m_k k})$ THEN merge O_{ij} with $O_{m_k k}$ such that $\min_{k \in connect_8(O_{ij})} \{\mu_t(O_{m_k k}, R_k)\}$.

5. EXPERIMENTS

The new MEFRIS, EFRIS, and GFRIS systems were implemented using MATLAB 6.0 (The Mathworks, Inc.) For the implementation of the membership functions defined in (1) and (2), the contour of the regions and their *main objects* were

determined using their respective convex hulls. The two reference images in Fig. 1(a) and (c) were used for empirical evaluation of the MEFRIS algorithm.
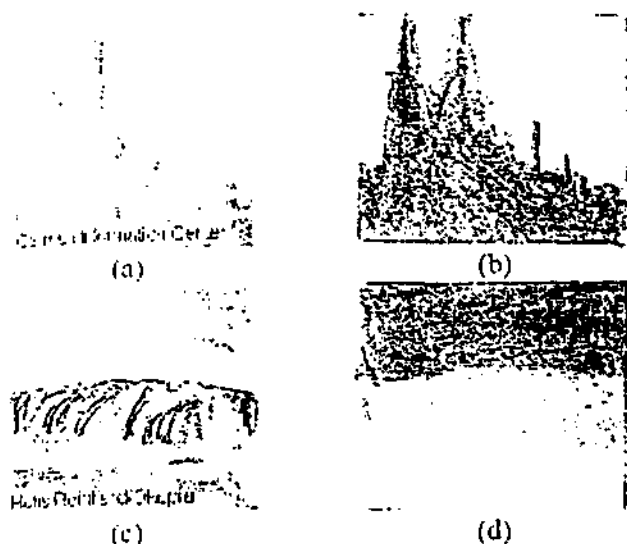
Fig 1: Original images and reference regions. (a): Church image. (b): Ref. regions for church image, (c): Sand image, (d): Ref. regions for Sand image.
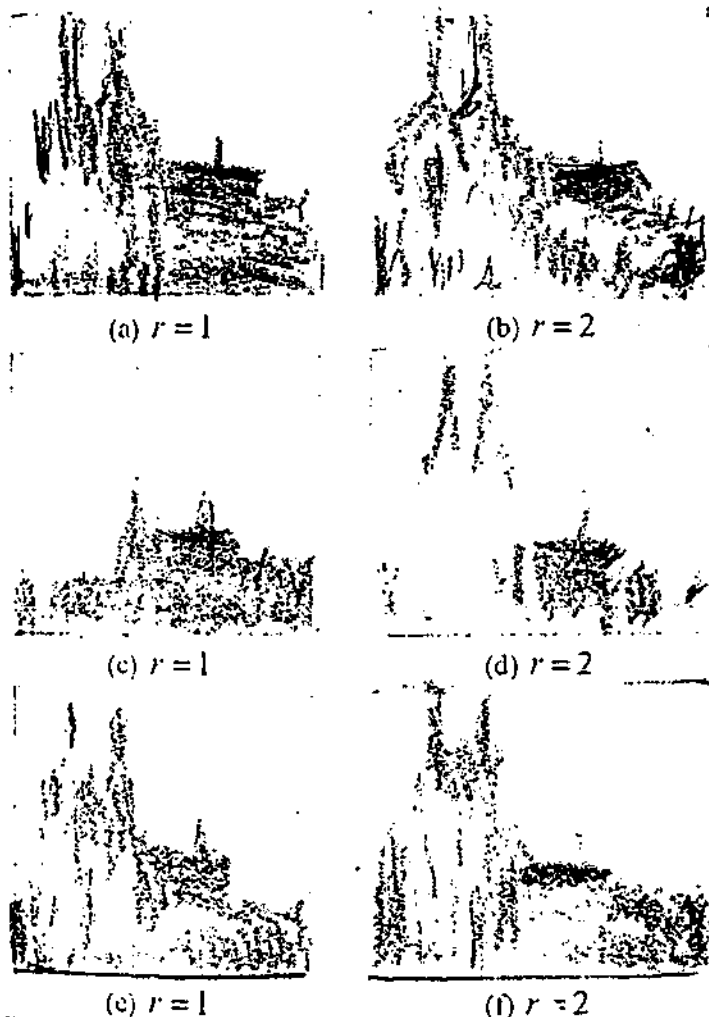
Fig. 2. The segmented results of the church image into two regions by GFRIS (a) & (b), EFRIS (c) & (d), and MEFRIS (e) & (f).

For the MEFRIS algorithm, the initial segmentation was carried out using GFRIS [6]. In GFRIS, the membership function for a region's pixel distribution $\mu_{DR_j}(P_{s,t})$ was developed using the clusters produced by the fuzzy c-means (FCM) algorithm [11] and their centre values were used to initialize the centres of the clusters required to define the membership function for closeness of a region $\mu_{CR_j}(P_{s,t})$. The values of the three thresholds ξ, λ_1, and λ_2 were empirically selected as 0.8, 0.7 and 0.9 respectively. The values of τ was also intuitively chosen as 1 and 0.8 for the *growing up* (definition 1) and *preventive* (definition 2) rules respectively, while a neighbourhood radius (r) of 1 and 2 was chosen. The results of segmenting the church image (Fig. 1(a)) into two regions, namely the church (R_1) and the sky (R_2), using the GFRIS, EFRIS, and MEFRIS algorithms are displayed in Fig. 2.

If the results shown in Fig. 2(a)-2(d) are compared with the results presented in Fig. 2(e)-2(f), it is visually apparent that the MEFRIS algorithm separated more distinct regions (church and sky) than the GFRIS and EFRIS algorithms. The reason for the poor EFRIS performance in not achieving superior results was as alluded earlier, because of small *main objects* and merging similar objects with other *main objects* (Fig. 2(c)-2(d)).
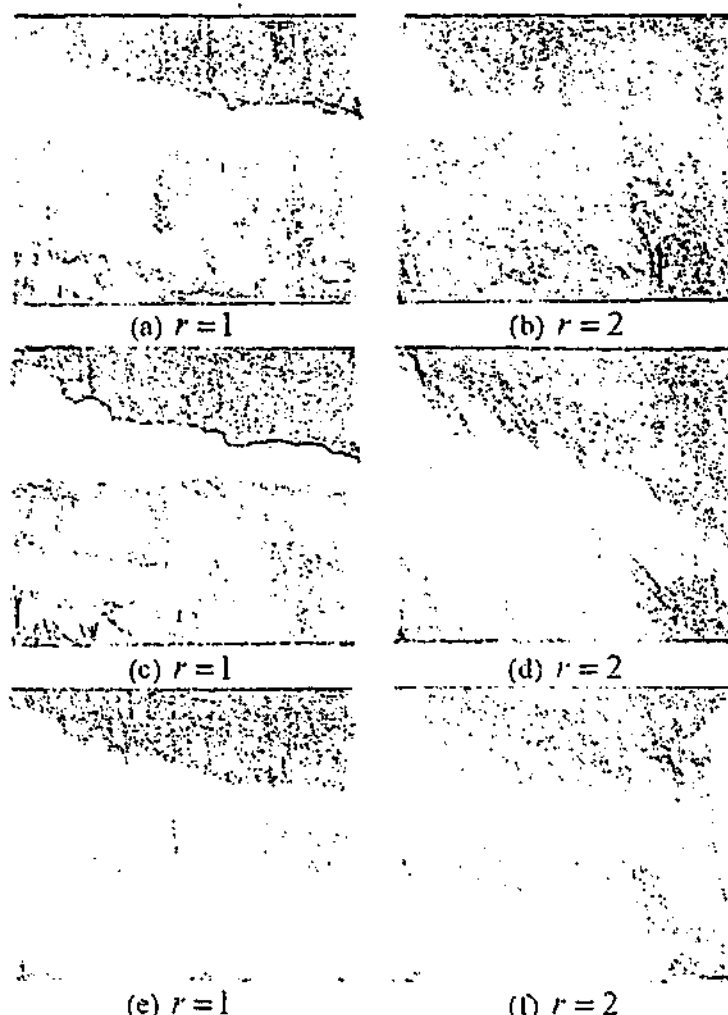
Fig. 3: The segmented results of the image into three regions by GFRIS (a) & (b), EFRIS (c) & (d), and MEFRIS (e) & (f).

All segmentation results were quantitatively evaluated using the powerful *discrepancy based on the number mis-*

segmented pixels [8] objective assessment method. Type I, errorI$_i$ represents the percentage error of ith region pixels that are not classified in the ith region, whereas Type II, errorII$_i$, is the percentage error of all other region pixels that are wrongly classified in the ith region. The numerical segmentation results of the church region for the Fig 1(a) segmentation with respect to manually segmented reference images are shown in Table 1. This reveals that the error rates (Type I) of MEFRIS are considerably lower than those of both GFRIS and EFRIS for all values of r.

Another series of experiments were performed using the image in Fig. 1(c), which comprised three distinct regions, namely sky (R_1), sand (R_2), and rock (R_3). The segmentation performance for the three regions using GFRIS, EFRIS and MEFRIS is presented in Fig. 3. EFRIS produced almost exactly the same results as GFRIS because of having small *main objects*. It is perceptually apparent that the MEFRIS algorithm exhibited significantly improved results compared with both GFRIS and EFRIS for both values of the neighbourhood radius. The numerical error rates of the sand image segmentation with respect to the manually segmented reference images are shown in Table 2. Both error rates for MEFRIS are noticeably lower than the GFRIS and EFRIS for both values of r. The best result is achieved by using MEFRIS at $r = 1$. A statistical significance test, called sign test was also conducted, and confirmed the significance improvements of MEFRIS over GFRIS and EFRIS [13].

Table 1: Error percentages for the church region (R$_1$) in Fig. 1(a).

Algorithm	Error r=1		Error r=2	
	Type I	Type II	Type I	Type II
GFRIS	53.5207	0.4700	52.8810	0.3302
EFRIS	67.3970	0.1588	54.0143	0.2286
MEFRIS	48.9272	0.4700	42.6816	0.3302

Table 2: Error percentages of the sand image in Fig. 1(b).

Algorithm	Region	Error r=1		Error r=2	
		Type I	Type II	Type I	Type II
GFRIS	Sky	36.916	33.980	19.067	31.542
	Sand	66.092	22.831	87.714	12.037
	Rock	19.125	7.619	10.583	15.153
EFRIS	Sky	36.988	33.533	18.995	16.732
	Sand	66.092	23.241	87.714	11.928
	Rock	19.125	7.619	6.479	25.288
MEFRIS	Sky	37.155	3.3451	19.212	13.093
	Sand	21.100	30.081	54.128	13.775
	Rock	19.073	6.196	10.614	14.067

6. CONCLUSIONS

This paper has addressed the three fundamental limitations of the *extended fuzzy rules for image segmentation* (EFRIS) algorithm by proposing a new general segmentation technique called *modified extended fuzzy rule based image segmentation* (MEFRIS). New rules for growing a small *main object*, preventing similar siblings from merging with another *main object*, and selecting the best surrounding *main object* have been incorporated into this new algorithm. Experimental results and

statistical significance test have conclusively shown that the MEFRIS significantly outperformed both the EFRIS and GFRIS algorithms for different image types. Since the proposed technique is fuzzy rule based, it is capable of incorporating any type of attribute of any special application domain. It is therefore possible to add membership functions for high-level semantics of an object for object based image segmentation.

7. REFERENCES

[1] Z. Chi, and H. Yan, "Segmentation of geographic map images using fuzzy rules", Proceedings of DICTA-93, Digital Image Computing, Techniques and applications, Australian Pattern Recognition Soc., 1, 95-101, Broadway, NSW, Australia, 1993.

[2] L.O. Hall, and A Namasivayam, "Using adaptive fuzzy rules for image segmentation", FUZZ-IEEE'98, 1998. http://modern.csee.usf.edu/~hall/adrules/segment.html.

[3] T. Sasaki, Y. Hata, Y. Ando, M. Ishikawa, and H Ishikawa, "Fuzzy rule based approach to segment the menisci region from MR images", Proceedings of SPIE Medical Imaging, 3661, 258-, San Diego, California, USA, 1999.

[4] W. Park, E. A. Hoffman, and M. Sonka, "Segmentation of intrathoracic airway trees: a fuzzy logic approach", IEEE Transactions on Medical Imaging, 17(4), 489-497, 1998.

[5] G.C. Karmakar, and L. Dooley, "Generic fuzzy rule based technique for image segmentation", IEEE International Conference on Acoustics, Speech, and Signal Processing, Salt Lake City, Utah, 3, III-1577-III-1580, 2001.

[6] G.C. Karmakar, and L.S. Dooley, "A Generic fuzzy rule based image segmentation algorithm", Accepted for publication in Pattern Recognition Letters, 2002.

[7] G.C. Karmakar, and L.S. Dooley; "Extended fuzzy rule for image segmentation", IEEE International Conference on Image Processing (ICIP2001), 3, 1099-1102, Thessaloniki, Greece, 2001.

[8] Y.J. Zhang, "A survey on evaluation methods for image segmentation", Pattern Recognition, 29, 8, 1335-1346, 1996.

[9] H. Tamura, S. Mori, and T. Yamawaki, "Textural features corresponding to visual perception", IEEE Transactions on Systems, Man, and Cybernetics, Vol: SMC-8, No: 6, pp: 460-473, June, 1978.

[10] G.C. Karmakar, "Shape and texture based feature extraction for object ranking using neural networks", Master Thesis, Gippsland School of Computing and Information Technology, Monash University, Australia, 1998.

[11] J.C. Bezdek, "Pattern Recognition with Fuzzy Objective Function Algorithms", New York: Plenum, 1981.

[12] E. Horch, "Basic Principles of Imaging Science II" Lecture Notes 8, 2001, http://www.cis.rit.edu/class/Simg712/lectures/lect_08/lect_08.pdf.

[13] W.J. Popham and K.A. Sirotnik, "Educational Statistics: Use and Interpretation", Harper & Row, Publishers, New York, second edition, 1973.

944

Supplementary Original and Their Manually Segmented Reference Images

(a)　　　　　(b)　　　　　(c)　　　　　(d)

(e)　　　　　(f)　　　　　(g)　　　　　(h)

(i)　　　　　(j)　　　　　(k)　　　　　(l)
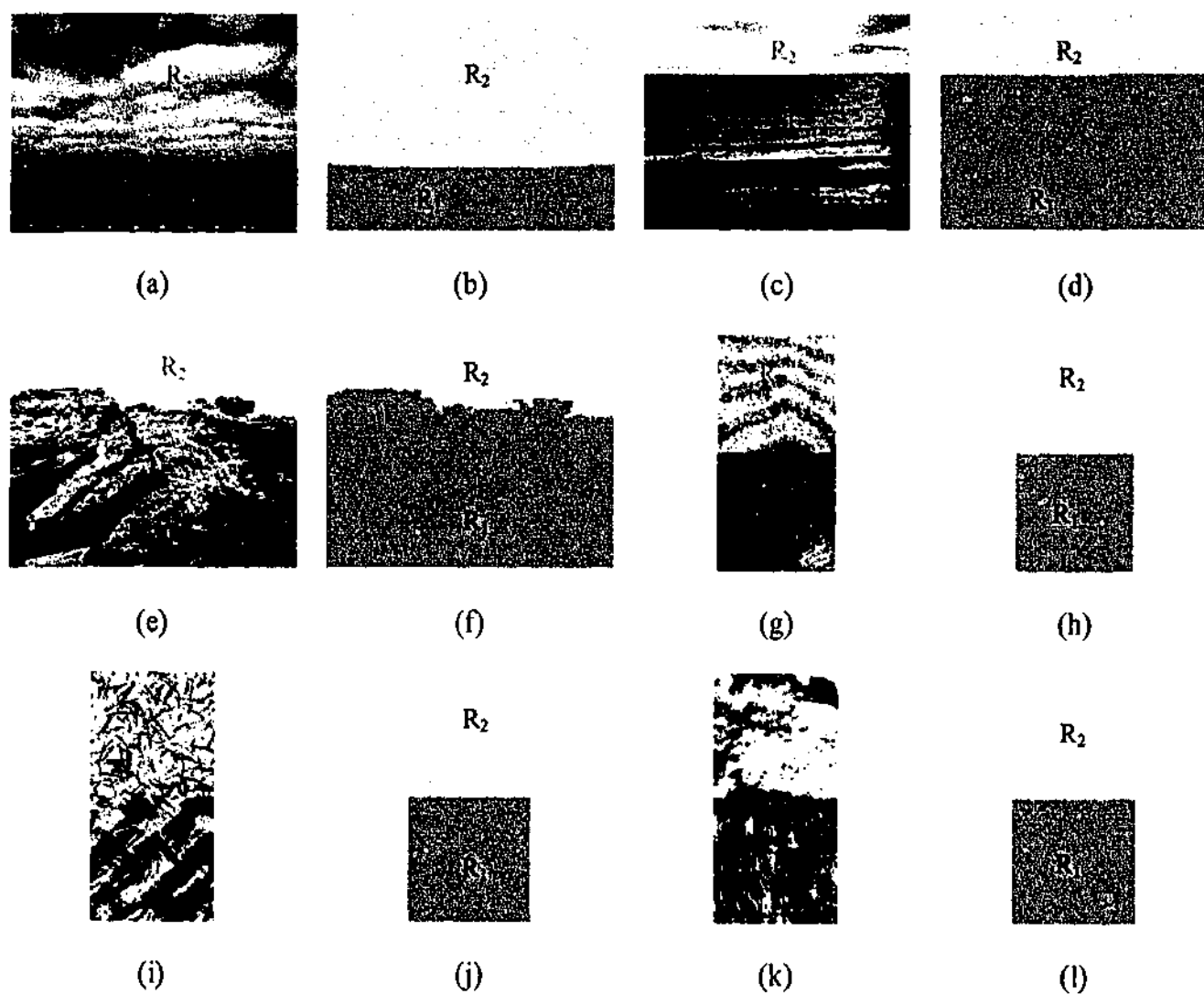
Fig. B.1: The other gray level original and their manually segmented reference images used in the evaluation in Chapter 7 for two regions.
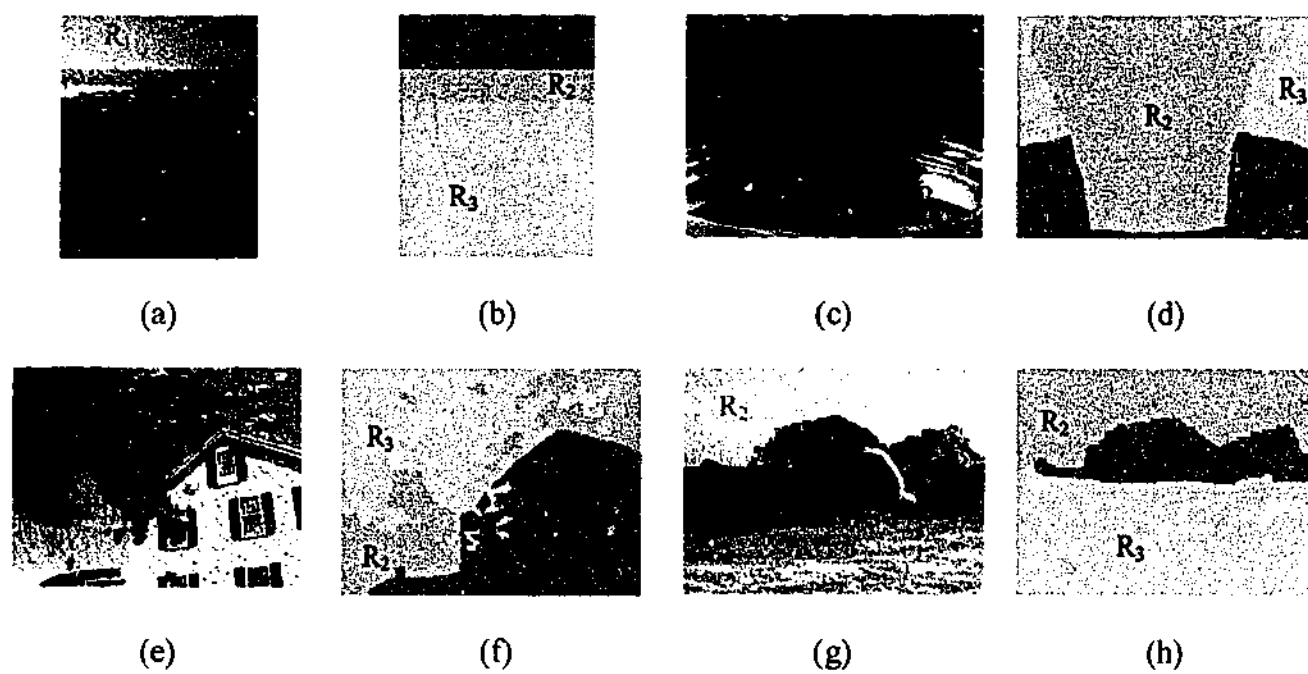
Fig. B.2: The other gray level original and their manually segmented reference images used in the evaluation in Chapter 7 for three regions.

The Segmentation Results for Supplementary Images
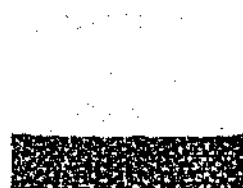
(a) GFRIS, $r = 1$ (b) GFRIS, $r = 2$ (c) GFRIS, $r = 4$ (d) FCM   (e) PCM
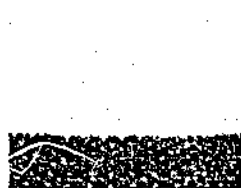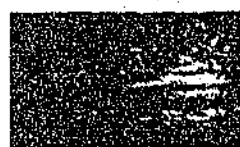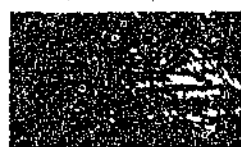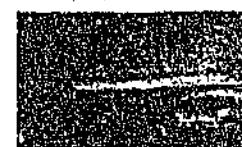
(f) GFRIS, $r = 1$ (g) GFRIS, $r = 2$ (h) GFRIS, $r = 4$ (i) FCM   (j) PCM

(k) GFRIS, $r = 1$ (l) GFRIS, $r = 2$ (m) GFRIS, $r = 4$ (n) FCM   (o) PCM

(p) GFRIS, $r = 1$ (q) GFRIS, $r = 2$ (r) GFRIS, $r = 4$ (s) FCM   (t) PCM

(u) GFRIS, $r=1$ (v) GFRIS, $r=2$ (w) GFRIS, $r=4$ (x) FCM   (y) PCM
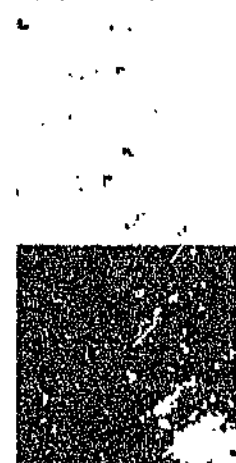
(z) GFRIS, $r=1$ (aa) GFRIS, $r=2$ (ab) GFRIS, $r=4$ (ac) FCM   (ad) PCM

Fig. C.1: The segmented results of the images shown in Fig. B.1(a), B.1(c), B.1(e), B.1(g), B.1(i), and B.1(k) are (a) to (e), (f) to (j), (k) to (o), (p) to (t), (u) to (y), and (z) to (ad) respectively for two regions using the GFRIS, FCM, and PCM algorithms.

(a) GFRIS, $r = 1$ (b) GFRIS, $r = 2$ (c) GFRIS, $r = 4$ (d) FCM   (e) PCM

(f) GFRIS, $r = 1$ (g) GFRIS, $r = 2$ (h) GFRIS, $r = 4$ (i) FCM   (j) PCM

(k) GFRIS, $r = 1$ (l) GFRIS, $r = 2$ (m) GFRIS, $r = 4$ (n) FCM   (o) PCM

(p) GFRIS, $r = 1$ (q) GFRIS, $r = 2$ (r) GFRIS, $r = 4$ (s) FCM   (t) PCM

Fig. C.2: The segmented results of the images shown in Fig. B.2(a), B.2(c), B.2(e), and B.2(g) are (a) to (e), (f) to (j), (k) to (o), and (p) to (t) respectively for three regions using the GFRIS, FCM, and PCM algorithms.

(a) GFRIS, $r = 1$ (b) GFRIS, $r = 2$ (c) GFRIS, $r = 4$ (d) FCM   (e) PCM

(f) GFRIS, $r = 1$ (g) GFRIS, $r = 2$ (h) GFRIS, $r = 4$ (i) FCM   (j) PCM

(k) GFRIS, $r = 1$ (l) GFRIS, $r = 2$ (m) GFRIS, $r = 4$ (n) FCM   (o) PCM

(p) GFRIS, $r = 1$ (q) GFRIS, $r = 2$ (r) GFRIS, $r = 4$ (s) FCM   (t) PCM

(u) GFRIS, $r = 1$ (v) GFRIS, $r = 2$ (w) GFRIS, $r = 4$ (x) FCM   (y) PCM

(z) GFRIS, $r=1$ (aa) GFRIS, $r=2$ (ab) GFRIS, $r=4$ (ac) FCM   (ad) PCM

Fig. C.3: The segmented results of the images shown in Fig. B.1(a), B.1(c), B.1(e), B.1(g), B.1(i), and B.1(k) are (a) to (e), (f) to (j), (k) to (o), (p) to (t), (u) to (y), and (z) to (ad) respectively for two regions using FRIS with the GFRIS, FCM, and PCM algorithms.

(a) GFRIS, $r = 1$ (b) GFRIS, $r = 2$ (c) GFRIS, $r = 4$ (d) FCM   (e) PCM

(f) GFRIS, $r = 1$ (g) GFRIS, $r = 2$ (h) GFRIS, $r = 4$ (i) FCM   (j) PCM

(k) GFRIS, $r = 1$ (l) GFRIS, $r = 2$ (m) GFRIS, $r = 4$ (n) FCM   (o) PCM

(p) GFRIS, $r = 1$ (q) GFRIS, $r = 2$ (r) GFRIS, $r = 4$ (s) FCM   (t) PCM
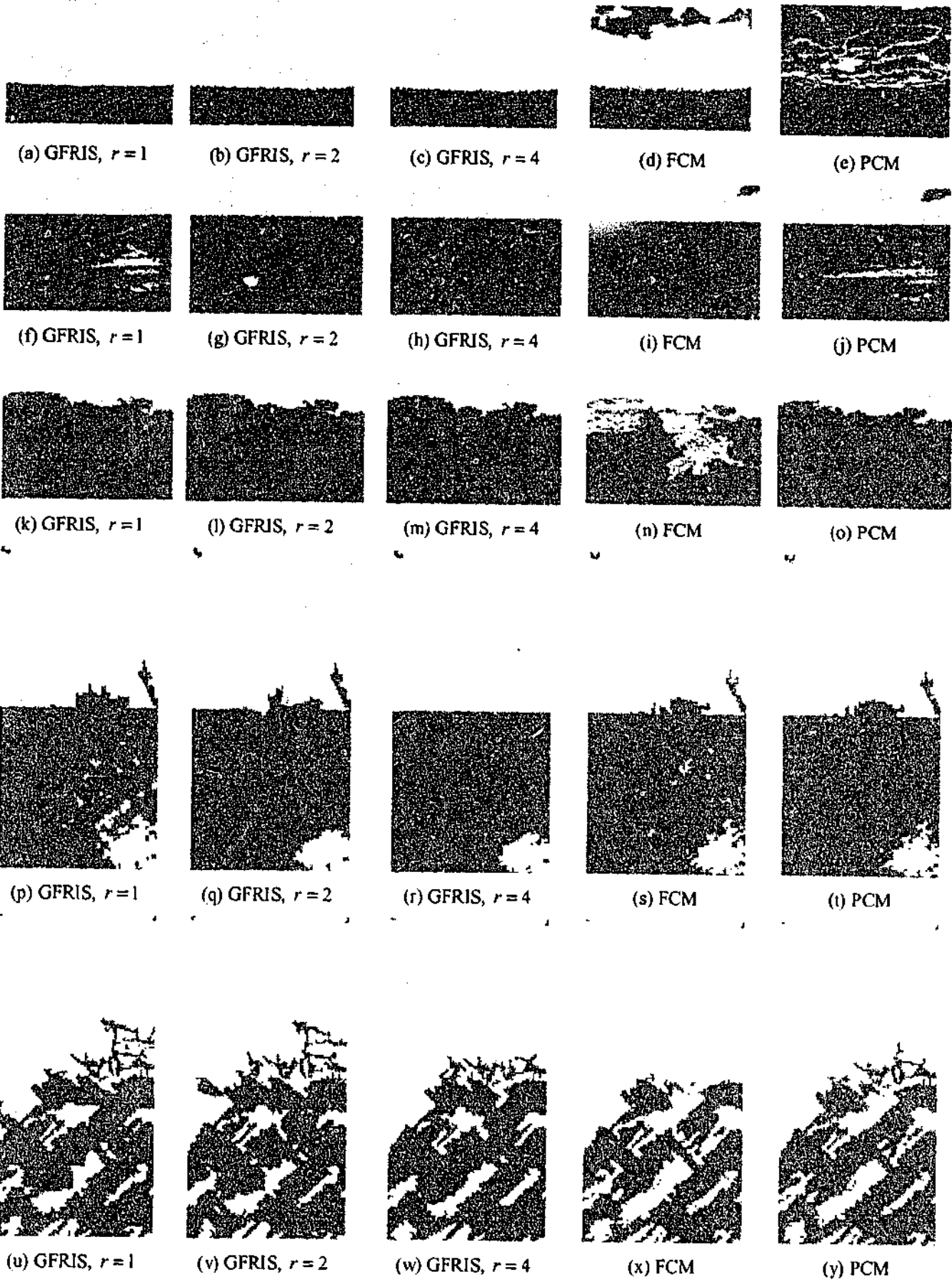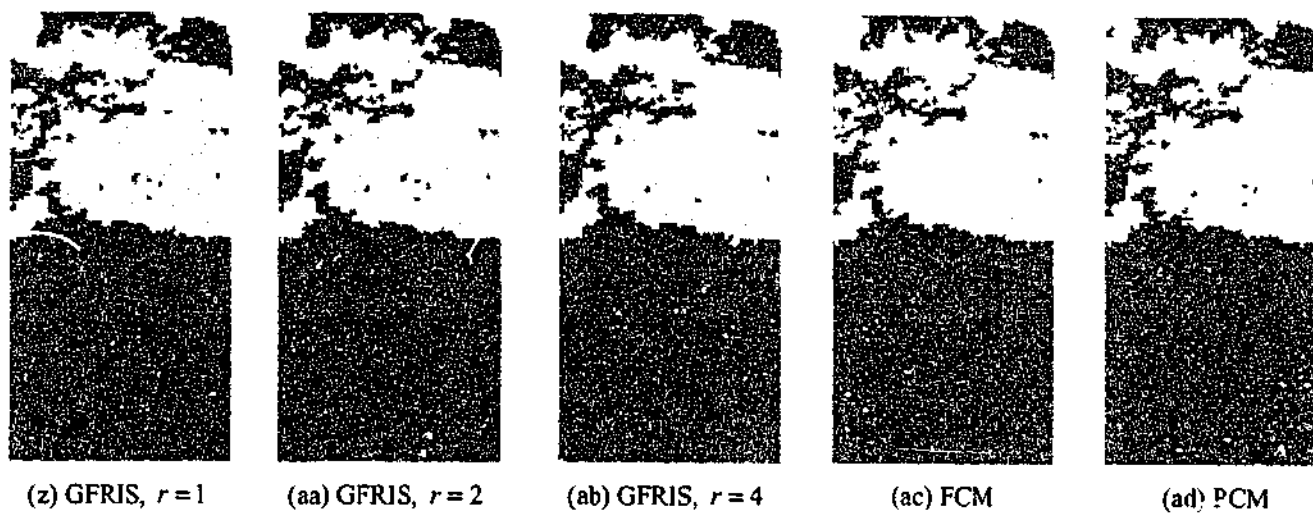
Fig. C.4: The segmented results of the images shown in Fig B.2(a), B.2(c), B.2(e), and B.2(g) are (a) to (e), (f) to (j), (k) to (o), and (p) to (t) respectively for three regions using FRIS with GFRIS, FCM, and PCM algorithms.
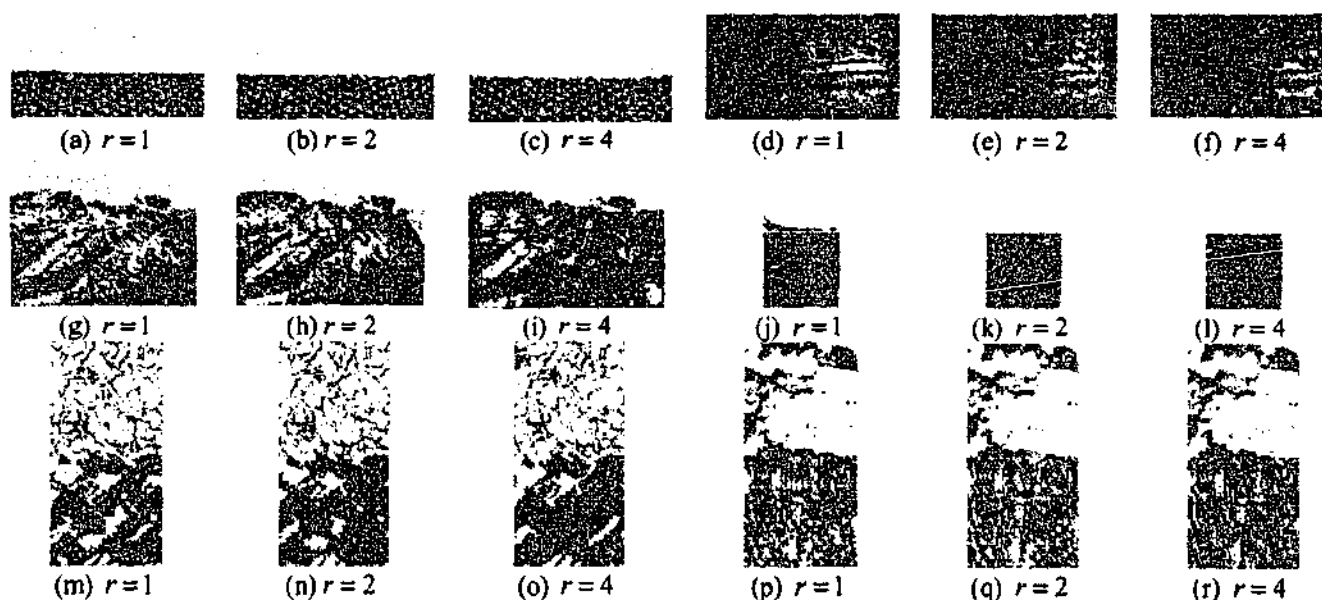
Fig. C.5: The segmented results of the images shown in Fig. B.1(a), B.1(c), B.1(e), B.1(g), B.1(i), and B.1(k) are (a) to (c), (d) to (f), (g) to (i), (j) to (l), (m) to (o), and (p) to (r) respectively for two regions using the FRIST algorithm.
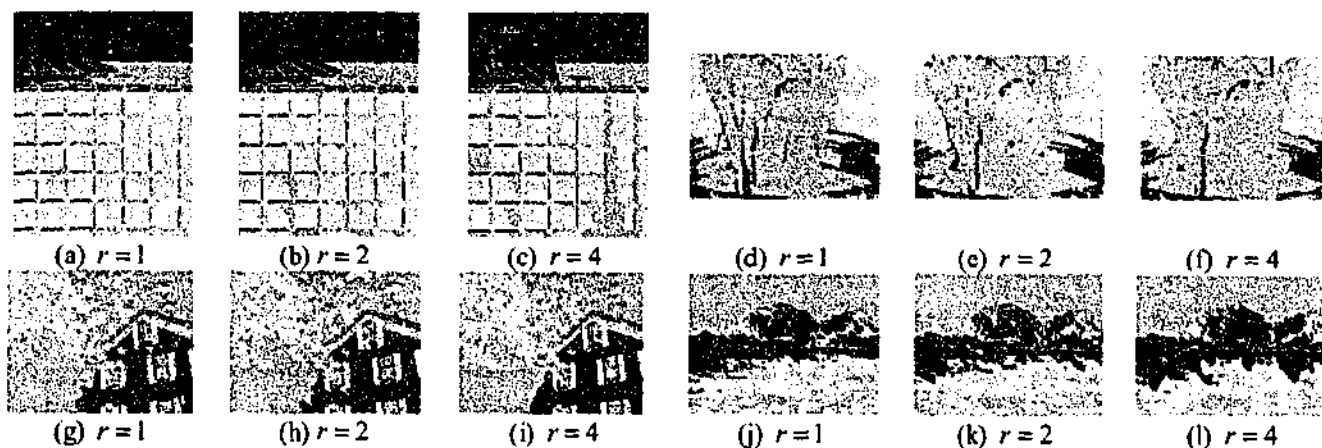

Fig. C.6: The segmented results of the images shown in Fig. B.2(a), B.2(c), B.2(e), and B.2(g) are (a) to (c), (d) to (f), (g) to (i), and (j) to (l) respectively for three regions using the FRIST algorithm.

Numerical Segmentation Results for Supplementary Images

Table D.1: Error percentages, average errors (average of Type I and II), and probability of object count agreement P(OCA) for other images shown in Fig. B.1, having two regions using the GFRIS, FCM, and PCM algorithms.

Algorithm	Region	Type I	Type II	Average	P(OCA)	Region	Type I	Type II	Average	P(OCA)
GFRIS r=1		7.97	1.17	4.57	0.344		5.24	0.00	2.62	0.465
GFRIS r=2	Texture in	7.95	0.89	4.42	0.352	Water in	4.17	0.00	2.08	0.491
GFRIS r=4	Fig. B.1(a)	7.84	0.67	4.25	0.352	Fig. B.1(c)	2.99	0.00	1.49	0.543
FCM		7.52	24.35	15.94	0.231		12.45	3.91	8.18	0.210
PCM		0.74	87.24	43.99	0.244		5.47	7.65	6.56	0.300
GFRIS r=1		20.85	0.17	10.51	0.200		10.28	13.05	11.66	0.517
GFRIS r=2	Hill in	18.89	0.17	9.53	0.263	Lower half	9.05	9.96	9.50	0.543
GFRIS r=4	Fig. B.1(e)	10.02	0.15	5.09	0.337	(d69) in	8.16	0.98	4.57	0.590
FCM		34.02	0.06	17.04	0.170	Fig. B.1(g)	10.01	8.21	9.11	0.404
PCM		23.83	0.10	11.96	0.175		9.19	9.72	9.46	0.398
GFRIS r=1		25.17	28.66	26.92	0.411		16.85	29.32	23.08	0.328
GFRIS r=2	Lower half	23.50	27.89	25.70	0.446	Lower half	16.48	29.48	22.98	0.343
GFRIS r=4	(d18) in	25.00	27.95	26.47	0.431	(d81) in	12.68	30.42	21.55	0.364
FCM	Fig. B.1(i)	36.68	23.11	29.89	0.374	Fig. B.1(k)	22.79	27.43	25.11	0.279
PCM		32.53	25.99	29.26	0.390		15.86	30.33	23.09	0.290

Table D.2: Error percentages, average errors (average of Type I and II), and probability of object count agreement P(OCA) for other images shown in Fig. B.2, having three regions using the GFRIS, FCM, and PCM algorithms.

Algorithm	Image and its Regions	Type I R_1	R_2	R_3	Type II R_1	R_2	R_3	Average	P(OCA)
GFRIS r=1	Wall1 (R₁),	0.00	49.00	10.16	9.14	5.61	2.94	12.81	0.486
GFRIS r=2	floor (R₂), and	0.00	49.94	14.44	9.36	8.71	3.01	14.24	0.492
GFRIS r=4	wall2 (R₃) of	0.00	49.33	34.43	9.67	23.32	2.66	19.90	0.554
FCM	Fig. B.2(a)	30.23	44.03	6.87	6.83	11.67	4.43	17.34	0.449
PCM		87.99	16.06	6.95	0.87	27.75	4.34	23.99	0.457
GFRIS r=1	Pot (R₁),	58.89	8.81	6.39	4.90	33.29	2.51	19.13	0.698
GFRIS r=2	asparagus (R₂), and	61.44	6.19	7.73	3.62	33.81	2.69	19.25	0.707
GFRIS r=4	background (R₃) of	62.58	6.80	3.91	3.29	33.30	3.11	18.83	0.725
FCM	Fig. B.2(c)	64.48	40.38	0.86	1.82	32.05	28.58	28.03	0.562
PCM		14.41	78.27	4.83	52.59	7.28	6.56	27.32	0.445
GFRIS r=1	House (R₁),	48.21	2.88	27.06	1.28	26.12	6.41	18.66	0.688
GFRIS r=2	sky (R₂), and	48.21	3.08	27.59	1.32	26.23	6.54	18.83	0.694
GFRIS r=4	tree (R₃) of	47.41	3.48	27.04	1.56	25.36	6.59	18.57	0.694
FCM	Fig. B.2(e)	45.87	22.93	23.83	6.85	22.32	7.22	21.50	0.600
PCM		48.88	8.35	25.69	2.60	25.72	6.62	19.64	0.649
GFRIS r=1	Hill (R₁),	36.57	1.87	34.85	15.12	8.42	13.13	18.33	0.414
GFRIS r=2	sky (R₂), and	37.97	1.55	38.15	16.78	8.95	13.29	19.45	0.444
GFRIS r=4	water (R₃) of	35.47	1.56	40.32	20.11	6.54	12.44	19.40	0.452
FCM	Fig. B.2(g)	40.76	1.78	47.11	14.37	19.01	13.88	22.82	0.276
PCM		65.06	63.70	30.11	41.01	1.42	23.95	37.54	0.229

D-1

Table D.3: Error percentages, average (average of Type I and II), probability of object count agreement P(OCA) for other images shown in Fig. B.1, having two regions using FRIS with the GFRIS, FCM, and PCM algorithms.

Algorithm	Region	Type I	Type II	Average	P(OCA)	Region	Type I	Type II	Average	P(OCA)
GFRIS $r=1$		0.00	1.17	0.59	1.000		4.09	0.00	2.05	0.713
GFRIS $r=2$	Texture in	0.17	0.89	0.53	1.000	Water in	0.26	0.00	0.13	1.000
GFRIS $r=4$	Fig. B.1(a)	0.40	0.66	0.53	1.000	Fig. B.1(c)	0.21	0.00	0.11	1.000
FCM		0.00	23.64	11.82	0.764		0.08	3.13	1.60	0.920
PCM		0.67	86.31	43.49	0.294		3.91	4.92	4.42	0.651
GFRIS $r=1$		0.79	0.19	0.49	0.931		8.94	4.48	6.71	0.746
GFRIS $r=2$	Hill in	0.73	0.19	0.46	0.960	Lower half	6.29	4.09	5.19	0.888
GFRIS $r=4$	Fig. B.1(e)	0.74	0.17	0.46	1.000	(d69) in	5.74	0.20	2.97	0.862
FCM		20.37	0.08	10.22	0.669	Fig. B.1(g)	6.86	3.64	5.25	0.777
PCM		1.50	0.11	0.80	0.931		5.81	4.16	4.99	0.841
GFRIS $r=1$		25.23	5.97	15.60	0.689		0.07	28.87	14.47	0.689
GFRIS $r=2$	Lower half	24.18	6.19	15.18	0.685	Lower half	0.07	28.85	14.46	0.708
GFRIS $r=4$	(d18) in	25.64	4.55	15.09	0.752	(d81) in	0.21	29.78	15.00	0.718
FCM	Fig. B.1(i)	35.84	0.43	18.13	0.724	Fig. B.1(k)	0.07	26.93	13.50	0.718
PCM		32.14	3.96	18.05	0.703		0.07	29.65	14.86	0.699

Table D.4: Error percentages, average errors (average of Type I and II), and probability of object count agreement P(OCA) for other images shown in Fig. B.2, having three regions using FRIS with the GFRIS, FCM, and PCM algorithms.

Algorithm	image and its Regions	Type I			Type II			Average	P(OCA)
		R_1	R_2	R_3	R_1	R_2	R_3		
GFRIS $r=1$	Wall1 (R_1),	0.00	31.39	7.31	5.44	5.38	0.04	8.26	0.689
GFRIS $r=2$	floor (R_2), and	0.00	31.68	13.75	5.37	10.20	0.04	10.17	0.805
GFRIS $r=4$	wall2 (R_3) of	0.00	46.56	31.44	5.20	23.32	5.94	18.74	0.705
FCM	Fig. B.2(a)	30.25	32.76	5.47	6.16	11.21	0.31	14.36	0.760
PCM		88.08	4.30	3.58	0.60	25.34	0.42	20.39	0.777
GFRIS $r=1$	Pot (R_1),	56.19	7.61	7.98	4.95	32.36	1.71	18.47	0.722
GFRIS $r=2$	asparagus (R_2), and	56.35	6.01	9.47	3.89	31.89	2.27	18.31	0.745
GFRIS $r=4$	background (R_3) of	56.78	6.88	5.44	4.85	30.19	2.02	17.69	0.768
FCM	Fig. B.2(c)	59.22	41.52	1.26	8.09	29.28	23.46	27.14	0.621
PCM		14.91	77.39	4.73	51.74	7.77	6.59	27.19	0.569
GFRIS $r=1$	House (R_1),	32.17	7.10	9.15	0.92	9.79	8.05	11.20	0.890
GFRIS $r=2$	sky (R_2), and	32.32	6.41	16.10	1.12	13.16	7.47	12.77	0.866
GFRIS $r=4$	tree (R_3) of	33.39	4.11	20.45	1.38	15.79	6.52	13.61	0.840
FCM	Fig. B.2(e)	26.24	27.90	10.21	7.66	7.41	8.01	14.57	0.811
PCM		33.23	12.05	11.29	2.26	11.65	7.72	13.03	0.862
GFRIS $r=1$	Hill (R_1),	33.44	1.60	22.81	14.23	0.81	11.33	14.04	0.807
GFRIS $r=2$	sky (R_2), and	36.98	1.40	27.51	16.20	1.86	12.58	16.09	0.659
GFRIS $r=4$	water (R_3) of	33.64	1.27	35.90	20.69	2.75	11.27	17.59	0.752
FCM	Fig. B.2(g)	42.02	1.69	41.49	13.16	16.47	13.95	21.46	0.497
PCM		74.73	37.54	28.21	28.48	5.41	24.07	33.07	0.342

Table D.5: Error percentages, average errors (average of Type I and II), and probability of object count agreement P(OCA) for other images shown in Fig. B.1, having two regions using the FRIST algorithm.

Algorithm FRIST	Region	Type I	Type II	Average	P(OCA)	Region	Type I	Type II	Average	P(OCA)
r=1	Texture in Fig. B.1(a)	7.45	1.43	4.44	0.357	Water in Fig. B.1(c)	4.74	0.00	2.37	0.462
r=2		7.70	0.60	4.15	0.361		3.68	0.00	1.84	0.493
r=4		7.78	0.39	4.08	0.361		2.89	0.00	1.45	0.551
r=1	Hill in Fig. B.1(e)	19.95	0.17	10.06	0.205	Lower half (d69) in Fig. B.1(g)	0.23	6.17	3.20	0.815
r=2		17.75	0.18	8.97	0.263		0.23	0.21	0.22	0.841
r=4		9.66	0.15	4.90	0.341		0.20	0.20	0.20	0.852
r=1	Lower half (d18) in Fig. B.1(i)	23.50	27.63	25.56	0.418	Lower half (d81) in Fig. B.1(k)	16.32	29.72	23.02	0.334
r=2		17.94	27.43	22.68	0.458		15.70	29.60	22.65	0.347
r=4		17.42	28.50	22.96	0.444		11.66	30.44	21.05	0.376

Table D.6: Error percentages, average errors (average of Type I and II), and probability of object count agreement P(OCA) for other images shown in Fig. B.2, having three regions using the FRIST algorithms.

Algorithm FRIST	Image and its Regions	Type I			Type II			Average	P(OCA)
		R_1	R_2	R_3	R_1	R_2	R_3		
r=1	Wall1 (R_1), floor (R_2), and wall2 (R_3) of Fig. B.2(a)	0.00	48.56	10.04	9.13	5.52	2.81	12.68	0.489
r=2		0.00	49.53	13.91	9.32	8.34	2.87	13.99	0.500
r=4		0.00	48.70	24.76	9.56	16.24	2.42	16.94	0.543
r=1	Pot (R_1), asparagus (R_2), and background (R_3) of Fig. B.2(c)	59.00	7.80	6.50	4.90	33.40	1.79	18.90	0.697
r=2		61.46	6.14	7.73	3.58	33.83	2.68	19.24	0.707
r=4		62.80	6.28	3.91	2.90	33.42	3.11	18.74	0.726
r=1	House (R_1), sky (R_2), and tree (R_3) of Fig. B.2(e)	50.29	2.94	24.01	1.00	26.24	6.34	18.47	0.702
r=2		51.72	3.07	25.26	1.04	27.68	6.29	19.18	0.708
r=4		49.55	3.61	24.65	1.23	26.11	6.33	18.58	0.705
r=1	Hill (R_1), sky (R_2), and water (R_3) of Fig. B.2(g)	36.45	1.87	34.65	15.30	8.05	13.08	18.23	0.418
r=2		37.91	1.53	37.92	16.79	8.77	13.25	19.36	0.449
r=4		35.47	1.56	41.00	20.58	6.47	12.44	19.59	0.457